Tampere University

TANJA HYVÄRINEN

Building Neural *in vitro* Models with Human Pluripotent Stem Cells

Neuronal Functionality and the Role of Astrocytes in the Networks

Tampere University Dissertations 216

Tampere University Dissertations 216

TANJA HYVÄRINEN

Building Neural *in vitro* Models with Human Pluripotent Stem Cells

Neuronal Functionality and the Role of Astrocytes in the Networks

ACADEMIC DISSERTATION
To be presented, with the permission of
the Faculty of Medicine and Health Technology
of Tampere University,
for public discussion in the auditorium 1096
of the Pinni B building, Kanslerinrinne 1, Tampere,
on 6 March 2020, at 12 o'clock.

ACADEMIC DISSERTATION
Tampere University, Faculty of Medicine and Health Technology
Finland

Responsible supervisor and Custos	Docent Susanna Narkilahti Tampere University Finland	
Supervisor	PhD Laura Ylä-Outinen Tampere University Finland	
Pre-examiners	Docent Šárka Lehtonen University of Eastern Finland Finland	Assistant professor Monica Frega University of Twente Netherlands
Opponent	Professor Ellen Fritsche Heinrich Heine University Düsseldorf Germany	

The originality of this thesis has been checked using the Turnitin OriginalityCheck service.

Cover design: Roihu Inc.

ISBN 978-952-03-1454-5 (print)
ISBN 978-952-03-1455-2 (pdf)
ISSN 2489-9860 (print)
ISSN 2490-0028 (pdf)
http://urn.fi/URN:ISBN:978-952-03-1455-2

PunaMusta Oy – Yliopistopaino
Tampere 2020

"Humor is by far the most significant activity of the human brain."

- Edward de Bono

ACKNOWLEDGEMENTS

The research for this thesis was carried out at the Faculty of Medicine and Health Technology, Tampere University during 2014-2019. I would like to thank all personnel who have advised and helped me over the years.

I wish to express my gratitude to all the financial supporters of this dissertation: the 3DNeuroN project in the European Union's Seventh Framework Programme, Future and Emerging Technologies; the Human Spare Parts Programme, Business Finland; and the Modular platform for epilepsy modeling in vitro (MEMO) project, Academy of Finland. I would also like to thank foundations for personal grants: the Tampere City Science Fund, the Oskar Öflunds Foundation, the Alfred Kordelin Foundation, the Finnish Cultural Foundation and the Graduate Program at the Faculty of Medicine and Health Technology, Tampere University.

I would like to express my sincere gratitude to the leader of Neuro Group, Docent Susanna Narkilahti, for supervising my thesis work. Joining your lab as a trainee really inspired my interest in stem cells and neuroscience. Later during my PhD studies, your support has allowed me to grow as an independent scientist. Thank you for placing your trust in my abilities. I truly feel I have learned a lot from you! I also present my gratefulness for my other supervisor PhD Laura Ylä-Outinen for helping me define the path of my research. You have a talent for seeing the big picture and finding the right words to encourage and advice.

Members of my thesis follow-up group Professor Karin Forsberg Nilsson and Associate Professor Susanna Miettinen are warmly thanked for their scientific expertise and insightful comments during my project. It was always a pleasure to invite you for my annual meetings. You are both inspiring women in science.

I would also like to express my gratitude to Docent Šárka Lehtonen and Assistant Professor Monica Frega for the valuable comments that helped me improve this thesis.

I am grateful for the support of all co-authors that made this research possible; Anssi Pelkonen, Sanna Hagman, Meeri Mäkinen, Marja Peltola, Heini Huhtala, Dmitriy Fayuk, Anu Hyysalo, Emre Kapucu, Laura Aarnos, Andrey Vinogradov, Stephen Eglen, Laura, Ylä-Outinen, Mervi Ristola, Lassi Sukki, Katariina Veijula, Joose Kreutzer, Pasi Kallio.

It is a great pleasure to acknowledge my dear colleagues and friends in the Neuro Group. Hanna Mäkelä, Eija Hannuksela and Juha Heikkilä, your help and expertise in the lab has been priceless and always highly appreciated. Thank you Outi Paloheimo for helping me with your admirable artistic talents and always offering help with the microscopes. Previous PhD students Anu Hyysalo, Tiina Joki and Meeri Mäkinen, you provided amazing peer support during my thesis project. I want to thank you for all the deep conversations, advice and most importantly your friendship over the years. I have also many great memories with the next generation of PhD students Venla Harju, Ropafadzo Mzezewa, Laura Honkamäki and Andrey Vinogradov, and I wish you best of luck for the coming challenges! I want to thank our past and present post docs who have helped me during my thesis work. Dmitriy Fayuk is highly acknowledged for having the time and patience to teach me calcium imaging experiments. Anssi Pelkonen, you were invaluable help and support in the finalization of the first project in the thesis, which at times felt like an endless process. Emre Kapucu is thanked for all input in the second project of the thesis and I hope to continue our fruitful collaboration. Sanna Hagman, I have certainly had the most fun memories of lab work with you. It is amazing how much laughter can be combined with effective working among friends! Mervi Ristola, I am grateful for our friendship and mutual understanding. Your support has been very important and guided me many times.

Last but not least, I want to thank all my friends and family for listening to me and being there for me. I also want to thank my amazing in-laws for always asking how we are holding up, and for your kindness and support. I owe my greatest gratitude to my parents for giving me experiences and opportunities in life but also for expecting a lot from me. Your endless encouragement and believe in me has allowed me to do my thing. Finally, I cannot thank enough my husband, Reeti for the understanding and support we can share. Thank you for making my life easier, happier and better!

Tampere, November 2019

Tanja

ABSTRACT

Our understanding of human brain development and function is still incomplete. Unfortunately, the field of neuroscience lacks representative human-specific models to accompany the animal studies. Access to human brain tissue for research purposes is limited, encouraging the utilization of novel approaches such as human pluripotent stem cell (hPSC)-derived neurons. Within the last few decades, research on hPSCs has undergone enormous expansion. Growing expectations are aimed at the application of stem cells and their derivatives in regenerative medicine, drug screening and disease modeling.

The main focus of this thesis was to evaluate the potential of hPSC-derived neural cultures in mimicking certain characteristics of central nervous system (CNS) development and functionality. The results were intended to help validate the utility of stem cell models for translational neuroscience applications. For this purpose, the differentiation capacities of hPSC-derived neuronal cells generated with two generally used differentiation methodologies were compared. The functional maturation of neurons following a prolonged differentiation time and optimization of culture conditions was assessed in network-level analyses. The results were complemented with a functional comparison to the widely used rodent *in vitro* model. Since astrocytes are the cells surrounding neurons and supporting neuronal functionality in the CNS, special focus was also placed on their role in both normal and neuroinflammatory conditions, the latter of which is typical of CNS insults.

The results of this thesis suggest that hPSC-derived neuronal cultures recapitulate many of the characteristics of CNS development *in vivo*. Specific chemical induction accelerated neural differentiation, leading to high cell purity and yield. Prolongation of the differentiation time increased the proportion of endogenously formed astrocytes and promoted the functionally mature activity type of neurons. Furthermore, the emergence of robust neuronal activity and the long-term maintenance of functional networks were achieved with the selection of defined laminin isoform as a culture substrate. With this improvement, the hPSC-derived networks exhibited time frames and stages of activity development similar to those of their rodent counterparts. However, marked variability was detected in the activity patterns between the rodent and human networks, which could relate to differences

in their maturation stage or interspecies dissimilarities. Finally, hPSC-derived astrocytes were exposed to specific inflammatory stimuli. Their response showed distinct characteristics of astrogliosis observed in CNS diseases, and the studied neuronal effects suggested polarization into a neurosupportive phenotype. Established controlled co-cultures with human neurons and astrocytes provide an alternative hPSC-based platform for modeling cell interactions in the context of health and disease.

In conclusion, the work presented in this thesis advances the development of functional hPSC-derived neuronal networks, confirms the role of astrocytes as significant partners in these networks, and encourages their translation into human-specific models for neuroscience research.

TIIVISTELMÄ

Ymmärryksemme ihmisaivojen kehityksestä ja toiminnasta on edelleen puutteellista. Valitettavasti neurotieteiden alalta puuttuu edustavia ihmisspesifisiä malleja, jotka täydentäisivät eläinmalleilla tehtäviä tutkimuksia. Ihmisaivokudoksen saatavuus tutkimustarkoituksiin on rajoitettua, mikä kannustaa uusien lähestymistapojen, kuten ihmisen monikykyisistä kantasoluista johdettujen hermosolujen hyödyntämistä. Muutaman viime vuosikymmenen aikana ihmisen monikykyisiin kantasoluihin liittyvä tutkimusala on laajentunut valtavasti. Kasvavat odotukset kohdistuvat kantasolujen ja niiden johdannaisten soveltamiseen regeneratiivisessa lääketieteessä, lääkkeiden seulonnassa ja tautien mallinnuksessa.

Tämän tutkimuksen pääpainona oli arvioida ihmisen monikykyisistä kantasoluista johdettujen hermosoluviljelmien potentiaalia jäljitellä tiettyjä keskushermoston kehityksen ja toiminnallisuuden tunnusmerkkejä. Tulosten on tarkoitus auttaa validoimaan kantasolumallien hyödyllisyys soveltavan neurotieteen käyttötarkoituksissa. Tätä varten verrattiin kahdella yleisesti käytetyllä erilaistusmenetelmällä tuotettujen ihmisen monikykyisistä kantasoluista johdettujen hermosolujen erilaistumiskykyä. Hermosolujen toiminnallista kypsymistä arvioitiin sekä pidennetyn erilaistusajan jälkeen, että viljelyolosuhteiden optimoinnin seurauksena verkostotason analyyseillä. Tuloksia täydennettiin vertailemalla näiden verkostojen toiminnallisuutta laajalti käytettyyn jyrsijäperäiseen solumalliin. Koska astrosyytit ovat hermosoluja ympäröiviä soluja ja ne tukevat keskushermoston toiminnallisuutta, erityistä huomiota kiinnitettiin myös astrosyyttien rooliin sekä normaaleissa että tulehduksellisissa olosuhteissa, joista jälkimmäinen on tyypillinen tila keskushermoston vaurioissa.

Tämän väitöskirjan tulokset viittaavat siihen, että ihmisen monikykyisistä kantasoluista johdetut hermosoluviljelmät toistavat useita *in vivo* olosuhteissa tapahtuvia keskushermoston kehityksen vaiheita. Erityinen kemiallinen induktio tehosti hermosoluerilaistusta johtaen korkeaan solupuhtauteen ja saantoon. Erilaistusajan pidennys lisäsi endogeenisesti muodostuvien astrosyyttien osuutta viljelmässä ja edisti hermosolujen toiminnallisuudessa havaittua kypsää aktiivisuustyyppiä. Lisäksi valitsemalla viljelypinnoitteeksi tietty laminiini-isoformi saavutettiin vahva, pitkäkestoinen hermosoluaktiivisuus muodostuneissa

verkostoissa. Tämän kehitystyön ansiosta kantasoluista johdetut hermoverkot osoittivat samankaltaista ajallista ja vaiheittaista toiminnallisuuden kehitystä, kuin vastaavat jyrsijöistä eristetyt hermosolut. Jyrsijä- ja ihmisverkostojen toiminnallisuuden muodoissa havaittiin kuitenkin myös huomattavia eroavaisuuksia, mikä saattaa liittyä eroihin niiden kypsyysasteissa tai lajien välisiin eroavaisuuksiin. Lopuksi ihmisen monikykyisistä kantasoluista johdetut astrosyytit altistettiin tietyille tulehduksellisille tekijöille. Niiden vaste osoitti keskushermoston sairauksissa tyypillisesti havaitun astroglioosin erityispiirteitä, ja tutkitut hermosoluihin kohdistuvat vaikutukset viittasivat polarisaatioon hermosoluja tukevaksi fenotyyppiksi. Tutkimuksessa luodut kontrolloidut ihmisen hermosolujen ja astrosyyttien yhteisviljelmät tarjoavat vaihtoehtoisen kantasolupohjaisen alustan solujen vuorovaikutusten mallintamiseksi sekä terveessä että sairauskonteksteissa.

Yhteenvetona voidaan todeta, että tämän väitöskirjan tulokset edistävät toiminnallisten ihmisen monikykyisistä kantasoluista johdettujen hermosoluverkkojen kehittämistä, ne vahvistavat astrosyyttien roolia merkittävinä kumppaneina näissä verkostoissa sekä rohkaisevat kantasolujen soveltamiseen ihmisspesifisinä malleina neurotieteen tutkimuksissa.

CONTENTS

ABBREVIATIONS

ACM	Astrocyte conditioned medium
AMPA	α-amino-3-hydroxy-5-methyl-4-isoxazolepropionic acid
ASCL1	Achate-schute complex homolog-like 1
ATP	Adenosine triphosphate
Aβ42	Beta-amyloid 42
BDNF	Brain-derived neurotrophic factor
BMP	Bone morphogenic protein
BRN2	Brain-specific homeobox/POU domain protein 2
BSA	Bovine serum albumin
B-TUB	Beta-tubulinIII
cAMP	Cyclic adenosine monophosphate
CCL5	C-C motif chemokine ligand 5
CHI3L1	Chitinase-3 like 1
CMA	Cumulative moving average
CMOS	Complementary metal-oxide-semiconductor
C-MYC	V-Myc avian myelocytomatosis viral oncogene homolog
CNS	Central nervous system
CNTF	Ciliary neurotrophic factor
CorSE	Correlated spectral entropy
CT-1	Cardiotriphin-1
CTIP2	COUP-TF-interacting protein 2
CUX1	Homeobox protein cut-like 1
DAPI	4´6-diamidino-2-phenylindole
DAPT	N-[N-(3,5-difluorophenacetyl)-L-alanyl]-S-phenylglycine t-butyl ester
DKK1	Dickkopf related protein 1
DMEM	Dulbecco's Modified Eagle`s Medium
EAP	Extracellular action potential
EB	Embryoid body
ECM	Extracellular matrix

EEG	Electroencephalography
EGF	Epidermal growth factor
EGO	Early gamma oscillation
ELISA	Enzyme-linked immunosorbent assay
ENO	Early network oscillation
FACS	Fluorescence associated cell sorting
FBS	Fetal bovine serum
FGF	Fibroblast growth factor
FOXG1	Forkhead box G1
GABA	Gamma-aminobutyric acid
GAD67	Glutamic acid decarboxylase 67
GAPDH	Glyceraldehyde 3-phosphate dehydrogenase
GBX2	Gastrulation brain homeobox 2
GDNF	Glial cell line-derived neurotrophic factor
GDP	Giant depolarizing potential
GFAP	Glial fibrillary acidic protein
GSK	Glycogen synthase kinase 3
GUSB	Beta-glucuronidase
hESC	Human embryonic stem cell
hiPSC	Human induced pluripotent stem cell
hPSC	Human pluripotent stem cell
IBI	Inter-burst interval
IFN	Interferon
IGF	Insulin-like growth factor
IL-6	Interleukin-6
iN	Induced neuronal cell
IP3	Inositol trisphosphate
ISI	Inter-spike interval
KCC2	Potassium chloride cotransporter 2
KI67	Ki-67 protein
KLF4	Kruppel-like factor 4
LCN2	Lipocalin 2
LFP	Local field potential
LIF	Leukemia inhibitory factor
LMX1A	LIM homeobox transcription factor 1 alpha
LN	Laminin

LPS	Lipopolysaccharide
MAP2	Microtubule-associated protein 2
MCS	Multichannel Systems
MEA	Microelectrode array
mLN	Mouse laminin
MYT1L	Myelin transcription factor 1-like
NEUROD1	Neurogenic differentiation factor 1
NFIA	Nuclear factor 1A
NF-κB	Nuclear factor kappa-light-chain-enhancer of activated B cells
NGN1	Neurogenin 1
NKCC1	Sodium-potassium-chloride cotransporter 1
NMDA	N-methyl-D-aspartate
NPC	Neural progenitor cell
OCT3/4	Octamer-binding transcription factor 3/4
OPN	Osteopontin
OTX2	Orthodenticle homeobox 2
PAX6	Paired box 6
PBS	Phosphate-buffered saline
PCA	Principal component analysis
PDL	Poly-D-lysine
PEI	Polyethyleneimine
PNS	Peripheral nervous system
PO	Poly-L-ornithine
Poly(I:C)	Polyinosinic-polycytidylic acid
PTX3	Pentraxin-3
PSD-95	Postsynaptic density protein 95
qRT-PCR	Quantitative real time polymerase chain reaction
RA	Retinoic acid
RT-PCR	Reverse transcription-polymerase chain reaction
S100β	S100 calcium binding protein B
SATB2	Special AT-rich sequence-binding protein 2
SATs	Spontaneous activity transients
SHH	Sonic hedgehog
SOX2	SRY (sex determining region Y)-box 2
SPA	Synchronous plateau assemblies
STTC	Spike time tiling coefficient

SVZ	Subventricular zone
SWTTEO	Stationary wavelet transform-based Teager energy operator
SYN	Synaptophysin
TBR1	T-box brain 1
TGF-β	Transforming growth factor-β
vCAM	Vascular cell adhesion molecule-1
VGLUT1	Vesicular glutamate transporter 1
VIM	Vimentin
VZ	Ventricular zone
WNT	Wingless- related integration site

ORIGINAL PUBLICATIONS

This thesis is based on three original publications listed below. The publications are referred to in the text by Roman numerals (**I**-**III**).

I **Paavilainen T***, Pelkonen A*, Mäkinen ME, Peltola M, Huhtala H, Fayuk D, Narkilahti S. Effect of prolonged differentiation on functional maturation of human pluripotent stem cell-derived neuronal cultures. Stem Cell Research. 2018. 27:151-61. doi: 10.1016/j.scr.2018.01.018.

II **Hyvärinen T**, Hyysalo A, Kapucu FE, Aarnos L, Vinogradov A, Eglen SJ, Ylä-Outinen L, Narkilahti S. Functional characterization of human pluripotent stem cell-derived cortical networks differentiated on laminin-521 substrate: comparison to rat cortical cultures. Scientific Reports. 2019. 9(1):17125. doi:10.1038/s41598-019-53647-8.

III **Hyvärinen T***, Hagman S*, Ristola M, Sukki L, Veijula K, Kreutzer J, Kallio P, Narkilahti S. Co-stimulation with IL-1β and TNF-α induces an inflammatory reactive astrocyte phenotype with neurosupportive characteristics in a human pluripotent stem cell model system. Scientific Reports. 2019. 9(1):16944. doi:10.1038/s41598-019-53414-9.

* Authors contributed equally.

1 INTRODUCTION

Derivation of human embryonic stem cells (hESCs) and the later discovery of human induced pluripotent stem cells (hiPSCs) hold promise for the establishment of human-specific models in the field of neuroscience (Paşca, 2018; Takahashi et al., 2007; Thomson et al., 1998). Collectively, these two cell types are termed human pluripotent stem cells (hPSCs) due to their capacity for self-renewal and differentiation into all cell types of the body, including those in the central nervous system (CNS) (Avior et al., 2016; Zirra et al., 2016). Regenerative medicine was among the first application targets for stem cells, and development of stem cell therapies to replace lost neurons in neurodegenerative diseases provides hope for the patients (Parmar, 2018; Steinbeck and Studer, 2015). Stem cell-derived neurons also offer novel tools for basic and translational research, including human neurodevelopmental biology and toxicity studies (Hofrichter et al., 2017; Kirwan et al., 2015). hiPSCs maintain the genetic background of the patient thus presenting opportunities for modeling genetic disorders and opening avenues for personalized medicine and drug discovery (Avior et al., 2016; Chung et al., 2013). Use of human-specific cells may help to translate results from animals to humans, for example in the case of drug testing. However, the stem cell field still requires development of methodologies and system validation.

Since the first reports on hPSC-derived neuronal cultures, numerous differentiation protocols have been introduced (Lancaster et al., 2013; Mertens et al., 2016; Shi, Yichen et al., 2012; Zhang, S-C et al., 2001b; Zhang, Yingsha et al., 2013). The protocols try to mimic the general principles learned from developmental neurobiology, for example the timed exposure to growth factors and morphogens guiding neural fate (Suzuki and Vanderhaeghen, 2015). Over the years, the methods for neuronal differentiation have advanced, leading to the acquisition of more homogenous populations of neuronal cells that closely represent their *in vivo* equivalents and contain lower number of undesired cell types (Floruta et al., 2017; Kirkeby et al., 2012). Culture media with defined chemical compositions have been refined to direct neuronal cell fate, support maturation and decrease experimental variation (Bardy et al., 2015; Chambers et al., 2009; Gunhanlar et al., 2018). The

extracellular matrix (ECM) components used as culture substrates provide additional signals influencing neuronal differentiation and maturation, but these have not been studied as extensively (Hagbard et al., 2018).

The structural development of the CNS is largely intertwined with functional development (Luhmann et al., 2016). The functional activity of neurons arises well before the postnatal period and is closely linked to the developmental migration, differentiation and apoptosis of neurons (Golbs et al., 2011; Luhmann and Khazipov, 2018). Aberrant neuronal function underlies neurodevelopmental disorders as well as neurodegenerative diseases in adults (Ebert and Greenberg, 2013; Pievani et al., 2014). Therefore, the functionality of the generated neurons has always been a major focus of research in the stem cell field. Unfortunately, functional maturation is not obtained with many of the available neuronal differentiation protocols. Also, improving the functional maturation of hPSC-derived neurons that currently best represent the midgestational fetal stage is an important step towards creating more representative models (Livesey et al., 2016; Weick, 2016).

Astrocytes, the major glial cell type of the CNS, play a pivotal role in the promotion of neuronal synaptogenesis and functional maturation (Clarke and Barres, 2013; Verkhratsky and Nedergaard, 2018). Astrocyte support has been considered a requisite for the development of functional activity in hPSC-derived neuronal cultures (Johnson et al., 2007; Odawara et al., 2014). Interestingly, astrocytes also have a very distinct response to and role in pathological conditions. Upon CNS injury or disease, they undergo dramatic phenotypic changes, termed astrocyte reactivation (Ben Haim et al., 2015). Astrocytes alter their morphological appearance and modulate many of their homeostatic and metabolic functions (Sofroniew and Vinters, 2010). The resulting effects on neuronal cells can be either beneficial or detrimental depending on the cellular milieu, which brings another dimension of complexity to the mechanisms of pathological conditions (Liddelow, S. A. et al., 2017; Zamanian et al., 2012). hPSC-derived models provide an alternative, human-specific system for better understanding neuron-astrocyte interactions (Oksanen et al., 2017; Park et al., 2018; Santos et al., 2017).

The focus of this thesis was to study the potential of hPSC-derived neuronal cells as human-specific models for neuroscience. This research shows ability of hPSC-derived neuronal cells to form mature functional networks, which is essential for hPSC model utility in different applications. Additionally, the role of astrocytes in the neuronal networks during normal and inflammatory environments was presented. Results consolidate the utility of hPSC-derived neural platforms for future studies involving both healthy and detrimental conditions.

2 LITERATURE REVIEW

2.1 Central nervous system

The central nervous system (CNS) comprises the brain and the spinal cord, which receives, processes and transfers information from all parts of the body by interfacing with the peripheral nervous system (PNS) (Stiles and Jernigan, 2010). Anatomically, the CNS can be roughly divided into the forebrain, midbrain, hindbrain, and spinal cord. At the macroscopic scale, the superficial part of the brain contains the cortex, wherein most neuronal cell somas are situated in a layered structure. This is also referred to as the gray matter. The more internal white matter contains axons extending from neuronal cell somas that form tracks between brain regions. The brain stem also contains several nuclei, wherein neuronal cell bodies are concentrated, and relays information to and from the cortex (Stiles and Jernigan, 2010). At the microscopic scale, the main cell types of the CNS include neurons and supporting glial cells, that is, astrocytes, oligodendrocytes and microglia. Neurons receive and transfer information in the form of electrical activity (Budday et al., 2015). Neurons typically have one longer projection called an axon, which transfers the information to a recipient cell. Multiple shorter branching projections, called dendrites, are responsible for collecting signals arising from the surrounding cells and transferring them to the neuronal soma (Budday et al., 2015; Stiles and Jernigan, 2010). Connections serving as points of information transfer are called synapses and are generally formed between a presynaptic axon and a postsynaptic dendrite (Stiles and Jernigan, 2010). Astrocytes maintain the homeostatic balance and provide metabolic and structural support for neurons (Verkhratsky and Nedergaard, 2018). They also take charge of the enormous energy demand caused by the electrical signaling of neurons. In past decades, research has focused on the role of astrocytes in synaptogenesis, the maintenance of healthy synaptic communication and the regulation of synaptic transmission (Verkhratsky and Nedergaard, 2018). Astrocyte-specific functions are discussed in more detail in chapter 2.5. Oligodendrocytes are the myelinating glial cells, and their main task is to insulate neuronal axons with myelin sheaths, thereby facilitating and accelerating information transfer (Stadelmann et al., 2019). The brain also includes microglial cells, which are the

nervous system derivative of macrophages participating in immune surveillance and clearance of metabolites (Ginhoux et al., 2010).

2.1.1 Development of the central nervous system

Nervous system development begins with the multipotent ectodermal cells of the gastrula-stage embryo (Zirra et al., 2016). The developmental process of neurulation begins as the neuroepithelial cells start forming the neural groove along the midline of the neural plate (Figure 1A) (Stiles and Jernigan, 2010). As the groove further folds into the neural tube, the neuroepithelial cells transition to radial glial cells, which undergo asymmetric cell division to produce neurons or intermediate cells, including intermediate progenitors and basal radial glia. The differentiated cell types migrate outward from the apicobasally oriented radial glia and ultimately generate neurons and glial cells (Kelava and Lancaster, 2016). Later, as a result of neural patterning, these cells form various brain regions, including the forebrain, midbrain and hindbrain. The spinal cord forms from the lower part of the neural tube, whereas the PNS originates from the tissue above the neural tube, which is called the neural crest (Zirra et al., 2016).

The molecular signals leading to neural induction from the ectoderm involve suppression of the bone morphogenic protein (BMP) and Nodal pathways (Mertens et al., 2016; Suzuki and Vanderhaeghen, 2015; Zirra et al., 2016). In addition to this so-called default pathway, fibroblast growth factor (FGF) and wingless (Wnt) signaling have been shown to mediate neural induction (Martynoga et al., 2012; Muñoz-Sanjuán and Brivanlou, 2002). Following neural induction, the different anatomical brain domains start to specify along the rostrocaudal and dorsoventral axes (Suzuki and Vanderhaeghen, 2015). Gradients of different morphogens from several organizing centers control the regional specification of the future forebrain, midbrain, hindbrain and spinal cord. The "default" pathway results in rostral phenotypes, while caudalization can be induced by retinoic acid (RA), Wnts or FGFs (Figure 1B). Specification in the dorsoventral axis is controlled by BMP, Wnt and Sonic hedgehog (Shh) signaling. This intricate regional patterning of neural progenitor cells enables the later formation of a large diversity of neurons and glial cells (Suzuki and Vanderhaeghen, 2015; Tao and Zhang, 2016).

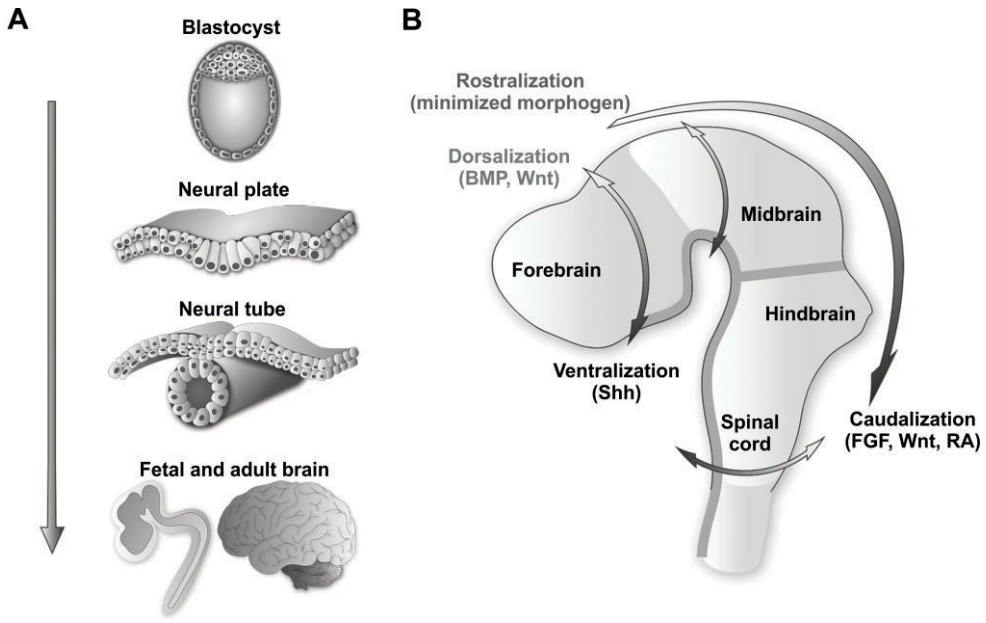

Figure 1. Neural development of the central nervous system. (A) Neural induction through the process of neurulation leading to the fetal brain and eventually to the adult brain. (B) Signaling cues involved in dorsoventral and rostrocaudal regional patterning of the CNS. Abbreviations: BMP, bone morphogenetic protein; Wnt, Wingless-related integration site; Shh, sonic hedgehog; FGF, fibroblast growth factor; RA, retinoic acid. Image is modified from Mertens et al. 2016 and Suzuki and Vanderhaeghen 2015.

Temporal development, during which neurons are generated first followed by glia, has been widely conserved across different species. In rodents, this switch from neurogenesis to astrogenesis occurs at late embryonic stages (approximately E18), and the development of astrocytes peaks postnatally (Miller and Gauthier, 2007). In humans, astrocytes appear at midgestation and develop in fetal and postnatal periods (Semple et al., 2013). Astrocytes are initially generated from the radial glia in the ventricular zone (VZ) and subventricular zone (SVZ) and are later developed by the division of local astrocytes (Jiang and Nardelli, 2016). The switch from neurogenesis to gliogenesis is controlled by several intrinsic signaling cues and requires both the inhibition of neurogenic factors and the induction of gliogenic factors (Okano and Temple, 2009). For example, neurogenin 1 (Ngn1) attenuates gliogenesis, while the proglial genes nuclear factors 1A and 1B (NFIA/B) initiate the formation of glial cells. In addition, a series of epigenetic changes, including histone modifications and DNA demethylation, enables the transcription of glial-specific genes upon stimulation (Okano and Temple, 2009). The IL-6 family members ciliary

neurotrophic factor (CNTF), leukemia inhibitor factor (LIF) and cardiotriphin-1 (CT-1) have been recognized as secreted signals promoting astrogenesis (Sloan and Barres, 2014). Additionally, the BMP and Notch signaling molecules play a role in inducing the development of astrocytes (Sloan and Barres, 2014).

2.1.2 Corticogenesis

The cerebral cortex is a complex structure consisting of six layers in which layer-specific neurons are produced in a sequential order. In rodents, neurogenesis begins on approximately E9.5 and continues through the first two postnatal weeks (Semple et al., 2013). In humans, neurogenesis occurs mainly during gestation. It is initiated at approximately 5 gestational weeks and completed by 28 weeks (Meyer et al., 2000). Corticogenesis begins in the VZ and proceeds to form a neighboring proliferative area termed the SVZ (Figure 2). In these regions, the cortical progenitors are generated in a temporal inside-out manner, meaning that the early-born deep-layer neurons are produced first, followed by late-born superficial-layer neurons (Kelava and Lancaster, 2016). The newly born neurons in the cerebral cortex are guided by radial glia to migrate basally to their particular cortical locations. The cortical plate starts to form all the different cortical layers as late-born neurons migrate past the pre-existing early-born neurons (Molyneaux et al., 2007). The different cortical layer-specific neurons have their own characteristic patterns of gene expression and connectivity, which result from temporal patterning (Toma and Hanashima, 2015). Deep-layer neurons, at layers V and VI, typically express transcription factors such as Tbr1 and Ctip2 and extend mostly to subcortical targets. Upper-layer neurons, layers II-IV, express the transcription factors Brn1/2, Cux1/2 and Satb2, form intracortical connections and promote thalamocortical communication (Toma and Hanashima, 2015). Most neurons generated in the dorsal forebrain are excitatory neurons. Cortical inhibitory interneurons are mostly formed ventrally, after which they tangentially migrate to the cortical plate (Kelava and Lancaster, 2016; Letinic et al., 2002; Yu, X. and Zecevic, 2011).

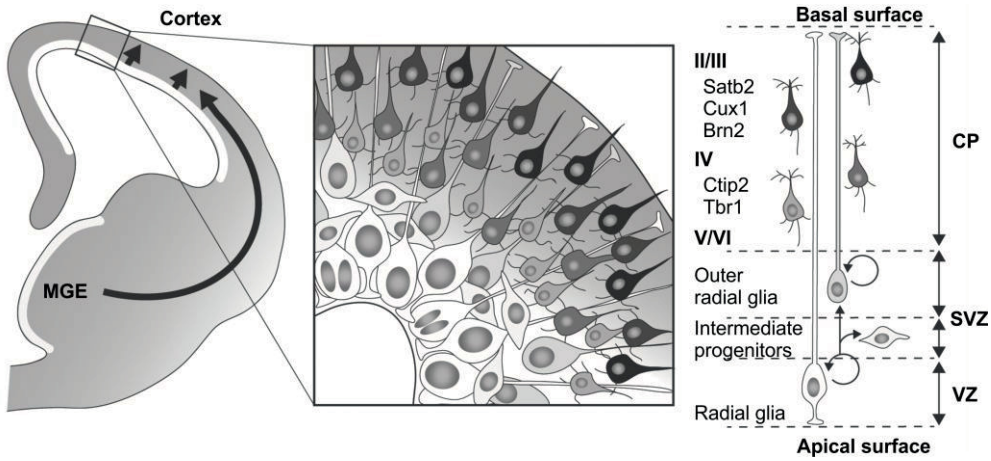

Figure 2. Cortical neurogenesis. Cortical excitatory neurons are produced at the dorsal part of the cortex, whereas interneurons are generated ventrally at the medial ganglionic eminence, from where they migrate dorsally and integrate into the excitatory neuronal network. The cortical plate forms in an inside-out manner from the progenitor pool in the ventricular and subventricular zones. Abbreviations: MGE, medial ganglionic eminence; VZ, ventricular zone; SVZ, subventricular zone; CP, cortical plate; Satb2, Special AT-rich sequence-binding protein 2; Cux1, Homeobox protein cut-like 1; Brn2, Brain-specific homeobox/POU domain protein 2; Ctip2, COUP-TF-interacting protein 2; Tbr1, T-box brain 1. Image is modified from Andersson and Vanderhaegen 2014 and Suzuki and Vanderhaeghen 2015.

2.1.3 Human-specific features of neural development

The development of the human CNS has long attracted the interest of researchers, and despite experimental challenges, studies have confirmed that many aspects of development follow the same principles as those observed in animal models (Kelava and Lancaster, 2016). However, some of the features differ, and many of these differences give rise to the improved cognitive abilities of humans (Sherwood et al., 2006). Humans have the largest brain size in relation to their body size, and the neuron density in humans is several times higher than that in the rodent brain (Herculano-Houzel, 2014; Kelava and Lancaster, 2016). In particular, the surface and thickness of the neocortex have been considerably enlarged throughout hominid evolution, resulting in increased cell numbers and diversity of cortical neurons (Suzuki and Vanderhaeghen, 2015).

Another distinct feature of human brain development is its prolonged cell division, amplification of progenitor cells and generation of neurons (Kelava and Lancaster, 2016). In the developing cortex, the neurogenic zones and their

progenitor pools are vastly more elaborate than their rodent counterparts (Lancaster et al., 2013). Similarly, axonal growth, dendritic spine maturation and synaptogenesis last for an extended time. Human neurons also exhibit prolonged electrophysiological maturation and variation in the neurotransmitter system (Semple et al., 2013). In human systems, full maturation of neurons can take months or even years (Figure 3) (Suzuki and Vanderhaeghen, 2015).

Astrocytic complexity in the human brain is distinctive and has increased throughout primate evolution with respect to both the morphology and density of astrocytes (Oberheim et al., 2006; Oberheim et al., 2009; Sherwood et al., 2006). Furthermore, transcriptional comparison between human and mouse astrocytes has revealed that only 30% of human astrocyte-enriched genes are found in mice astrocytes (Zhang, Ye et al., 2016). In the cerebral cortex, the neuron-glial cell ratio has increased from 0.4 in rodents to an estimated 1.4 in humans (Oberheim Bush and Nedergaard, 2017). Human astrocytes are on average 3 times larger, contain 10 times more processes, and present faster calcium waves than rodent astrocytes (Oberheim et al., 2009). At the same time, through this development, human astrocytes are expected to be capable of contacting and controlling ~2 million

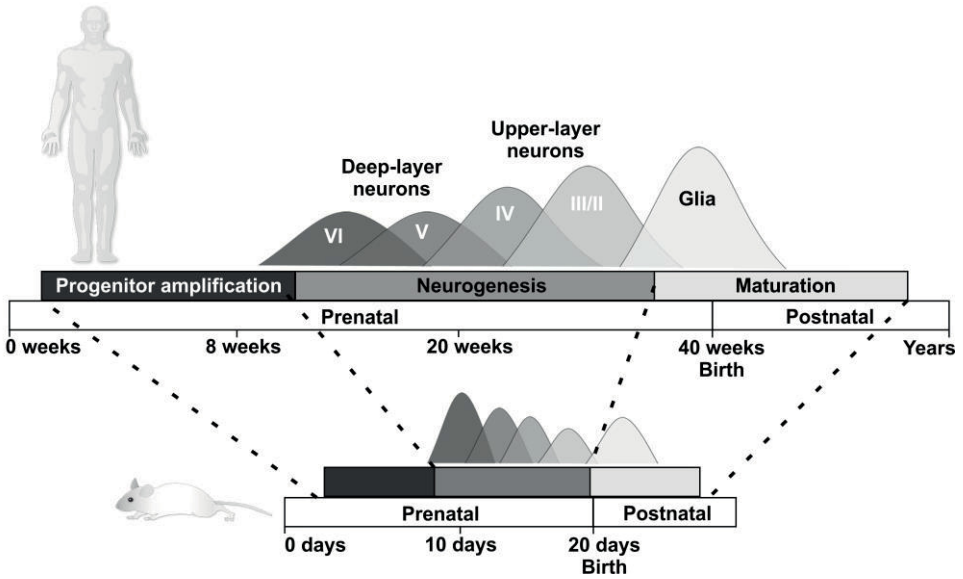

Figure 3. Timeline for cortical development in humans and rodents. Human development is characterized by extended progenitor cell amplification, neurogenesis and maturation. The sequential generation of cortical layer-specific neurons followed by gliogenesis is shown. Image is modified from Andersson and Vanderhaegen 2014.

synapses, while in rodents, the estimate is only 0.1 million synapses (Oberheim et al., 2006). In addition to the two main classes of astrocytes, the protoplasmic gray matter and fibrous white matter astrocytes, primates also possess additional astrocyte subtypes. Interlaminar and polarized astrocytes are found only in primates (Oberheim et al., 2006).

2.2 Stem cells

Stem cells are undifferentiated cells that have the ability to become specific cells of various tissue types depending on their differentiation capacity and environmental conditions. They are usually characterized by their ability to divide either unlimitedly, such as pluripotent embryonic stem cells, or with certain limitations, such as adult tissue-specific stem cells (Zakrzewski et al., 2019). Stem cells with these differing capacities originate mainly from two sources: embryos and adult tissues (Thomson et al., 1998; Zakrzewski et al., 2019). Stem cells can also be derived from fully differentiated adult cells via genetic reprogramming technologies (Takahashi et al., 2007). In adult tissues, stem cells can be found, for example, in the brain, blood, bone marrow, skin and skeletal muscles, and they reside in specific locations called the stem cell niche (Zakrzewski et al., 2019). In the brain, a small population of radial glia remains in specific regions in the subventricular zone of the lateral ventricles and the dentate gyrus of the hippocampus (Martynoga et al., 2012). Next, human pluripotent stem cells and their neural derivatives are described in more detail.

2.2.1 Human pluripotent stem cells

Human pluripotent stem cells (hPSCs) are defined by their unlimited capacity to divide and produce cells of all three germ layers: the endoderm, mesoderm and ectoderm (Zirra et al., 2016). hPSCs include human embryonic stem cells (hESCs) derived from the inner cell mass of blastocyst-stage embryos and human induced pluripotent stem cells (hiPSCs) genetically reprogrammed from adult somatic cells (Takahashi et al., 2007; Thomson et al., 1998). The derivation of hESC lines is highly regulated, and in Finland, couples undergoing *in vitro* fertilization treatments can donate surplus, poor-quality embryos for research use (Skottman, 2010). The hiPSCs are often preferred because they do not raise ethical concerns as severe as research utilizing embryos (Shi, Yanhong et al., 2017). Derivation of pluripotent cells from

human somatic cells using reprogramming methods was first described in 2007 by Yamanaka and colleagues (Takahashi et al., 2007). In short, somatic cells were introduced with four pluripotency-inducing transcription factors, called the "Yamanaka factors". The original research included retroviral transfection with the transcription factors octamer-binding transcription factor 3/4 (OCT3/4), SRY-box 2 (SOX2), Kruppel-like factor 4 (KLF4) and V-Myc avian myelocytomatosis viral oncogene homolog (C-MYC) (Takahashi et al., 2007). Since then, other combinations of transcription factors and other viral or nonviral means of transporting or expressing specific factors have been experimented successfully (Shi, Yanhong et al., 2017; Yu, J. et al., 2007). Despite their different origins, hESCs and hiPSCs are generally considered to resemble each other and to have similar surface marker expression, self-renewal abilities and capacities to differentiate into mature cell types (Avior et al., 2016). However, there are known differences; for example, persistence of the former epigenetic memory of somatic cells has been observed in hiPSCs. Both hESCs and hiPSCs are considerably promising for use in regenerative medicine and drug development, and hiPSCs derived from human patient-specific cells are a major target for modeling human disorders due to the genetic background of the donor (Avior et al., 2016; Steinbeck and Studer, 2015).

2.2.2 Neuronal differentiation

The neurodevelopmental events discovered *in vivo* can be mimicked to achieve neuronal differentiation *in vitro*. For example, timed applications of different environmental cues, such as mitogens and morphogens, can be used to generate neurons showing a high level of brain regional specificity (Suzuki and Vanderhaeghen, 2015). The very first reports on neuronal differentiation from hESCs date back to the early 21st century (Reubinoff et al., 2000; Reubinoff et al., 2001; Zhang, S-C et al., 2001a). Neural induction was established using the three-dimensional (3D) embryoid body (EB) method, which resulted in the formation of neural rosette structures resembling early neural tube development (Zhang, S-C et al., 2001a). When these EBs were plated in adherent cultures, the neural rosettes could be further mechanically or enzymatically isolated to enrich the neuronal population. Neural conversion could also be induced in the presence of FGF2-containing media, and these cultures could be continuously maintained, passaged and enriched in 3D; thus, they were commonly termed neurospheres (Lappalainen et al., 2010; Nat et al., 2007).

An important advance in the field of *in vitro* neuronal differentiation was the development of the so-called dual SMAD inhibition method (Chambers et al., 2009). Neural induction is achieved in more controlled conditions using combined inhibition of the BMP pathway and the Noggin and Activin/Transforming growth factor-β (TGF-β) pathway with SB431542. This protocol enabled the differentiation of homogenous neural cultures in fully adherent conditions without the need for rosette isolation. The principle of dual SMAD inhibition has been used in various differentiation methods, including adherent cultures, neurospheres and, most recently, brain organoid cultures (Pasca et al., 2015; Shi, Y. et al., 2012).

Three-dimensional cultures beneficially allow neural cells to acquire a more elaborate morphology and form a cytoarchitecture that better recapitulates brain complexity (Lehmann et al., 2019). Within the last few years, cerebral organoids have become increasingly popular to research because neural cells can self-assemble into large tissues with defined brain regions within organoids (Lancaster et al., 2013). Organoid culture starts with the same principles as the EB protocol, but the cells are usually encapsulated in a Matrigel matrix droplet. Organoids are cultured and expanded for an extended time in a spinning bioreactor to ensure efficient nutrient exchange. The development of organoids can be established in the absence of external cues or alternatively directed with timed exposure to morphogens (Amin and Paşca, 2018; Lancaster et al., 2013). Depending on the culture conditions and maturation time, the organoids can grow over several millimeters in diameter and contain multiple brain regions with variable populations of progenitor cells and mature neural cell types, including neurons, astrocytes and oligodendrocytes (Madhavan et al., 2018; Pasca et al., 2015).

Following technological advances in hiPSC reprogramming, approaches involving the direct conversion of fibroblasts or hPSCs into induced neuronal (iN) cells have become more common (Mertens et al., 2016; Zhang, Yingsha et al., 2013). Genetic reprogramming by viral delivery of specific transcription factors generally results in highly homogenous neuronal populations in a short period of time. Direct conversion from fibroblasts also has the advantage of better preserving the aging-specific signatures of the cells (Mertens et al., 2016). However, the conversion efficiency of somatic cells is still not as good as the neuronal reprogramming of hiPSCs (Zhang, Yingsha et al., 2013). Direct conversion from mouse fibroblasts was originally established by introducing three transcription factors (BAM factors): Brn2, Ascl1 and Myt1L (Mertens et al., 2016). In human cells, a fourth transcription factor, NeuroD1, or specific microRNAs are required (Wapinski et al., 2013). On the other hand, neurogenin 2 (Ngn2) has also been shown to efficiently convert adult human

fibroblasts into iN cells (Zhang, Yingsha et al., 2013). This approach is also most commonly used for the generation of iN cells from hiPSCs. The specification of different neuronal subtypes upon direct conversion can be further influenced by the simultaneous application of extrinsic cues, morphogens or small molecules, as was elegantly shown by Liu and colleagues (Liu et al., 2013).

The production of regional- or neurotransmitter-specific neurons is usually an important goal in all of these neuronal differentiation approaches (Suzuki and Vanderhaeghen, 2015). Regional patterning of hPSC-derived neural progenitor cells (NPCs) follows the same principles as those previously described for *in vivo* neural development (Figure 1B). Without specific morphogens, hPSCs differentiate into a dorsal forebrain phenotype and generate mostly neurons with glutamatergic properties (Espuny-Camacho et al., 2013; Shi, Y. et al., 2012). The dorsal forebrain identity of NPCs can be maintained with dual SMAD inhibition and simultaneous blockage of the Wnt pathway with molecules such as Dickkopf-related protein1 (DKK1) (Mariani et al., 2012). More ventrally derived inhibitory neurons can be generated with the introduction of Shh (Floruta et al., 2017; Maroof et al., 2013). Patterning along the rostrocaudal axis has been established with the dose-dependent activation of Wnt signaling using glycogen synthase kinase 3 (GSK3) inhibitors, including CHIR99021 (CHIR) (Suzuki and Vanderhaeghen, 2015). Together with Shh and FGF8 signaling, this establishment leads to midbrain dopaminergic phenotypes (Kirkeby et al., 2012). Increasing activation WNT signaling will result in posterior hindbrain phenotypes (Kirkeby et al., 2012). Furthermore, the posterior hindbrain cerebellar and spinal cord motor neuron identities are obtained with concomitant manipulation of RA and FGFs (Suzuki and Vanderhaeghen, 2015; Zirra et al., 2016).

Within the past two decades, substantial progress has been made regarding the differentiation of hPSC-derived neuronal cultures. Many protocols follow common principles inspired by *in vivo* development. Temporal development *in vitro* also presents prolonged neurogenesis, similar to that observed in humans.

2.2.3 Astrocyte differentiation

Astrogenesis follows neurogenesis, but the signaling mechanisms important for astrocyte specification and heterogeneity are not as well established (Jiang and Nardelli, 2016). Traditional neuronal differentiation methods based on chemical cues typically produce a certain proportion of astrocytes, especially after extended culture

times (Lappalainen et al., 2010). The first report on directed astrocyte differentiation from hPSCs was published in 2011 by Krencik and colleagues (Krencik, R. et al., 2011). They used the EB method to induce neural fate, continued culturing neurospheres in medium containing FGF and epidermal growth factor (EGF) for several weeks, and matured the differentiated astrocytes in the presence of LIF, ciliary neurotrophic factor (CNTF) or fetal bovine serum (FBS). Interestingly, they were also able to show regional specification of astrocytes along the rostrocaudal and dorsoventral axes using RA, Shh and FGF8, similar to what has been established with neurons (Krencik, R. et al., 2011). Since then, most efforts to generate pure populations of astrocytes rely on the expansion of glial progenitors after the neurogenic stage established either with the EB method or the dual SMAD inhibition protocol (Tao and Zhang, 2016; Tcw et al., 2017). These glial progenitors can be further regionally specified with RA or Shh and differentiated into mature astrocytes in the presence of different combinations of growth factors, such as CNTF, BMP, brain-derived neurotrophic factor (BDNF), glial cell line-derived neurotrophic factor (GDNF) and insulin-like growth factor (IGF) (Lundin et al., 2018; Roybon et al., 2013; Serio et al., 2013; Shaltouki et al., 2013; Tcw et al., 2017). More recently, genetic approaches have also been introduced to achieve efficient and fast astrocyte differentiation. Expression of the transcription factors Sox9 and NFIB or NFIA results in the rapid conversion of astrocytes from pluripotent stem cells (Canals et al., 2018; Li et al., 2018).

In general, the astrocyte differentiation protocols utilizing chemical induction are lengthy, potentially taking up to six months. Astrocyte characterization is also lacking, and identifying the different astrocyte subtypes is currently challenging due to a shortage of suitable markers (Krencik, Robert and Ullian, 2013).

2.3 Functional development of the brain

Functional activity depends on membrane potential, which is established during development by the distribution of ions across the plasma membrane owing to the expression of specific ion channels and pumps (Bean, 2007). In mature neurons, the resting membrane potential is approximately -65 mV. The information transfer between neurons is carried by an action potential, which occurs as changes in neuron membrane potential cross a threshold (Bean, 2007). The opening of plasma membrane voltage-gated ion channels quickly depolarizes the neuron, and action potential is propagated along the axon all the way to the presynaptic boutons

(Radivojevic et al., 2017). The two major types of synapses include electrical synapses that arise in the early stages of functional development and chemical synapses that are formed later (Luhmann and Khazipov, 2018). In the latter, synaptic vesicles containing neurotransmitters are released into the synaptic cleft as a result of action potential arrival. Neurotransmitters can have either excitatory or inhibitory effects when binding to their specific receptors on the postsynaptic site, resulting in either depolarization or hyperpolarization of the postsynaptic neuron (Bean, 2007; Luhmann and Khazipov, 2018; Radivojevic et al., 2017).

2.3.1 Stages of activity development

Spontaneous activity arises early in various regions of the developing CNS and is developed largely through similar sequences of events in both rodents and humans (Kilb et al., 2011; Luhmann and Khazipov, 2018). Activity development follows a temporal sequence of patterns that is similarly reproduced in most CNS regions, such as the cortex, spinal cord, cerebellum and hippocampus (Luhmann and Khazipov, 2018). Additionally, the mechanisms that shape the various patterns of activity are surprisingly similar between these regions. These include electrical coupling, excitatory effects of γ-aminobutyric acid (GABA), pacemaker-like hub neurons and synaptic and extrasynaptic effects of neurotransmitters (Blankenship and Feller, 2010; Kilb et al., 2011). In the cortex, the earliest born neurons present more mature functional properties than those born later and may act as hub neurons during development (Luhmann et al., 2016). In addition, inputs are received from the subcortical areas, including the thalamus, which helps drive the activity (Luhmann et al., 2016). The development of spontaneous activity in the mouse cortex can be described in four distinct sequences to illustrate the general stages and mechanisms involved (Figure 4).

The initial form of activity is asynchronous firing consisting of sparse spikes originating from single neurons. Calcium has a central role in the early activity before the appearance of voltage-gated sodium and potassium channels and the generation of sodium-dependent action potentials (Corlew et al., 2004). With further development, the glutamatergic and GABAergic neurons in the cortex start firing their first action potentials (Egorov and Draguhn, 2013). However, during these early stages, the neurons are not yet functionally connected to electrical or chemical synapses (Luhmann and Khazipov, 2018).

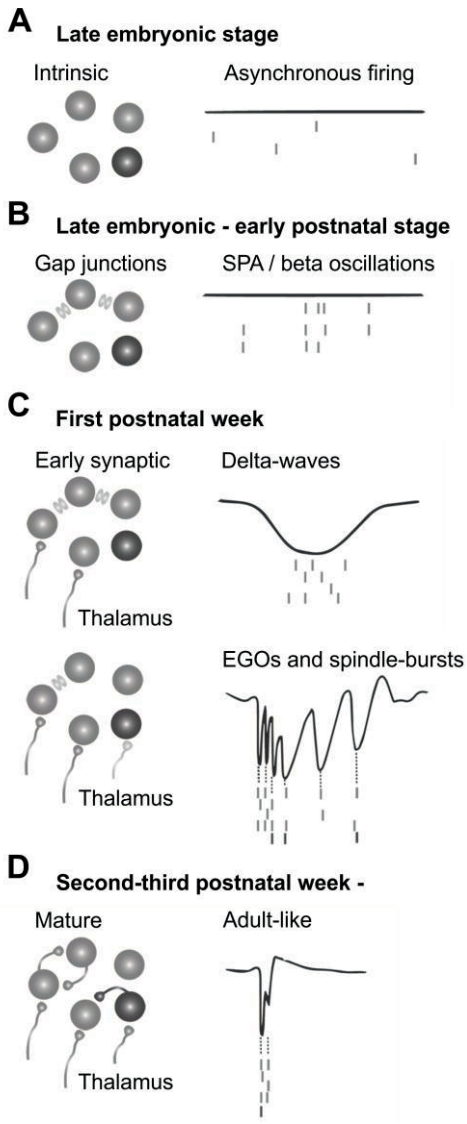

Figure 4. Development of functional activity in the cortex. Four distinct stages can be recognized in the functional development of the cortex. (A) The initial sign of functional activity is uncorrelated single-cell firing. (B) The first form of correlated firing is mediated by gap junction-coupled electrical synapses. (C) Chemical synapses are formed between glutamatergic (light gray) neurons, and most electrical synapses are ultimately removed. Eventually, inhibitory GABAergic neurons (dark gray) are involved in bursting, and the activity also includes thalamic inputs. (D) In the final stages, the adult type of activity is achieved. Abbreviations: SPA, synchronous plateau assemblies; EGO, early gamma oscillations. Image is modified from Luhmann and Khazipov, 2018.

Next, the first correlated activity emerges, which relies mostly on electrical synapses formed by connexin-containing gap junctions between adjacent neurons (Dupont et al., 2006; Uhlén et al., 2015). Gap junctional coupling allows the spread of calcium transients between cells contributing to synchronic activity, but these events are still local, extending only short distances (Egorov and Draguhn, 2013). Several different activity patterns relying on electrical synapses and calcium ions between groups of cells are reported; examples include the synchronous plateau assemblies (SPAs, 0.001 Hz) and beta-oscillations (Allène et al., 2008; Dupont et al., 2006). These activity patterns take place during the late embryonic and early postnatal periods in mice (Egorov and Draguhn, 2013).

In the third stage, electrical synapses, which serve as templates for the development of chemical synapses, are mostly removed as the formation of chemical synapses between glutamatergic neurons begins (Luhmann and Khazipov, 2018). One immature pattern of activity is the slow delta waves, which arise during postnatal development and extend over larger areas of the networks involving many neurons (Luhmann and Khazipov, 2018). While delta waves involve the subcortical thalamic inputs and can therefore be observed only in *vivo*, comparable activity patterns termed early network oscillations (ENOs, frequency ~0.01 Hz) dependent on corticocortical connections are also reproduced in preparations *in vitro* (Garaschuk et al., 2000). Delta waves may or may not contain additional oscillatory components, such as early gamma oscillations (EGOs, 30-50 Hz) and spindle bursts (5-25 Hz) (Luhmann and Khazipov, 2018). Both EGOs and spindle bursts are transient activity patterns during development, and they cease in rodents after approximately the first postnatal week. They initially involve only glutamatergic input, but with further development, they also show temporal increase in GABAergic currents (Luhmann and Khazipov, 2018).

The giant depolarizing potentials (GDPs, ~0.1 Hz) observed in the hippocampus and cortex after the first postnatal week require GABA-dependent connections and are coordinated by GABAergic hub neurons (Blankenship and Feller, 2010; Egorov and Draguhn, 2013). It is important to note that GABA actions are initially excitatory due to the high intracellular chloride concentration in neurons (Ben-Ari et al., 2007). This excitation is eventually switched to inhibition as chloride transporter expression is altered, resulting in changes in the chloride balance and the hyperpolarizing effect of GABA (Ben-Ari et al., 2007).

Finally, the adult type of activity is formed after three to four postnatal weeks and is strongly modified by input from the sensory systems, including vision and hearing, and by motor activity (Egorov and Draguhn, 2013). In adult animals, cortical activity

is described by adult type-specific response discharges, which are superimposed by a continuous background of network oscillations. These processes depend on both excitatory and inhibitory signaling and can be very complex, propagating assemblies of signals (Egorov and Draguhn, 2013).

In the cortices of human preterm babies, spontaneous bursting is known as spontaneous activity transients (SATs) (Arichi et al., 2017). The most well-described activity patterns are delta brushes, which are equivalent to spindle bursts in rodents (Arichi et al., 2017; Khazipov and Luhmann, 2006). Although the exact neuroanatomical source of activity in humans has not been described in detail, delta brushes play an important role in the structural and functional development of the cortex (Arichi et al., 2017; Tolonen et al., 2007). Electroencephalography (EEG) recordings of infants have indicated that a high incidence of delta brushes is linked to normal mental development (Iyer et al., 2015).

2.3.2 Functions of early activity

It is not always acknowledged that electrical activity affects embryonic and postnatal developmental processes as much as genetic programs (Luhmann et al., 2016). It is important for the generation of neurons, cell death, migration, differentiation and formation of networks (Kilb et al., 2011). Calcium activity in the ventricular zone directly affects neurogenesis and progenitor cell proliferation (Luhmann et al., 2015). Early asynchronous activity also has a trophic effect and guides the migration of neurons (Egorov and Draguhn, 2013). Trophic factors further affect dendritic branching in neurons via an activity-dependent mechanism, and electrical activity plays an important role in axonal arborization, supporting neuronal maturation (Kilb et al., 2011). The programmed cell death mechanism, apoptosis is partly controlled by network activity, and disturbances or silencing of activity during development can have drastic effects on the normal apoptosis rate and elevate neuronal cell death rates (Golbs et al., 2011). Waves of activity have been linked to the generation of specific cortical architectures. They can also elicit activity-dependent potentiation of connections, following to some extent the "cells that fire together wire together" principle (Luhmann and Khazipov, 2018).

2.4 Neuronal functionality *in vitro*

2.4.1 Measurements of functional activity *in vitro*

Neuronal activity *in vitro* is traditionally measured from acute or organotypic slices of brain tissue or from dissociated cell cultures. Brain slices maintain the cytoarchitecture of the brain, although some tissue damage and cell death occur as a result of the slice preparation procedure. Dissociated cultures can re-establish axonal networks and recapitulate some activity patterns observed in *vivo* despite the loss or the original structural tissue complexity (Pasquale et al., 2008). The activity of neurons can be measured at many levels, starting from microscale recordings using the patch clamp method, via which single cells are poked with very sharp patch pipettes, and the ionic currents across the membrane and voltage changes are measured (Petersen, 2017). Network-level electrical activity events of several neurons can be evaluated with optical methods, such as fluorescent calcium imaging (Grienberger and Konnerth, 2012). Additionally, extracellular recordings of the activity of a group of neurons can be achieved simultaneously with microelectrode array (MEA) measurements (Obien et al., 2014). In addition to conventional pharmacological and electrical neuronal stimulation, novel selective stimulation approaches have been reported. A technique called optogenetics, in which genetically encoded light-sensitive ion channels or pumps are activated by light, has become an increasingly popular tool (Klapper et al., 2017). Next, the methods for measuring network functionality *in vitro* utilized in this thesis, calcium imaging and MEA measurements, are described in more detail.

2.4.1.1 Calcium imaging

Calcium is a very important second messenger involved in the regulation of many cellular processes (Grienberger and Konnerth, 2012; Gu et al., 1994). Calcium influx can originate from two sources, via specific channels on the plasma membrane or via release from internal stores, mostly from the endoplasmic reticulum; however, mitochondria are also involved in calcium homeostasis (Grienberger and Konnerth, 2012). Calcium imaging has been established as a reliable tool for studying functional activity at the network level (Forostyak et al., 2013; Gu et al., 1994; Kerr et al., 2005).

During action potentials, the depolarization of a neuron opens voltage-gated ion channels, including voltage-gated calcium channels, which results in calcium transients (Grienberger and Konnerth, 2012). These calcium transients can be imaged utilizing specialized dyes, fluorescent calcium indicators that bind to calcium (Bootman et al., 2013). The resulting image series of several neurons experiencing transient calcium concentration increases depict the functional activity of neurons. The benefit of calcium imaging is its single-cell resolution in a network of cells; however, the temporal resolution is poor owing to the slow kinetics of calcium transients compared to action potential currents (seconds vs. milliseconds) (Kerr et al., 2005).

2.4.1.2 Microelectrode array measurements

MEAs represent a technique for recording neuronal activity at the network level with very high (millisecond) temporal resolution. The array of microelectrodes measures changes in the extracellular field resulting from the activity of neuronal cells cultured on top of embedded electrodes (Obien et al., 2014). The method is thus noninvasive and can be used to follow the development of networks over several weeks of culture (Charlesworth et al., 2015; Ito et al., 2014). The trade-off of MEAs is spatial resolution. Neuronal activity results from the transmembrane current, which can be detected by electrodes even across tens to hundreds of micrometer distances (Egert et al., 2002). Therefore, the resulting recorded electric field depends on the number of active neurons and on the magnitude and distance of the signal from the recording electrode (Obien et al., 2014). The single-unit activity, which is known as the extracellular action potential (EAP), or spike, results from the rapid intracellular influx of Na^+ ions followed by efflux of K^+ ions, producing extracellularly recorded signals characteristic of negative spikes and small positive increases thereafter (Buzsáki et al., 2012). Usually, the recorded signal consists of the multiunit activity of several neurons firing action potentials in close vicinity to the electrodes (Obien et al., 2014). MEAs can also detect local field potentials (LFPs) arising from the activity of a very large population of neurons, which presents a low-frequency band signal (less than 300 Hz) and is usually filtered out from the analysis (Einevoll et al., 2013). Several different MEA device types are on the market, from single-well MEAs to multiwell plate format MEAs enabling more high-throughput analyses. An interesting upcoming technology is CMOS-based high-density MEAs, which contain an array of thousands of electrodes, improving the special resolution of the measurements (Obien et al., 2014).

2.4.2 Functionality of hPSC-derived neuronal cultures

Neuronal activity and functional circuits are the key elements that underlie the information processing required for complex behavior and cognitive properties. hPSC-derived neurons provide a unique human-specific model for studying network function during development, in disease and during pharmacological exposure (Hartlaub et al., 2019). Many CNS disorders present abnormalities in the channels and synapses affecting normal synaptic signaling of neurons. The functional maturity level of hPSC-derived neurons has been a common topic of research since the neural identity must closely match that of the *in vivo* counterparts to reliably model pathological processes.

2.4.2.1 Functional properties of hPSC-derived neurons

Ion channel composition affects the membrane properties driving the functionality of neurons, and therefore membrane properties were among the first functional traits of hPSC-derived neurons to be studied (Johnson et al., 2007). Single-cell patch clamp studies have repeatedly shown that the passive membrane properties of hPSC-derived neurons resemble those of the late embryonic stages in rodents and those of the mid to late gestational stages in humans with some maturation after extended culture times (Johnson et al., 2007; Weick, 2016). The active membrane properties directly linked to action potential generation have also been shown to be partially underdeveloped, resulting in immature spiking patterns (Chinchalongporn et al., 2015; Gunhanlar et al., 2018; Johnson et al., 2007).

As mentioned in previous chapters, hPSC-derived neurons differentiate by default into forebrain glutamatergic subtypes with varying proportions of GABAergic neurons (Suzuki and Vanderhaeghen, 2015). Glutamatergic excitatory neurotransmission is a major driver of cortical type activity through N-methyl-D-aspartate (NMDA) and α-amino-3-hydroxy-5-methyl-4-isoxazolepropionic acid (AMPA) receptors (Livesey et al., 2016). Both immature and mature receptor subtype compositions have been characterized in hPSC-derived neurons and shown to exhibit the expected maturation over time (Kirwan et al., 2015; Livesey et al., 2014). Reports have even shown that hPSC-derived networks can support NMDA-dependent synaptic plasticity, suggestive of functional maturation (Kirwan et al., 2015).

The GABAergic system is a very important local controller of excitatory networks. Studies on hPSC-derived excitatory networks revealed $GABA_A$ receptor-

mediated currents, but pharmacological dissection demonstrated immature receptor composition (James et al., 2014; Livesey et al., 2014). In time, GABAergic neurons also demonstrate spiking pattern maturation and increased sensitivity to GABAergic antagonists (Nicholas et al., 2013; Weick, 2016). During early development, GABA binding to the $GABA_A$ receptor exerts an excitatory depolarizing effect due to the high intracellular chloride concentration (Ben-Ari, 2002). The chloride concentration decreases during development as a shift occurs in the expression of the chloride transporters NKCC1 and KCC2 (Ben-Ari, 2002). Similar development has been observed in the maturation of hPSC-derived networks (Livesey et al., 2014).

The network level activity of hPSC-derived neurons is scantily described in the literature (Table 1), partly because achieving robust network activity has been difficult with the current culture methods. The first stem cell studies reporting network activity with MEAs were performed with mouse ESC-derived cultures (Illes et al., 2007), and hESC-derived neuron reports followed shortly thereafter (Heikkilä et al., 2009). In both reports, the network activity developed from sparse spiking to more pronounced spike trains and, finally, to mature bursting phenotypes (Heikkilä et al., 2009; Illes et al., 2007). More recently, elaborate network level analyses have been performed with calcium imaging (Kirwan et al., 2015; Mäkinen et al., 2018) and MEA setups (Frega et al., 2017; Izsak et al., 2019; Mäkinen et al., 2018; Odawara et al., 2016; Trujillo et al., 2019). These networks have demonstrated sensitivity to common glutamatergic and GABAergic receptor blockers (Heikkilä et al., 2009; Odawara et al., 2016). However, many other MEA studies still show very low bursting activity and localization of synchronic activity to clustered areas instead of wider participation of the network.

Table 1. Network activity in hPSC-derived neuronal cultures.

Study	Culture methods	Method	Main findings
Frega et al. 2018	Ngn2 expression, for maturation +rat cortical astrocytes, +NT-3, BDNF, FBS	MEA	Excitatory glutamatergic networks. Spike rate increased between 16 to 23 days after induction, reaching ~2.5 Hz. At day 23, the network burst rate was ~4 burst/min.
Izsak et al. 2018	Adherent dual SMAD inhibition, maturation in BrainPhys, +BDNF, GDNF, NT-3, FGF8, TGF-β, DAPT, AA	MEA	Cortical glutamatergic and GABAergic neurons. Network bursts arose during 2-3 wks on MEA, 10-20 burst/min after days 20-37 on MEA. Super network bursts could contain several bursts with a duration of ~1-1.5 sec, and an IBI of ~20 sec existed between super network bursts. Inhibitory GABAergic input.
Kirwan et al. 2015	Adherent dual SMAD inhibition	CA	Cortical excitatory glutamatergic neurons. Synchronized calcium oscillations arose by 8 wks after induction. Peak of ~10 bursts/min at 10 wks. After 14 wks, synchronicity decreased and was replaced by complex patterns of activity. Variation in timing of bursting. No inhibitory input.
Kuijlaars et al. 2016	Adherent dual SMAD inhibition, for maturation ±DAPT, ±human fetal astrocytes, +cAMP, BDNF, GDNF	CA	Cortical glutamatergic and GABAergic neurons. Network bursts arose during 3-4 wks on MEA at a rate of ~3 bursts/min. In the presence of both DAPT and human astrocytes, the percentages of active neurons, bursting and synchronicity were increased. Co-culture with rat but not human astrocytes improved activity. GABAergic inhibition was present at later time points.
Odawara et al. 2014	Commercial hiPSC-neurons (CDI, iCell), +rat ACM or rat astrocytes	MEA	Spike rate was increased by the humoral effect and co-culture with rat astrocytes.
Odawara et al. 2016	Commercial cortical hiPSC-neurons (Axol Bioscience), +rat astrocytes	MEA	Cortical glutamatergic and GABAergic neurons. Occasional synchronous burst firing at 10-13 wks on MEA, increasing frequency towards 30 wks. After 30 wks, the network burst rate was ~6 burst/min. GABAergic input was evident at both time points.

Study	Culture methods	Method	Main findings
Odawara et al. 2018	Commercial cortical hiPSC-neurons (XCell Science), maturation in BrainPhys, +LN511, ±hiPSC-astrocytes (XCell Science)	MEA	Cortical glutamatergic and GABAergic neurons. Higher spike rate with astrocyte co-culture. Network bursting arising after 6 wks with neurons only and after 5 wks with astrocyte co-culture. A $GABA_AR$ antagonist increased the network burst rate.
Trujillo et al. 2019	Organoid dual SMAD inhibition, for maturation +BDNF, GDNF, NT-3, AA, cAMP	MEA	Cortical glutamatergic and GABAergic neurons. Network bursts arising after 2 months on MEA. A network bursting rate of 0.05 Hz (every 20 sec) developed into super network bursts containing two bursts from 4-6 months. Glutamatergic and GABAergic signaling.
Tukker et al. 2018	(Co-)cultures of commercial 90% glutamatergic neurons (CDI, iCell Glutaneurons), 30%/70% glutamatergic/GABAergic neurons (iCell neurons), maturation in BrainPhys, ±hiPSC-astrocytes (iCell)	MEA	Addition of inhibitory neurons or astrocytes had limited effect on the spike rate, but astrocyte co-culture increased the percentage of active wells and the burst rate. After 3 wks of co-culture with astrocytes, synchronous network bursts developed at a rate of 3 bursts/min. In cultures with inhibitory neurons and astrocytes, a $GABA_AR$ antagonist increased the burst rate.

Ngn2, neurogenin 2; NT-3, neurotrophin-3; BDNF, brain-derived neurotrophic factor; FBS, fetal bovine serum; MEA, microelectrode array; GDNF, glial cell line-derived neurotrophic factor; FGF, fibroblast growth factor; TGF-β, transforming growth factor-β; DAPT, N-[N-(3,5-difluorophenacetyl)-L-alanyl]-S-phenylglycine t-butyl ester; AA, ascorbic acid; GABA, γ-aminobutyric acid; IBI, interburst interval; CA, calcium imaging; cAMP, cyclic adenosine monophosphate; ACM, astrocyte-conditioned medium; LN511, laminin-511.

2.4.2.2 Improving the functional maturation of hPSC-derived neurons

Enhancement of the functional maturation of hPSC-derived neurons and optimization of culture conditions to support electrical activity has been important for the generation of representative *in vitro* models. hPSC-derived neuronal cultures have been shown to undergo spontaneous maturation in time (Weick, 2016). Additionally, specialized culture media have been developed with the idea of improving electrical activity and allowing long-term maintenance of functional hPSC-derived neurons (Bardy et al., 2015). These media are chemically defined, and with appropriate supplements, it is suggested that they better match the *in vivo* environment. In the optimized medium, the concentration of inorganic salts was adjusted closer to the physiological range, and the amount of neuroactive amino acids was decreased. Additionally, the energy levels, mainly glucose, and osmolarity, were adjusted to mimic more native brain conditions. The culture medium was demonstrated to mediate its effect via strengthening silent synapses and may therefore indirectly enhance neuronal maturation (Bardy et al., 2015).

Selective supplements are regularly used with basal media to improve long-term survival, neurite outgrowth and synaptogenesis. The most commonly used supplements include the N2 and B27 commercial products in place of serum (Bardy et al., 2015). In addition, several neurotrophic and other factors are used, such as BDNF, GDNF, cyclic adenosine monophosphate (cAMP), RA, ascorbic acid (AA), the γ-secretase inhibitor N-[N-(3,5-difluorophenacetyl)-L-alanyl]-S-phenylglycine t-butyl ester (DAPT) and laminin (Bardy et al., 2015; Borghese et al., 2010; Gunhanlar et al., 2018; Shi, Y. et al., 2012). The selection of factors should always be performed with caution because these can have very specific effects on the functional development of neurons (Lepski et al., 2013; Livesey et al., 2014).

The effect of the extracellular matrix (ECM) on the development of hPSC-derived neuronal cultures has not been addressed often in the literature, although the ECM is known to mediate important signals regulating cellular effects (Long and Huttner, 2019; Zhang, Dawei et al., 2017). Laminins are heterotrimeric ECM glycoproteins, and the different laminin isoforms contain varying combinations of three subunits: alpha, beta and gamma chains (Domogatskaya et al., 2012). In particular, the animal-derived basement membrane extracts Matrigel and mouse laminin, which contains mostly laminin-111 (α1, β1, γ1), are often used as culture substrates in neuronal differentiation (Hagbard et al., 2018). However, improved survival and functional maturation has been demonstrated on laminin alpha5 chain substrates (Hyysalo et al., 2017; Odawara et al., 2018; Zhang, Dawei et al., 2017).

These defined human recombinant ECM proteins are also more attractive options than animal-derived components that suffer from batch-to-batch variation (Kirkeby et al., 2017; Niclis et al., 2017).

Glial cells, astrocytes, have also been shown to play a critical role in supporting neuronal maturation and functionality, specifically by inducing synaptogenesis. Rodent astrocytes are succesfully used as feeder layers for hPSC-derived neurons in functional studies (Johnson et al., 2007; Odawara et al., 2014), but results obtained with hPSC-derived astrocyte co-cultures are still variable (Klapper et al., 2019; Kuijlaars et al., 2016; Lischka et al., 2018; Odawara et al., 2018). In addition, the role of endogenously generated astrocytes in hPSC-derived neuronal cultures is scantily described (Izsak et al., 2019; Lappalainen et al., 2010). Astrocyte functions are next discussed in more detail.

2.5 Astrocytes

Astrocytes are the most numerous cell type in the CNS and have aroused increasing research interest in recent decades thanks to new findings regarding their functions. Astrocytes were first believed to serve only as structural support and substance between neurons, giving rise to the historical neuroglia name "nerve glue" (Kettenmann and Verkhratsky, 2008). Astrocytes are a heterogeneous population of cells that possess distinct properties in different areas of the CNS. They also have a very different role in disease states, termed astrocyte reactivation (Sofroniew and Vinters, 2010)

2.5.1 Physiological functions of astrocytes

The morphological complexity and locations of numerous astrocyte processes enables them to actively monitor and regulate their microenvironment. Astrocytes regulate brain homeostasis via the extracellular buffering of water, ion and pH levels (Allaman et al., 2011). They can control local cerebral blood flow based on the activity and energy demand of neurons and participate in the maintenance of blood-brain barrier integrity (Marina et al., 2018; Takano et al., 2006). One key function of astrocytes is to provide structural support for neurons and synthesize extracellular matrix proteins and adhesion molecules (Sofroniew and Vinters, 2010). They also take part in the sustainment of neuronal activity by releasing energy substrates and

trophic factors (Clarke and Barres, 2013). Close positioning with synapses also protects neurons from excitotoxic insults via the recycling of neurotransmitters from the synaptic cleft (Allen, 2014). The gap junctional coupling between astrocytes allows the formation of functional networks and the spreading of second messengers such as calcium and inositol trisphosphate (IP3) and metabolic products, glucose and adenosine trisphosphate (ATP) (Sofroniew and Vinters, 2010). Thus, astrocytes have a major role in maintaining the homeostatic and metabolic balance in the CNS.

2.5.2 Astrocyte-neuron communication

Astrocytes have a central role in the control of synapse formation and function (Baldwin and Eroglu, 2017; Clarke and Barres, 2013; Craig et al., 2006). Several synaptogenic astrocyte-secreted factors have been identified that contribute to the initial synapse formation, transformation of silent synapses into active ones and pruning of unnecessary synapses (Clarke and Barres, 2013). These secreted molecules include thrombospondins and glypicans (Allen et al., 2012; Christopherson et al., 2005). Astrocytes are in tight contact with synapses, particularly the postsynaptic dendritic spines, and have contact-mediated effects on synapse development and stabilization (Clarke and Barres, 2013).

Astrocytes have their own communication system that is based on calcium transients (Cornell-Bell et al., 1990). Calcium can spread within a network of gap junction-coupled astrocytes, but local calcium increases in the soma and processes of astrocytes are also detected, and functions of these local calcium transients are only beginning to be understood (Volterra et al., 2014). Astrocytes also express receptors for a variety of neurotransmitters and other signaling molecules, allowing them to communicate and respond to environmental cues. At least half of the synaptic connections in the CNS are estimated to contain an enshrouding astrocyte (Verkhratsky and Nedergaard, 2018). These observations have led to hypotheses and debate about the direct role of astrocytes in regulating synaptic transmission in the so-called tripartite synapse (Araque, A. et al., 1999; Araque, Alfonso et al., 2014; Nedergaard and Verkhratsky, 2012). In this paradigm, the activation of astrocytes by neurotransmitters induces calcium transients and the release of neuroactive molecules called gliotransmitters (such as ATP, glutamate and D-serine), further regulating synaptic transmission and plasticity (Araque, Alfonso et al., 2014). Considering the intricate communication and cooperation between neurons and

astrocytes, it is not difficult to comprehend the problems arising from the loss of normal functions in disease states.

2.5.3 Astrocyte reactivation

Following CNS injury or disease, astrocytes undergo transformation into a reactive state that is characterized by altered gene expression and morphological and functional changes that may depend on the severity of the insult (Ben Haim et al., 2015; Blanco-Suárez et al., 2017; Dossi et al., 2018). Different environmental stimuli, such as infection, CNS trauma, systemic inflammation, and chronic neurodegeneration, can elicit astrogliosis (Sofroniew and Vinters, 2010). These stimuli are mediated by a variety of molecular triggers, such as inflammatory cytokines, microbial antigens, myelin debris, aggregated proteins typical for neurodegenerative diseases and hypoxic conditions present during stroke (Pekny et al., 2019; Ponath et al., 2018; Sofroniew and Vinters, 2010). Reactivation is often accompanied by infiltration of immune cells and interaction with microglia, increasing the complexity of the subsequent events (Sommer et al., 2019; Yun et al., 2018).

Astrocyte heterogeneity is also evident in their reactive state, as both neuroprotective and neurotoxic phenotypes have been reported (Anderson, M. A. et al., 2016; Rodríguez-Arellano et al., 2016). Reactivation can lead to excess proliferation, astrocyte scar formation and inhibition of axonal growth (Sofroniew and Vinters, 2010). Astrocytes can secrete cytokines and chemokines that further increase the inflammatory reaction and release excitotoxic levels of glutamate, nitric oxide or other toxic molecules compromising neuronal survival (Sofroniew and Vinters, 2010). On the other hand, astrocytes may limit inflammation and tissue damage and facilitate regeneration (Colombo and Farina, 2016). In fact, an elegant study has demonstrated that distinct astrocyte phenotypes result from different environmental stimuli. Treatment of mice with bacterial lipopolysaccharide led to a harmful reactive astrocyte phenotype, while ischemic insult by middle cerebral artery occlusion resulted in a more beneficial state (Zamanian et al., 2012). These two phenotypes were named neurotoxic A1 and neuroprotective A2 astrocytes, although there is still speculation about several other unidentified reactive astrocyte phenotypes (Liddelow, Shane A. and Barres, 2017).

Astrocyte reactivation has been reproduced *in vitro*. Liddelow and colleagues provided evidence that the neurotoxic A1 astrocyte phenotype can be replicated *in*

vitro by combinatorial treatment with IL-1α, TNF-α and complement component C1q (Liddelow, S. A. et al., 2017). Many other studies have also experimented with a variety of cytokines and inflammatory factors to create representative *in vitro* models for reactive astrocytes (Hamby et al., 2012; Perriot et al., 2018; Ronco et al., 2014). To better understand human astrocytes and disease, fetal-derived astrocytes and glioma cell lines have been utilized (Hoffmann et al., 2015; van Scheppingen et al., 2018; Zhang, Ye et al., 2016). More recently, an increasing number of papers on hPSC-derived reactive astrocytes have been published (Lundin et al., 2018; Perriot et al., 2018; Roybon et al., 2013; Tcw et al., 2017), and the first reports combined other cell types, such as neurons, microglia and leukocytes, to better understand their interplay in disease (Park et al., 2018; Santos et al., 2017; Sommer et al., 2019). Table 2 lists some of the key publications in which hPSC-derived astrocyte reactivation has been explored.

Table 2. Reactivation of hPSC-derived astrocytes.

Study	Stimulation	Reactive astrocyte characterization	Neuron-specific effects
Lundin et al. 2018	IL-1β (10, 50 ng/ml) or TNF-α (10, 50 ng/ml), for 24 h or 48 h	Time- and dose-dependent IL-6 and IL-8 secretion.	NA
Perriot et al. 2018	IL-1β (10 ng/ml) and/or TNF-α (10 ng/ml) or IL-6 (100 ng/ml), for 5 days	As single stimulation TNF-α induced the most significant transcriptomic chances. All stimulants resulted in differing secretion profiles of pro- and anti-inflammatory factors. Co-stimulation with TNF-α and IL-1β led to a further shift in the transcriptomic profile and had a synergistic effect on secretion.	NA
Ponath et al. 2018	TNF-α (50 ng/ml), IL-1β (10 ng/ml) and IFNγ (100 U/ml), for 10 min, 16 h or 48 h	Induction of NF-κB signaling by TNF-α and IL-1β stimulation. Impaired glutamate uptake and lactate release by all three stimulants.	NA
Roybon et al. 2013	IL-1β (10 ng/ml) or TNF-α (50 ng/ml), for 7 days	Upregulation of IL-8, CCL5, and Lcn2 and secretion of IL-6. IL-1β increased and TNF-α decreased GFAP-positive cell portion.	NA
Santos et al. 2017	IL-1β (10 ng/ml) or TNF-α (50 ng/ml), for 5 h or 24 h	Larger portion of cells secreted IL-6 and IL-8 with IL-1β stimulation than with TNF-α stimulation. IL-1β elicited transcriptomic changes related to inflammation.	48 h of co-culture with IL-1β-treated astrocytes reduced neuron survival and dendritic length.
Tcw et al. 2018	poly(I:C) (50, 100 ng/ml) or LPS (10, 50 μg/ml) or Aβ42 (5, 10 μM), for 24 h	Response to inflammatory stimulation with dose-dependent IL-6 secretion. Aβ42 induced secretion of a wide range of inflammatory molecules.	NA

IL, interleukin; TNF, tumor necrosis factor; IFN, interferon; NF-κB, nuclear factor kappa-light-chain-enhancer of activated B cells; CCL5, C-C motif chemokine ligand 5; Lcn2, lipocalin 2; Poly(I:C), polyinosinic-polycytidylic acid; LPS, lipopolysaccharide; Aβ42, β-amyloid 42.

2.6 Applications of stem cell-derived neuronal networks

In addition to therapeutic applications in regenerative medicine, hPSC-derived neuronal networks are considered potential human models in many translational stem cell applications (Yap et al., 2015). hPSC-derived models have allowed researchers to show that similar mechanisms in neural development are conserved through the evolution of humans and rodents (Suzuki and Vanderhaeghen, 2015). Some of the major species-specific differences have also been confirmed with these models, such as the prolonged progenitor amplification of hominid species (Eiraku and Sasai, 2012; Shi, Yichen et al., 2012).

hiPSCs can be derived from the somatic cells of patients suffering from genetic disorders and differentiated into a specific neuronal cell types to study diseased cell phenotypes and mechanisms *in vitro* (Avior et al., 2016; Sandoe and Eggan, 2013). hPSC-derived neurons represent the fetal stage of development and are thus best suited for modeling neurodevelopmental disorders (Deneault et al., 2018; Frega et al., 2019; Russo et al., 2018). Additionally, many neurodegenerative diseases with typically late onset have been studied (García-León et al., 2018; Kouroupi et al., 2017; Mehta et al., 2018). Despite great discoveries in neuroscience, the development of therapeutic molecules in the treatment of neurological disorders has not been successful (Cummings, 2018). Many drugs have been shown to be effective in preclinical animal studies but still fail in clinical trials. The reasoning behind this could point to interspecies differences or the fact that animal models do not properly represent human diseases (Cummings, 2018; Pankevich et al., 2014). hPSC-derived neuronal cells can also be utilized for screening new, prospective drugs as an alternative to animal models (Elitt et al., 2018; Lee et al., 2012).

We are constantly exposed to numerous chemicals, and there is enormous pressure to perform chemical safety tests, including neurotoxicological assessments using animal studies, which are laborious, costly, and ethically problematic (Yap et al., 2015). The application of hPSC-derived neuronal models for developmental neurotoxicology is advantageous and may reveal interspecies differences regarding the effects of different chemicals (Baumann et al., 2016; Ylä-Outinen et al., 2010).

Understanding the potential and recognizing the limitations of stem cells and their derivatives is of high importance, as it will improve the utility of hPSC-derived networks as human-specific model systems.

3 AIMS OF THE STUDY

The aim of this thesis was to evaluate the potential of hPSC-derived neuronal cells for studying the development and maturation of functional networks. Special focus was placed on the role of astrocytes in healthy and detrimental conditions. The specific aims of the studies are as follows:

1. To compare the differentiation of hPSC-derived neuronal cultures with neurosphere and adherent methods (Studies **I** and **II**).

2. To improve the functional maturation of hPSC-derived neurons through prolonged differentiation time and selection of defined culture substrate (Studies **I** and **II**).

3. To compare the activity development of hPSC-derived neurons and rat cortical cultures, and distinguish their specific activity feature profiles (Study **II**).

4. To study astrocyte reactivation and astrocyte-neuron interactions using the hPSC-based platform (Study **III**).

4 MATERIALS AND METHODS

4.1 Cell culture

4.1.1 Ethical issues

The National Authority for Medicolegal Affairs Finland approved research with human embryos (Dnro 1426/32/300/05). The Pirkanmaa Hospital District ethics committee provided supportive statements for the derivation, culture and expansion of hESC (R05116) and hiPSC lines (R08070) for research purposes.

A local authority approved the animal license (ELLA-Animal Experiment Board of Regional State Administrative Agency for Southern Finland, ESAVI/10300/04.10.07/2016). Rat cortical cultures were prepared according to the institutional guidelines of the University of Helsinki (license number KEK17-016).

4.1.2 hPSC culture

The hESC and hiPSC lines used in this study and their specific information are listed in Table 3. The hPSCs were cultured on top of the human feeder cell layer (CRL 2429, ATTC, Manassas, VA, USA) in Dulbecco's Modified Eagle's Medium (DMEM) containing 20% KnockOut serum replacement (both from Gibco, Thermo Fisher Scientific, Waltham, MA, USA) as described previously (Rajala et al., 2007). For Studies **II** and **III**, before differentiation, the hPSCs were transferred and expanded in feeder-free conditions on plates coated with the human recombinant laminin isoform LN521 (BioLamina, Sundbyberg, Sweden) and with Essential 8 Flex medium according to previously published method (Hongisto et al., 2017).

The pluripotency of the hPSC lines was confirmed regularly with immunocytochemical staining, and the differentiation capacity was confirmed using an embryoid body formation assay. All cultures maintained a normal karyotype and were mycoplasma free.

Table 3. The hPSC lines used in this thesis.

hPSC line	Type	Gender	Method	Publication	Study
Regea 08/023	hESC	male	NA	(Skottman, 2010)	I, II, III
04311.WTs	hiPSC	female	Sendai virus	(Ojala et al., 2016; Paavilainen et al., 2018)	I
10212.EURCCs	hiPSC	female	Sendai virus	(Kiamehr et al., 2019)	II, III
IMR90-4*	hiPSC	female	retrovirus	(Yu, J. et al., 2007)	II

*Commercial cell line from WiCell, Madison, Wisconsin, USA

4.1.3 Neurosphere differentiation

Neurosphere differentiation was performed according to Lappalainen et al. (2010) to obtain a mixed population of neurons and astrocytes (Study **I**). Briefly, hPSC colonies were mechanically removed and transferred onto ultra-low-attachment plates for formation of embryoid bodies and differentiation of neurospheres. The neural differentiation medium consisted of 1:1 DMEM/F-12 and Neurobasal, 1× B27, 1× N2, 2 mM Glutamax (all from Gibco, Thermo Fisher Scientific), 25 U/ml penicillin/streptomycin (Lonza Group Ltd., Bazel, Switzerland) and 20 ng/ml FGF2 (R&D Systems Inc., Minneapolis, MN, USA). The medium was refreshed every two to three days, and neurospheres were mechanically passaged once a week. Cultured cells were maintained for 8 or 15 wks, mechanically cut into small aggregates 50-200 μm in diameter (Ø) containing 5,000-10,000 cells, and plated in adherent culture for up to 5 wks. Plastic plates were coated with 10 μg/ml mouse laminin, and MEA plates were coated with 0.05% polyethyleneimine (PEI) and 20 μg/ml mouse laminin (both from Sigma-Aldrich, St. Louis, MO, USA). After the final plating, FGF2 was omitted to promote differentiation, and after one week, 4 ng/ml FGF2 (R&D Systems Inc.) and 5 ng/ml BDNF (ProSpec-Tany TechnoGene Ltd., Rehovot, Israel) were added to support maturation.

4.1.4 Adherent neuronal differentiation

Adherent differentiation of mixed neuron and astrocyte culture was performed according to Shi et al. (2012) with some modifications (Studies **II** and **III**). First, a single-cell suspension of hPSCs was established enzymatically with Tryple Select (Gibco, Thermo Fisher Scientific), and cells were plated at a density of 5×10^5

cells/cm^2 on plates coated with 100 μg/ml poly-L-ornithine (PO, Sigma-Aldrich) and 15 μg/ml LN521 (BioLamina) or Matrigel (Corning, New York, USA) in E8 medium supplemented with 10 μM Rock inhibitor (Y-27632, Sigma-Aldrich). Neural maintenance medium (NMM) consisted of 1:1 DMEM/F12 containing Glutamax and Neurobasal, 1% B27 containing retinoid acid, 0.5% N2, 0.5 mM Glutamax, 0.5% NEEA, 50 μM 2-mercaptoethanol (all from Thermo Fisher Scientific), 2.5 μg/ml insulin (Sigma-Aldrich) and 0.1% penicillin/streptomycin (Thermo Fisher Scientific). For neural induction on days 1-12, the NMM was supplemented with 100 nM LDN193189 and 10 μM SB431542 (both from Sigma-Aldrich), and the medium was refreshed daily. Single-cell passaging on day 12 was carried out with StemPro Accutase (Thermo Fisher Scientific), and cells were plated at a density of 2.5×10^5 cells/cm^2 on plates coated with 100 μg/ml PO and 15 μg/ml LN521 or mouse laminin in neural induction medium supplemented with 10 μM Rock inhibitor. For NPC proliferation on days 13-25, the NMM was supplemented with 20 ng/ml FGF2 (Thermo Fisher Scientific). NPCs were passaged on days 17, 21 and 25 with StemPro Accutase and cryopreserved on day 21 in neural proliferation medium containing 10 μM Rock inhibitor and 10% DMSO (Sigma-Aldrich). From day 26 onwards, the NMM was supplemented with 20 ng/ml BDNF, 10 ng/ml GDNF (both from R&D Systems Inc.), 500 μM cAMP and 200 μM AA (both from Sigma-Aldrich) for neuronal maturation. At the final plating on day 32, the cells were plated at a 50,000 cells/cm^2 density on plastic plates and at a 1×10^6 cells/cm^2 density on MEAs in neural maturation medium supplemented with 10 μM Rock inhibitor. Plastic plates were coated with PO and LN521 or with mouse laminin as described previously, and MEAs were coated with 0.1% PEI and 50 μg/ml LN521 or mouse laminin. The medium was refreshed every two to three days.

4.1.5 Astrocyte culture

Commercial hiPSC-derived astrocyte progenitor cells were cultured according to the manufacturer's instructions (ax0083, Axol Bioscience Inc., UK; Study **III**). In short, astrocyte progenitors were cultured in Astrocyte Basal Medium containing Supplements A-C. Cells were expanded at a 100,000 cells/cm^2 density on plastic plates coated with Matrigel (Corning). Astrocytes were differentiated for 24 days before experiments and passaged with StemPro Accutase once a week; the medium was refreshed every other day. The cell density at the final plating prior to experiments was 80,000 cells/cm^2.

For astrocyte reactivation, cells were treated with 10 ng/ml human recombinant TNF-α and 10 ng/ml human recombinant IL-1β (both from PeproTech Inc., New York, USA) for seven days. Astrocyte-conditioned medium (ACM) was collected from control and treated astrocytes to characterize the astrocyte-secreted factors and evaluate the neuron-specific effects of ACM on viability and functionality. Additionally, a control medium not incubated with astrocytes was prepared.

4.1.6 Rat cortical cultures

Cortex tissue was harvested from E17-18 Wistar rat embryos according to a published protocol (Sahu et al., 2019) (Study **II**). Cortical cells were cultured in Neurobasal Medium supplemented with 2% B27, 2 mM Glutamax and 1% penicillin/streptomycin (all from Thermo Fisher Scientific). Cells were plated at a 100,000 cells/cm^2 density on plastic plates and at a 2.5×10^5 cells/cm^2 density on MEAs coated with 25 μg/ml poly-D-lysine (PDL, Sigma-Aldrich). The medium was changed every two to three days.

4.2 Molecular biology characterization

4.2.1 Gene expression analysis

Reverse transcription-polymerase chain reaction (RT-PCR) was performed in Study **I**, and quantitative real-time PCR (qRT-PCR) was performed in Study **III**. RNA was isolated with a NucleoSpin RNA Kit (Macherey-Nagel, Düren, Germany). cDNA was generated using a High Capacity cDNA Reverse Transcription Kit (Thermo Fischer Scientific). The RT-PCR and qRT-PCR protocols and primers are described in detail in the original publications (Studies **I** and **III**). The RT-PCR products were separated electrophoretically, and qRT-PCR data were analyzed using the delta Ct method (Livak and Schmittgen, 2001). The gene expression levels were normalized to that of the GAPDH or GUSB housekeeping gene. Information on the analyzed genes is listed in Table 4.

Table 4. Genes analyzed with RT-PCR and qRT-PCR.

Gene symbol	Gene name	Method	Study
FOXG1	Forkhead box G1	RT-PCR	I
GAPDH	Glyceraldehyde-3-phosphate dehydrogenase	RT-PCR, qRT-PCR	I, III
GBX2	Gastrulation brain homeobox 2	RT-PCR	I
GFAP	Glial fibrillary acidic protein	qRT-PCR	III
GUSB	Glucuronidase beta	qRT-PCR	III
KCC2	Potassium chloride cotransporter 2	RT-PCR	I
LMX1A	LIM homeobox transcription factor 1 alpha	RT-PCR	I
NKCC1	Na-K-Cl cotransporter 1	RT-PCR	I
OTX2	Orthodenticle homeobox 2	RT-PCR	I

4.2.2 Immunocytochemical staining

Immunocytochemical staining was performed on 4% paraformaldehyde-fixed samples according to the original publications (Studies **I**-**III**). The primary antibodies used in the staining protocol are listed in Table 5. Secondary antibodies consisted of AlexaFluor-488, AlexaFluor-568, and AlexaFluor-647 dyes diluted 1:200 or 1:400 (all from Thermo Fisher Scientific). Samples were imaged with an Olympus IX51 microscope equipped with an Olympus DP30BW camera (Olympus Corporation, Hamburg, Germany), a LSM780 Laser Scanning Confocal Microscope equipped with a Quasar spectral GaAsP detector (Carl Zeiss, Jena, Germany) or a Nikon A1R+ Laser Scanning Confocal Microscope equipped with an A1-DUG GaAsP Multi Detector Unit (Nikon, Tokyo, Japan). Image data were quantified with CellProfiler and CellProfiler Analyst software (Carpenter et al., 2006; Jones et al., 2008).

Table 5. Primary antibodies used for immunocytochemical staining.

Antibody symbol	Protein name	Species	Dilution	Supplier	Study
Brn2	Brain-specific homeobox/POU domain protein 2	goat	1:400	GenScript	II
β-tubulin	Beta tubulin III	chicken	1:4000	Abcam	I, II
β-tubulin	Beta tubulin III	mouse	1:1000	Sigma-Aldrich	I-III
β-tubulin	Beta tubulin III	rabbit	1:2000	GenScript	I-III
Ctip2	COUP-TF-interacting protein 2	rat	1:500	Abcam	II
FoxG1	Forkhead box G1	rabbit	1:500	Abcam	II
GABA	γ-aminobutyric acid	rabbit	1:1000	Sigma-Aldrich	I, II
GAD67	Glutamic acid decarboxylase 67	mouse	1:100	Millipore	I, II
GFAP	Glial fibrillary acidic protein	chicken	1:4000	Abcam	I-III
Ki67	Ki-67 protein	rabbit	1:800	Millipore	III
MAP2	Microtubule-associated protein 2	chicken	1:4000	Novus Biologicals	I
MAP2	Microtubule-associated protein 2	rabbit	1:400	Millipore	I-III
Pax6	Paired box 6	rabbit	1:1000	BioLegend	II
PSD-95	Postsynaptic density protein 95	mouse	1:50	Abcam	II
PSD-95	Postsynaptic density protein 95	rabbit	1:100	Cell Signaling Technology	I
Satb2	Special AT-rich sequence-binding protein 2	mouse	1:200	Abcam	II
S100β	S100 calcium binding protein B	mouse	1:500	Abcam	I, II
Syn	Synaptophysin	mouse	1:2000	Sigma-Aldrich	I
Syn	Synaptophysin	rabbit	1:2000	Abcam	II
Tbr1	T-box brain protein 1	rabbit	1:1500	Abcam	II
vGlut1	Vesicular glutamate transporter 1	guinea pig	1:1000	Millipore	I
vGlut1	Vesicular glutamate transporter 1	rabbit	1:2000	Synaptic Systems	II
Vim	Vimentin	mouse	1:500	Dako	III

4.2.3 Western blot

Western blot analysis was carried out to measure the total levels of glial fibrillary acidic protein (GFAP) in astrocytes (Study **III**). Cultures were washed with phosphate-buffered saline (PBS) and lysed with Laemmli sample buffer (Bio-Rad Laboratories Inc., Hercules, CA, USA). Proteins were separated on 10% Mini-Protean TGX Precast Gels and transferred to PVDF membranes using a Trans-Blot Turbo Transfer System (both from Bio-Rad Laboratories Inc.). The membranes were blocked with 5% milk in 0.05% Tween 20/TBS buffer for 1 h. The primary antibodies anti-GFAP (chicken, 1:30000, Abcam, Cambridge, UK) and anti-β-actin (mouse, 1:2000, Santa Cruz Biotechnology, Dallas, Texas) were incubated for 1 h at RT. The secondary antibodies used were goat anti-mouse IgG-HRP (goat, 1:2000, Santa Cruz Biotechnology) and goat anti-chicken IgY-HRP (goat, 1:30,000, Thermo Fisher Scientific). Proteins were detected using ECL Prime Western Blotting System reagent (Sigma-Aldrich) and imaged with a ChemiDoc XRS+ System (Bio-Rad Laboratories Inc.).

4.2.4 Glutamate uptake

Glutamate uptake by astrocytes was analyzed with a Glutamate Assay Kit (Abcam; Study **III**). First, cells were washed with PBS supplemented with 1% bovine serum albumin (BSA) for 30 min at 37 °C. Then, the cells were incubated with 100 μM glutamate in PBS for 1 h at 37 °C. After the PBS wash and lysis with the assay buffer, the cell lysate concentration was analyzed according to the manufacturer`s instructions.

4.2.5 ELISA and cytokine array

The secretion profile of astrocytes was evaluated in Study **III**. The secretion of IL-6 into the culture medium was analyzed with a Human IL-6 Uncoated ELISA Kit (Thermo Fisher Scientific). Absorbance was measured at 450 nm (Wallac Victor 1420).

A wider secretion profile was measured with a Proteome Profiler Array (Human XL Cytokine Kit, R&D Systems Inc.). The resulting membranes were imaged with a ChemiDoc imaging system (Bio-Rad Laboratories). A total of 105 different

cytokines, chemokines and other inflammatory molecules were analyzed. A full list of analytes can be found in the original publication (Study **III**).

4.2.6 Viability assays

The viability, cytotoxicity and apoptosis of neurons were evaluated after 48 h of ACM treatment with the Apo-Tox-Glo Triplex assay according to the manufacturer's protocol (Promega, Madison, WI, USA). Additionally, the viability of neurons during co-culture with astrocytes in a microfluidic device was assessed using the Live/Dead Viability/Cytotoxicity Kit (Thermo Fisher Scientific) (Study **III**). Live staining with 0.1 μM calcein-AM was applied for 30 min, and samples were imaged immediately. The area covered by live-stained neuronal axons was quantified with CellProfiler software.

4.3 Functional characterization

4.3.1 Microelectrode array measurements

MEA measurements of neurosphere-differentiated cells were performed with an MEA60 amplifier (Multi Channels System, MCS, Reutlingen, Germany; Study **I**), and those of adherent differentiated cells were performed with the Axion Maestro system (Axion Biosystems, Atlanta, GA, USA; Studies **II** and **III**).

With the MEA60 system, 60-6well MEA200/30iR-Ti-w/o arrays (MCS) with 9 electrodes per well were used. Culture wells were separated with a 6-well silicone chamber, SpikeBooster (Kreutzer et al., 2012). Measurements were performed at 37 °C twice a week for 10 min. Recordings were obtained using MC_Rack software at a 50 kHz sampling frequency.

For the Axion Maestro system measurements, cells were plated on CytoView MEA 48 or CytoView MEA 12 plates with 16 and 64 electrodes per well, respectively (both from Axion Biosystems). Measurements were obtained with AxIS software at a 12.5 kHz sampling frequency. Recordings were performed at 37 °C, and a 5% CO_2 atmosphere control was used for recordings over 10 min. Spontaneous activity was measured twice a week for 10 min. Pharmacological responses (Study **II**) were recorded for 30 min. The pharmacological reagents included γ-aminobutyric acid (GABA, 10 μM, Sigma-Aldrich) and the $GABA_A$ receptor antagonist gabazine

(30 μM, Sigma-Aldrich). In the ACM experiments (Study **III**), 50% of the medium was replaced with ACM, and recordings were performed for 10 min immediately, after 1 h, 4 h and 24 h exposure.

4.3.2 Microelectrode array data analysis

The spike detection from MCS data (Study **I**) was performed with MC_Rack, and spikes were detected from 200 Hz high-pass filtered data when their amplitude crossed the threshold of 5 × the standard deviation of noise. The active electrode criterion was experimentally set to 2 spikes/min. Burst analysis was performed with the cumulative moving average (CMA) method (Kapucu et al., 2012) embedded in a custom MATLAB script (Mathworks, Natick, MA, USA). Burst analysis was performed for electrodes with over 10 spikes/min, and additional criteria included a minimum of three spikes per burst and a maximum of 2000 ms interspike interval (ISI) in the burst.

For Axion data analysis (Studies **II** and **III**), data were filtered with a 200 Hz lower passband frequency and a 3000 Hz upper passband frequency. Spike detection was performed with a threshold value of 4.5 × the estimate of the noise standard deviation according to a previous publication (Quiroga et al., 2004), followed by processing with a stationary wavelet transform-based Teager energy operator (SWTTEO) algorithm (Mayer et al., 2018) embedded in a custom MATLAB script. The criterion for an active electrode was 10 spikes/min. Burst analysis was performed with the logISI algorithm (Pasquale et al., 2010) embedded in the R package meaRtools (Gelfman et al., 2018). Burst analysis was performed only for burst-detecting electrodes. Additionally, a minimum of five spikes constituted a burst, and short bursts were merged when the computed ISI threshold was less than 100 ms. A cutoff of 100 ms was applied as the minimum time required between bursts. Connectivity analysis was performed according to the correlated spectral entropy (CorSE) method reported previously (Kapucu et al., 2016). Connectivity maps were plotted for electrode pairs with a CorSE value >0.7. Principal component analysis (PCA) was performed in MATLAB according to a previous publication (Ylä-Outinen et al., 2019). In short, a total of seven MEA activity features were included: spike rate, spike time tiling coefficient (STTC, using a default time bin of 50 msec), burst rate, burst duration, spike frequency in burst, spikes in burst and percentage of spikes in bursts. Values were normalized using the standard score method and plotted against three major principal components.

4.3.3 Calcium imaging and data analysis

Calcium imaging was performed in Study **I**. For calcium imaging experiments, cells were loaded with 4 μM Fluo-4 AM (Thermo Fisher Scientific) in neural differentiation medium for 30 min in an incubator. Before imaging, the cells were washed with culture medium. During acquisition, cultures were imaged every 0.5 sec at 36±0.5 °C and under perfusion with a physiological solution containing 140 mM NaCl, 10 mM HEPES, 10 mM D-glucose, 3.5 mM KCl, 1.25 mM NaH_2PO_4, 2 mM $CaCl_2$ and 1 mM $MgCl_2$ (all from Sigma-Aldrich) dissolved in dH_2O. Imaging was performed with an Olympus IX61 inverted microscope, an Andor iXon 885 EMCCD camera (Andor Technology, Belfast, Northern Ireland) and a Polychrom V monochromator (TILL Photonics, Munich, Germany). Images were acquired with TILL Photonics Live Acquisition software and analyzed with the SimplePCI software package (Hamamatsu Corporation, Sewickley, PA, USA). Neurons were identified based on a fast response to a high K^+ concentration (50 mM). The percentage of neurons responding to GABA (100 μM, Sigma) application with a calcium increase was quantified.

4.4 Microfluidic device

To create controlled neuron/astrocyte co-cultures, a microfluidic device developed in-house was used (patent: WO2015092141A1). The three cell compartments (two neuronal compartments and one astrocyte compartment) are connected to an axonal compartment via microtunnels. The small microtunnels restrict the cell somas to the cell compartments while allowing interactions between cell processes in the axonal compartment. The detailed design, fabrication and assembly of the microfluidic device is described in the original publication (Study **III**).

The hPSC-derived neurons and astrocytes were plated in the neuronal and astrocyte compartments, respectively. Neurons were plated at a density of 1.5×10^5 cells/cm^2, and the astrocyte density was 50,000 cells/compartment. The same coating, comprising 250 μg/ml PO (Sigma-Aldrich) and 20 μg/ml LN521 (BioLamina), was used for both neurons and astrocytes. After three days, the astrocyte compartment was treated with 10 ng/ml human recombinant TNF-α and 10 ng/ml human recombinant IL-1β (both from PeproTech Inc.) for 72 h. Experimental groups included 1) a group with neurons only (Neu), 2) a group with neurons only and cytokine treatment via the astrocyte compartment (Neu+IL-

1β/TNF-α), 3) a group with neurons and astrocytes (Neu+Ctrl astro), and 4) a group with neurons and astrocytes and cytokine treatment via the astrocyte compartment (Neu+Reactive astro). Cultures were stained for neuronal and astrocyte markers, and viability staining was performed to visualize the effect of treatment on the axonal density in the axonal compartment, as described previously.

4.5 Statistical analysis

For data with a Gaussian distribution, a parametric independent-sample T-test was used. When the data followed a non-Gaussian distribution, a nonparametric Kruskal-Wallis test followed by the Mann-Whitney U test was performed. When differences between ACM treatment groups were analyzed from the MEA data, delta values were calculated by subtracting the baseline value from the treatment value. Bonferroni correction was used for multiple comparisons. Correlations were assessed with Spearman's rho. Statistical tests were performed with SPSS Statistics software (IBM Corp., Armonk, NY, USA). A p-value of <0.05 was considered statistically significant. University statistician Heini Huhtala, MSc, was consulted regarding the statistical tests.

5 RESULTS

5.1 Neuronal differentiation with suspension neurosphere and adherent methods

The neuronal cells used in this study were differentiated with either a suspension neurosphere method (Study **I**) or an adherent method with dual SMAD inhibition (Studies **II** and **III**). In the first part of the results section, neuronal cells produced with the two methods are characterized. Both of the differentiation methods are presented in detail in the schematic illustrations, which indicate the timelines, culture matrices, growth factors and small molecules used for chemical induction (Figure 5A-B). In short, via the neurosphere method, hPSCs were differentiated in the presence of FGF2 for the standard 8 weeks or, alternatively, for a prolonged period of 15 weeks to increase the proportion of glial cells and improve maturation. Cells were plated on mouse laminin substrate in adherent culture for up to 5 weeks for final maturation, which was further promoted by FGF2 and BDNF treatments.

The adherent differentiation process can be divided into three stages: 12-day neural induction with dual SMAD inhibition, NPC proliferation with FGF2, and final maturation in the presence of the neurotrophic factors BDNF, GDNF, cAMP and AA. The neural induction was carried out on either a Matrigel matrix or on a more defined LN521 culture substrate. Similarly, subsequent differentiation was performed on either mouse laminin or LN521 substrates. The produced NPCs could be stored in cryobanks and further differentiated into neurons and astrocytes for use in experiments. To evaluate the neurosphere differentiation method, the hESC line 08/023 and the hiPSC line 04311.WTs were used. The adherent neuronal differentiation method was established with the same hESC line 08/023 and two hiPSC lines, 10212.EURCCs and IMR90-4. Data from the different hPSC lines are mostly pooled in the results section but are shown separately in the original publications.

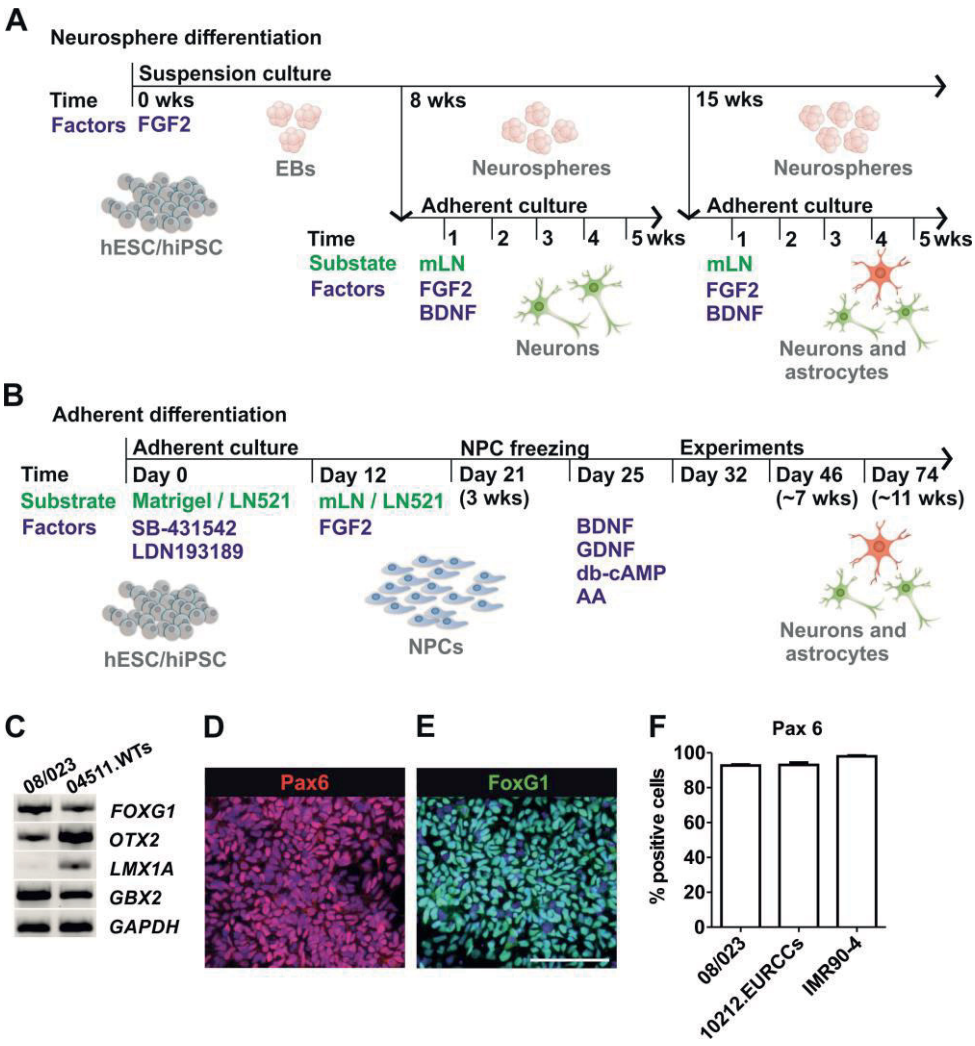

Figure 5. Neuronal differentiation with the neurosphere and adherent methods. Schematic illustrations of (A) the neurosphere and (B) adherent methods depicting the time frame, stages of differentiation, culture substrate and factors involved. (C) RT-PCR analysis of the expression of forebrain (*FOXG1*, *OTX2*), midbrain (*LMX1A*) and hindbrain (*GBX2*) transcripts in two of the neurosphere-differentiated hPSC lines at the 8+1 wk time point (hESC line 08/023 and hiPSC line 04311.WTs). *GAPDH* was used as a housekeeping gene. Immunocytochemical staining of the neuroectodermal markers (D) Pax6 and (E) FoxG1 after 12 days of neural induction with the adherent method. The scale bar represents 100 μm. (F) The percentage of Pax6-positive cells in all three hPSC lines (hESC line 08/023 and hiPSC lines 10212.EURCCs, IMR90-4) was quantified on day 12 of adherent differentiation. Abbreviations: EB, embryoid body; NPC, neural progenitor cell; mLN, mouse laminin.

5.1.1 Specification of neural progenitor cells and generation of neurons

Without additional regional specifications, the neural differentiation of hPSCs is known to follow the "default" pathway, where the rostral forebrain phenotype is the first to emerge (Suzuki and Vanderhaeghen, 2015). Here, successful neural induction and brain region identities in neurosphere-differentiated cultures were evaluated from determining the expression of transcripts in the forebrain (*FOXG1*, *OTX2*), midbrain (*EN1*) and hindbrain (*GBX2*) (Study **I**). Analysis revealed that the cultures represent a mixed CNS culture with strong expression levels of the forebrain markers *FOXG1* and *OTX2* (Figure 5C). Additionally, the efficiency of neural induction with the adherent differentiation method was assessed (Study **II**). Staining and quantification of the neuroectodermal marker Pax6 revealed that over 90% of the cells were Pax6-positive (Figure 5D and F). The produced NPCs were further characterized by staining for FoxG1, an important transcription factor for specification of the rostral cortex (Figure 5E).

To evaluate the differentiation capacity, the amount of MAP2- and/or β-tubulin-positive neurons was quantified after differentiation with both the neurosphere method (Study **I**) and the adherent method (Study **II**). First, the neurosphere method produced neurons efficiently, as the portion of neurons was 74% after 8 weeks of neurosphere differentiation followed by 4 weeks of adherent maturation (8+4 wks, Figure 6A). A significant decrease in the proportion of neurons to 66% was observed after prolonged neurosphere differentiation for 15+4 wks (8+4 wks vs. 15+4 wks, $p=0.008$; Figure 6A). In adherent neuronal differentiation, the neuron percentage was 72% after 7 wks (Figure 6B). Similarly, it decreased later, as 49% of the cells were neuronal at the 11 wks time point (7 wks vs. 11 wks, $p<0.001$; Figure 6B).

Analysis of the neuronal subtypes confirmed that both neuronal differentiation methods (Studies **I-II)** primarily produced glutamatergic excitatory neurons expressing vGlut1 (Figure 6A-B). Cultures also contained GABAergic inhibitory neurons, as determined by GABA and GAD67 staining (Figure 6A-B). Furthermore, synaptic connections were formed and identified with presynaptic synaptophysin and postsynaptic PSD-95 staining (neurosphere method, after 8+4 wks; adherent method, after 11 wks; Figure 6A-B).

Different cortical layer markers from the adherent-differentiated neurons were stained (Study **II**). Expression of the early-born deep cortical layer-specific markers Ctip2 and Tbr1 was detected after 7 wks of differentiation (Figure 6C-D). The generation of late-born upper layer-specific neurons was initiated after 7 wks as

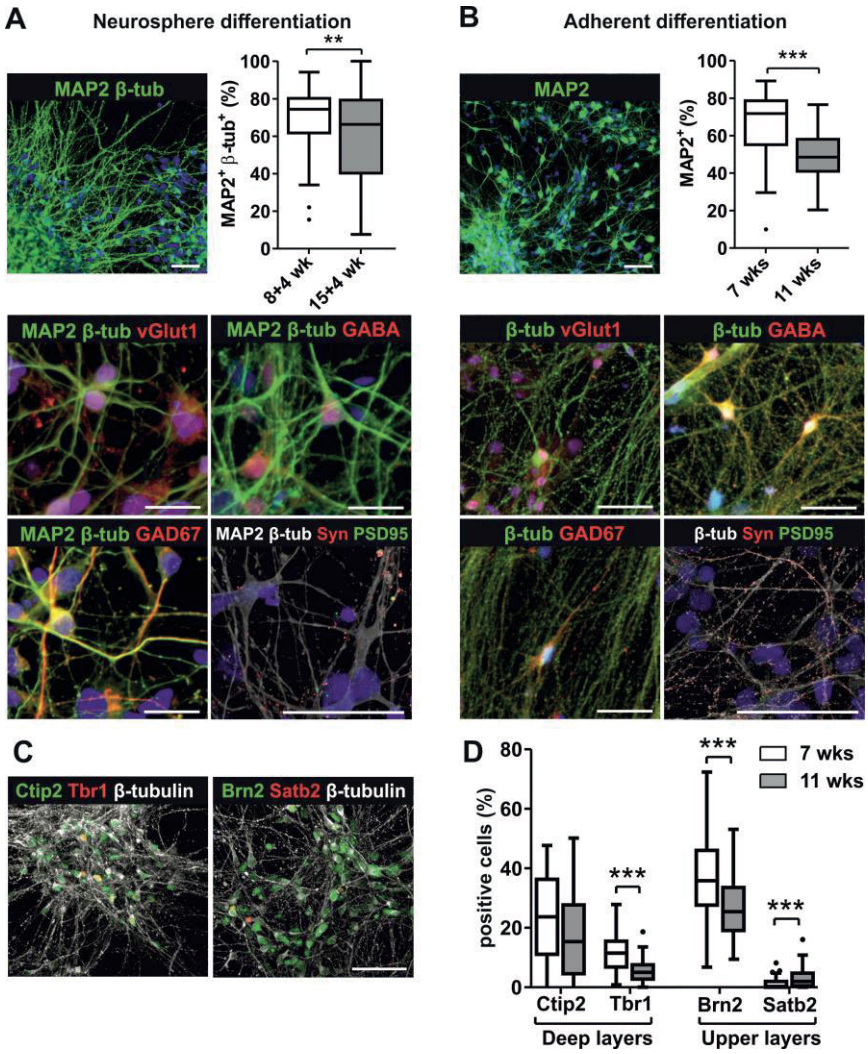

Figure 6. Differentiation of neuronal cell types. The neuronal population was characterized following (A) neurosphere differentiation and (B) adherent differentiation. The number of neurons was quantified by MAP2 and/or β-tubulin staining. Glutamatergic neurons were stained with vGlut1, and GABAergic neurons were stained with GABA and GAD67. The formation of synapses was assessed with synaptophysin (Syn) and PSD-95 staining. (C) Generation of cortical layer-specific neurons from adherent-differentiated cultures was evaluated with staining of the early-born deep layer-specific markers Ctip2 and Tbr1 and the late-born upper layer-specific markers Brn2 and Satb2. Neurons were labeled with β-tubulin. The scale bar is 50 μm in all images. (D) The proportions of different layer-specific neurons among the whole cell population were quantified after 7 and 11 weeks. For quantification, data are pooled from all hPSC lines. Data are presented as Tukey box plots showing median and interquartile range with whiskers extending out to min and max values within 1.5 times the interquartile range. Statistical analyses with the Mann-Whitney U test show differences between time points (* $p<0.05$, ** $p<0.01$, *** $p<0.001$).

shown by Brn2 staining. However, it continued during the follow-up period because only a few Satb2-positive cells were present after 11 wks (Figure 6D).

Together, these results show that both differentiation methods produced neuronal cells efficiently, and cultures contained mixed populations of glutamatergic and GABAergic neurons. The adherent method resulted in the typical sequential generation of cortical layer-specific neurons. Overall, the neurogenesis period starting from pluripotent stage was shorter with the adherent method than with the neurosphere method.

5.1.2 Generation of endogenous astrocytes

Many neuronal differentiation protocols are known to produce a certain amount of endogenous astrocytes from the same neural progenitors that give rise to neurons. Here, the capability of the neurosphere (Study **I**) and adherent (Study **II**) differentiation protocols to produce astrocytes was evaluated with S100β and GFAP staining. Quantification of the percentage of GFAP-positive cells revealed that the neurosphere differentiation method produced only a modest 3% of astrocytes after 8+4 wks (Figure 7A). After 15+4 wks of differentiation, the astrocyte proportion was significantly increased to 15% (8+4 wks vs. 15+4 wks, $p<0.001$; Figure 7A). The adherent differentiation protocol also produced a considerable portion of astrocytes. The astrocyte percentage was quantified using the results from both S100β and GFAP staining. The percentage of S100β-positive astrocytes increased from 5% at 7 wks to 38% at 11 wks (7 wks vs. 11 wks, $p<0.001$; Figure 7B). The increase in the portion of GFAP-positive astrocytes was also significant, from 0.5% at 7 wks to 20% at 11 wks (7 wks vs. 11 wks, $p<0.001$; Figure 7B). These results indicate that both differentiation methods produce endogenous astrocytes after an extended period of differentiation, but this time frame starting from pluripotent stage is shorter with the adherent method.

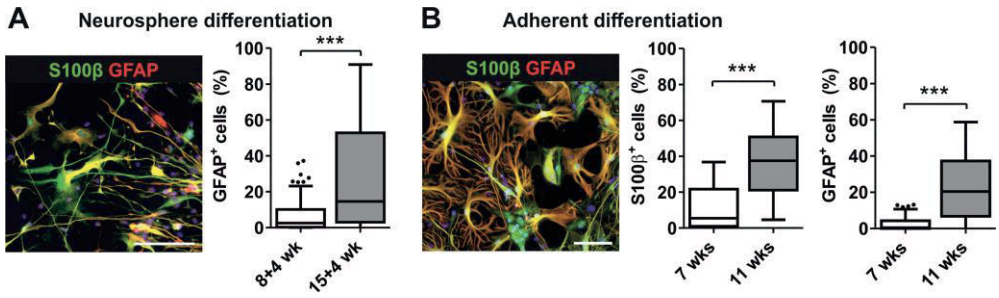

Figure 7. Generation of endogenous astrocytes. The numbers of astrocytes in the (A) neurosphere-differentiated and (B) adherent-differentiated cultures was evaluated by staining for GFAP and S100β. The scale bar represents 100 µm. Quantifications are of pooled data from different hPSC lines and are shown as Tukey box plots. Significant differences between time points were determined by the Mann-Whitney U test (* $p<0.05$, ** $p<0.01$, *** $p<0.001$).

5.2 Functional maturation of the hPSC-derived neuronal networks

Functional activity is initially observed as uncorrelated single spikes and tonic spike trains, but with maturation, increased bursting and connectivity is observed, as the activity is orchestrated into synchronous network bursts (Heikkilä et al., 2009; Wagenaar et al., 2006). Neuronal cultures differentiated using both the neurosphere and adherent methods generated electrophysiologically active networks (Studies **I** and **II**). However, MEA measurements demonstrate that the activity levels were substantially different between the networks produced using the two differentiation methods (Figure 8A-B). Raster plots presenting the spike intensities of single networks show that the neurosphere-differentiated neurons presented mainly uncorrelated spiking and bursting activity (Figure 8A), while the adherent-differentiated neurons achieved synchronous network level bursting (Figure 8B). Further maturation of the activity was achieved via the neurosphere method with a prolonged differentiation time (Study **I**) and via the adherent method with optimization of the culture substrate (Study **II**), which are described in more detail. Additionally, maturation of the GABAergic system was observed with both methods (Studies **I** and **II**).

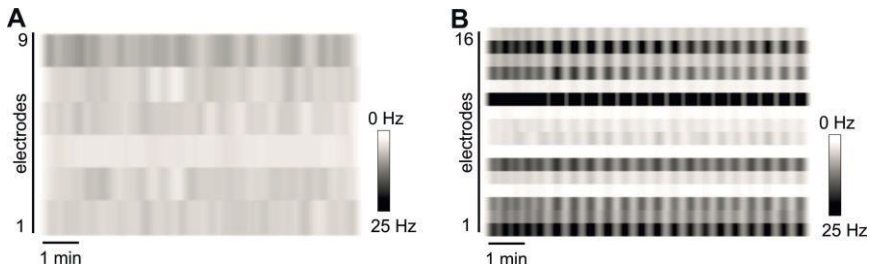

Figure 8. Functional activity of neurons as measured with microelectrode arrays. Spike intensity raster plots presenting the activity of (A) neurosphere- and (B) adherent-differentiated neurons as determined by microelectrode arrays (MEAs). Both images show a 10-minute measurement of a single MEA well with 9 or 16 electrodes after approximately 8 weeks of differentiation from the pluripotent stage. The intensity scale bar on the right represents the spike frequency (Hz).

5.2.1 Prolonged neurosphere differentiation results in an increased burst rate and burst compaction

Neural cells were differentiated with the neurosphere method for either the standard 8 wks or for a prolonged period of 15 wks (Study **I**). After this, the neurospheres were dissociated and plated on MEA plates for functional measurements over 5 wks. The studied hPSC lines (hESC line 08/023 and hiPSC line 04311.WTs) developed spiking activity after both differentiation periods (8 wks and 15 wks), but the detection of mature bursting activity was the specific focus of the study. A significant increase in the number of bursts was observed after the prolonged differentiation time, suggesting functional maturation (Figure 9A-B).

Characterization of the burst features, spike frequencies in bursts and burst durations revealed differences between the two studied hPSC lines. When data from the five weeks of measurements were combined and divided into groups by hPSC line (08/023 and 04311.WTs) and differentiation time (8 wks and 15 wks), all groups showed a strong correlation between the two features, as the spike frequency in bursts increased with a decreasing burst duration (Spearman's rho, Figure 9C-D). However, unlike the hiPSC line 04311.WTs, the hESC line 08/023 showed an increased spike frequency in bursts and a shortened burst duration after the prolonged 15 wk differentiation period. This burst compaction was more distinct in the 08/023 line than in the 04311.WTs line, suggesting efficient functional maturation (Figure 9C). Taken together, these results suggest that prolonged differentiation can improve functional maturation, as determined by the observation of increased burst rates and burst compaction.

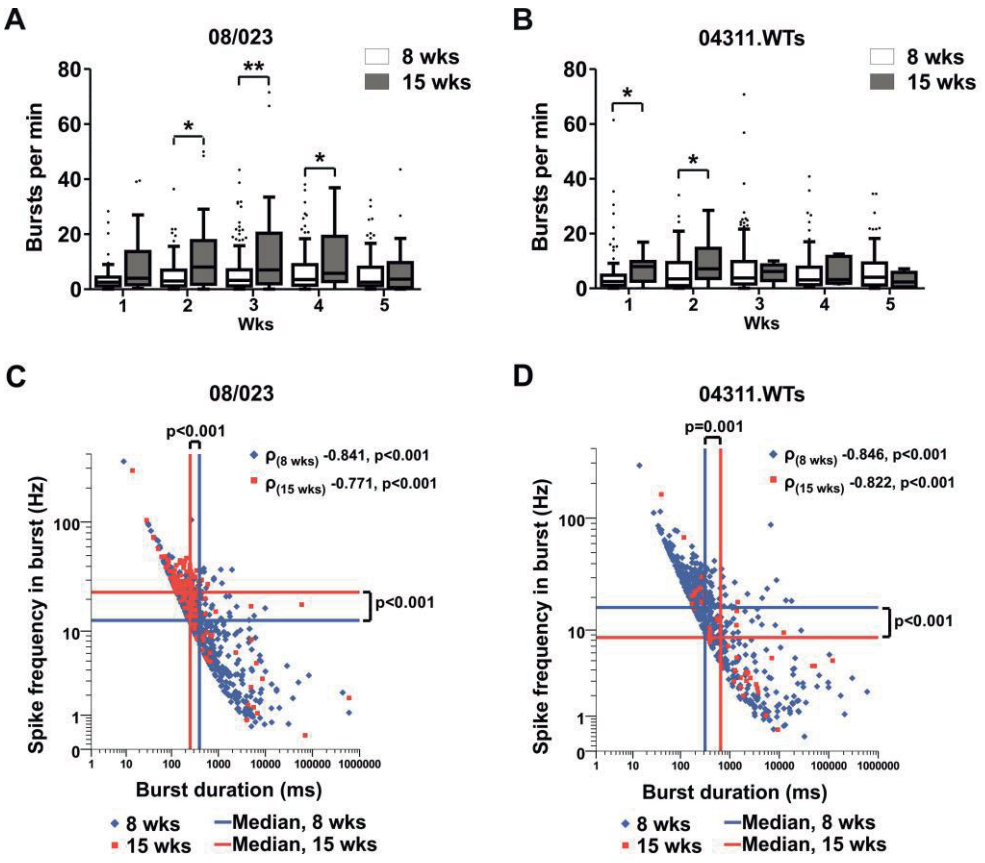

Figure 9. Bursting activity in neurosphere-differentiated networks on MEA. The number of bursts per minute was increased in (A) 08/023 hESC-derived and (B) 04311.WTs hiPSC-derived neural networks as a result of prolonged differentiation for 15 wks. Statistical significance at each time point on MEA was assessed with the Mann-Whitney U test, and significant differences are denoted as * $p<0.05$, ** $p<0.01$, and *** $p<0.001$. Correlations between the spike frequency in burst and burst duration were determined from data obtained from five weeks of measurement from the (C) 08/023 and (D) 04311.WTs lines. The median result for each feature and time point are marked with a solid line. The Mann-Whitney U test was used for statistical assessment, and correlations were determined using Spearman's rho (ρ). Significance differences are marked in the images.

5.2.2 The laminin-521 substrate improves the functional activity of adherent-differentiated neuronal networks

The effect of α5 laminin substrates on the promotion of functional activity on the MEA has previously been shown for neurosphere-differentiated cultures (Hyysalo et al., 2017). Here, the human recombinant laminin isoform LN521 was optimized as a culture substrate for adherent neural differentiation with the aim of improving functional development (Study **II**). As a comparison, cells were also cultured with the commonly used mouse laminin substrate. Both substrates supported the generation of MAP2- and β-tubulin-positive neurons and S100β-positive astrocytes (Figure 10A). However, when activity was measured on MEA, there was a substantial increase in the percentage of active electrodes observed in the networks cultured on LN521 compared to those cultured on mouse laminin (Figure 10B). Additionally, the spike and burst rates of neurons cultured on LN521 were higher than those of neurons cultured on mouse laminin (Figure 10 C-D). This result demonstrated the superiority of the LN521 substrate for the functional development of neurons, and LN521 was thereafter used as the sole substrate for adherent differentiation.

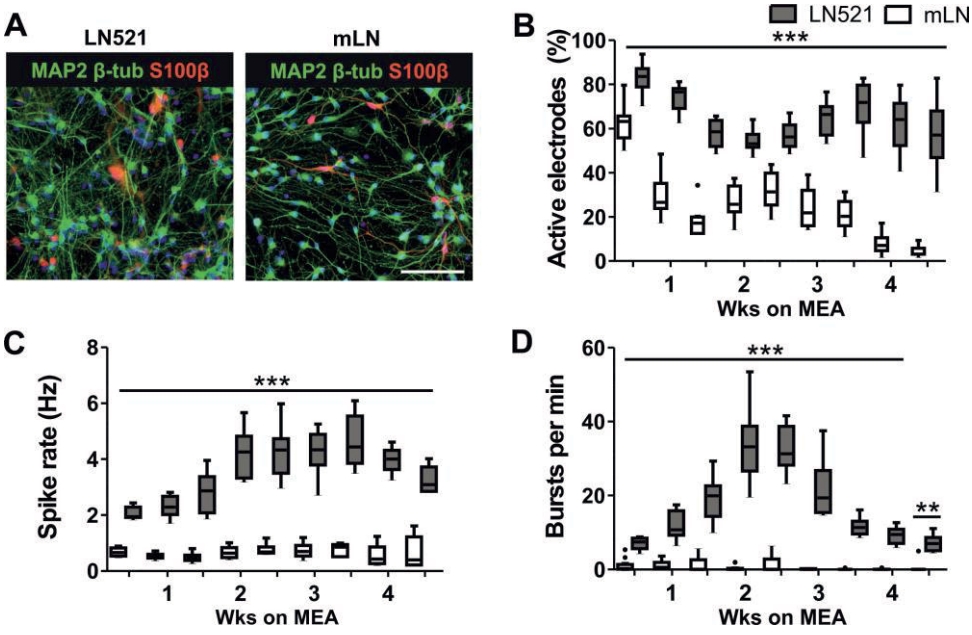

Figure 10. Functional activity of neurons differentiated on mouse laminin and human recombinant laminin-521 substrates. (A) Immunocytochemical staining showing the differentiation of neurons (MAP2 and β-tubulin) and astrocyte progenitors (S100β) on mouse laminin (mLN) and human recombinant laminin-521 (LN521). The scale bar is 100 µm. MEA

measurements of cultures differentiated on either mLN and LN521 demonstrate differences in the development of the (B) percentage of active electrodes, (C) spike rate (Hz) and (D) number of bursts per minute. Data are presented as Tukey box plots. Significant differences between substrates at each time point were determined by the Mann-Whitney U test (* $p<0.05$, ** $p<0.01$, *** $p<0.001$).

5.2.3 GABAergic maturation and inhibitory input in hPSC-derived networks

The presence of GABAergic cells, determined by immunocytochemical staining, in both neurosphere- and adherent-differentiated cultures raised the question of whether maturation of the GABAergic system and inhibitory networks modulating the activity were observable (Studies **I** and **II**).

Maturation of the GABAergic system was assessed via calcium imaging of the neurosphere-differentiated networks (Study **I**, Figure 11A). After the standard 8 wks of differentiation, the neuronal responses to GABA application were largely excitatory (Figure 11B), but occasionally, GABA was also found to inhibit spontaneous activity (Figure 11C). With a prolonged 15 wk differentiation time period and adherent maturation, the excitatory effect of GABA was decreased in both of the studied hPSC lines (Figure 11D-E). Gene expression analysis simultaneously revealed change in the chloride transporter subtype from NKCC1 to KCC2 (Figure 11F), which has been demonstrated to be important for the excitatory to inhibitory switch occurring during the development of the GABAergic system (Ben-Ari et al., 2007).

The inhibitory GABAergic input associated with network activity was inspected in the adherent-differentiated cultures (Study **II**). MEA measurements were performed until synchronic network activity was well established after 4 wks on the MEA. Then, pharmacological modulation of the network with GABA and the $GABA_AR$ antagonist gabazine was tested. Application of GABA resulted in a typical silencing of the network activity (Figure 11G-H). Few irregular spikes were detected, but clear bursts of activity were absent (Figure 11 G). Gabazine had the opposite effect, as it significantly increased the overall spike rate (Figure 11 G-H). In summary, the functional results obtained from both calcium imaging and the MEA experiments show that GABAergic maturation occurs in hPSC-derived networks and that inhibitory networks modulating synchronic burst activity are present.

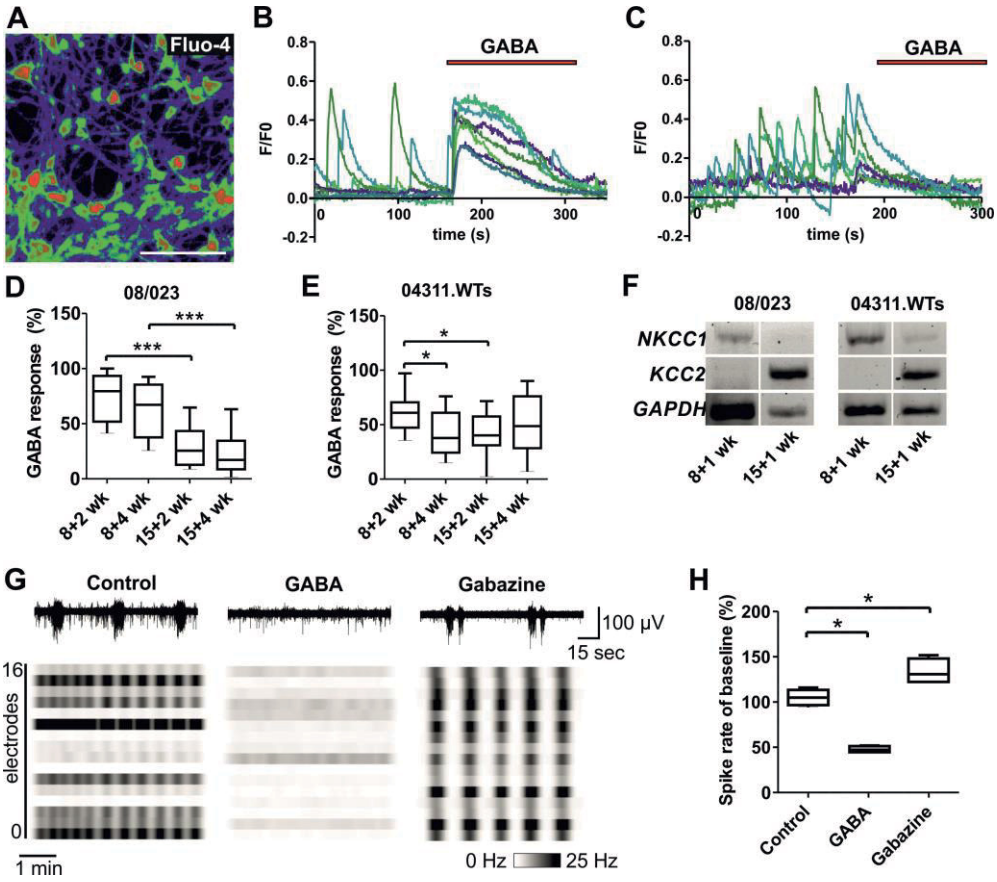

Figure 11. Roles of GABAergic maturation and input in the functionality of hPSC-derived neuronal networks. (A) To perform the calcium imaging experiments, neurosphere-differentiated cells were loaded with the fluorescent calcium indicator Fluo-4 AM. The pseudocolor image shows the high calcium concentration in red. The scale bar is 100 µm. Typical calcium traces of (B) the excitatory effect of GABA and the (C) inhibition of spontaneous activity after GABA application. (D, E) Percentages of neuronal cells responding to GABA application with excitation in the studied hPSC. (F) Expression of the chloride transporters *NKCC1* and *KCC2* in the hPSC lines differentiated by the neurosphere method. The analyzed hPSC lines are hESC line 08/023 and hiPSC line 04311.WTs. (G) Example images of adherent-differentiated neuronal MEA signals under control conditions and pharmacological treatment with GABA and gabazine. The raw MEA signal from one electrode over one minute is shown above, and the spike intensity raster blots from the entire MEA well over a 5-minute recording is shown below. (H) Spike rate changes after pharmacological treatments. Quantifications are presented as Tukey box plots, and statistical analyses were performed with the Kruskal Wallis test followed by the Mann-Whitney U test (* $p<0.05$, ** $p<0.01$, *** $p<0.001$).

5.3 Functional comparison of hPSC-derived neuronal networks and rodent *in vitro* counterparts

5.3.1 Temporal development of network activity

Rat embryonic cortical cultures have been established as the gold standard in the MEA field (Charlesworth et al., 2015; Wagenaar et al., 2006). Therefore, the development of spontaneous activity of the adherent-differentiated human cortical networks was compared with that of their rodent counterparts (Study **II**). hPSC-neurons were pre-differentiated for 32 days to begin active neurogenesis and rat neurons were isolated from day 17-18 embryos following plating on MEA. The time frames and stages of activity development were similar between hPSC-derived and rat networks. Representative images of typical firing patterns show that asynchronous spike activity was detected during the first two weeks of measurement on MEA (Figure 12A-B). Occasional spiking was followed by tonic spike trains before the organization of activity into network-level synchronous bursts (Figure 12A-B). The highest activity peak, determined by median spike and burst rates, was detected between 2-4 wks on MEA in both hPSC-derived and rat networks (Figure 12C-D). The rat networks presented higher spike and burst rates than the hPSC-derived networks after the initiation of network-level activity at approximately 3-4 wks on MEA. While the rat networks were mostly silenced after five weeks *in vitro*, the hPSC-derived networks were maintained for several weeks (Figure 12C-D).

The functional connectivity between spatially distant areas of the network was determined by analyzing the entropy between a pair of electrodes (Kapucu et al., 2016). Functional connectivity maps from as set of MEA recordings revealed a gradual increase in connectivity over time (Figure 12E). The formation of functional connections was observed in hPSC networks after 3 wks on MEA and in rat networks after 2 wks on MEA. After 4 wks, the networks expanded over the 64-channel array and subsequently declined as the 5 wk time point approached (Figure 12E). Further network level analysis was performed by calculating the synchrony measure spike time tiling coefficient (STTC) (Cutts and Eglen, 2014). According to quantification, the rat networks presented earlier initiation and exhibited higher levels of synchrony than the hPSC-derived networks (Figure 12F). Overall, in both hPSC-derived and rat networks, the activity developed through similar activity states and on the same time scale, but the level of activity was more pronounced in the rat networks.

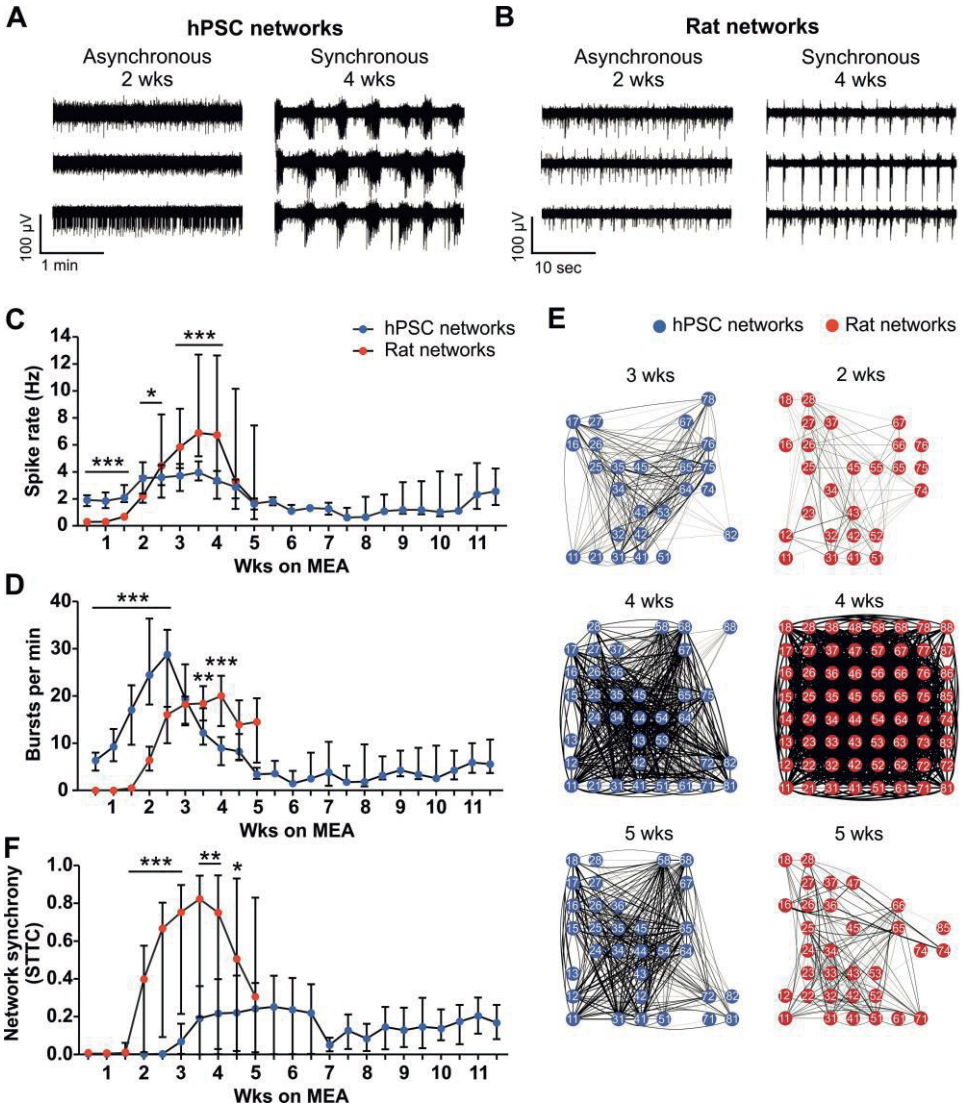

Figure 12. Temporal development of spontaneous activity in hPSC-derived and rat cortical networks. Typical asynchronous and synchronous firing patterns of (A) hPSC-derived and (B) rat networks recorded from three electrodes at the 2 and 4 wk time points. (C) Development of the spike rate and (D) bursting activity over 11 wks on MEA. Data are pooled from three experiments with two different hPSC lines. (E) Functional connectivity maps of 10-minute recordings showing the development of hPSC-derived and rat networks over time. A connectivity strength (CorSE) value of 0.7 was used for plotting. (F) Quantification of network synchrony using the spike time tiling coefficient (STTC). Quantitative data are shown as the median and interquartile range. Significant differences between hPSC-derived and rat networks at each time point were determined by the Mann-Whitney U test (* $p<0.05$, ** $p<0.01$, *** $p<0.001$).

5.3.2 Principal component analysis reveals distinct activity features of hPSC-derived neurons

Principal component analysis (PCA) was utilized to efficiently summarize the functional profiles of the hPSC-derived and rat networks (Study **II**). Analysis was performed on data from three cell batches and on recordings from three subsequent days at the peak of activity. We assessed seven different activity features, including the spike rate, STTC, burst rate, burst duration, spike frequency in bursts, number of spikes in bursts and percentage of spikes in bursts. The 7-dimensional feature vector was plotted in 3-dimensional space to visually assess the differences between hPSC-derived and rat networks. A clear segregation of the two network types was observed, with very little overlap between some of the analyzed wells (Figure 13). Most of the differences were explained by the first principal component (PC), which accounted for over 50% of the variation. Overall, the first three principal components described 94% of the variation between hPSC-derived and rat networks, confirming the distinct activity feature profile of hPSC-derived neurons.

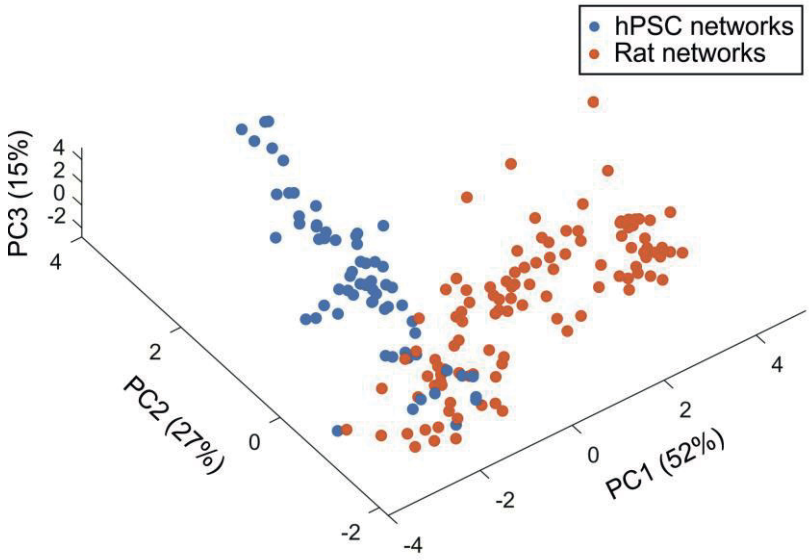

Figure 13. Principal component analysis of hPSC-derived and rat network activity features. Principal component analysis (PCA) was utilized to separate hPSC- and rat-derived networks based on variation in MEA activity consisting of seven spike, burst and network activity features. Data from several cell batches and three subsequent time points showing the highest spike rates were analyzed. The data points are plotted in 3-dimensional space, where each dot represents one MEA well. The three principal components account for the amount of variation of the data shown in parenthesis.

5.4 Modeling astrocyte-neuron interactions *in vitro*

Astrocytes play an important role in both brain development and pathology (Sofroniew and Vinters, 2010). To mimic the pathological state, hiPSC-derived astrocytes were stimulated with inflammatory cytokines, and their characteristics and neuron-specific effects were investigated (Study **III**).

5.4.1 Reactivation of hiPSC-derived astrocytes

CNS injury and disease elicit inflammatory conditions, as numerous proinflammatory factors are released at the affected region, changing the local homeostasis and cell behavior (Colombo and Farina, 2016). A 7-day cytokine treatment regimen with IL-1β and TNF-α was followed to stimulate astrocyte activation *in vitro* (Study **III**). The morphology of astrocytes was monitored, and a typical change from a filamentous to a polygonal shape was observed within 7 days of cytokine administration (Figure 14A-B). Inflammatory conditions also induced modest astrocyte proliferation, as determined by Ki67 staining (Figure 14C). Additionally, modifications of the astrocyte-specific structural intermediate filament network were observed, as GFAP downregulation was observed at both the mRNA and protein levels (Figure 14D-E). Astrocytes have an important role in the homeostatic control of extracellular space, and functional impairment was observed in the glutamate uptake mechanisms following cytokine treatment (Figure 14F). The response to cytokine exposure was also time-dependent, as the secretion of the inflammatory cytokine IL-6 was gradually increased over time (Figure 14G). In addition, a wide profile of secretion of other inflammatory factors from the culture medium was detected (Figure 14H). These included several chemokines, cytokines, and other inflammatory proteins, such as chitinase-3-like 1 (CHI3L1), osteopontin (OPN), pentraxin-3 (PTX3), serpine1 and vascular cell adhesion molecule-1 (vCAM). Thus, hPSC-derived astrocytes readily respond to the inflammatory environment and exhibit multiple reactive astrocyte characteristics.

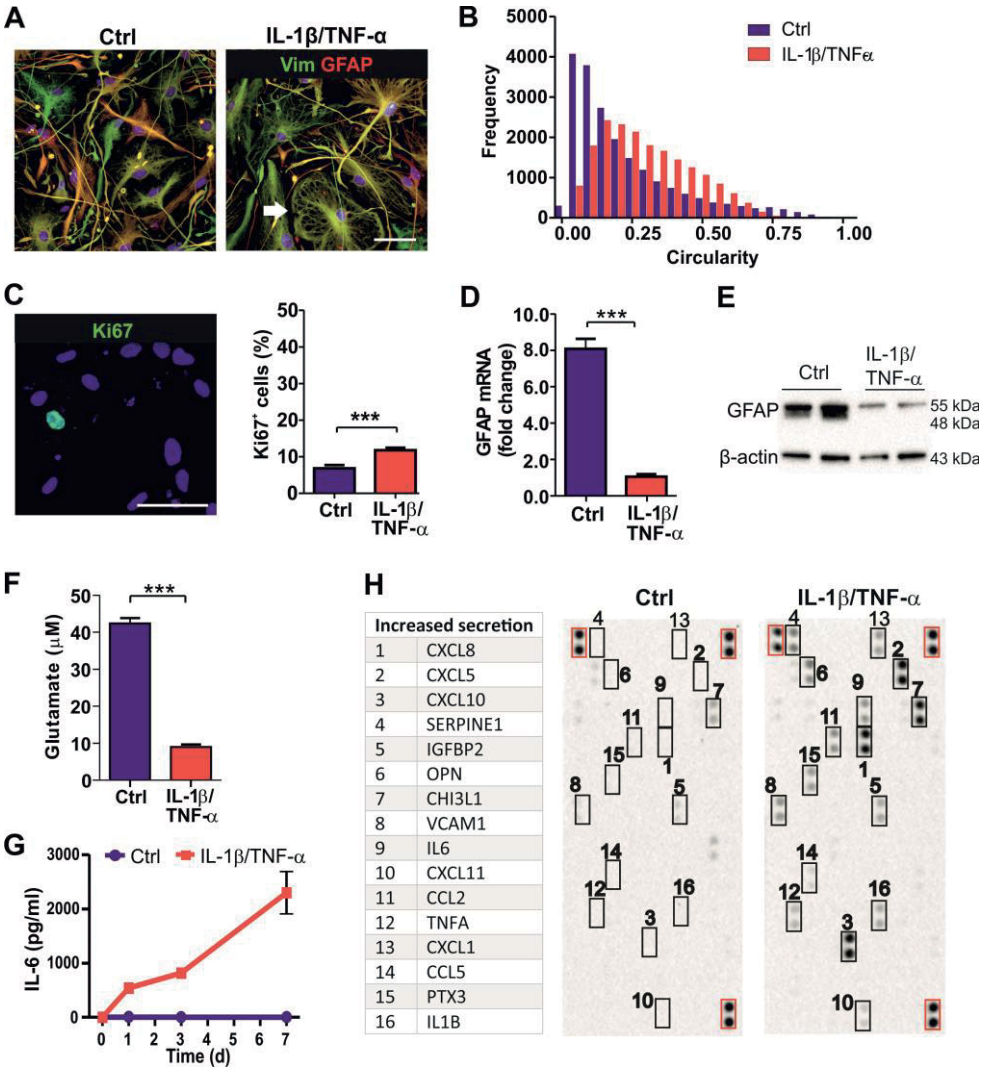

Figure 14. Stimulation of the reactive astrocyte phenotype. (A) Morphological changes in response to cytokine treatment were evident with vimentin (Vim) and GFAP staining (white arrow). (B) Astrocyte morphology was quantified from vimentin-stained samples and presented as a histogram of circularity. The bin size is 0.05, and a value of 1.0 represents a perfectly circular object. (C) Increased proliferation following cytokine treatment was determined with Ki67 staining. The DAPI nuclear stain is shown in blue, and the scale bar is 50 μm in all images. (D) Gene expression analysis showing downregulation of *GFAP* after cytokine treatment. (E) Lower GFAP protein levels in the stimulation group than in the control were also observed by Western Blot. β-actin was used as a loading control. (F) Glutamate uptake was impaired in treated astrocytes. (G) ELISA was carried out to detect IL-6 levels in the culture medium over time. (H) A proteome array was used to screen wider secretion profiles of cytokine-treated astrocytes. Factors with increased secretion are marked with a black rectangle and listed in the table. Red boxes indicate positive controls.

5.4.2 Neuron-specific effects of astrocytes

The effects of astrocytes on neuronal cells were studied by assessing secreted factors in the astrocyte-conditioned medium (ACM) and in controlled co-cultures utilizing a microfluidic device (Study **III**). First, ACM experiments were performed to investigate whether the astrocyte secretion profile was directly neurotoxic. Astrocytes were treated over 7 days as previously described, and the culture medium was refreshed; ACM was collected from control and treated astrocytes 48 h later. A viability assay of neuronal cultures after 48 h of ACM exposure verified that the secreted factors did not compromise the morphology or survival of neurons, as no significant differences were observed when compared to the control medium (Figure 15A-B). More sensitive functional measurements were performed with the MEA system. The ACM effect was studied on mature neuronal networks directly after application (acute) and at the 1 h, 4 h and 24 h time points. Functional measurements revealed that the ACM collected from both control and reactive astrocytes supported spike and burst activity over 24 h (Figure 15C-D). There were no statistically significant differences between the control (Ctrl) and reactive ACM groups. However, when compared to the control group, spike rates were increased directly after application in reactive ACM group and spike and burst rate were increased at 1 h time point in control ACM group (Figure 15 C-D).

Finally, controlled co-cultures of neurons and astrocytes were established utilizing microfluidics technology. The designed microfluidic device enabled the separation of astrocytes, neurons and their axons into different compartments that were connected via microchannels (Figure 15E). These microchannels permitted cell-to-cell contacts between neuronal axons and astrocytes and allowed fluid flow selectively across axonal and astrocyte compartments (Figure 15F-G; Study **III** Figure 6G-H). The effects of reactive astrocytes and the inflammatory milieu on axonal growth were examined in the microfluidic device. Cytokine treatment was applied solely to the astrocyte compartment (groups: Neurons [Neu]+Ctrl astrocyte [astro] and Neu+Reactive astro), and devices without astrocytes were prepared as controls (groups: Neu and Neu+IL-1β/TNF-α). After 72 h, the axonal density in their compartment was evaluated with the live stain calcein-AM (Figure 15H). Axonal density was found to be higher in the presence of cytokine-treated astrocytes than in control astrocytes (Figure 15I). These data, together with the viability and functional results, indicate that the reactive astrocyte phenotype is supportive of neurons.

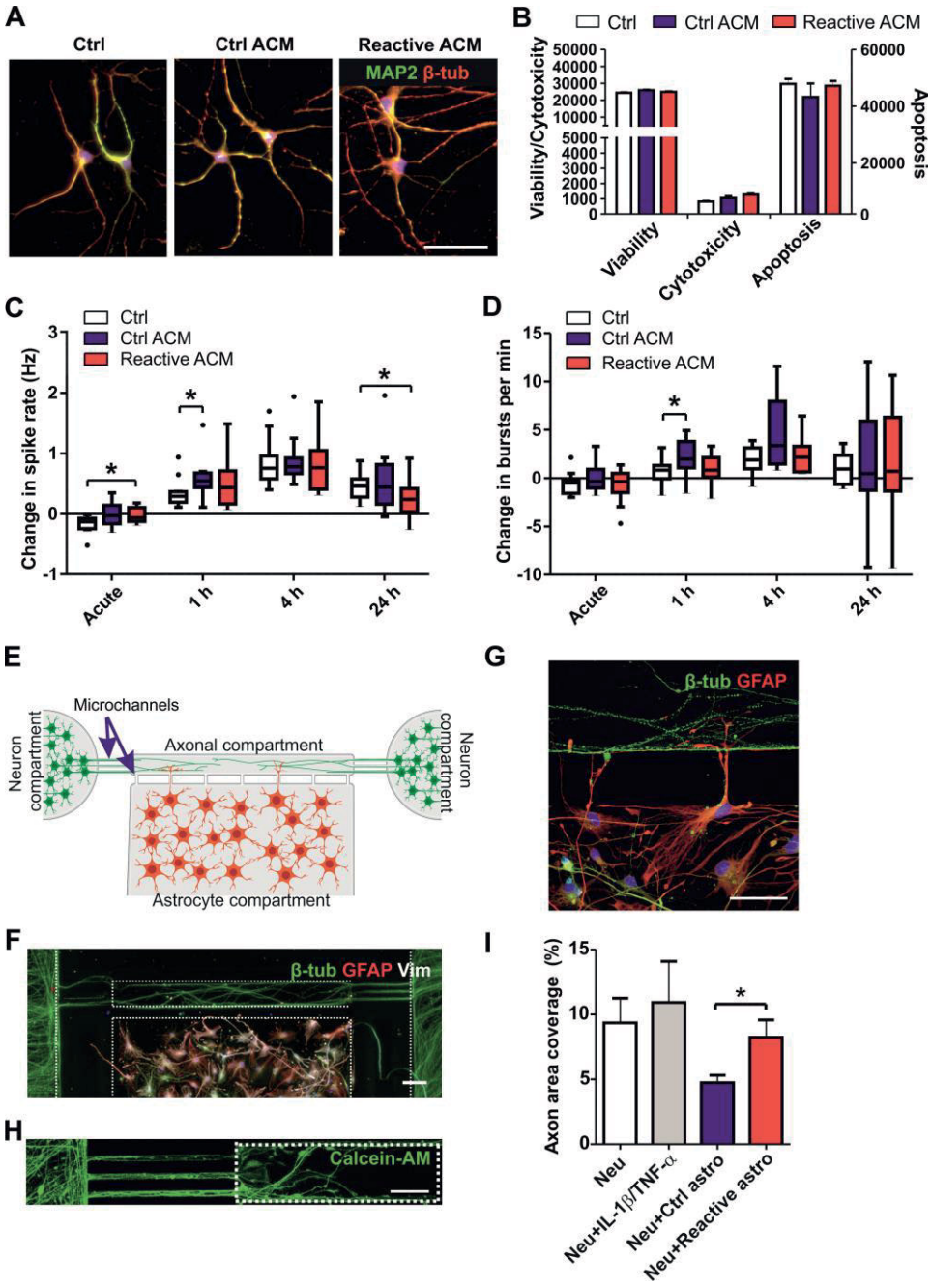

Figure 15. Neuron-specific actions of reactive astrocytes. (A) Immunocytochemical staining of neurons (MAP2+β-tubulin) treated with control medium (Ctrl), control astrocyte-conditioned medium (Ctrl ACM) or reactive ACM. (B) The viability, cytotoxicity and apoptosis of ACM-treated neurons was quantified after 48 h. (C) Functional measurements with MEA show changes in the spike rate after ACM exposure. (D) Additionally, the change in bursting activity was

evaluated following ACM treatments. Data are shown as Tukey box plots, and statistical analyses were performed with the Kruskal-Wallis test followed by the Mann-Whitney U test (*p<0.05). (E) Schematic representation of the microfluidic device used to co-culture neurons and astrocytes. (F) Neurons (β-tubulin) and astrocytes (GFAP, Vimentin) are restricted in their compartments by microchannels. (F, G) Neuronal axons and astrocyte processes can grow and interact in the axonal compartment. (H) The density of axons in the axonal compartment (white dotted box) was quantified from the calcein-AM live-stained samples. The scale bar represents 50 μm except for that in panel F, which is 100 μm. (I) Quantification of the area covered by axons in microfluidic devices containing only neurons (Neu), neurons with cytokine treatment of the astrocyte compartment (Neu+IL-1β/TNF-α), neurons and control astrocytes (Neu+Ctrl astro) and neurons and reactive astrocytes (Neu+Reactive astro). Data are presented as the mean±s.e.m. and statistical analyses were performed with independent-sample t-tests (*p<0.05).

6 DISCUSSION

6.1 Considerations of the neurosphere and adherent neuronal differentiation methods

Since the first reports on hPSC-derived neuronal cells, several differentiation methods and approaches have been developed to increase the purity of cultures and better mimic *in vivo* development (Chambers et al., 2009; Nat et al., 2007; Pasca et al., 2015; Shi, Y. et al., 2012; Zhang, S-C et al., 2001a). In the first two studies included in this thesis, neuronal cells were differentiated using two widely used methods, the neurosphere differentiation method (Study **I**) described previously by Lappalainen et al. (2010) and the adherent monolayer method with dual SMAD inhibition (Study **II**) that was modified from Shi et al. (2012) and further optimized in this thesis. The first aim of the thesis was to evaluate the outcomes of differentiation with gene and protein expression analysis.

During development, neural fate is the "default" pathway that is triggered when cells are deprived of morphogens or treated with morphogen inhibitors such as SB431542 and LDN193189 targeting the TGFβ and BMP pathways (Suzuki and Vanderhaeghen, 2015). Here, without external patterning factors, the neuronal cells from both differentiation methods first exhibited a forebrain phenotype, as determined by FoxG1 expression (Studies **I** and **II**). Cells resulting from the neurosphere differentiation method were also found to express transcripts typical of midbrain and hindbrain phenotypes (Study **I**). This can be an expected outcome, as without additional inhibition of caudalizing signals, the extended culture and passaging of hPSC-derived neural cultures in the presence of FGF2 drives them to eventually adapt caudal identities (Shi, Yichen et al., 2012; Suzuki and Vanderhaeghen, 2015). Neural induction was particularly efficient with the adherent dual SMAD inhibition method, resulting in homogenous expression of the neuroectodermal marker Pax6 in all of the studied hPSC lines (Study **II**).

The NPCs derived with both methods differentiated into neurons at similar efficiencies (Studies **I** and **II**). The proportion of neurons was over 70%, while the rest of the cultures consisted of glial cells and the remaining neural progenitors. Additionally, the timing for neurogenesis was comparable between the two methods.

However, the adherent method, which included more directed chemical induction with a variety of factors, seemed to be beneficial and promote faster differentiation. Overall, the time scale of neurogenesis reflects the prolonged development observed in humans compared to rodents. In general, the first hPSC-derived neurons are generated after one month of differentiation on average, while for example, mouse PSCs produce neurons within one week (Espuny-Camacho et al., 2013).

Cortical neurogenesis of hPSC-derived cells largely follows the temporal patterns observed *in vivo,* where the six-layered structure is generated in an inside-out manner, with deep layer neurons born first and upper layer neurons migrating past later (Molyneaux et al., 2007). Analysis of the cortical layer-specific markers in the adherent-differentiated neurons revealed expression of the early-born deep-layer markers Ctip2 and Tbr1 (Study **II**). The upper layer marker Brn2 was present at the analyzed time points, but very few Satb2-positive cells were detected. Satb2 is usually detected in very late-born cortical neurons, and in fact, earlier reports on hPSC-derived neurons have reported upregulation of Satb2 even as late as after 100 days of differentiation (Pasca et al., 2015; Shi, Y. et al., 2012).

The emergence of endogenous astrocytes was also studied because they are known to arise from the common neural progenitor pool as neurons and are important for the support of neuronal maturation (Johnson et al., 2007; Qian et al., 2000). In both methods, the proportion of astrocytes increased in long-term culture (Studies **I** and **II**), confirming other previous reports on hPSC-derived cultures (Espuny-Camacho et al., 2013; Pasca et al., 2015). The neurosphere method produced 15% GFAP-positive astrocytes after a prolonged differentiation period of 15 wks, while the adherent method produced 20% astrocytes after 11 wks of differentiation as detected with the same marker. Thus, it seems that with the studied hPSC lines, the adherent protocol was more efficient at producing astrocytes. Additionally, as GFAP is not an optimal marker for astrocytes, the proportions of S100β-positive astrocytes and astrocyte progenitors were also quantified (Study **II**). A considerably larger portion of cells, 38%, were S100β-positive after 11 wks of adherent differentiation, indicating that GFAP should not be used as the sole marker for evaluating the astrocyte content in cultures, as suggested by several other studies (Krencik, Robert and Ullian, 2013; Lundin et al., 2018).

In conclusion, some temporal differences were observed in the differentiation efficiencies of the two methods. Additionally, the original publications (Studies **I** and **II**) revealed variation in the differentiation capacity depending on the hPSC line. This is widely acknowledged in the literature showing that the intrinsic differentiation propensity of a particular hPSC line may affect the result (Kim et al.,

2010; Osafune et al., 2008; Toivonen et al., 2013). Cell line-specific properties can be overcome, to some extent, with selection steps, such as rosette isolation and FACS sorting, which may improve the consistency and help remove undesired cell types (Muratore et al., 2014). Manipulation of signaling pathways with dual SMAD inhibition has been effectively shown to reduce the variability between cell lines during differentiation (Kim et al., 2010), and this strategy has been applied to both adherent and suspension cultures (Chambers et al., 2009; Pasca et al., 2015). Additionally, in adherent monolayer cultures, the cells are better exposed to an even distribution of growth factors and nutrients, whereas in aggregates, the increasing size creates concentration gradients (Muratore et al., 2014). Due to the vast number of differentiation protocols currently available for hPSC-derived neurons, it seems unlikely that any standardization will follow. Additionally, different types of protocols may be practical for particular applications. For example, 3D suspension cultures such as neurospheres and organoids may be more suited for studying the morphology and cytoarchitecture of the cells. On the other hand, adherent cultures achieved with chemical induction are often more homogenous and scalable.

6.2 Achievement of mature functional activity in hPSC-derived neuronal cultures

Understanding the genetic and protein-level characteristics of hPSC-derived neuronal cultures is important. To utilize these cells for studying human development or disease, their functional properties need to be determined. The second aim of the thesis was to assess functional maturation under different culture conditions. With the current differentiation protocols presented in the first two studies of this thesis, the development of functionally active networks on MEA was strikingly different between the two methods (Studies **I** and **II**). While the neurosphere-differentiated cultures presented merely uncorrelated spikes and bursts, the adherent-differentiated cultures developed highly correlated network bursting activity. Despite these different innate basal activities, functional maturation could be promoted with long-term differentiation and optimization of culture conditions.

6.2.1 Prolonged differentiation time for promotion of functional maturation

It is well established that human brain development follows a very different temporal pattern from that of rodents, and the final maturation of neuronal cells takes months if not years (Anderson, S. and Vanderhaeghen, 2014). Therefore, the aim of Study **I** was to address how functional properties on MEAs change during the long-term differentiation of hPSC-derived neuronal cultures. Interestingly, the mature bursting activity was increased in neurosphere cultures differentiated for a prolonged period of 15 wks compared to that in cultures differentiated for the standard 8 wks. We also observed a correlation between burst features: increased spike frequency in the burst resulted in a shorter burst duration. The prolonged differentiation time had opposing effects on these features in the two studied hPSC lines. The studied hESC line showed burst compaction after prolonged differentiation, a phenomenon that has since been described in other studies (Tourigny et al., 2019). This could potentially result from the maturation of membrane ion channel composition, allowing faster repetitive action potential firing (Weick, 2016). The studied hiPSC line, however, did not show the same behavior, which could in part relate to the difficulty of maintaining hPSC-derived cultures for extended times. During prolonged expansion, undesired cell types may arise in the culture and affect development (Muratore et al., 2014).

It is tempting to speculate that the variation in the amount of endogenously generated astrocytes between the two studied hPSC lines described in the original publication (Study **I**) could partially affect the functional maturation. It has been demonstrated that astrocyte metabolic functions, glutamate and potassium uptake, are critical for the recurrent bursting activity of neurons (Karus et al., 2015). In mature synapses, astrocyte endfeet are known to enshroud and control synapses forming the so-called tripartite synapse (Araque, Alfonso et al., 2014). Additionally, in developing networks, astrocyte-secreted factors and direct contact can control synapse formation and maturation (Clarke and Barres, 2013). Both rodent and human astrocytes have been shown to induce synapse maturation and increase the excitability of hPSC-derived neurons, further supporting this viewpoint (Klapper et al., 2019; Odawara et al., 2014).

In conclusion, extended culture times would be a natural approach for the functional maturation of neurons, and previous studies have shown successful long-term culture for up to one year with the help of a rodent astrocyte feeder layer (Odawara et al., 2016). However, experiments involving the observation of hPSC-derived neuron maturation for many months to years is not the most practical

approach considering the possible medical applications, such as drug screening and disease modeling.

6.2.2 Use of the Laminin-521 substrate for development of functionally active cortical networks

Our research group has previously shown that α5 laminin substrates can improve the attachment, outgrowth and functionality of neurosphere-differentiated cells upon plating in adherent culture on polystyrene plastic wells and MEA surfaces (Hyysalo et al., 2017). Our aim was to establish LN521 as a culture substrate for adherent neuronal differentiation (Study **II**), replacing the animal-derived Matrigel and mouse laminin substrates, which suffer from batch-to-batch variation (Muratore et al., 2014; Niclis et al., 2017).

Over the years, new approaches have been developed to improve hPSC culture and the functionality of their neural derivatives. Focus has been largely on specific medium compositions, growth factors and small molecules (Bardy et al., 2015; Chambers et al., 2009; Chen et al., 2011; Niclis et al., 2017). However, ECM-cell interactions have proven to play an important role in providing signals guiding the cell phenotype (Hagbard et al., 2018). Here, the hPSCs were cultured according to the protocol described by Hongisto et al. (2017) utilizing feeder-free conditions on the LN521 substrate, which has been shown to support the pluripotent state according to other reports (Lu et al., 2014; Niclis et al., 2017). The following neural induction on Matrigel or LN521 and the neural differentiation on mouse laminin or LN521 equally supported the growth and morphological maturation of hPSC-derived neurons and astrocytes. Previous studies have demonstrated the suitability of the α5 laminin substrates LN521 and LN511 in dopaminergic neuron differentiation (Doi et al., 2014; Lu et al., 2014; Niclis et al., 2017) and LN521 in astrocyte differentiation (Lundin et al., 2018). Our results further confirm that the LN521 substrate is suitable for cortical neural differentiation. Furthermore, it is encouraging that the same substrate could be used for both hPSC culture and subsequent neural differentiation without undesired pluripotent cells after neural induction. Better defined culture components, such as LN521, are preferred, especially in clinical research aimed at cell therapy, but basic research can also benefit from increased experimental reproducibility.

The most remarkable difference between the mouse laminin- and LN521-differentiated cultures was in functional development. The functional activity of

neurons differentiated on mouse laminin was very modest compared to that of networks differentiated on LN521. Compared to the mouse laminin differentiated neuronal cultures, the LN521-differentiated neurons presented a higher percentage of active electrodes, higher spike rate and higher burst rate over the follow-up period. This finding was in line with the group's previous results obtained using neurosphere-differentiated cultures (Hyysalo et al., 2017). A recent publication has shed light on the possible mechanism of LN521 and neuron functionality. Omar and colleagues (2017) reported that laminin α5 regulates synapse stability during postnatal CNS development in mice (Omar et al., 2017). They were able to show spine stabilization of laminin α5-deficient neurons with the application of LN521 but not with LN111, the major constituent that is also in mouse laminin. Furthermore, laminin α5 was required for normal synapse density and function. In mouse hippocampal neurons, laminin α5 is deposited at the synapse by postsynaptic dendrite, and it acts through the integrin α3β1 adhesion receptor (Omar et al., 2017). Determining whether the observed LN521 effect is mediated via a similar mechanism in the hPSC-derived neuronal network would be an interesting direction for future studies.

In summary, the superiority of LN521 over mouse laminin has now been verified with both the neurosphere method (Hyysalo et al., 2017) and the adherent differentiation with dual SMAD inhibition method. For LN521 adherent-differentiated neurons, the level of activity corresponds with that of neurons resulting from the co-culture of rodent astrocytes (Frega et al., 2017; Odawara et al., 2016), and LN521 is therefore considered the most suitable substrate for supporting functional maturation of hPSC-derived networks without externally applied astrocytes in fully humanized conditions.

6.2.3 Inhibitory system in hPSC-derived networks

Inhibitory neurons expressing GABA and GAD67 were present in the neuronal cultures, and we were interested in elucidating their role in maintaining the excitatory-inhibitory balance of the network. Calcium imaging experiments showed that in the neurosphere-differentiated cultures, a decreasing proportion of neurons showed an excitatory response to GABA application after prolonged differentiation, which is suggestive of functional maturation (Study **I**). In line with this, changes in the expression of the chloride transporters NKCC1 and KCC2 were observed. During early development, high intracellular chloride concentrations in neurons,

mainly due to NKCC1 transporter expression, results in depolarization upon GABA binding to its receptor (Ben-Ari et al., 2007; Ben-Ari et al., 2012). Increasing KCC2 expression during development eventually causes changes in the chloride balance, allowing the hyperpolarizing inhibitory effect of GABA. Our data are consistent with previous patch clamp studies on hPSC-derived neurons showing a reduction in intracellular chloride levels and changes in chloride transporter expression as a result of prolonged differentiation (Livesey et al., 2014).

The actual inhibitory input on network activity was investigated with adherent-differentiated neurons (Study **II**). The actions of a GABAergic agonist and antagonist were evaluated once the synchronous network level activity developed on the MEA. The presence of GABA receptors was confirmed by the application of GABA, which silenced the network bursts, leaving only a low level of asynchronous spiking. The $GABA_A$ receptor antagonist gabazine blocked the inhibitory GABAergic networks, increasing the total activity. These results demonstrate that cortical networks exhibit a functional inhibitory system that regulates their activity. GABAergic signaling emerges before glutamatergic signaling during development and is thus a potential player in the initiation of network activity, a theme that is widely discussed in the literature (Allène et al., 2008; Ben-Ari et al., 2007; Garaschuk et al., 2000). The presence or absence of interneurons has been speculated to affect the initiation of robust network activity in hPSC-derived cultures (Livesey et al., 2016; Weick, 2016). Previous reports on hPSC-derived cortical networks have, however, shown that inhibitory input is not necessary for the development of network oscillations (Kirwan et al., 2015; Mäkinen et al., 2018; Tukker et al., 2018). Nevertheless, our results, along with those of others, have demonstrated that inhibitory GABAergic systems can develop and modulate the synchronous activity of hPSC-derived networks (Ishii et al., 2017; Izsak et al., 2019; Odawara et al., 2016).

Given these different observations, the amount and maturity of interneurons produced with various differentiation methods should be carefully considered, especially in disease modeling, as perturbation of excitatory-inhibitory balance is a key feature of numerous diseases (Blaesse et al., 2009; Livesey et al., 2016).

6.3 Evaluation of the *in vitro* activity of human and rodent networks

The third aim of this thesis was to compare the network activity of hPSC-derived neurons differentiated via the adherent protocol with those of rat cortical cultures,

often referred to as the "gold standard" for MEA recordings (Study **II**). One drawback prohibiting wider utilization of hPSC-derived neurons instead of rat cortical neurons is the time required for the detection of robust network activity. Here, we found that the activities of the pre-differentiated hPSC-derived neurons and rat cortical neurons developed in comparable time frames, as early as 3-4 wks after plating on MEAs. Very few studies have previously shown direct network-level comparisons between human and rat neurons *in vitro*. Tukker and colleagues (2016) followed the activity development of rat cortical cultures and commercially available hiPSC-derived neurons for 9 days on MEA (Tukker et al., 2016). During that time, they concluded that these two networks showed comparable results with respect to the numbers of active wells, electrodes and spikes. However, after only 9 days, they showed no bursting or synchronous activity (Tukker et al., 2016). Napoli and colleagues (2015) compared midgestational human fetal neurons and E18 rat neurons on MEAs (Napoli and Obeid, 2016). Rat neurons produced robust network activity after 10 days on MEA, exhibiting numerous active electrodes and high spike rates, while human fetal neurons showed a lower level of activity even after 40 days. However, they noted that human-derived cells might be less mature than rodent neurons and depend more on glial support and extracellular environment control (Napoli and Obeid, 2016).

The stages of activity development were similar between the hPSC-derived and rat networks originating as asynchronous spikes, followed by more abundant spike trains and, finally, organization into highly synchronous network bursts (Study **II**). Thus, achieving human cortical type network bursting is now possible in the same time period as that required for rat cortical neurons. Until recently, synchronously active hPSC-derived neuronal networks were not often reported. Despite variations in cell culture protocols, measurement methods and data analyses, network bursting has been described to arise in a similar time frame and present comparable frequencies in most previous publications (Frega et al., 2017; Izsak et al., 2019; Kirwan et al., 2015; Kuijlaars et al., 2016; Odawara et al., 2016; Odawara et al., 2018; Tukker et al., 2018). Odawara and colleagues (2016) first reported a very long time period, up to 20 wks, for the complete maturation of networks. Later, they further refined culture systems showing network activity as early as 5 wks after beginning to measure (Odawara et al., 2018). More recently, Izsak and colleagues (2019) presented network bursting after 2 wks on MEA. Clearly, the time frame in which robust network activity can be achieved with hPSC-derived neurons is closing in on that achievable with their *in vitro* rodent counterparts.

Distinct differences between hPSC-derived and rat cultures were also observed in our experiments (Study **II**). Principal component analysis involving several spike, burst and network features demonstrated variation in the activity of the two network types. Segregation of data into separate clusters could indicate differences in the maturation stage or species-specific differences between the hPSC-derived and rat networks. Previous gene expression analyses point to the similarities of hPSC-derived neurons and midgestational (~19-24 wks) human fetuses, which are known to resemble late-stage rodent embryos (embryonic development days 18-23) (Pasca et al., 2015; Stein et al., 2014; Weick, 2016). Distinct functional characteristics may arise for example from differing ion channel, receptor and transporter expression levels specific to maturation stage. On the other hand, species differences between human- and rodent-expressed genes are also acknowledged (Masjosthusmann et al., 2018; Xu et al., 2018). Furthermore, differences in the neuron cytoarchitecture or, for example, the location or spreading of proteins can largely influence neuron functional properties and responses to external conditions (Beaulieu-Laroche et al., 2018). Investigation of the maturation stage and interspecies differences between the human and rodent models can help validate the utility of hPSC-derived networks as platforms for *in vitro* studies including human neurological disorders.

6.4 Development of *in vitro* models for astrogliosis

The fourth aim of the thesis focused directly on astrocytes, specifically on how they respond to specific inflammatory conditions and how their response affects neuronal viability and function (Study **III**). In neuropathological conditions, the astrocyte response depends on the degree and type of stimulation and is therefore highly context dependent (Liddelow, S. A. et al., 2017). In study **III**, astrocytes were treated with cytokines IL-1β and TNF-α for seven days to mimic neuroinflammatory conditions, in which microglia activation and cytokine secretion stimulate astrogliosis (Clausen et al., 2008; Shinozaki et al., 2017). Because the biological characterization of hPSC-derived reactive astrocyte models is limited, the most common properties known to be involved in astrogliosis were evaluated. Detailed characterization revealed considerable changes in the astrocyte intermediate filament network, proliferation, homeostatic role and secretion profile, suggesting a change to a reactive state. Most other reports on stem cell-derived reactive astrocytes have been published within the past few years (Lundin et al., 2018; Perriot et al., 2018; Ponath et al., 2018; Roybon et al., 2013; Santos et al., 2017; Tcw et al., 2017). These

publications are still mostly focused on treatment with a limited set of stimulants and analysis of a few well-characterized inflammatory factors from astrocytes. Nevertheless, some interesting observations have already been made regarding hiPSC-derived astrocytes. First, they are able to respond to cytokine treatments and are thus immunocompetent (Lundin et al., 2018; Perriot et al., 2018; Roybon et al., 2013). Second, they are sensitive to inflammatory treatment in a time- and dose-dependent manner (Lundin et al., 2018; Tcw et al., 2017), and co-stimulation with different cytokines may elicit synergistic effects (Perriot et al., 2018). Third, the percentage of astrocytes responding to the stimulation may vary depending on the stimulant used and the analyzed factors describing activation (Santos et al., 2017). Together, these data elucidate the complex nature of astrocyte reactivation in hPSC models.

Interestingly, in our study, the neuron-specific effects of astrocytes were mostly beneficial, and no directly toxic responses were reported (Study **III**). Analysis was based on astrocyte-secreted factors, and the collected ACM did not compromise neuronal viability during the 48 h of exposure. Previous work involving different combinations of astrocyte stimulants and varying exposure times demonstrated a decreased number of neurons and directly toxic effects on human neurons (Liddelow, S. A. et al., 2017; Santos et al., 2017). Continuation of this work would require careful consideration of stimulants, optimization of exposure times and even concentration of the factors found in ACM. Showing responses of hPSC-derived neurons has been challenging and may need more sensitive detection methods. One potential approach is the analysis of neuronal functionality. In this setup, both control and reactive astrocyte ACM were shown to induce transient increases in spike and burst rates, further demonstrating that astrocytes do not secrete significant levels of detrimental factors that would silence network activity (Study **III**). ACM has been previously shown to promote functional activity on MEA and even more so when astrocytes are in direct contact with the neurons (Fukushima et al., 2016; Odawara et al., 2014). Due to a lack of previous studies, an interesting future direction would be co-culturing reactive astrocytes and neurons on MEAs; however, selective astrocyte stimulation and sustainment of a reactive phenotype should be controlled.

Astrocyte direct contact and ACM-mediated influence on axonal growth were studied under controlled conditions utilizing a microfluidic platform (Study **III**). With microfluidic devices, it is possible to create compartmentalized culture environments and study specific cell-to-cell interactions (Neto et al., 2016; Ristola et al., 2019; Sarkar et al., 2018; Taylor et al., 2005). Here, the utilized microfluidic device

isolated neuronal and astrocyte somas and allowed the study of axonal growth and axonal interaction with astrocytes. At the same time, fluidic isolation provided by the narrow microtunnels connecting cell areas restricted fluid flow and allowed selective stimulation of astrocytes. The inflammatory niche created by stimulated astrocytes was supportive of axonal growth, confirming the polarization of astrocytes into a neurosupportive phenotype. The interactions of neurons and astrocytes in inflammatory conditions elucidated by the controlled microfluidic platform have not been previously described in the literature. However, an interesting report from Park and colleagues (2018) presented the use of microfluidics technology to study the recruitment of microglia and their toxic actions on a mixed neuron-astrocyte culture in an Alzheimer's disease model. Creating more elaborate culture setups in which the complexity of the brain can be mimicked and the interactions of several contributing cell types can be dissected will be the direction of future studies.

6.5 Future perspectives

Evaluating the properties of the developed stem cell models and how they compare with the validated rodent models provides important information for future studies. The last chapter follows the major topics discussed in this thesis and provides some important critiques and options for future avenues. These are the four underlined points: 1) differentiation and maturation of hPSC-derived neurons, 2) increasing functional activity of neurons, 3) role of astrocytes in neuronal signaling in health and disease, and 4) complex co-culture settings for *in vitro* modeling.

The hPSC-derived neuronal cells generated with various methods, including those described here in studies **I** and **II**, represent fetal-stage cells that, according to gene expression analysis, do not mature even after months of *in vitro* culture to match the adult expression profile (Stein et al., 2014). Considering this imperfect match is important, especially when applying hiPSC-derived neurons for modeling late-onset neurodegenerative diseases, such as Alzheimer's disease and Parkinson's disease. An increasing number of papers are carefully describing the plausible pathophysiological phenotypes of disease-specific hiPSC-derived neurons (Brennand et al., 2015). MEA technology is also attracting interest as a high-throughput method for characterizing functional deficits (García-León et al., 2018; Mehta et al., 2018; Wakeman et al., 2017). It will be important to verify how the observed functional changes in these developing stage networks relate to the network dysfunctions observed in the adult and aging brain.

Because hPSC-derived networks mimic many of the cellular and functional properties of *in vivo* networks, as shown in studies **I** and **II**, they provide a valuable tool for investigating both fundamental questions in human developmental biology as well as mechanisms of disease. Further development of culture methods has resulted in even better resemblance. Improvements in culture conditions utilizing an increasing number of different neuroactive factors and high glucose levels may eventually risk altering normal development and lead to unnatural, almost epileptic firing. Chronic exposure to growth factors is reported to change, for example, ion channel and transporter expression (Lepski et al., 2013; Livesey et al., 2014). These issues should be considered when designing culture conditions for particular experiments.

Astrocytes play an important role in neurodevelopment by promoting synaptogenesis and synapse remodeling (Clarke and Barres, 2013) and therefore provide perhaps a more natural option for the support of neuron growth and functionality. The development of neurons and astrocytes is intertwined, and astrocytes provide important cues for neuronal differentiation and maturation and *vice versa* (Baldwin and Eroglu, 2017; Stogsdill et al., 2017). In our culture systems (Studies **I** and **II**), astrocytes were generated endogenously, and they developed alongside neurons. Adding rodent astrocytes, especially in later stages of neuronal differentiation, is not the most physiological approach (Klapper et al., 2019). Despite the many benefits of astrocyte co-culture, it is also good to keep in mind the powerful metabolic role of astrocytes. They can protect neurons against toxicants and mask defective neuronal phenotypes in models of neurodegenerative disease or insult (Engle et al., 2018; Tieu et al., 2001).

Astrocyte reactivation is dominant in all neurodegenerative diseases and injuries of the CNS. We presented a detailed characterization of hPSC-derived reactive astrocytes in one set of conditions (Study **III**). According to previous rodent work, it is now clear that astrocyte reactivation does not represent a single cellular phenotype but rather a mixture of two or more unidentified reactive astrocyte polarization states (Liddelow, Shane A. and Barres, 2017). How the reactivation of hiPSC-derived astrocytes corresponds to the extreme astrogliosis observed in *vivo* is not currently known. The use of more elaborate gene expression panels or single-cell RNA sequencing to classify different reactive astrocyte phenotypes and how they match the *in vivo* setting could clarify the validity of hiPSC models. It is unclear whether astrocytes are beneficial or detrimental under pathological circumstances and how they interact with other CNS cells. These questions will be at the forefront of future studies.

To our knowledge, study **III** of this thesis was the first report showing a controlled co-culture setting involving human stem cell-derived neurons, astrocytes and inflammatory components utilizing microfluidics technology. Including astrocytes and possibly other CNS cells, such as oligodendrocytes and microglia together with neurons, will make the *in vitro* model more credible and *in vivo*-like. Cytoarchitecturally intricate cultures such as brain organoids could also provide an interesting possibility for co-cultures. Furthermore, organoids with different cell types or brain region-specific cells can be combined into so-called brain assembloids and even organized in a controlled way using microfluidic devices for studying circuitries (Amin and Paşca, 2018; Hartlaub et al., 2019; Kelava and Lancaster, 2016).

7 SUMMARY AND CONCLUSIONS

This research aimed to evaluate the potential of hPSC-derived neuronal cells to form mature functional networks, which are essential for hPSC model utility in neuroscience applications. Additionally, the role of astrocytes in the neuronal networks during normal and inflammatory conditions was considered. Based on these results, the following conclusions can be drawn:

1. Both of the tested differentiation methods, neurosphere and adherent culture, recapitulate the developmental events occurring *in vivo*. Directed chemical induction can accelerate development and improve culture homogeneity over more spontaneous differentiation. The suitability of the selected method should be considered based on target applications.

2. The extended differentiation time of hPSC-derived networks increases the share of endogenously formed astrocytes and promotes the development of functionally mature activity types. Furthermore, a specific LN521 culture substrate supports the emergence of electrical activity and stabilizes the maintenance of functional networks, providing more representable, completely human-specific models.

3. The similar time frames and stages of activity development between hPSC-derived neuronal cultures and rodent counterparts validates the stem cell systems for studying network biology. The observed variation in the activity features between rodents and humans can be linked to maturation stage or interspecies differences. This could provide new insights into the low predictive value of rodent models for human outcomes.

4. Reactivation of healthy hPSC-derived astrocytes shows many characteristics distinctive of astrogliosis and the astrocytes transform into a neurosupportive phenotype, inducing neuronal responses at the functional level. Astrocytes can be combined in a controlled co-culture

model together with neurons to assess cell interactions during inflammation. Experiments combining several CNS cell types under disease-specific settings to better mimic *in vivo* conditions are warranted in future studies.

REFERENCES

Allaman, I., Belanger, M. and Magistretti, P. J. (2011). Astrocyte-Neuron Metabolic Relationships: For Better and for Worse. *Trends Neurosci.* 34, 76-87.

Allen, N. J. (2014). Astrocyte Regulation of Synaptic Behavior. *Annu. Rev. Cell Dev. Biol.* 30, 439-463.

Allen, N. J., Bennett, M. L., Foo, L. C., Wang, G. X., Chakraborty, C., Smith, S. J. and Barres, B. A. (2012). Astrocyte Glypicans 4 and 6 Promote Formation of Excitatory Synapses Via GluA1 AMPA Receptors. *Nature* 486, 410-414.

Allène, C., Cattani, A., Ackman, J. B., Bonifazi, P., Aniksztejn, L., Ben-Ari, Y. and Cossart, R. (2008). Sequential Generation of Two Distinct Synapse-Driven Network Patterns in Developing Neocortex. *J. Neurosci.* 28, 12851-12863.

Amin, N. D. and Paşca, S. P. (2018). Building Models of Brain Disorders with Three-Dimensional Organoids. *Neuron* 100, 389-405.

Anderson, M. A., Burda, J. E., Ren, Y., Ao, Y., O'Shea, T. M., Kawaguchi, R., Coppola, G., Khakh, B. S., Deming, T. J. and Sofroniew, M. V. (2016). Astrocyte Scar Formation Aids Central Nervous System Axon Regeneration. *Nature* 532, 195-200.

Anderson, S. and Vanderhaeghen, P. (2014). Cortical Neurogenesis from Pluripotent Stem Cells: Complexity Emerging from Simplicity. *Curr. Opin. Neurobiol.* 27, 151-157.

Araque, A., Parpura, V., Sanzgiri, R. P. and Haydon, P. G. (1999). Tripartite Synapses: Glia, the Unacknowledged Partner. *Trends Neurosci.* 22, 208-215.

Araque, A., Carmignoto, G., Haydon, P. G., Oliet, S. H. R., Robitaille, R. and Volterra, A. (2014). Gliotransmitters Travel in Time and Space. *Neuron* 81, 728-739.

Arichi, T., Whitehead, K., Barone, G., Pressler, R., Padormo, F., Edwards, A. D. and Fabrizi, L. (2017). Localization of Spontaneous Bursting Neuronal Activity in the Preterm Human Brain with Simultaneous EEG-fMRI. *Elife* 6,.

Avior, Y., Sagi, I. and Benvenisty, N. (2016). Pluripotent Stem Cells in Disease Modelling and Drug Discovery. *Nat. Rev. Mol. Cell Biol.* 17, 170-182.

Baldwin, K. T. and Eroglu, C. (2017). Molecular Mechanisms of Astrocyte-Induced Synaptogenesis. *Curr. Opin. Neurobiol.* 45, 113-120.

Bardy, C., Van Den Hurk, M., Eames, T., Marchand, C., Hernandez, R. V., Kellogg, M., Gorris, M., Galet, B., Palomares, V., Brown, J. et al. (2015). Neuronal Medium that Supports Basic Synaptic Functions and Activity of Human Neurons in Vitro. *Proc. Natl. Acad. Sci. U. S. A.* 112, E2725-E2734.

Baumann, J., Gassmann, K., Masjosthusmann, S., DeBoer, D., Bendt, F., Giersiefer, S. and Fritsche, E. (2016). Comparative Human and Rat Neurospheres Reveal Species Differences in Chemical Effects on Neurodevelopmental Key Events. *Arch. Toxicol.* 90, 1415-1427.

Bean, B. P. (2007). The Action Potential in Mammalian Central Neurons. *Nat. Rev. Neurosci.* 8, 451-465.

Beaulieu-Laroche, L., Toloza, E. H. S., van der Goes, M., Lafourcade, M., Barnagian, D., Williams, Z. M., Eskandar, E. N., Frosch, M. P., Cash, S. S. and Harnett, M. T. (2018). Enhanced Dendritic Compartmentalization in Human Cortical Neurons. *Cell* 175, 643-651.e14.

Ben Haim, L., Carrillo-de Sauvage, M., Ceyzériat, K. and Escartin, C. (2015). Elusive Roles for Reactive Astrocytes in Neurodegenerative Diseases. *Front Cell Neurosci* 9, 278.

Ben-Ari, Y. (2002). Excitatory Actions of Gaba during Development: The Nature of the Nurture. *Nat. Rev. Neurosci.* 3, 728-739.

Ben-Ari, Y., Gaiarsa, J., Tyzio, R. and Khazipov, R. (2007). GABA: A Pioneer Transmitter that Excites Immature Neurons and Generates Primitive Oscillations. *Physiol. Rev.* 87, 1215-1284.

Ben-Ari, Y., Khalilov, I., Kahle, K. T. and Cherubini, E. (2012). The GABA Excitatory/Inhibitory Shift in Brain Maturation and Neurological Disorders. *Neuroscientist* 18, 467-486.

Blaesse, P., Airaksinen, M. S., Rivera, C. and Kaila, K. (2009). Cation-Chloride Cotransporters and Neuronal Function. *Neuron* 61, 820-838.

Blanco-Suárez, E., Caldwell, A. L. M. and Allen, N. J. (2017). Role of Astrocyte-Synapse Interactions in CNS Disorders. *J. Physiol. (Lond.)* 595, 1903-1916.

Blankenship, A. G. and Feller, M. B. (2010). Mechanisms Underlying Spontaneous Patterned Activity in Developing Neural Circuits. *Nat. Rev. Neurosci.* 11, 18-29.

Bootman, M. D., Rietdorf, K., Collins, T., Walker, S. and Sanderson, M. (2013). Ca2+-Sensitive Fluorescent Dyes and Intracellular Ca2+ Imaging. *Cold Spring Harb Protoc* 2013, 83-99.

Borghese, L., Dolezalova, D., Opitz, T., Haupt, S., Leinhaas, A., Steinfarz, B., Koch, P., Edenhofer, F., Hampl, A. and Brüstle, O. (2010). Inhibition of Notch Signaling in Human Embryonic Stem Cell-Derived Neural Stem Cells Delays G1/S Phase Transition and Accelerates Neuronal Differentiation in Vitro and in Vivo. *Stem Cells* 28, 955-964.

Brennand, K. J., Marchetto, M. C., Benvenisty, N., Brüstle, O., Ebert, A., Izpisua Belmonte, J. C., Kaykas, A., Lancaster, M. A., Livesey, F. J., McConnell, M. J. et al. (2015). Creating Patient-Specific Neural Cells for the in Vitro Study of Brain Disorders. *Stem Cell Reports* 5, 933-945.

Budday, S., Steinmann, P. and Kuhl, E. (2015). Physical Biology of Human Brain Development. *Front Cell Neurosci* 9, 257.

Buzsáki, G., Anastassiou, C. A. and Koch, C. (2012). The Origin of Extracellular Fields and Currents--EEG, ECoG, LFP and Spikes. *Nat. Rev. Neurosci.* 13, 407-420.

Canals, I., Ginisty, A., Quist, E., Timmerman, R., Fritze, J., Miskinyte, G., Monni, E., Hansen, M. G., Hidalgo, I., Bryder, D. et al. (2018). Rapid and Efficient Induction of Functional Astrocytes from Human Pluripotent Stem Cells. *Nat. Methods* 15, 693-696.

Carpenter, A. E., Jones, T. R., Lamprecht, M. R., Clarke, C., Kang, I. H., Friman, O., Guertin, D. A., Chang, J. H., Lindquist, R. A., Moffat, J. et al. (2006). CellProfiler: Image Analysis Software for Identifying and Quantifying Cell Phenotypes. *Genome Biol.* 7,.

Chambers, S. M., Fasano, C. A., Papapetrou, E. P., Tomishima, M., Sadelain, M. and Studer, L. (2009). Highly Efficient Neural Conversion of Human ES and iPS Cells by Dual Inhibition of SMAD Signaling. *Nat. Biotechnol.* 27, 275.

Charlesworth, P., Cotterill, E., Morton, A., Grant, S. G. N. and Eglen, S. J. (2015). Quantitative Differences in Developmental Profiles of Spontaneous Activity in Cortical and Hippocampal Cultures. *Neural Dev* 10,.

Chen, G., Gulbranson, D. R., Hou, Z., Bolin, J. M., Ruotti, V., Probasco, M. D., Smuga-Otto, K., Howden, S. E., Diol, N. R., Propson, N. E. et al. (2011). Chemically Defined Conditions for Human iPSC Derivation and Culture. *Nat. Methods* 8, 424-429.

Chinchalongporn, V., Koppensteiner, P., Prè, D., Thangnipon, W., Bilo, L. and Arancio, O. (2015). Connectivity and Circuitry in a Dish Versus in a Brain. *Alzheimers Res Ther* 7, 44.

Christopherson, K. S., Ullian, E. M., Stokes, C. C. A., Mullowney, C. E., Hell, J. W., Agah, A., Lawler, J., Mosher, D. F., Bornstein, P. and Barres, B. A. (2005). Thrombospondins are Astrocyte-Secreted Proteins that Promote CNS Synaptogenesis. *Cell* 120, 421-433.

Chung, C. Y., Khurana, V., Auluck, P. K., Tardiff, D. F., Mazzulli, J. R., Soldner, F., Baru, V., Lou, Y., Freyzon, Y., Cho, S. et al. (2013). Identification and Rescue of A-Synuclein Toxicity in Parkinson Patient-Derived Neurons. *Science* 342, 983-987.

Clarke, L. E. and Barres, B. A. (2013). Emerging Roles of Astrocytes in Neural Circuit Development. *Nat. Rev. Neurosci.* 14, 311-321.

Clausen, B. H., Lambertsen, K. L., Babcock, A. A., Holm, T. H., Dagnaes-Hansen, F. and Finsen, B. (2008). Interleukin-1beta and Tumor Necrosis Factor-Alpha are Expressed by Different Subsets of Microglia and Macrophages After Ischemic Stroke in Mice. *J Neuroinflammation* 5, 46.

Colombo, E. and Farina, C. (2016). Astrocytes: Key Regulators of Neuroinflammation. *Trends Immunol.* 37, 608-620.

Corlew, R., Bosma, M. M. and Moody, W. J. (2004). Spontaneous, Synchronous Electrical Activity in Neonatal Mouse Cortical Neurones. *J. Physiol.* 560, 377-390.

Cornell-Bell, A. H., Finkbeiner, S. M., Cooper, M. S. and Smith, S. J. (1990). Glutamate Induces Calcium Waves in Cultured Astrocytes: Long-Range Glial Signaling. *Science* 247, 470-473.

Craig, A. M., Graf, E. R. and Linhoff, M. W. (2006). How to Build a Central Synapse: Clues from Cell Culture. *Trends Neurosci.* 29, 8-20.

Cummings, J. (2018). Lessons Learned from Alzheimer Disease: Clinical Trials with Negative Outcomes. *Clin Transl Sci* 11, 147-152.

Cutts, C. S. and Eglen, S. J. (2014). Detecting Pairwise Correlations in Spike Trains: An Objective Comparison of Methods and Application to the Study of Retinal Waves. *J. Neurosci.* 34, 14288-14303.

Deneault, E., White, S. H., Rodrigues, D. C., Ross, P. J., Faheem, M., Zaslavsky, K., Wang, Z., Alexandrova, R., Pellecchia, G., Wei, W. et al. (2018). Complete Disruption of Autism-Susceptibility Genes by Gene Editing Predominantly Reduces Functional Connectivity of Isogenic Human Neurons. *Stem Cell. Reports* 11, 1211-1225.

Doi, D., Samata, B., Katsukawa, M., Kikuchi, T., Morizane, A., Ono, Y., Sekiguchi, K., Nakagawa, M., Parmar, M. and Takahashi, J. (2014). Isolation of Human Induced Pluripotent Stem Cell-Derived Dopaminergic Progenitors by Cell Sorting for Successful Transplantation. *Stem Cell Reports* 2, 337-350.

Domogatskaya, A., Rodin, S. and Tryggvason, K. (2012). Functional Diversity of Laminins. *Annu. Rev. Cell Dev. Biol.* 28, 523-553.

Dossi, E., Vasile, F. and Rouach, N. (2018). Human Astrocytes in the Diseased Brain. *Brain Res. Bull.* 136, 139-156.

Dupont, E., Hanganu, I. L., Kilb, W., Hirsch, S. and Luhmann, H. J. (2006). Rapid Developmental Switch in the Mechanisms Driving Early Cortical Columnar Networks. *Nature* 439, 79-83.

Ebert, D. H. and Greenberg, M. E. (2013). Activity-Dependent Neuronal Signalling and Autism Spectrum Disorder. *Nature* 493, 327-337.

Egert, U., Heck, D. and Aertsen, A. (2002). Two-Dimensional Monitoring of Spiking Networks in Acute Brain Slices. *Exp Brain Res* 142, 268-274.

Egorov, A. V. and Draguhn, A. (2013). Development of Coherent Neuronal Activity Patterns in Mammalian Cortical Networks: Common Principles and Local Hetereogeneity. *Mech. Dev.* 130, 412-423.

Einevoll, G. T., Kayser, C., Logothetis, N. K. and Panzeri, S. (2013). Modelling and Analysis of Local Field Potentials for Studying the Function of Cortical Circuits. *Nat. Rev. Neurosci.* 14, 770-785.

Eiraku, M. and Sasai, Y. (2012). Self-Formation of Layered Neural Structures in Three-Dimensional Culture of ES Cells. *Curr. Opin. Neurobiol.* 22, 768-777.

Elitt, M. S., Barbar, L. and Tesar, P. J. (2018). Drug Screening for Human Genetic Diseases using iPSC Models. *Hum. Mol. Genet.* 27, R89-R98.

Engle, S. J., Blaha, L. and Kleiman, R. J. (2018). Best Practices for Translational Disease Modeling using Human iPSC-Derived Neurons. *Neuron* 100, 783-797.

Espuny-Camacho, I., Michelsen, K. A., Gall, D., Linaro, D., Hasche, A., Bonnefont, J., Bali, C., Orduz, D., Bilheu, A., Herpoel, A. et al. (2013). Pyramidal Neurons Derived from Human Pluripotent Stem Cells Integrate Efficiently into Mouse Brain Circuits in Vivo. *Neuron* 77, 440-456.

Floruta, C. M., Du, R., Kang, H., Stein, J. L. and Weick, J. P. (2017). Default Patterning Produces Pan-Cortical Glutamatergic and CGE/LGE-Like GABAergic Neurons from Human Pluripotent Stem Cells. *Stem Cell Reports* 9, 1463-1476.

Forostyak, O., Romanyuk, N., Verkhratsky, A., Sykova, E. and Dayanithi, G. (2013). Plasticity of Calcium Signaling Cascades in Human Embryonic Stem Cell-Derived Neural Precursors. *Stem Cells Dev.* 22, 1506-1521.

Frega, M., Linda, K., Keller, J. M., Gümüş-Akay, G., Mossink, B., van Rhijn, J., Negwer, M., Klein Gunnewiek, T., Foreman, K., Kompier, N. et al. (2019). Neuronal Network Dysfunction in a Model for Kleefstra Syndrome Mediated by Enhanced NMDAR Signaling. *Nat Commun* 10, 4928.

Frega, M., van Gestel, Sebastianus H. C., Linda, K., van der Raadt, J., Keller, J., Van Rhijn, J., Schubert, D., Albers, C. A. and Nadif Kasri, N. (2017). Rapid Neuronal Differentiation of Induced Pluripotent Stem Cells for Measuring Network Activity on Micro-Electrode Arrays. *J Vis Exp.*

Fukushima, K., Miura, Y., Sawada, K., Yamazaki, K. and Ito, M. (2016). Establishment of a Human Neuronal Network Assessment System by using a Human Neuron/Astrocyte Co-Culture Derived from Fetal Neural Stem/Progenitor Cells. *J Biomol Screen* 21, 54-64.

Garaschuk, O., Linn, J., Eilers, J. and Konnerth, A. (2000). Large-Scale Oscillatory Calcium Waves in the Immature Cortex. *Nat. Neurosci.* 3, 452-459.

García-León, J. A., Cabrera-Socorro, A., Eggermont, K., Swijsen, A., Terryn, J., Fazal, R., Nami, F., Ordovás, L., Quiles, A., Lluis, F. et al. (2018). Generation of a Human Induced Pluripotent Stem Cell-Based Model for Tauopathies Combining Three Microtubule-Associated Protein TAU Mutations which Displays several Phenotypes Linked to Neurodegeneration. *Alzheimers Dement* 14, 1261-1280.

Gelfman, S., Wang, Q., Lu, Y. F., Hall, D., Bostick, C. D., Dhindsa, R., Halvorsen, M., McSweeney, K. M., Cotterill, E., Edinburgh, T. et al. (2018). meaRtools: An R

Package for the Analysis of Neuronal Networks Recorded on Microelectrode Arrays. *PLoS Comput. Biol.* 14, e1006506.

Ginhoux, F., Greter, M., Leboeuf, M., Nandi, S., See, P., Gokhan, S., Mehler, M. F., Conway, S. J., Ng, L. G., Stanley, E. R. et al. (2010). Fate Mapping Analysis Reveals that Adult Microglia Derive from Primitive Macrophages. *Science* 330, 841-845.

Golbs, A., Nimmervoll, B., Sun, J., Sava, I. E. and Luhmann, H. J. (2011). Control of Programmed Cell Death by Distinct Electrical Activity Patterns. *Cereb. Cortex* 21, 1192-1202.

Grainger, A. I., King, M. C., Nagel, D. A., Parri, H. R., Coleman, M. D. and Hill, E. J. (2018). In Vitro Models for Seizure-Liability Testing using Induced Pluripotent Stem Cells. *Front Neurosci* 12, 590.

Grienberger, C. and Konnerth, A. (2012). Imaging Calcium in Neurons. *Neuron* 73, 862-885.

Gu, X., Olson, E. C. and Spitzer, N. C. (1994). Spontaneous Neuronal Calcium Spikes and Waves during Early Differentiation. *J. Neurosci.* 14, 6325-6335.

Gunhanlar, N., Shpak, G., van der Kroeg, M., Gouty-Colomer, L. A., Munshi, S. T., Lendemeijer, B., Ghazvini, M., Dupont, C., Hoogendijk, W. J. G., Gribnau, J. et al. (2018). A Simplified Protocol for Differentiation of Electrophysiologically Mature Neuronal Networks from Human Induced Pluripotent Stem Cells. *Mol. Psychiatry* 23, 1336-1344.

Hagbard, L., Cameron, K., August, P., Penton, C., Parmar, M., Hay, D. C. and Kallur, T. (2018). Developing Defined Substrates for Stem Cell Culture and Differentiation. *Philos. Trans. R. Soc. Lond. , B, Biol. Sci.* 373,.

Hamby, M. E., Coppola, G., Ao, Y., Geschwind, D. H., Khakh, B. S. and Sofroniew, M. V. (2012). Inflammatory Mediators Alter the Astrocyte Transcriptome and Calcium Signaling Elicited by Multiple G-Protein-Coupled Receptors. *J. Neurosci.* 32, 14489-14510.

Hartlaub, A. M., McElroy, C. A., Maitre, N. L. and Hester, M. E. (2019). Modeling Human Brain Circuitry using Pluripotent Stem Cell Platforms. *Front Pediatr* 7, 57.

Heikkilä, T. J., Ylä-Outinen, L., Tanskanen, J. M. A., Lappalainen, R. S., Skottman, H., Suuronen, R., Mikkonen, J. E., Hyttinen, J. A. K. and Narkilahti, S. (2009). Human Embryonic Stem Cell-Derived Neuronal Cells Form Spontaneously Active Neuronal Networks in Vitro. *Exp. Neurol.* 218, 109-116.

Herculano-Houzel, S. (2014). The Glia/Neuron Ratio: How it Varies Uniformly Across Brain Structures and Species and what that Means for Brain Physiology and Evolution. *Glia* 62, 1377-1391.

Hoffmann, F. S., Hofereiter, J., Rübsamen, H., Melms, J., Schwarz, S., Faber, H., Weber, P., Pütz, B., Loleit, V., Weber, F. et al. (2015). Fingolimod Induces Neuroprotective Factors in Human Astrocytes. *J Neuroinflammation* 12, 184.

Hofrichter, M., Nimtz, L., Tigges, J., Kabiri, Y., Schröter, F., Royer-Pokora, B., Hildebrandt, B., Schmuck, M., Epanchintsev, A., Theiss, S. et al. (2017). Comparative Performance Analysis of Human iPSC-Derived and Primary Neural Progenitor Cells (NPC) Grown as Neurospheres in Vitro. *Stem Cell Res* 25, 72-82.

Hongisto, H., Ilmarinen, T., Vattulainen, M., Mikhailova, A. and Skottman, H. (2017). Xeno- and Feeder-Free Differentiation of Human Pluripotent Stem Cells to Two Distinct Ocular Epithelial Cell Types using Simple Modifications of One Method. *Stem Cell Res Ther* 8, 291.

Hyysalo, A., Ristola, M., Makinen, M. E., Hayrynen, S., Nykter, M. and Narkilahti, S. (2017). Laminin Alpha5 Substrates Promote Survival, Network Formation and Functional

Development of Human Pluripotent Stem Cell-Derived Neurons in Vitro. *Stem Cell. Res.* 24, 118-127.

Illes, S., Fleischer, W., Siebler, M., Hartung, H. and Dihné, M. (2007). Development and Pharmacological Modulation of Embryonic Stem Cell-Derived Neuronal Network Activity. *Exp. Neurol.* 207, 171-176.

Ishii, M. N., Yamamoto, K., Shoji, M., Asami, A. and Kawamata, Y. (2017). Human Induced Pluripotent Stem Cell (hiPSC)-Derived Neurons Respond to Convulsant Drugs when Co-Cultured with hiPSC-Derived Astrocytes. *Toxicology* 389, 130-138.

Ito, S., Yeh, F., Hiolski, E., Rydygier, P., Gunning, D. E., Hottowy, P., Timme, N., Litke, A. M. and Beggs, J. M. (2014). Large-Scale, High-Resolution Multielectrode-Array Recording Depicts Functional Network Differences of Cortical and Hippocampal Cultures. *PLoS ONE* 9, e105324.

Iyer, K. K., Roberts, J. A., Hellström-Westas, L., Wikström, S., Hansen Pupp, I., Ley, D., Vanhatalo, S. and Breakspear, M. (2015). Cortical Burst Dynamics Predict Clinical Outcome Early in Extremely Preterm Infants. *Brain* 138, 2206-2218.

Izsak, J., Seth, H., Andersson, M., Vizlin-Hodzic, D., Theiss, S., Hanse, E., Ågren, H., Funa, K. and Illes, S. (2019). Robust Generation of Person-Specific, Synchronously Active Neuronal Networks using Purely Isogenic Human iPSC-3D Neural Aggregate Cultures. *Front Neurosci* 13, 351.

James, O. T., Livesey, M. R., Qiu, J., Dando, O., Bilican, B., Haghi, G., Rajan, R., Burr, K., Hardingham, G. E., Chandran, S. et al. (2014). Ionotropic GABA and Glycine Receptor Subunit Composition in Human Pluripotent Stem Cell-Derived Excitatory Cortical Neurones. *J. Physiol. (Lond.)* 592, 4353-4363.

Jiang, X. and Nardelli, J. (2016). Cellular and Molecular Introduction to Brain Development. *Neurobiol. Dis.* 92, 3-17.

Johnson, M. A., Weick, J. P., Pearce, R. A. and Zhang, S. C. (2007). Functional Neural Development from Human Embryonic Stem Cells: Accelerated Synaptic Activity Via Astrocyte Coculture. *J. Neurosci.* 27, 3069-3077.

Jones, T. R., Kang, I. H., Wheeler, D. B., Lindquist, R. A., Papallo, A., Sabatini, D. M., Golland, P. and Carpenter, A. E. (2008). CellProfiler Analyst: Data Exploration and Analysis Software for Complex Image-Based Screens. *BMC Bioinform.* 9,.

Kapucu, F. E., Tanskanen, J. M. A., Mikkonen, J., Ylä-Outinen, L., Narkilahti, S. and Hyttinen, J. A. K. (2012). Burst Analysis Tool for Developing Neuronal Networks Exhibiting Highly Varying Action Potential Dynamics. *Front. Comp. Neurosci.* 6,.

Kapucu, F. E., Välkki, I., Mikkonen, J. E., Leone, C., Lenk, K., Tanskanen, J. M. A. and Hyttinen, J. A. K. (2016). Spectral Entropy Based Neuronal Network Synchronization Analysis Based on Microelectrode Array Measurements. *Front Comput Neurosci* 10, 112.

Karus, C., Mondragao, M. A., Ziemens, D. and Rose, C. R. (2015). Astrocytes Restrict Discharge Duration and Neuronal Sodium Loads during Recurrent Network Activity. *Glia* 63, 936-957.

Kelava, I. and Lancaster, M. A. (2016). Stem Cell Models of Human Brain Development. *Cell Stem Cell* 18, 736-748.

Kerr, J. N. D., Greenberg, D. and Helmchen, F. (2005). Imaging Input and Output of Neocortical Networks in Vivo. *Proc. Natl. Acad. Sci. U. S. A.* 102, 14063-14068.

Kettenmann, H. and Verkhratsky, A. (2008). Neuroglia: The 150 Years After. *Trends Neurosci.* 31, 653-659.

Khazipov, R. and Luhmann, H. J. (2006). Early Patterns of Electrical Activity in the Developing Cerebral Cortex of Humans and Rodents. *Trends Neurosci.* 29, 414-418.

Kiamehr, M., Klettner, A., Richert, E., Koskela, A., Koistinen, A., Skottman, H., Kaarniranta, K., Aalto-Setälä, K. and Juuti-Uusitalo, K. (2019). Compromised Barrier Function in Human Induced Pluripotent Stem-Cell-Derived Retinal Pigment Epithelial Cells from Type 2 Diabetic Patients. *Int J Mol Sci* 20,.

Kilb, W., Kirischuk, S. and Luhmann, H. J. (2011). Electrical Activity Patterns and the Functional Maturation of the Neocortex. *Eur. J. Neurosci.* 34, 1677-1686.

Kim, K., Doi, A., Wen, B., Ng, K., Zhao, R., Cahan, P., Kim, J., Aryee, M. J., Ji, H., Ehrlich, L. I. R. et al. (2010). Epigenetic Memory in Induced Pluripotent Stem Cells. *Nature* 467, 285-290.

Kirkeby, A., Grealish, S., Wolf, D. A., Nelander, J., Wood, J., Lundblad, M., Lindvall, O. and Parmar, M. (2012). Generation of Regionally Specified Neural Progenitors and Functional Neurons from Human Embryonic Stem Cells Under Defined Conditions. *Cell Rep* 1, 703-714.

Kirkeby, A., Nolbrant, S., Tiklova, K., Heuer, A., Kee, N., Cardoso, T., Ottosson, D. R., Lelos, M. J., Rifes, P., Dunnett, S. B. et al. (2017). Predictive Markers Guide Differentiation to Improve Graft Outcome in Clinical Translation of hESC-Based Therapy for Parkinson's Disease. *Cell Stem Cell* 20, 135-148.

Kirwan, P., Turner-Bridger, B., Peter, M., Momoh, A., Arambepola, D., Robinson, H. P. C. and Livesey, F. J. (2015). Development and Function of Human Cerebral Cortex Neural Networks from Pluripotent Stem Cells in Vitro. *Development* 142, 3178-3187.

Klapper, S. D., Garg, P., Dagar, S., Lenk, K., Gottmann, K. and Nieweg, K. (2019). Astrocyte Lineage Cells are Essential for Functional Neuronal Differentiation and Synapse Maturation in Human iPSC-Derived Neural Networks. *Glia*.

Klapper, S. D., Sauter, E. J., Swiersy, A., Hyman, M. A. E., Bamann, C., Bamberg, E. and Busskamp, V. (2017). On-Demand Optogenetic Activation of Human Stem-Cell-Derived Neurons. *Sci Rep* 7, 14450.

Kouroupi, G., Taoufik, E., Vlachos, I. S., Tsioras, K., Antoniou, N., Papastefanaki, F., Chroni-Tzartou, D., Wrasidlo, W., Bohl, D., Stellas, D. et al. (2017). Defective Synaptic Connectivity and Axonal Neuropathology in a Human iPSC-Based Model of Familial Parkinson's Disease. *Proc. Natl. Acad. Sci. U. S. A.* 114, E3679-E3688.

Krencik, R., Weick, J. P., Liu, Y., Zhang, Z. J. and Zhang, S. C. (2011). Specification of Transplantable Astroglial Subtypes from Human Pluripotent Stem Cells. *Nat. Biotechnol.* 29, 528-534.

Krencik, R. and Ullian, E. M. (2013). A Cellular Star Atlas: Using Astrocytes from Human Pluripotent Stem Cells for Disease Studies. *Front Cell Neurosci* 7, 25.

Kreutzer, J., Ylä-Outinen, L., Kärnä, P., Kaarela, T., Mikkonen, J., Skottman, H., Narkilahti, S. and Kallio, P. (2012). Structured PDMS Chambers for Enhanced Human Neuronal Cell Activity on MEA Platforms. *Journal of Bionic Engineering* 9, 1-10.

Kuijlaars, J., Oyelami, T., Diels, A., Rohrbacher, J., Versweyveld, S., Meneghello, G., Tuefferd, M., Verstraelen, P., Detrez, J. R., Verschuuren, M. et al. (2016). Sustained Synchronized Neuronal Network Activity in a Human Astrocyte Co-Culture System. *Scientific Reports* 6, 36529.

Lancaster, M. A., Renner, M., Martin, C., Wenzel, D., Bicknell, L. S., Hurles, M. E., Homfray, T., Penninger, J. M., Jackson, A. P. and Knoblich, J. A. (2013). Cerebral Organoids Model Human Brain Development and Microcephaly. *Nature* 501, 373-379.

Lappalainen, R. S., Salomäki, M., Ylä-Outinen, L., Heikkilä, T. J., Hyttinen, J. A., Pihlajamäki, H., Suuronen, R., Skottman, H. and Narkilahti, S. (2010). Similarly Derived and

Cultured hESC Lines show Variation in their Developmental Potential Towards Neuronal Cells in Long-Term Culture. *Regenerative Med.* 5, 749-762.

Lee, G., Ramirez, C. N., Kim, H., Zeltner, N., Liu, B., Radu, C., Bhinder, B., Kim, Y. J., Choi, I. Y., Mukherjee-Clavin, B. et al. (2012). Large-Scale Screening using Familial Dysautonomia Induced Pluripotent Stem Cells Identifies Compounds that Rescue IKBKAP Expression. *Nat. Biotechnol.* 30, 1244-1248.

Lehmann, R., Lee, C. M., Shugart, E. C., Benedetti, M., Charo, R. A., Gartner, Z., Hogan, B., Knoblich, J., Nelson, C. M. and Wilson, K. M. (2019). Human Organoids: A New Dimension in Cell Biology. *Mol. Biol. Cell* 30, 1129-1137.

Lepski, G., Jannes, C. E., Nikkhah, G. and Bischofberger, J. (2013). cAMP Promotes the Differentiation of Neural Progenitor Cells in Vitro Via Modulation of Voltage-Gated Calcium Channels. *Front Cell Neurosci* 7, 155.

Letinic, K., Zoncu, R. and Rakic, P. (2002). Origin of GABAergic Neurons in the Human Neocortex. *Nature* 417, 645-649.

Li, X., Tao, Y., Bradley, R., Du, Z., Tao, Y., Kong, L., Dong, Y., Jones, J., Yan, Y., Harder, C. R. K. et al. (2018). Fast Generation of Functional Subtype Astrocytes from Human Pluripotent Stem Cells. *Stem Cell Reports* 11, 998-1008.

Liddelow, S. A., Guttenplan, K. A., Clarke, L. E., Bennett, F. C., Bohlen, C. J., Schirmer, L., Bennett, M. L., Münch, A. E., Chung, W., Peterson, T. C. et al. (2017). Neurotoxic Reactive Astrocytes are Induced by Activated Microglia. *Nature* 541, 481-487.

Liddelow, S. A. and Barres, B. A. (2017). Reactive Astrocytes: Production, Function, and Therapeutic Potential. *Immunity* 46, 957-967.

Lischka, F. W., Efthymiou, A., Zhou, Q., Nieves, M. D., McCormack, N. M., Wilkerson, M. D., Sukumar, G., Dalgard, C. L. and Doughty, M. L. (2018). Neonatal Mouse Cortical but Not Isogenic Human Astrocyte Feeder Layers Enhance the Functional Maturation of Induced Pluripotent Stem Cell-Derived Neurons in Culture. *Glia* 66, 725-748.

Liu, M., Zang, T., Zou, Y., Chang, J. C., Gibson, J. R., Huber, K. M. and Zhang, C. (2013). Small Molecules Enable Neurogenin 2 to Efficiently Convert Human Fibroblasts into Cholinergic Neurons. *Nat Commun* 4, 2183.

Livak, K. J. and Schmittgen, T. D. (2001). Analysis of Relative Gene Expression Data using Real-Time Quantitative PCR and the 2-ΔΔCT Method. *Methods* 25, 402-408.

Livesey, M. R., Bilican, B., Qiu, J., Rzechorzek, N. M., Haghi, G., Burr, K., Hardingham, G. E., Chandran, S. and Wyllie, D. J. A. (2014). Maturation of AMPAR Composition and the GABAAR Reversal Potential in hPSC-Derived Cortical Neurons. *J. Neurosci.* 34, 4070-4075.

Livesey, M. R., Magnani, D., Hardingham, G. E., Chandran, S. and Wyllie, D. J. A. (2016). Functional Properties of in Vitro Excitatory Cortical Neurons Derived from Human Pluripotent Stem Cells. *J. Physiol. (Lond.)* 594, 6573-6582.

Long, K. R. and Huttner, W. B. (2019). How the Extracellular Matrix Shapes Neural Development. *Open Biol* 9, 180216.

Lu, H. F., Chai, C., Lim, T. C., Leong, M. F., Lim, J. K., Gao, S., Lim, K. L. and Wan, A. C. A. (2014). A Defined Xeno-Free and Feeder-Free Culture System for the Derivation, Expansion and Direct Differentiation of Transgene-Free Patient-Specific Induced Pluripotent Stem Cells. *Biomaterials* 35, 2816-2826.

Luhmann, H. J., Fukuda, A. and Kilb, W. (2015). Control of Cortical Neuronal Migration by Glutamate and GABA. *Front Cell Neurosci* 9, 4.

Luhmann, H. J. and Khazipov, R. (2018). Neuronal Activity Patterns in the Developing Barrel Cortex. *Neuroscience* 368, 256-267.

Luhmann, H. J., Sinning, A., Yang, J., Reyes-Puerta, V., Stüttgen, M. C., Kirischuk, S. and Kilb, W. (2016). Spontaneous Neuronal Activity in Developing Neocortical Networks: From Single Cells to Large-Scale Interactions. *Front Neural Circuits* 10, 40.

Lundin, A., Delsing, L., Clausen, M., Ricchiuto, P., Sanchez, J., Sabirsh, A., Ding, M., Synnergren, J., Zetterberg, H., Brolen, G. et al. (2018). Human iPS-Derived Astroglia from a Stable Neural Precursor State show Improved Functionality Compared with Conventional Astrocytic Models. *Stem Cell. Reports* 10, 1030-1045.

Madhavan, M., Nevin, Z. S., Shick, H. E., Garrison, E., Clarkson-Paredes, C., Karl, M., Clayton, B. L. L., Factor, D. C., Allan, K. C., Barbar, L. et al. (2018). Induction of Myelinating Oligodendrocytes in Human Cortical Spheroids. *Nat. Methods* 15, 700-706.

Mäkinen, M. E., Ylä-Outinen, L. and Narkilahti, S. (2018). GABA and Gap Junctions in the Development of Synchronized Activity in Human Pluripotent Stem Cell-Derived Neural Networks. *Front Cell Neurosci* 12, 56.

Mariani, J., Simonini, M. V., Palejev, D., Tomasini, L., Coppola, G., Szekely, A. M., Horvath, T. L. and Vaccarino, F. M. (2012). Modeling Human Cortical Development in Vitro using Induced Pluripotent Stem Cells. *Proc. Natl. Acad. Sci. U. S. A.* 109, 12770-12775.

Marina, N., Turovsky, E., Christie, I. N., Hosford, P. S., Hadjihambi, A., Korsak, A., Ang, R., Mastitskaya, S., Sheikhbahaei, S., Theparambil, S. M. et al. (2018). Brain Metabolic Sensing and Metabolic Signaling at the Level of an Astrocyte. *Glia* 66, 1185-1199.

Maroof, A. M., Keros, S., Tyson, J. A., Ying, S., Ganat, Y. M., Merkle, F. T., Liu, B., Goulburn, A., Stanley, E. G., Elefanty, A. G. et al. (2013). Directed Differentiation and Functional Maturation of Cortical Interneurons from Human Embryonic Stem Cells. *Cell Stem Cell* 12, 559-572.

Martynoga, B., Drechsel, D. and Guillemot, F. (2012). Molecular Control of Neurogenesis: A View from the Mammalian Cerebral Cortex. *Cold Spring Harb Perspect Biol* 4,.

Masjosthusmann, S., Becker, D., Petzuch, B., Klose, J., Siebert, C., Deenen, R., Barenys, M., Baumann, J., Dach, K., Tigges, J. et al. (2018). A Transcriptome Comparison of Time-Matched Developing Human, Mouse and Rat Neural Progenitor Cells Reveals Human Uniqueness. *Toxicol. Appl. Pharmacol.* 354, 40-55.

Mayer, M., Arrizabalaga, O., Lieb, F., Ciba, M., Ritter, S. and Thielemann, C. (2018). Electrophysiological Investigation of Human Embryonic Stem Cell Derived Neurospheres using a Novel Spike Detection Algorithm. *Biosens. Bioelectron.* 100, 462-468.

Mehta, S. R., Tom, C. M., Wang, Y., Bresee, C., Rushton, D., Mathkar, P. P., Tang, J. and Mattis, V. B. (2018). Human Huntington's Disease iPSC-Derived Cortical Neurons Display Altered Transcriptomics, Morphology, and Maturation. *Cell Rep* 25, 1081-1096.e6.

Mertens, J., Marchetto, M. C., Bardy, C. and Gage, F. H. (2016). Evaluating Cell Reprogramming, Differentiation and Conversion Technologies in Neuroscience. *Nat. Rev. Neurosci.* 17, 424-437.

Meyer, G., Schaaps, J. P., Moreau, L. and Goffinet, A. M. (2000). Embryonic and Early Fetal Development of the Human Neocortex. *J. Neurosci.* 20, 1858-1868.

Miller, F. D. and Gauthier, A. S. (2007). Timing is Everything: Making Neurons Versus Glia in the Developing Cortex. *Neuron* 54, 357-369.

Molyneaux, B. J., Arlotta, P., Menezes, J. R. L. and Macklis, J. D. (2007). Neuronal Subtype Specification in the Cerebral Cortex. *Nat. Rev. Neurosci.* 8, 427-437.

Muñoz-Sanjuán, I. and Brivanlou, A. H. (2002). Neural Induction, the Default Model and Embryonic Stem Cells. *Nat. Rev. Neurosci.* 3, 271-280.

Muratore, C. R., Srikanth, P., Callahan, D. G. and Young-Pearse, T. L. (2014). Comparison and Optimization of hiPSC Forebrain Cortical Differentiation Protocols. *PLoS ONE* 9, e105807.

Napoli, A. and Obeid, I. (2016). Comparative Analysis of Human and Rodent Brain Primary Neuronal Culture Spontaneous Activity using Micro-Electrode Array Technology. *J. Cell. Biochem.* 117, 559-565.

Nat, R., Nilbratt, M., Narkilahti, S., Winblad, B., Hovatta, O. and Nordberg, A. (2007). Neurogenic Neuroepithelial and Radial Glial Cells Generated from Six Human Embryonic Stem Cell Lines in Serum-Free Suspension and Adherent Cultures. *Glia* 55, 385-399.

Nedergaard, M. and Verkhratsky, A. (2012). Artifact Versus Reality--how Astrocytes Contribute to Synaptic Events. *Glia* 60, 1013-1023.

Neto, E., Leitão, L., Sousa, D. M., Alves, C. J., Alencastre, I. S., Aguiar, P. and Lamghari, M. (2016). Compartmentalized Microfluidic Platforms: The Unrivaled Breakthrough of in Vitro Tools for Neurobiological Research. *J. Neurosci.* 36, 11573-11584.

Nicholas, C. R., Chen, J., Tang, Y., Southwell, D. G., Chalmers, N., Vogt, D., Arnold, C. M., Chen, Y. J., Stanley, E. G., Elefanty, A. G. et al. (2013). Functional Maturation of hPSC-Derived Forebrain Interneurons Requires an Extended Timeline and Mimics Human Neural Development. *Cell Stem Cell* 12, 573-586.

Niclis, J. C., Gantner, C. W., Alsanie, W. F., McDougall, S. J., Bye, C. R., Elefanty, A. G., Stanley, E. G., Haynes, J. M., Pouton, C. W., Thompson, L. H. et al. (2017). Efficiently Specified Ventral Midbrain Dopamine Neurons from Human Pluripotent Stem Cells Under Xeno-Free Conditions Restore Motor Deficits in Parkinsonian Rodents. *Stem Cells Transl Med* 6, 937-948.

Oberheim Bush, N. A. and Nedergaard, M. (2017). Do Evolutionary Changes in Astrocytes Contribute to the Computational Power of the Hominid Brain? *Neurochem. Res.* 42, 2577-2587.

Oberheim, N. A., Takano, T., Han, X., He, W., Lin, J. H. C., Wang, F., Xu, Q., Wyatt, J. D., Pilcher, W., Ojemann, J. G. et al. (2009). Uniquely Hominid Features of Adult Human Astrocytes. *J. Neurosci.* 29, 3276-3287.

Oberheim, N. A., Wang, X., Goldman, S. and Nedergaard, M. (2006). Astrocytic Complexity Distinguishes the Human Brain. *Trends Neurosci.* 29, 547-553.

Obien, M. E. J., Deligkaris, K., Bullmann, T., Bakkum, D. J. and Frey, U. (2014). Revealing Neuronal Function through Microelectrode Array Recordings. *Front Neurosci* 8, 423.

Odawara, A., Matsuda, N., Ishibashi, Y., Yokoi, R. and Suzuki, I. (2018). Toxicological Evaluation of Convulsant and Anticonvulsant Drugs in Human Induced Pluripotent Stem Cell-Derived Cortical Neuronal Networks using an MEA System. *Sci Rep* 8, 10416.

Odawara, A., Saitoh, Y., Alhebshi, A. H., Gotoh, M. and Suzuki, I. (2014). Long-Term Electrophysiological Activity and Pharmacological Response of a Human Induced Pluripotent Stem Cell-Derived Neuron and Astrocyte Co-Culture. *Biochem. Biophys. Res. Commun.* 443, 1176-1181.

Odawara, A., Katoh, H., Matsuda, N. and Suzuki, I. (2016). Physiological Maturation and Drug Responses of Human Induced Pluripotent Stem Cell-Derived Cortical Neuronal Networks in Long-Term Culture. *Sci Rep* 6, 26181.

Ojala, M., Prajapati, C., Pölönen, R., Rajala, K., Pekkanen-Mattila, M., Rasku, J., Larsson, K. and Aalto-Setälä, K. (2016). Mutation-Specific Phenotypes in hiPSC-Derived Cardiomyocytes Carrying either Myosin-Binding Protein C Or A-Tropomyosin Mutation for Hypertrophic Cardiomyopathy. *Stem Cells International* 2016, 1684792.

Okano, H. and Temple, S. (2009). Cell Types to Order: Temporal Specification of CNS Stem Cells. *Curr. Opin. Neurobiol.* 19, 112-119.

Oksanen, M., Petersen, A. J., Naumenko, N., Puttonen, K., Lehtonen, Š, Gubert Olivé, M., Shakirzyanova, A., Leskelä, S., Sarajärvi, T., Viitanen, M. et al. (2017). PSEN1 Mutant iPSC-Derived Model Reveals Severe Astrocyte Pathology in Alzheimer's Disease. *Stem Cell Reports* 9, 1885-1897.

Omar, M. H., Kerrisk Campbell, M., Xiao, X., Zhong, Q., Brunken, W. J., Miner, J. H., Greer, C. A. and Koleske, A. J. (2017). CNS Neurons Deposit Laminin A5 to Stabilize Synapses. *Cell Reports* 21, 1281-1292.

Osafune, K., Caron, L., Borowiak, M., Martinez, R. J., Fitz-Gerald, C. S., Sato, Y., Cowan, C. A., Chien, K. R. and Melton, D. A. (2008). Marked Differences in Differentiation Propensity among Human Embryonic Stem Cell Lines. *Nat. Biotechnol.* 26, 313-315.

Paavilainen, T., Pelkonen, A., Mäkinen, M. E. -., Peltola, M., Huhtala, H., Fayuk, D. and Narkilahti, S. (2018). Effect of Prolonged Differentiation on Functional Maturation of Human Pluripotent Stem Cell-Derived Neuronal Cultures. *Stem Cell Res* 27, 151-161.

Pankevich, D., Altevogt, B., Dunlop, J., Gage, F. and Hyman, S. (2014). Improving and Accelerating Drug Development for Nervous System Disorders. *Neuron* 84, 546-553.

Park, J., Wetzel, I., Marriott, I., Dréau, D., D'Avanzo, C., Kim, D. Y., Tanzi, R. E. and Cho, H. (2018). A 3D Human Triculture System Modeling Neurodegeneration and Neuroinflammation in Alzheimer's Disease. *Nat. Neurosci.* 21, 941-951.

Parmar, M. (2018). Towards Stem Cell Based Therapies for Parkinson's Disease. *Development* 145,.

Pasca, A. M., Sloan, S. A., Clarke, L. E., Tian, Y., Makinson, C. D., Huber, N., Kim, C. H., Park, J., O'Rourke, N. A., Nguyen, K. D. et al. (2015). Functional Cortical Neurons and Astrocytes from Human Pluripotent Stem Cells in 3D Culture. *Nat. Methods* 12, 671-678.

Paşca, S. P. (2018). The Rise of Three-Dimensional Human Brain Cultures. *Nature* 553, 437-445.

Pasquale, V., Martinoia, S. and Chiappalone, M. (2010). A Self-Adapting Approach for the Detection of Bursts and Network Bursts in Neuronal Cultures. *J. Comput. Neurosci.* 29, 213-229.

Pasquale, V., Massobrio, P., Bologna, L. L., Chiappalone, M. and Martinoia, S. (2008). Self-Organization and Neuronal Avalanches in Networks of Dissociated Cortical Neurons. *Neuroscience* 153, 1354-1369.

Pekny, M., Wilhelmsson, U., Tatlisumak, T. and Pekna, M. (2019). Astrocyte Activation and Reactive Gliosis-A New Target in Stroke? *Neurosci. Lett.* 689, 45-55.

Perriot, S., Mathias, A., Perriard, G., Canales, M., Jonkmans, N., Merienne, N., Meunier, C., El Kassar, L., Perrier, A. L., Laplaud, D. et al. (2018). Human Induced Pluripotent

Stem Cell-Derived Astrocytes are Differentially Activated by Multiple Sclerosis-Associated Cytokines. *Stem Cell Reports* 11, 1199-1210.

Petersen, C. C. H. (2017). Whole-Cell Recording of Neuronal Membrane Potential during Behavior. *Neuron* 95, 1266-1281.

Pievani, M., Filippini, N., van den Heuvel, Martijn P., Cappa, S. F. and Frisoni, G. B. (2014). Brain Connectivity in Neurodegenerative Diseases--from Phenotype to Proteinopathy. *Nat Rev Neurol* 10, 620-633.

Ponath, G., Park, C. and Pitt, D. (2018). The Role of Astrocytes in Multiple Sclerosis. *Front Immunol* 9, 217.

Qian, X., Shen, Q., Goderie, S. K., He, W., Capela, A., Davis, A. A. and Temple, S. (2000). Timing of CNS Cell Generation: A Programmed Sequence of Neuron and Glial Cell Production from Isolated Murine Cortical Stem Cells. *Neuron* 28, 69-80.

Quiroga, R. Q., Nadasdy, Z. and Ben-Shaul, Y. (2004). Unsupervised Spike Detection and Sorting with Wavelets and Superparamagnetic Clustering. *Neural Comput* 16, 1661-1687.

Radivojevic, M., Franke, F., Altermatt, M., Müller, J., Hierlemann, A. and Bakkum, D. J. (2017). Tracking Individual Action Potentials Throughout Mammalian Axonal Arbors. *Elife* 6,.

Rajala, K., Hakala, H., Panula, S., Aivio, S., Pihlajamäki, H., Suuronen, R., Hovatta, O. and Skottman, H. (2007). Testing of Nine Different Xeno-Free Culture Media for Human Embryonic Stem Cell Cultures. *Hum. Reprod.* 22, 1231-1238.

Reubinoff, B. E., Itsykson, P., Turetsky, T., Pera, M. F., Reinhartz, E., Itzik, A. and Ben-Hur, T. (2001). Neural Progenitors from Human Embryonic Stem Cells. *Nat. Biotechnol.* 19, 1134-1140.

Reubinoff, B. E., Pera, M. F., Fong, C. Y., Trounson, A. and Bongso, A. (2000). Embryonic Stem Cell Lines from Human Blastocysts: Somatic Differentiation in Vitro. *Nat. Biotechnol.* 18, 399-404.

Ristola, M., Sukki, L., Azevedo, M. M., Seixas, A. I., Relvas, J. B., Narkilahti, S. and Kallio, P. (2019). A Compartmentalized Neuron-Oligodendrocyte Co-Culture Device for Myelin Research: Design, Fabrication and Functionality Testing. *J Micromech Microengineering* 29, 065009.

Rodríguez-Arellano, J. J., Parpura, V., Zorec, R. and Verkhratsky, A. (2016). Astrocytes in Physiological Aging and Alzheimer's Disease. *Neuroscience* 323, 170-182.

Ronco, V., Grolla, A. A., Glasnov, T. N., Canonico, P. L., Verkhratsky, A., Genazzani, A. A. and Lim, D. (2014). Differential Deregulation of Astrocytic Calcium Signalling by Amyloid-B, TNFα, IL-1β and LPS. *Cell Calcium* 55, 219-229.

Roybon, L., Lamas, N. J., Garcia, A. D., Yang, E. J., Sattler, R., Lewis, V. J., Kim, Y. A., Kachel, C. A., Rothstein, J. D., Przedborski, S. et al. (2013). Human Stem Cell-Derived Spinal Cord Astrocytes with Defined Mature Or Reactive Phenotypes. *Cell. Rep.* 4, 1035-1048.

Russo, F. B., Freitas, B. C., Pignatari, G. C., Fernandes, I. R., Sebat, J., Muotri, A. R. and Beltrão-Braga, P. C. B. (2018). Modeling the Interplay between Neurons and Astrocytes in Autism using Human Induced Pluripotent Stem Cells. *Biol. Psychiatry* 83, 569-578.

Sahu, M., Nikkilä, O., Lågas, S., Kolehmainen, S. and Castrén, E. (2019). Culturing Primary Neurons from Rat Hippocampus and Cortex. *Neuronal Signal.* 3, NS20180207.

Sandoe, J. and Eggan, K. (2013). Opportunities and Challenges of Pluripotent Stem Cell Neurodegenerative Disease Models. *Nat. Neurosci.* 16, 780.

Santos, R., Vadodaria, K. C., Jaeger, B. N., Mei, A., Lefcochilos-Fogelquist, S., Mendes, A. P. D., Erikson, G., Shokhirev, M., Randolph-Moore, L., Fredlender, C. et al. (2017). Differentiation of Inflammation-Responsive Astrocytes from Glial Progenitors Generated from Human Induced Pluripotent Stem Cells. *Stem Cell. Reports* 8, 1757-1769.

Sarkar, A., Mei, A., Paquola, A. C. M., Stern, S., Bardy, C., Klug, J. R., Kim, H. J., Kim, S., Neshat, N., Ku, M. et al. (2018). Efficient Generation of CA3 Neurons from Human Pluripotent Stem Cells Enables Modeling of Hippocampal Connectivity In Vitro. *Cell Stem Cell* 22, 684-697.e9.

Semple, B. D., Blomgren, K., Gimlin, K., Ferriero, D. M. and Noble-Haeusslein, L. J. (2013). Brain Development in Rodents and Humans: Identifying Benchmarks of Maturation and Vulnerability to Injury Across Species. *Prog. Neurobiol.* 106-107, 1-16.

Serio, A., Bilican, B., Barmada, S. J., Ando, D. M., Zhao, C., Siller, R., Burr, K., Haghi, G., Story, D., Nishimura, A. L. et al. (2013). Astrocyte Pathology and the Absence of Non-Cell Autonomy in an Induced Pluripotent Stem Cell Model of TDP-43 Proteinopathy. *Proc. Natl. Acad. Sci. U. S. A.* 110, 4697-4702.

Shaltouki, A., Peng, J., Liu, Q., Rao, M. S. and Zeng, X. (2013). Efficient Generation of Astrocytes from Human Pluripotent Stem Cells in Defined Conditions. *Stem Cells* 31, 941-952.

Sherwood, C. C., Stimpson, C. D., Raghanti, M. A., Wildman, D. E., Uddin, M., Grossman, L. I., Goodman, M., Redmond, J. C., Bonar, C. J., Erwin, J. M. et al. (2006). Evolution of Increased Glia-Neuron Ratios in the Human Frontal Cortex. *Proc. Natl. Acad. Sci. U. S. A.* 103, 13606-13611.

Shi, Y., Kirwan, P., Smith, J., Robinson, H. P. and Livesey, F. J. (2012). Human Cerebral Cortex Development from Pluripotent Stem Cells to Functional Excitatory Synapses. *Nat. Neurosci.* 15, 477-86, S1.

Shi, Y., Inoue, H., Wu, J. C. and Yamanaka, S. (2017). Induced Pluripotent Stem Cell Technology: A Decade of Progress. *Nat Rev Drug Discov* 16, 115-130.

Shi, Y., Kirwan, P. and Livesey, F. J. (2012). Directed Differentiation of Human Pluripotent Stem Cells to Cerebral Cortex Neurons and Neural Networks. *Nat Protoc* 7, 1836-1846.

Shinozaki, Y., Shibata, K., Yoshida, K., Shigetomi, E., Gachet, C., Ikenaka, K., Tanaka, K. F. and Koizumi, S. (2017). Transformation of Astrocytes to a Neuroprotective Phenotype by Microglia Via P2Y1 Receptor Downregulation. *Cell Rep* 19, 1151-1164.

Skottman, H. (2010). Derivation and Characterization of Three New Human Embryonic Stem Cell Lines in Finland. *In Vitro Cell. Dev. Biol. Anim.* 46, 206-209.

Sloan, S. A. and Barres, B. A. (2014). Mechanisms of Astrocyte Development and their Contributions to Neurodevelopmental Disorders. *Curr. Opin. Neurobiol.* 27, 75-81.

Sofroniew, M. V. and Vinters, H. V. (2010). Astrocytes: Biology and Pathology. *Acta Neuropathol.* 119, 7-35.

Sommer, A., Marxreiter, F., Krach, F., Fadler, T., Grosch, J., Maroni, M., Graef, D., Eberhardt, E., Riemenschneider, M. J., Yeo, G. W. et al. (2019). Th17 Lymphocytes Induce Neuronal Cell Death in a Human iPSC-Based Model of Parkinson's Disease. *Cell Stem Cell* 24, 1006.

Stadelmann, C., Timmler, S., Barrantes-Freer, A. and Simons, M. (2019). Myelin in the Central Nervous System: Structure, Function, and Pathology. *Physiol. Rev.* 99, 1381-1431.

Stein, J. L., de la Torre-Ubieta, L., Tian, Y., Parikshak, N. N., Hernández, I. A., Marchetto, M. C., Baker, D. K., Lu, D., Hinman, C. R., Lowe, J. K. et al. (2014). A Quantitative Framework to Evaluate Modeling of Cortical Development by Neural Stem Cells. *Neuron* 83, 69-86.

Steinbeck, J. A. and Studer, L. (2015). Moving Stem Cells to the Clinic: Potential and Limitations for Brain Repair. *Neuron* 86, 187-206.

Stiles, J. and Jernigan, T. L. (2010). The Basics of Brain Development. *Neuropsychol Rev* 20, 327-348.

Stogsdill, J. A., Ramirez, J., Liu, D., Kim, Y. H., Baldwin, K. T., Enustun, E., Ejikeme, T., Ji, R. and Eroglu, C. (2017). Astrocytic Neuroligins Control Astrocyte Morphogenesis and Synaptogenesis. *Nature* 551, 192-197.

Suzuki, I. K. and Vanderhaeghen, P. (2015). Is this a Brain which I See before Me? Modeling Human Neural Development with Pluripotent Stem Cells. *Development* 142, 3138-3150.

Takahashi, K., Tanabe, K., Ohnuki, M., Narita, M., Ichisaka, T., Tomoda, K. and Yamanaka, S. (2007). Induction of Pluripotent Stem Cells from Adult Human Fibroblasts by Defined Factors. *Cell* 131, 861-872.

Takano, T., Tian, G., Peng, W., Lou, N., Libionka, W., Han, X. and Nedergaard, M. (2006). Astrocyte-Mediated Control of Cerebral Blood Flow. *Nat. Neurosci.* 9, 260-267.

Tao, Y. and Zhang, S. (2016). Neural Subtype Specification from Human Pluripotent Stem Cells. *Cell Stem Cell* 19, 573-586.

Taylor, A. M., Blurton-Jones, M., Rhee, S. W., Cribbs, D. H., Cotman, C. W. and Jeon, N. L. (2005). A Microfluidic Culture Platform for CNS Axonal Injury, Regeneration and Transport. *Nat. Methods* 2, 599-605.

Tcw, J., Wang, M., Pimenova, A. A., Bowles, K. R., Hartley, B. J., Lacin, E., Machlovi, S. I., Abdelaal, R., Karch, C. M., Phatnani, H. et al. (2017). An Efficient Platform for Astrocyte Differentiation from Human Induced Pluripotent Stem Cells. *Stem cell reports* 9, 600-614.

Thomson, J. A., Itskovitz-Eldor, J., Shapiro, S. S., Waknitz, M. A., Swiergiel, J. J., Marshall, V. S. and Jones, J. M. (1998). Embryonic Stem Cell Lines Derived from Human Blastocysts. *Science* 282, 1145-1147.

Tieu, K., Ashe, P. C., Zuo, D. M. and Yu, P. H. (2001). Inhibition of 6-Hydroxydopamine-Induced p53 Expression and Survival of Neuroblastoma Cells Following Interaction with Astrocytes. *Neuroscience* 103, 125-132.

Toivonen, S., Ojala, M., Hyysalo, A., Ilmarinen, T., Rajala, K., Pekkanen-Mattila, M., Äänismaa, R., Lundin, K., Palgi, J., Weltner, J. et al. (2013). Comparative Analysis of Targeted Differentiation of Human Induced Pluripotent Stem Cells (hiPSCs) and Human Embryonic Stem Cells Reveals Variability Associated with Incomplete Transgene Silencing in Retrovirally Derived hiPSCs Lines. *Stem Cells Transl. Med.* 2, 83-93.

Tolonen, M., Palva, J. M., Andersson, S. and Vanhatalo, S. (2007). Development of the Spontaneous Activity Transients and Ongoing Cortical Activity in Human Preterm Babies. *Neuroscience* 145, 997-1006.

Toma, K. and Hanashima, C. (2015). Switching Modes in Corticogenesis: Mechanisms of Neuronal Subtype Transitions and Integration in the Cerebral Cortex. *Front Neurosci* 9, 274.

Tourigny, D. S., Karim, M. K. A., Echeveste, R., Kotter, M. R. N. and O'Neill, J. S. (2019). Energetic Substrate Availability Regulates Synchronous Activity in an Excitatory Neural Network. *PLoS ONE* 14, e0220937.

Trujillo, C. A., Gao, R., Negraes, P. D., Gu, J., Buchanan, J., Preissl, S., Wang, A., Wu, W., Haddad, G. G., Chaim, I. A. et al. (2019). Complex Oscillatory Waves Emerging from Cortical Organoids Model Early Human Brain Network Development. *Cell Stem Cell* 25, 558-569.e7.

Tukker, A. M., de Groot, Martje W. G. D. M., Wijnolts, F. M. J., Kasteel, E. E. J., Hondebrink, L. and Westerink, R. H. S. (2016). Is the Time Right for in Vitro Neurotoxicity Testing using Human iPSC-Derived Neurons? *ALTEX* 33, 261-271.

Tukker, A. M., Wijnolts, F. M. J., de Groot, A. and Westerink, R. H. S. (2018). Human iPSC-Derived Neuronal Models for in Vitro Neurotoxicity Assessment. *Neurotoxicology* 67, 215-225.

Uhlén, P., Fritz, N., Smedler, E., Malmersjö, S. and Kanatani, S. (2015). Calcium Signaling in Neocortical Development. *Dev Neurobiol* 75, 360-368.

van Scheppingen, J., Mills, J. D., Zimmer, T. S., Broekaart, D. W. M., Iori, V., Bongaarts, A., Anink, J. J., Iyer, A. M., Korotkov, A., Jansen, F. E. et al. (2018). miR147b: A Novel Key Regulator of Interleukin 1 Beta-Mediated Inflammation in Human Astrocytes. *Glia* 66, 1082-1097.

Verkhratsky, A. and Nedergaard, M. (2018). Physiology of Astroglia. *Physiol. Rev.* 98, 239-389.

Volterra, A., Liaudet, N. and Savtchouk, I. (2014). Astrocyte Ca^{2+} Signalling: An Unexpected Complexity. *Nat. Rev. Neurosci.* 15, 327-335.

Wagenaar, D. A., Pine, J. and Potter, S. M. (2006). An Extremely Rich Repertoire of Bursting Patterns during the Development of Cortical Cultures. *BMC Neurosci.* 7,.

Wakeman, D. R., Hiller, B. M., Marmion, D. J., McMahon, C. W., Corbett, G. T., Mangan, K. P., Ma, J., Little, L. E., Xie, Z., Perez-Rosello, T. et al. (2017). Cryopreservation Maintains Functionality of Human iPSC Dopamine Neurons and Rescues Parkinsonian Phenotypes In Vivo. *Stem Cell Reports* 9, 149-161.

Wapinski, O. L., Vierbuchen, T., Qu, K., Lee, Q. Y., Chanda, S., Fuentes, D. R., Giresi, P. G., Ng, Y. H., Marro, S., Neff, N. F. et al. (2013). Hierarchical Mechanisms for Direct Reprogramming of Fibroblasts to Neurons. *Cell* 155, 621-635.

Weick, J. P. (2016). Functional Properties of Human Stem Cell-Derived Neurons in Health and Disease. *Stem Cells Int* 2016, 4190438.

Xu, X., Stoyanova, E. I., Lemiesz, A. E., Xing, J., Mash, D. C. and Heintz, N. (2018). Species and Cell-Type Properties of Classically Defined Human and Rodent Neurons and Glia. *Elife* 7,.

Yap, M. S., Nathan, K. R., Yeo, Y., Lim, L. W., Poh, C. L., Richards, M., Lim, W. L., Othman, I. and Heng, B. C. (2015). Neural Differentiation of Human Pluripotent Stem Cells for Nontherapeutic Applications: Toxicology, Pharmacology, and in Vitro Disease Modeling. *Stem Cells Int* 2015, 105172.

Ylä-Outinen, L., Harju, V., Joki, T., Koivisto, J. T., Karvinen, J., Kellomäki, M. and Narkilahti, S. (2019). Screening of Hydrogels for Human Pluripotent Stem Cell-Derived Neural Cells: Hyaluronan-Polyvinyl Alcohol-Collagen-Based Interpenetrating Polymer Network Provides an Improved Hydrogel Scaffold. *Macromol Biosci* 19, e1900096.

Ylä-Outinen, L., Heikkilä, J., Skottman, H., Suuronen, R., Aänismaa, R. and Narkilahti, S. (2010). Human Cell-Based Micro Electrode Array Platform for Studying Neurotoxicity. *Front Neuroeng* 3,.

Yu, J., Vodyanik, M. A., Smuga-Otto, K., Antosiewicz-Bourget, J., Frane, J. L., Tian, S., Nie, J., Jonsdottir, G. A., Ruotti, V., Stewart, R. et al. (2007). Induced Pluripotent Stem Cell Lines Derived from Human Somatic Cells. *Science* 318, 1917-1920.

Yu, X. and Zecevic, N. (2011). Dorsal Radial Glial Cells have the Potential to Generate Cortical Interneurons in Human but Not in Mouse Brain. *J. Neurosci.* 31, 2413-2420.

Yun, S. P., Kam, T., Panicker, N., Kim, S., Oh, Y., Park, J., Kwon, S., Park, Y. J., Karuppagounder, S. S., Park, H. et al. (2018). Block of A1 Astrocyte Conversion by Microglia is Neuroprotective in Models of Parkinson's Disease. *Nat. Med.* 24, 931-938.

Zakrzewski, W., Dobrzyński, M., Szymonowicz, M. and Rybak, Z. (2019). Stem Cells: Past, Present, and Future. *Stem Cell Res Ther* 10, 68.

Zamanian, J. L., Xu, L., Foo, L. C., Nouri, N., Zhou, L., Giffard, R. G. and Barres, B. A. (2012). Genomic Analysis of Reactive Astrogliosis. *J. Neurosci.* 32, 6391-6410.

Zhang, D., Yang, S., Toledo, E. M., Gyllborg, D., Saltó, C., Carlos Villaescusa, J. and Arenas, E. (2017). Niche-Derived Laminin-511 Promotes Midbrain Dopaminergic Neuron Survival and Differentiation through YAP. *Sci Signal* 10,.

Zhang, S., Wernig, M., Duncan, I. D., Brüstle, O. and Thomson, J. A. (2001a). In Vitro Differentiation of Transplantable Neural Precursors from Human Embryonic Stem Cells. *Nat. Biotechnol.* 19, 1129-1133.

Zhang, S., Wernig, M., Duncan, I. D., Brüstle, O. and Thomson, J. A. (2001b). In Vitro Differentiation of Transplantable Neural Precursors from Human Embryonic Stem Cells. *Nature biotechnology* 19, 1129-1133.

Zhang, Y., Sloan, S., Clarke, L., Caneda, C., Plaza, C., Blumenthal, P., Vogel, H., Steinberg, G., Edwards, M. B., Li, G. et al. (2016). Purification and Characterization of Progenitor and Mature Human Astrocytes Reveals Transcriptional and Functional Differences with Mouse. *Neuron* 89, 37-53.

Zhang, Y., Pak, C., Han, Y., Ahlenius, H., Zhang, Z., Chanda, S., Marro, S., Patzke, C., Acuna, C., Covy, J. et al. (2013). Rapid Single-Step Induction of Functional Neurons from Human Pluripotent Stem Cells. *Neuron* 78, 785-798.

Zirra, A., Wiethoff, S. and Patani, R. (2016). Neural Conversion and Patterning of Human Pluripotent Stem Cells: A Developmental Perspective. *Stem Cells Int* 2016, 8291260.

PUBLICATIONS

PUBLICATION I

Effect of prolonged differentiation on functional maturation of human pluripotent stem cell-derived neuronal cultures

Paavilainen T, Pelkonen A, Mäkinen ME, Peltola M, Huhtala H, Fayuk D, Narkilahti S

Stem Cell Research. 2018. 27:151-61.
doi: 10.1016/j.scr.2018.01.018

Stem Cell Research 27 (2018) 151–161

Contents lists available at ScienceDirect

Stem Cell Research

journal homepage: www.elsevier.com/locate/scr

Effect of prolonged differentiation on functional maturation of human pluripotent stem cell-derived neuronal cultures

Tanja Paavilainen [a,1], Anssi Pelkonen [a,1], Meeri E.-L. Mäkinen [a], Marja Peltola [a], Heini Huhtala [b], Dmitriy Fayuk [a], Susanna Narkilahti [a,*]

[a] NeuroGroup, BioMediTech and Faculty of Medicine and Life Sciences, University of Tampere, Arvo Ylpön katu 34, 33520 Tampere, Finland
[b] Faculty of Social Sciences, University of Tampere, Arvo Ylpön katu 34, 33520 Tampere, Finland

ARTICLE INFO

Article history:
Received 10 November 2017
Received in revised form 9 January 2018
Accepted 17 January 2018
Available online 31 January 2018

Keywords:
Astrocytes
Calcium signaling
Microelectrode array
Neural development
Neurons
Pluripotent stem cells

ABSTRACT

Long-term neural differentiation of human pluripotent stem cells (hPSCs) is associated with enhanced neuronal maturation, which is a necessity for creation of representative *in vitro* models. It also induces neurogenic-to-gliogenic fate switch, increasing proportion of endogenous astrocytes formed from the common neural progenitors. However, the significance of prolonged differentiation on the neural cell type composition and functional development of hPSC-derived neuronal cells has not been well characterized. Here, we studied two hPSC lines, both of which initially showed good neuronal differentiation capacity. However, the propensity for endogenous astrogenesis and maturation state after extended differentiation varied. Live cell calcium imaging revealed that prolonged differentiation facilitated maturation of GABAergic signaling. According to extracellular recordings with microelectrode array (MEA), neuronal activity was limited to fewer areas of the culture, which expressed more frequent burst activity. Efficient maturation after prolonged differentiation also promoted organization of spontaneous activity by burst compaction. These results suggest that although prolonged neural differentiation can be challenging, it has beneficial effect on functional maturation, which can also improve transition to different neural *in vitro* models and applications.

1. Introduction

Human pluripotent stem cell (hPSC)-derived neurons hold a great promise for modeling neurodevelopment as well as pathologies with genetic background (Suzuki and Vanderhaeghen, 2015). Additionally, hPSC-derived neuronal cultures represent a promising platform for neurotoxicity testing (Johnstone et al., 2010; Ylä-Outinen et al., 2010) and a therapy option, for example, in Parkinson's disease and spinal cord injury (Li et al., 2015; Lindvall, 2015). hPSCs include human embryonic stem cells (hESCs) (Thomson, 1998) and human induced pluripotent stem cells (hiPSCs) (Takahashi et al., 2007), both of which have their advantages and disadvantages. hESCs are considered to have fewer obstacles to differentiation because they do not carry any previous epigenetic memory of former cellular identity (Kim et al., 2010), whereas hiPSCs are associated with fewer ethical problems and wider utilization potential in applications such as modeling of hereditary diseases (Du and Parent, 2015). hPSCs can be differentiated into spontaneously active functional neuronal networks (Heikkilä et al., 2009; Toivonen et al., 2013), but to gain greater benefits from hPSC-derived neural cells for various applications, their basic characteristics need to be studied and evaluated in more detail *in vitro*, especially at the level of functional development.

Achieving functional maturation of hPSC-derived neuronal cells *in vitro* still remains a challenge in the field. When compared to rodent primary neurons, the functional state of hPSC-derived neuronal cultures can be considered immature. Traditionally, the survival in long-term culture and functional maturation of hPSC-derived neural cultures has been enhanced with primary rodent astrocytes in cocultures (Frega et al., 2017; Johnson et al., 2007; Odawara et al., 2014). After all, astrocytes have been recognized as active regulators of neuronal development and function (Clarke and Barres, 2013). However, for most hPSC-derived neuronal applications, for example disease modeling, a completely human cell-based system is a necessity. At the same time many differentiation protocols for hPSC-derived neurons typically produce a varying proportion of astrocytes from the common neural progenitors (Lappalainen et al., 2010; Pasca et al., 2015; Shi et al., 2012). Still this change in cell type composition is not often discussed. Overall, the significance of prolonged differentiation on neural cell type composition and network level functional studies describing this development are still largely lacking.

Here, we describe how prolonged neural differentiation affects the generation of endogenous astrocytes and impacts the functional

* Corresponding author.
E-mail address: susanna.narkilahti@uta.fi (S. Narkilahti).
[1] These authors contributed equally to this work.

https://doi.org/10.1016/j.scr.2018.01.018

development of hPSC-derived neural cultures. Typically, extended differentiation of hPSC-derived neurons is supported by rodent astrocyte coculture but here only hPSC-derived cultures were used. Our neurosphere differentiation method recapitulates the *in vivo* developmental stages in which the switch from neurogenesis to gliogenesis occurs over time (Lappalainen et al., 2010; Miller and Gauthier, 2007; Zhang et al., 2001). Accordingly, we selected two time points of neurosphere differentiation, the standard 8 week and the prolonged 15 week time point, which were quantitatively analyzed for neuronal and astrocytic markers using immunocytochemistry and gene expression analysis. Microelectrode array (MEA) technique was used to measure spontaneous electrical activity repeatedly in large populations of neurons. In contrast, calcium (Ca^{2+}) imaging allowed detection of individual cell type specific activity in neurons and astrocytes. Together, Ca^{2+} imaging and MEA system were validated as useful tools in providing extensive information about hPSC-derived neural cultures, and indicated functional maturation of neuronal cells after prolonged differentiation.

2. Materials and methods

2.1. Maintenance of human pluripotent stem cells

The human embryonic stem cell (hESC) line Regea 08/023 (passages 14–66) and the human induced pluripotent stem cell (hiPSC) line 04311.WT (passages 24–45) were used in this study. The cell lines were derived at the Institute of Biosciences and Medical Technology (BioMediTech), University of Tampere, Finland. BioMediTech received approval from the Finnish Medicines Agency (FIMEA) to perform research using human embryos (Dnro 1426/32/300/05). Supportive statements were also obtained from the regional ethics committee of Pirkanmaa Hospital District for the derivation, culture, and differentiation of hESCs (R05116) and hiPSCs (R08070). An informed consent was obtained from all subjects who provided cell samples. All methods were carried out in accordance with relevant guidelines and regulations. The hESC line Regea 08/023 was generated as previously described (Rajala et al., 2010; Skottman, 2010). The hiPSC line 04311.WT was derived from human skin fibroblasts following a previously published protocol using Sendai virus technology (Ojala et al., 2016) (Supplementary Fig. 1). The hPSC-lines were cultured on top of a human feeder cell layer (CRL-2429, ATCC, Manassas, VA, USA) and were passaged weekly (Rajala et al., 2007). The medium consisted of knockout Dulbecco's modified Eagle's medium (DMEM) supplemented with 20% knockout serum replacement, 2 mM Glutamax (all from Gibco, Thermo Fisher Scientific Waltham, MA USA), 1% nonessential amino acids, 50 U ml^{-1} penicillin/streptomycin (both from Lonza Group Ltd., Basel, Switzerland), 0.1 mM 2-mercaptoethanol (Gibco, Thermo Fisher Scientific) and 8 ng ml^{-1} basic fibroblast growth factor (bFGF, R&D Systems Inc., Minneapolis, MN, USA). The undifferentiated stage of both human pluripotent stem cell (hPSC) lines were regularly monitored with gene and protein expression analyses of pluripotency markers (Nanog, Oct-3/4, TRA-1-81 and TRA-1-60) and markers for different germ layers (human alpha-smooth muscle actin, human alpha-fetoprotein, and Nestin). All cultures maintained normal karyotypes and were mycoplasma free.

2.2. Neural differentiation

Neural differentiation of hESCs (Regea 08/023) and hiPSCs (04311.WT) was performed using a free-floating neurosphere culture (Lappalainen et al., 2010). hPSC colonies were mechanically cut into small clusters and transferred into six-well ultra-low attachment plates (Nunc, Thermo Fisher Scientific) for neural differentiation. Neural differentiation medium (NDM) consisted of 1:1 DMEM/F-12:Neurobasal medium supplemented with 1× B27, 1× N2, and 2 mM Glutamax (all from Gibco, Thermo Fisher Scientific), 25 U ml^{-1} penicillin/streptomycin (Lonza Group Ltd.) and 20 ng ml^{-1} bFGF (R&D Systems Inc.). The medium was changed three times per week, and the neurospheres were mechanically passaged once per week. Cells were differentiated in neurosphere culture for standard 8 weeks or prolonged 15 weeks and plated under adherent culture conditions for maturation up to 5 weeks (Fig. 1A, experimental setup). For adherent culture the neurospheres were mechanically cut into small 50–200 μm in diameter clusters containing on average 5000–10,000 cells. The number of plated clusters was relative to culture area: 10 clusters for MEA experiments, 20 clusters for calcium imaging experiments, 20 clusters for immunocytochemistry and PCR experiments. Cells were plated either on glass coverslips or MEA dishes coated with 0.05% PEI and 20 μg ml^{-1} mouse laminin (both from Sigma-Aldrich, St. Louis, MO, USA). For adherent culture bFGF was omitted from the NDM. After one week of adherent culture, 4 ng ml^{-1} bFGF and 5 ng ml^{-1} brain-derived neurotrophic factor (BDNF, Prospec, Rehovot, Israel) were added to the NDM to support neuronal maturation. The cultures were maintained with three medium changes per week.

2.3. Immunocytochemistry

Protein expression in cultures was characterized with immunocytochemical staining as previously described (Lappalainen et al., 2010). The following primary antibodies were used: MAP-2 (rabbit, 1:400, Millipore, Billerica, MA, USA: AB5622), MAP-2 (chicken, 1:4000, Novus Biologicals, Littleton, CO, USA: NB300-213), β_{III}-tubulin (rabbit, 1:2000, GenScript, Piscataway, NJ, USA: A01627), β_{III}-tubulin (chicken, 1:4000, Abcam, Cambridge, MA, USA: ab107216), GFAP (chicken, 1:4000, Abcam: ab4674), synaptophysin (mouse, 1:2000, Sigma-Aldrich: s5768), vGlut (guinea pig, 1:1000, Millipore: AB2251), GABA (rabbit, 1:1000, Sigma-Aldrich: A2052), GAD67 (mouse, 1:100, Millipore: MAB5406), TH (mouse, 1:800, Sigma-Aldrich: T1299), serotonin (rabbit, 1:800, Sigma-Aldrich: S5545), and S100β (mouse, 1:500, Abcam: ab11178). For secondary antibody labeling, Alexa Fluor 488 (1:400), Alexa Fluor 568 (1:400) or Alexa Fluor 647 (1:200) dye (Thermo Fisher Scientific) was used as appropriate. The cells were imaged using an Olympus IX51 microscope (10×, NA = 0.3 and 20×, NA = 0.45 objectives) equipped with an Olympus DP30BW camera (Olympus Corporation, Hamburg, Germany). For synaptophysin staining, an LSM780 Laser Scanning Confocal Microscope (40× objective, NA = 1.4) with a Quasar spectral GaAsP detector (all from Carl Zeiss, Jena, Germany) was used.

To quantify the neuron-to-astrocyte ratio at the 8 and 15 wk. time points, cells were plated under adherent culture conditions and were stained after 2 and 4 wks for neuronal (MAP-2 + β-tubulin) and astrocyte (GFAP) markers. The numbers of biological and technical repeats are listed in Supplementary Table 2. Distinct cell types were automatically counted using CellProfiler (Carpenter et al., 2006) and CellProfiler Analyst (Jones et al., 2008) software. The results of the automated analysis were evaluated manually, and samples with fewer than 200 cells or a false classification result were excluded from the final analysis.

2.4. RT-PCR analysis and qRT-PCR array

Total RNA was isolated from 8 + 5 wks and 15 + 5 wks differentiated cells using the NucleoSpin RNA XS kit (Macherey-Nagel, Düren, Germany) according to the manufacturer's instructions. The concentration and quality of the RNA were monitored spectroscopically. For each sample, 800 ng of total RNA was reverse transcribed into cDNA with the High Capacity cDNA Reverse Transcription kit (Applied Biosystems, Thermo Fisher Scientific, Foster City, CA, USA) according to the manufacturer's instructions.

To investigate brain region specificity and chloride transporter expression, a standard RT-PCR analysis was performed (target genes, primer sequences and exact annealing temperatures in Supplementary Table 1). For each reaction, an aliquot of 2.5 ng cDNA was used with

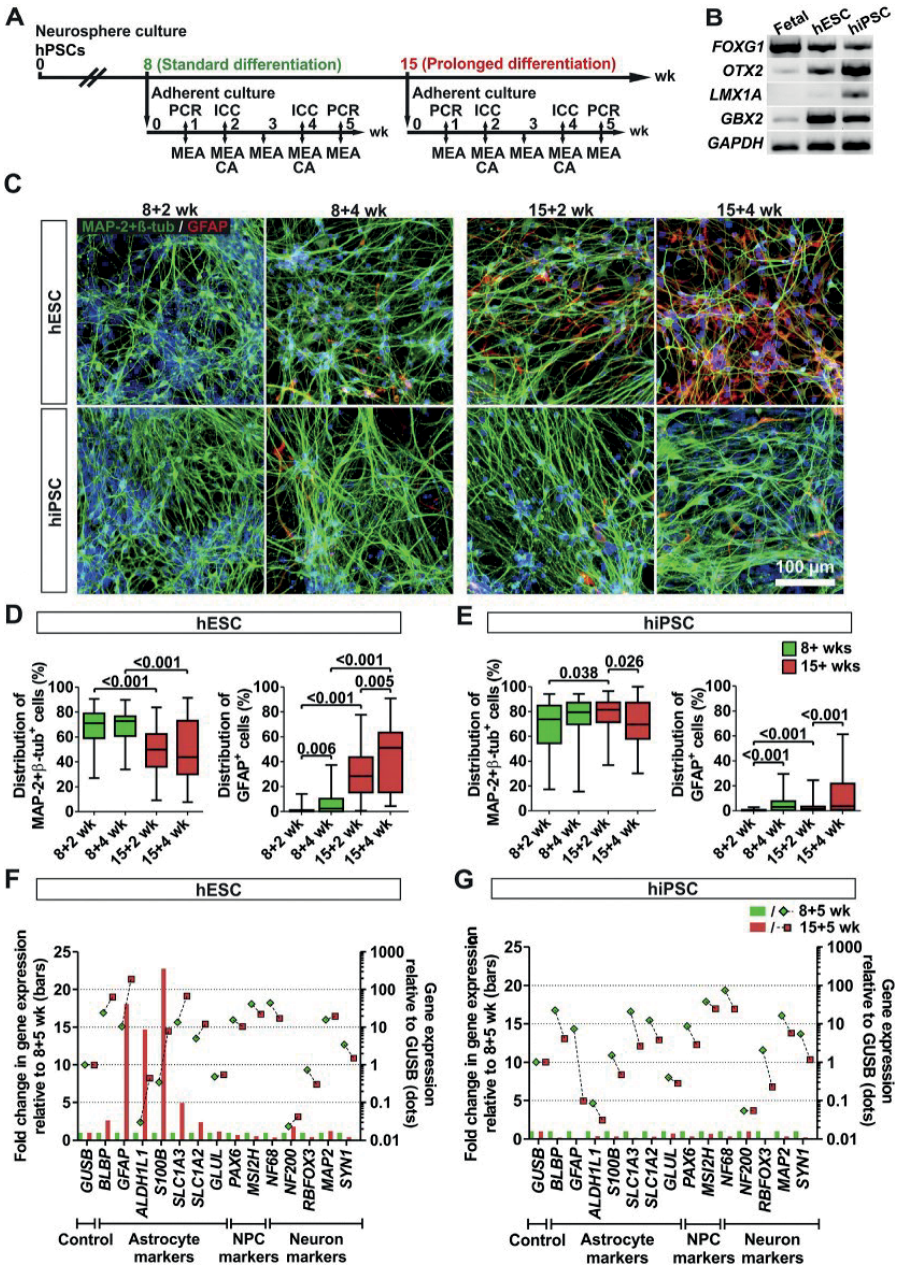

Fig. 1. Differentiation of hESC- and hiPSC-derived neurons and astrocytes. (A) hPSCs were first differentiated in neurosphere culture for 8 or 15 wks and then plated under adherent culture conditions for maturation up to five weeks before characterization with immunocytochemical staining (ICC), PCR, Ca^{2+} imaging (CA), and microelectrode array (MEA). (B) At 8 + 1 wk. time point RNA was extracted from cultures and RT-PCR was performed for forebrain (*FOXG1* and *OTX2*), midbrain (*LMX1A*) and hindbrain markers (*GBX2*) ($n = 1$). Human fetal brain RNA was used as control. The displayed bands were cropped from a single image of one gel (Supplementary Fig. 5A). (C) Representative images of immunocytochemical staining of neuronal (MAP-2 + β-tubulin) and astrocyte (GFAP) markers after standard (8 + wks) and prolonged (15 + wks) differentiation. 4′,6-diamidino-2-phenylindole (DAPI) nuclear staining is in blue. (D, E) The percentages of neurons and astrocytes were counted using CellProfiler analysis tools. The data are presented as the distribution of the percentages of neurons and astrocytes at each time point. The median and interquartile ranges are indicated by lines, and the whiskers indicate the minimum and maximum of the data. A non-parametric Mann-Whitney *U* test was used for the statistical analysis, and p-values <0.05 were considered significant. Significant p-values are presented in the images. The number of samples analyzed is presented in Supplementary Table 2. (F, G) At the 8 + 5 and 15 + 5 wk. time points, qPCR was performed to evaluate various neural precursor cell (NPC) markers and markers of mature neurons and astrocytes (n = 1, 3 technical replicates). The bars represent the fold change in gene expression between 8 + 5 and 15 + 5 wks, and they correspond to the left *y*-axis. The dots indicate the variable expression levels of genes compared to the housekeeping gene *GUSB*, and they correspond to the right *y*-axis (logarithmic).

0.2 mM of both forward and reverse primers, 1 × PCR buffer (−MgCl, +KCl), 1.5 mM $MgCl_2$, 0.1 mM dNTP mix and 0.25 U/μl Taq DNA polymerase (Qiagen, Hilden, Germany). The cDNA was amplified using 37 PCR cycles with an initializing step at 95 °C for 3 min, DNA denaturation at 95 °C for 30 s, annealing at 60–68 °C (Supplementary Table 1) for 30 s and elongation at 72 °C for 1 min. A 5 min elongation step finalized the reaction. The PCR products were separated electrophoretically on a 1.5% agarose gel in Tris/Borate/EDTA buffer containing GelRed (Biotium, Hayward, CA, USA) and visualized using BioRad ChemiDoc MP system (Bio-rad Laboratories, Inc., Hercules, CA, USA).

To investigate astrocyte, neural precursor and general neuron genes, a gene expression array analysis of a subset of 14 genes of interest (Supplementary Table 1) was performed using a custom TaqMan® Array (Applied Biosystems) according to the manufacturer's instructions. For each reaction, 6 ng of cDNA was used with TaqMan® Universal PCR Master Mix (Applied Biosystems). The analysis was performed using the ABI Prism 7300 real-time PCR system (Applied Biosystems). The data were normalized to the expression of the housekeeping gene GUSB, and the data from the 15 + 5 wks time point were further compared to the 8 + 5 wks time point. Relative expression values were determined using the comparative $2^{-\Delta\Delta Ct}$ method, and the quality of the PCR products was monitored with a melt curve analysis. The analysis consisted of three technical replicates.

2.5. Ca^{2+} imaging

Ca^{2+} signaling of 8 and 15 weeks differentiated cells was studied after 2 and 4 wks of adherent maturation. Cells were loaded with 4 μM of Fluo-4 AM (Thermo Fisher Scientific) diluted in NDM for 30 min at 37 °C and 5% CO_2, followed by washing with NDM for another 30 min at 37 °C and 5% CO_2. Culture were imaged every 0.5 s while being continuously perfused with physiological solution at 36 ± 0.5 °C at a rate of 2 ml/min (RC-22 perfusion chamber, TC-344C temperature controller, SH-27B in-line solution heater; Warner Instruments Inc., Hamden, USA). The physiological solution contained 140 mM NaCl, 10 mM HEPES, 10 mM D-glucose, 3.5 mM KCl, 1.25 mM NaH_2PO_4, 2 mM $CaCl_2$ and 1 mM $MgCl_2$ (all from Sigma-Aldrich) dissolved in dH_2O. The fluorescent imaging system consisted of an Olympus IX61 inverted microscope (10× and 20× objectives, NA = 0.5), an Andor iXon 885 EMCCD camera (Andor Technology, Belfast, Northern Ireland) and a Polychrom V monochromator (TILL Photonics, Munich, Germany). Images were acquired with TILL Photonics Live Acquisition software and analyzed with SimplePCI software package (Hamamatsu Corporation, Sewickley, PA, USA). Neuronal cells were identified by their morphology and ability to quickly respond to elevated extracellular K^+ (50 mM). Ca^{2+} signaling was considered related to action potentials if it was blocked by the voltage-gated sodium channel antagonist tetrodotoxin (TTX, 1 μM, Tocris Bioscience, Bristol, UK). GABA (100 μM, Sigma-Aldrich) and glutamate (50 μM, Sigma-Aldrich) were applied to test for the presence of functional receptors for these major neurotransmitters. The fluorescence intensity was normalized to the resting level, and amplitude of the GABA and glutamate responses in each cell was calculated as a fraction of the response to high-K^+ depolarization in the cell. The numbers of biological and technical repeats are listed in Supplementary Table 2.

2.6. Microelectrode arrays

The development of spontaneous electrical activity in 8 and 15 wks differentiated cells was measured for 5 wks with a MEA system (Heikkilä et al., 2009). Recordings were obtained with an MEA60 amplifier and 60-6wellMEA200/30iR-Ti-w/o arrays with 9 electrodes per well (Multi Channel Systems [MCS], Reutlingen, Germany; Fig. 4A). A custom-made 6-well silicone chamber, SpikeBooster, was used to culture neural cells on MEA dishes as previously described (Kreutzer et al., 2012). The temperature was maintained at 37 °C with a TC02 temperature controller (MCS). Cultures were measured twice per week for 10 min, and the two weekly measurements were averaged for analysis (Supplementary Table 2, experimental repeats). The control of measurements and the detection of spikes were performed with MC_Rack software (MCS). A sampling rate of 50 kHz was used for the measurements. Spikes were detected from 200 Hz high-pass filtered data when their amplitude crossed the threshold of −5 × standard deviation (SD) of noise. Electrodes with a total spike frequency >0.033 Hz (2/min) were experimentally determined to present biological activity (*i.e.*, to be active electrodes; Supplementary Fig. 4A–C). The spike count and burst analysis were performed using a custom-made script for MATLAB (MathWorks, Natick, MA, USA) (Kapucu et al., 2012) with further modifications. Additional conditions were applied to the analysis to ensure the validity of burst detection: burst detection was only applied to channels where the total spike frequency was at least 0.167 Hz (10/min), and a minimum of three spikes was considered to form a burst. Furthermore, if the automatically detected burst inter-spike interval threshold exceeded 2000 ms, the channel was considered not to have bursts and was excluded from the burst analysis.

2.7. Statistical analysis

Due to the non-Gaussian distribution of the data, the non-parametric Kruskal Wallis test (with Dunn's *post hoc* – test) and Mann-Whitney *U* test were used. All the statistical tests were performed with SPSS Statistics software (version 23.0).

3. Results

3.1. hPCS differentiate efficiently into neuronal population with varying proportion of astrocytes

Using our simple neurosphere differentiation method (Lappalainen et al., 2010), we have tested the neural differentiation capacity of several hESC and hiPSC lines (Lappalainen et al., 2010; Toivonen et al., 2013) and have chosen the in-house derived hESC line Regea 08/023 and the hiPSC line 04311.WT for a detailed study of neuron and astrocyte differentiation and functionality (Fig. 1A). Cells were differentiated in suspension for either standard 8 week period or prolonged 15 week period and plated in adherent culture for maturation and experiments. For clarity, the names of the study's time points refer to both differentiation and maturation time points. For example, 8 + 2 wks refers to 8 weeks of differentiation in neurosphere culture, and 2 weeks of adherent maturation (Fig. 1A).

To examine the brain regional identity of the cells, we performed RT-PCR to 8 + 1 wk. samples and detected strong expression of forebrain (*FOXG1*, *OTX2*) and hindbrain (*GBX2*) markers, and minor expression of midbrain marker (*LMX1A*) (Fig. 1B). Expression of midbrain marker *EN1* and hindbrain marker *HOXA2* were not detected. RT-PCR analysis confirmed that the culture represents a mixed neural cell population.

In order to determine the differentiation capacity of the two hPSC lines, neuronal cells were immunostained with microtubule-associated protein 2 (MAP-2) and β-tubulin antibodies, and astrocytes with glial fibrillary acidic protein (GFAP) antibody. Quantification of the neuron-to-astrocyte ratio in the hESC line revealed good capacity to give rise to both neurons and astrocytes (Fig. 1C and D, for cell counts see Supplementary Fig. 2). Neuronal cells were efficiently produced, but their proportion was decreased with prolonged differentiation time from 73% at 8 + 4 wks to 44% at 15 + 4 wks (Fig. 1D). Astrocyte proportion increased gradually at the expense of neuronal cells from 2% at 8 + 4 wks to 51% at 15 + 4 wks (Fig. 1C and D). At the same time, proportion of cells without any neural staining was diminished from 25% at 8 + 4 wks to 5% at 15 + 4 wks. In line with the immunocytochemical data, the gene expression analysis revealed upregulation of astrocyte markers (*BLBP, GFAP, ALDH1L1, S100B, SLC1A3, SLC1A2,* and *GLUL*) after prolonged differentiation (15 + 5 wks) (Fig. 1F). Such robust changes

were not observed with neural precursor cell (NPC) markers (*PAX6, MSI2H*) or neuron markers (*NF68, NF200, RBFOX3, MAP2, SYN1*) (Fig. 1F).

The hiPSC line was shown to have a good capacity for neuronal differentiation but limited astrogenesis (Fig. 1C and E). The hiPSC line efficiently produced neuronal cells after standard differentiation time, and the proportion remained also high after prolonged differentiation: 80% at 8 + 4 wks and 70% at 15 + 4 wks (Fig. 1E). Contrary to the results obtained with hESC line, the increase in astrocyte proportion in hiPSC line was very modest, from 3% at 8 + 4 wks to 5% at 15 + 5 wks (Fig. 1E). The proportion of cells without any neural staining slightly increased from 17% at 8 + 4 wks to 25% at 15 + 4 wks. Furthermore, at the gene expression level, astrocyte markers were not upregulated in the hiPSC line (Fig. 1G). To summarize, these findings demonstrate that the hiPSC line (04311.WT) did not undergo astrocyte enrichment

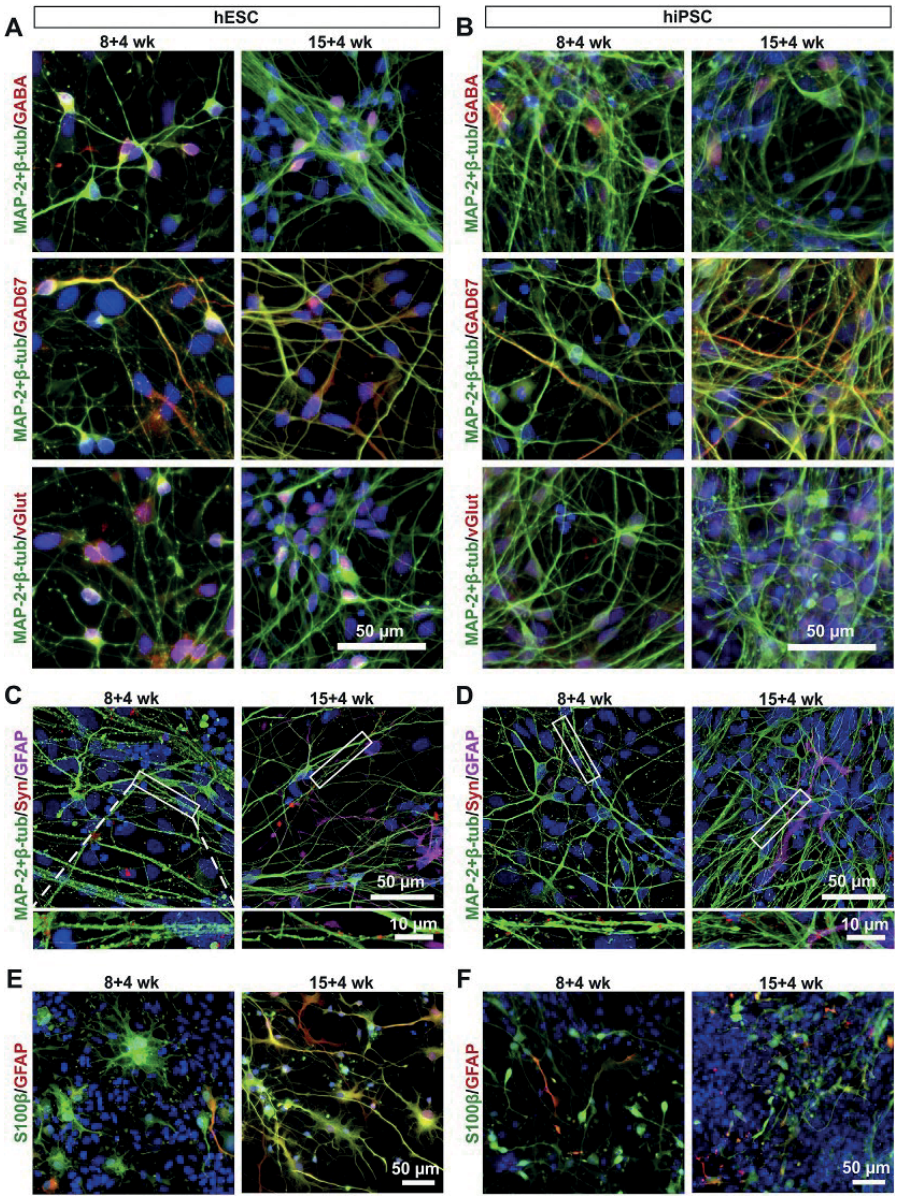

Fig. 2. Immunocytochemical characterization of neural cell types. Immunocytochemical staining verified specific neuronal subtypes expressing GABA, GAD67 and vGlut in both (A) hESC- and (B) hiPSC-derived 8 + 4 wks and 15 + 4 wks old cultures (n = 1). (C, D) Synaptophysin staining co-localized with the neuronal markers MAP-2 + β-tubulin in all analyzed cultures (*n* = 3). GFAP-positive astrocytes were sometimes found in close proximity to synaptophysin-positive neuronal processes after prolonged differentiation (15 + 4 wks). Insets below show a magnified view of synaptophysin staining along neuronal processes. (E, F) Astrocytes expressing the cell type-specific markers S100β and GFAP were found in all the cultures (n = 1). DAPI nuclear staining is shown in blue.

as efficiently as the hESC line (Regea 08/023). On the other hand, NPC and neuron markers were expressed at comparable level in both hPSC lines supporting overall good neuronal differentiation capacity.

3.2. Immunocytochemical characterization of hPSC-derived neural cultures

The majority of neurons were positive for GABAergic or glutamatergic markers in both 8 and 15 wk. differentiated cultures (Fig. 2A and B). Neurons expressing the presynaptic marker synaptophysin were detected at all the studied time points (Fig. 2C and D). Combined staining of synaptophysin with the neuronal markers revealed organized synaptophysin-positive boutons in neuronal processes. Occasionally, astrocyte processes were found aligned with synaptophysin-positive neuronal processes (Fig. 2C and D). Astrocytes were characterized with GFAP and S100 calcium-binding protein B (S100β) staining, and in most cases, both markers were co-localized (Fig. 2E and F). As stated earlier, the proportion of GFAP-positive astrocytes was increased after prolonged differentiation especially in the hESC line (Fig. 1) (Fig. 2E). Some astrocytes sent several-hundred-micrometer-long processes which often closely intertwined with neuronal axons and dendrites.

3.3. Prolonged differentiation enhances maturation of GABAergic system

To study the basic functional properties of the hESC- and hiPSC-derived neural cultures, we monitored intracellular Ca^{2+} dynamics using Fluo-4 AM dye (Fig. 3). First, we imaged spontaneous Ca^{2+} signaling and its blockage by tetrodotoxin (TTX). Next, γ-aminobutyric acid (GABA) and glutamate were applied to demonstrate for the presence of functional receptors for these major neurotransmitters. Finally, a high concentration of KCl was used to induce depolarization and voltage-gated Ca^{2+} channel activation. The subsequent immunocytochemical staining verified that Ca^{2+} signals were detected from both neurons and astrocytes (Fig. 3A–C). Examples of neuronal and astrocyte Ca^{2+} signals are presented in Supplementary Movies 1 and 2.

Spontaneous neuronal Ca^{2+} transients were detected at all the studied time points in both hPSC lines. Neurons exhibited Ca^{2+} events with single spikes and high-frequency oscillations (Fig. 3B and Movie 1). TTX reversibly blocked spontaneous Ca^{2+} signaling in a subset of neurons (Fig. 3B), indicating that the activation of Na^{+} voltage-gated channels due to depolarization is a critical step for spontaneous, action potential-related Ca^{2+} signaling in neuronal cells (Fig. 3E and F).

Responses to GABA and glutamate application confirmed the presence of functional receptor-operated channels in neurons. Glutamate induced an instant, strong Ca^{2+} elevation in the majority (85–99%) of the analyzed neurons (Fig. 3G and H). The amplitudes of the glutamate responses are presented in Supplementary Fig. 3A. In contrast to glutamate treatment, the neuronal responses to GABA application varied considerably between studied time points. In most cases, GABA had an excitatory effect increasing intracellular Ca^{2+} (Fig. 3B) but occasionally spontaneous activity of neurons was attenuated by GABA treatment (Fig. 3D). In the hESC line, the proportion of neurons responding to GABA with a Ca^{2+} rise (excitatory action) decreased progressively during both prolonged differentiation and adherent maturation. GABA response decreased from 76% at 8 + 2 wks to 24% at 15 + 4 wks (Fig. 3I). The reduction in excitatory GABA response over time was not as prominent in the hiPSC line as in the hESC line. In hiPSC line, proportion of GABA-responsive cells decreased from 61% at 8 + 2 wks to 51% at 15 + 4 wks (Fig. 3J). The changes in GABA response amplitudes are presented in Supplementary Fig. 3C and D. To support these results we performed RT-PCR analysis of chloride transporter genes *NKCC1* and *KCC2*, important for the developmental change of GABA response from excitatory to inhibitory (Ben-Ari et al., 2012). In both hPSC lines, the expression of *NKCC1*, a marker of early development, was strongest in 8 + 1 wk. time point after which it was down-regulated (Fig. 3K). *KCC2* expression, which starts later in development, was observed at 15 + 1 wk. time point (Fig. 3K).

All in all, both of the studied hPSC lines demonstrated similar trends in the development of pharmacological responses over time. Maturation of GABAergic system was observed as a result of prolonged differentiation.

3.4. Prolonged differentiation promotes maturation of spontaneous activity

Spontaneous electrical activity in neuronal cultures was measured using MEA (Fig. 4A and B) as previously described (Heikkilä et al., 2009). Significant differences between hPSC lines, as well as numerical details (medians and averages) are presented in Supplementary Table 3. To verify the dependency of activity on excitatory and inhibitory synaptic factors, we used a pharmacological test battery containing N-Methyl-D-aspartate (NMDA), α-amino-3-hydroxy-5-methyl-4-isoxazolepropionic acid (AMPA)/kainate and GABA receptor ligands (Supplementary Fig. 4).

The hESC-derived cultures followed an activity development curve after standard differentiation with a high-activity peak at 8 + 3 and 8 + 4 wks (Fig. 4C, E and G). Similar clear curves were not detected in the hiPSC-derived cultures after standard differentiation (8+ wks; Fig. 4D, F and H) or from either of the hPSC lines after prolonged differentiation (15+ wks; Fig. 4C–H). All in all, there were more active electrodes in the hESC-derived cultures, and prolonged differentiation significantly reduced the proportion of active electrodes per culture with both hPSC lines (Supplementary Table 2 and Fig. 4C and D).

Spike frequency in active electrodes is a frequently used measure of neuronal activity (Fukushima et al., 2016). The median and average spike frequency values are listed in Supplementary Table 3 (see also Supplementary Movie 3). In the hESC-derived cultures, the spike frequency reached a maximum during the high-activity peak at 8 + 4 wks, with a median value of 0.276 Hz (Fig. 4E). At the corresponding time point after prolonged differentiation (15 + 4 wks), the spike frequency was significantly reduced to 0.132 Hz ($p = 0.020$). Similar reductions in spike frequency were observed with the hiPSC-derived cultures (Fig. 4F).

Spontaneous bursts were detected in all the studied groups (Fig. 4C and D). Prolonged differentiation (15+ wks) significantly reduced the proportion of burst-detecting electrodes (Fig. 4C and D). Nonetheless, in those burst-detecting electrodes, burst counts increased significantly in both hPSC lines (Fig. 4G and H). In the hESC line, the greatest increase in burst number was detected between 8 + 2 and 15 + 2 wks, from 30 to 81 bursts per electrode ($p = 0.012$). In the hiPSC line, the highest increase was already between 8 + 1 and 15 + 1 wks, from 25 to 80 bursts per electrode ($p = 0.046$).

According to these results, prolonged differentiation affected the organization neuronal activity similarly in both hPSC lines by condensing the activity to fewer electrodes, which in turn expressed more frequent burst activity. The spike frequency and burst counts in active electrodes were similar between the hPSC lines verifying that the level of activity development was comparable.

3.5. Prolonged differentiation affects burst characteristics

After concluding that both hPCS lines develop similar bursting activity, we next studied in detail the basic burst characteristics: spike frequency in bursts, burst duration and number of spikes per burst (Fig. 5). Numerical details (median and mean values) of burst parameters and significant differences between the hPSC lines are presented in Supplementary Table 4. Prolonged differentiation (15+ wks) of the hESC-derived cultures significantly increased the spike frequency in bursts at 4 out of 5 time points (Fig. 5A). The difference was most notable between 8 + 3 and 15 + 3 wks, with median frequency values of 11 Hz and 25 Hz ($p < 0.001$). In contrast, in the hiPSC line, spike frequency in bursts was reduced as result of prolonged differentiation. This reduction was most evident between 8 + 3 and 15 + 3 wks, when the median values were 19 Hz and 5 Hz ($p = 0.002$, Fig. 5B).

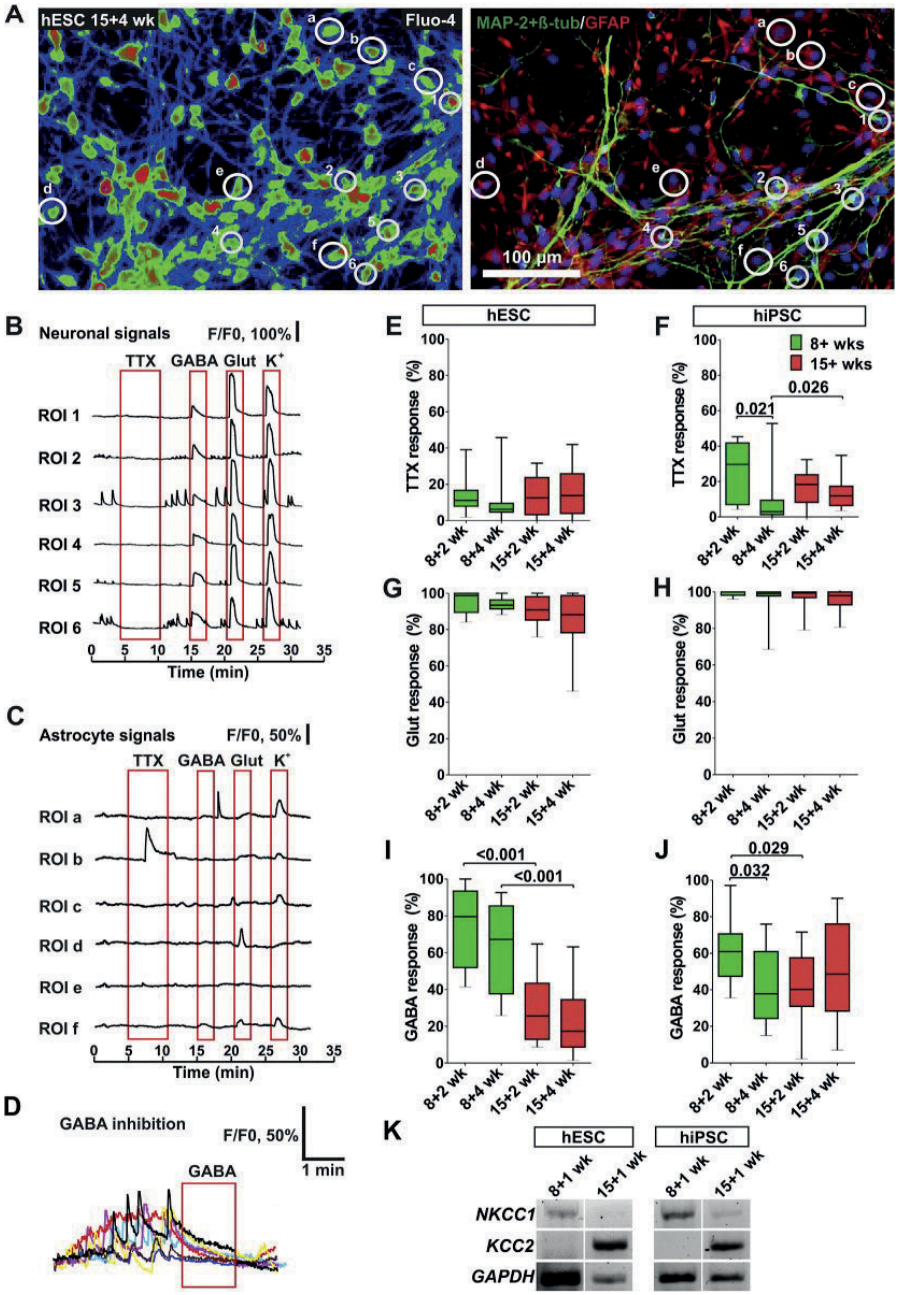

Fig. 3. Ca^{2+} signaling after standard and prolonged differentiation. (A) For calcium imaging experiments neural culture was loaded with Fluo-4 AM Ca^{2+} indicator. On the left a representative pseudocolor image of Fluo-4 loaded culture where red indicates high and blue indicates low Ca^{2+} levels. On the right is the same field after immunocytochemical staining of neuronal cells (MAP-2 + β-tubulin) and astrocytes (GFAP). DAPI nuclear staining is in blue. Neurons are marked with small region of interest (ROI) and numbering, and astrocytes are marked with large ROI and letters. Typical traces of (B) neuronal and (C) astrocyte Ca^{2+} signals. (D) Example traces showing attenuation of spontaneous neuronal Ca^{2+} signaling by GABA. Cultures showed both spontaneous activity and responses to pharmacological treatments. (E, F) Percentages of neuronal cells silenced by TTX (1 µM) treatment after standard and prolonged differentiation. Percentage of neuronal cells responding to (G, H) glutamate (Glut, 50 µM) and (I, J) GABA (100 µM) applications. The data are presented as the distribution of the percentages at each time point. The median and interquartile ranges are indicated by lines, and the whiskers indicate the minimum and maximum of the data. A non-parametric Mann-Whitney *U* test was used for the statistical analysis, and p-values <0.05 were considered significant. Significant p-values are presented in the images. See also Supplementary Fig. 3 for response amplitudes. The number of samples analyzed is presented in Supplementary Table 2. For all analyses (*E-J*), cells with neuronal morphology responding to high K^+ application were included. (K) The expression of chloride channel genes *NKCC1* and *KCC2* was determined with RT-PCR in both cell lines at 8 + 1 and 15 + 1 wk. time points ($n = 1$). The RT-PCR products from the two hPSC lines were analyzed on separate gels and image exposure times for the two gels were identical. Otherwise the bands representing different genes and time points were cropped from a single image of one gel (Supplementary Fig. 5B and C).

Burst duration was significantly reduced by prolonged differentiation (15+ wks) at 4 out of 5 time points in the hESC-derived cultures (Fig. 5C). The difference was most prominent between 8 + 3 wks and 15 + 3 wks, with median values of 476 ms and 223 ms ($p < 0.001$). In the hiPSC-derived cultures, however, prolonged differentiation increased the burst duration; the median duration was 286 ms at 8 + 3 wks and 1883 ms at 15 + 3 wks ($p = 0.001$, Fig. 5D). The number of spikes per burst was unaffected in most time points (medians between 4 and 6; Fig. 5E and F). Almost all the significant changes in spike frequency in burst and burst duration occurred at the same time points (Fig. 5A and B *vs.* C and D). Therefore, it appears that changes in burst duration were responsible for the differences in spike frequency in bursts.

To summarize, after prolonged differentiation the hESC-derived cultures demonstrated increased spike frequency in bursts, which was associated with reduced burst duration. Prolonged differentiation did not support similar burst development in the hiPSC-derived cultures.

4. Discussion

In our culture system, prolonged differentiation resulted in a switch from neurogenesis to astrogenesis recapitulating the *in vivo* developmental stages, as previously described (Itsykson et al., 2005; Nat et al., 2007). We characterized the effects of prolonged differentiation on cell type composition, and studied neuronal function using Ca^{2+} imaging and MEA. Here, we report that prolonged neuronal differentiation enhances the functional maturation of hPSC-derived neuronal cultures.

Propensity for astrogenesis varied substantially between the studied hPSC lines in long-term follow-up. The neuron-to-astrocyte ratio was similar in both hPSC lines after standard 8 weeks of differentiation but after prolonged 15 weeks of differentiation, the ratio was strikingly different. The astrocyte proportion in the hiPSC line was very modest, only 5%, whereas the hESC line produced up to 50% of astrocytes. Earlier studies also showed variation in neuron and astrocyte differentiation among hPSC lines regardless of their origin (Emdad et al., 2012; Toivonen et al., 2013). Especially in hiPSC lines, incomplete transgene silencing and epigenetic differences can affect differentiation capacity (Hatada et al., 2008; Kim et al., 2010). Although pluripotency-inducing transgenes were silenced in the hiPSC line used in the present work, possible methylation of astrocyte-specific genes might delay astrocyte differentiation (Hatada et al., 2008; Majumder et al., 2013). Generally, differentiation capacity is known to be related to intrinsic properties of the particular hPSC line (Emdad et al., 2012; Hu et al., 2010; Toivonen et al., 2013).

The neuronal cells produced a mixed population of glutamatergic neurons with a subset of GABAergic neurons, as demonstrated by immunocytochemistry and functional measurements. These results are in line with a recent report characterizing the generation of glutamatergic and GABAergic neurons from hPSCs using another neurosphere differentiation protocol (Floruta et al., 2017). Here, both hPSC lines showed similar properties respective to action potential generation and glutamate responsiveness. hPSC-derived neurons also responded at comparative levels to high K^+ and glutamate applications similarly as previously described by Forostyak et al. (2013). After standard 8 weeks differentiation, our GABAergic population was immature and responded to GABA application with excitation. Also, we detected expression of chloride transporter *NKCC1*, which is prominently expressed in early GABAergic development (Ben-Ari et al., 2012). During prolonged differentiation, we observed a typical reduction in the excitatory GABAergic response and concurrent increase chloride transporter *KCC2*, a mature marker for chloride transporter development (Ben-Ari et al., 2012). Together these changes imply developmental maturation of the GABAergic system as a result of prolonged differentiation.

MEA experiments showed that spontaneous neuronal activity could be repeatedly measured from all the studied time points. The analysis revealed varying electrical activity patterns, resulting in a non-Gaussian distribution of the data. A very comprehensive, large-scale study by Wagenaar and colleagues showed similar MEA data distribution with rodent primary neuronal networks (Wagenaar et al., 2006). Although MEA studies with rodent-derived neuronal cultures provide a well-established reference for future applications, even primary human and primary rodent cultures are far from comparable. Human cultures tend to have a significantly slower rate of activity development, lower percentage of active electrodes and spike counts in comparison to rodent cultures (Napoli and Obeid, 2016). The current results show that also human stem cell-derived cultures have a comparatively low percentage of active electrodes and low spike counts. Therefore the characteristics of hPSC-derived cultures need to be considered in MEA experimental design, execution and data analysis.

MEA analysis revealed that prolonged differentiation decreased the overall spike frequency and condensed electrical activity to particular areas in the culture. Although the overall level of activity seemed to decrease in prolonged differentiation, the remaining activity organized from single spikes into bursts with increasing bursting frequency. As bursts are thought to represent more mature neuronal function, the increase in burst number after prolonged differentiation should be expected. The observed reduction in the percentage of active and burst detecting electrodes could be attributed to synaptic pruning (Yamamoto and López-Bendito, 2012; Benders et al., 2015) or the increase in proportion of astrocytes at the expense of neurons after prolonged differentiation. Even though, the amount of spontaneous spike and burst activity was in a comparable level between the studied hPSC lines after prolonged differentiation, closer analysis revealed differences in their activity patterns. In the hESC line prolonged differentiation was associated with burst compaction. Mature compact bursts were not formed similarly in the hiPSC line. This, and the slight increase of non-neuronal and non-astrocytic cells in the hiPSC line after prolonged differentiation may reflect aberrant differentiation, which supports the observation that not all cell lines mature as efficiently after extended culture times (Emdad et al., 2012; Toivonen et al., 2013). Also, the studied hESC line produced a substantial amount of endogenous astrocytes (>50%) which could partly help in stabilizing neuronal activity and support compaction of burst activity in long-term culture. However, dissecting these processes pharmacologically in astrocytes alone is very challenging, and new approaches are needed to address these questions. Even though hPSC-derived neuron cocultures with rodent astrocytes are relatively well established, the cocultures with human astrocytes need to be better validated.

In conclusion, we found that the studied hPSC lines underwent neurogenic-to-gliogenic switch during prolonged differentiation. However, there were striking differences in the efficiency of astrogenesis which should be considered also more carefully in the field. Despite its challenges, prolonged neural differentiation induces functional changes which mimic the development occurring *in vivo*, and in the future it can be utilized in development of more representative hPSC-derived neural models.

Supplementary data to this article can be found online at https://doi.org/10.1016/j.scr.2018.01.018.

Author contributions

S.N., T.P., A.P. and D.F. designed the study; T.P., A.P., D.F. and M.P. performed experiments; M.M. contributed new analytic tools; T.P., A.P. and D.F. analyzed data; H.H. assisted with the statistical analysis; and T.P., A. P. and S.N. wrote the paper. T.P. and A.P. contributed equally to this work. All authors edited the article.

Competing financial interests

Authors declare no competing financial interests.

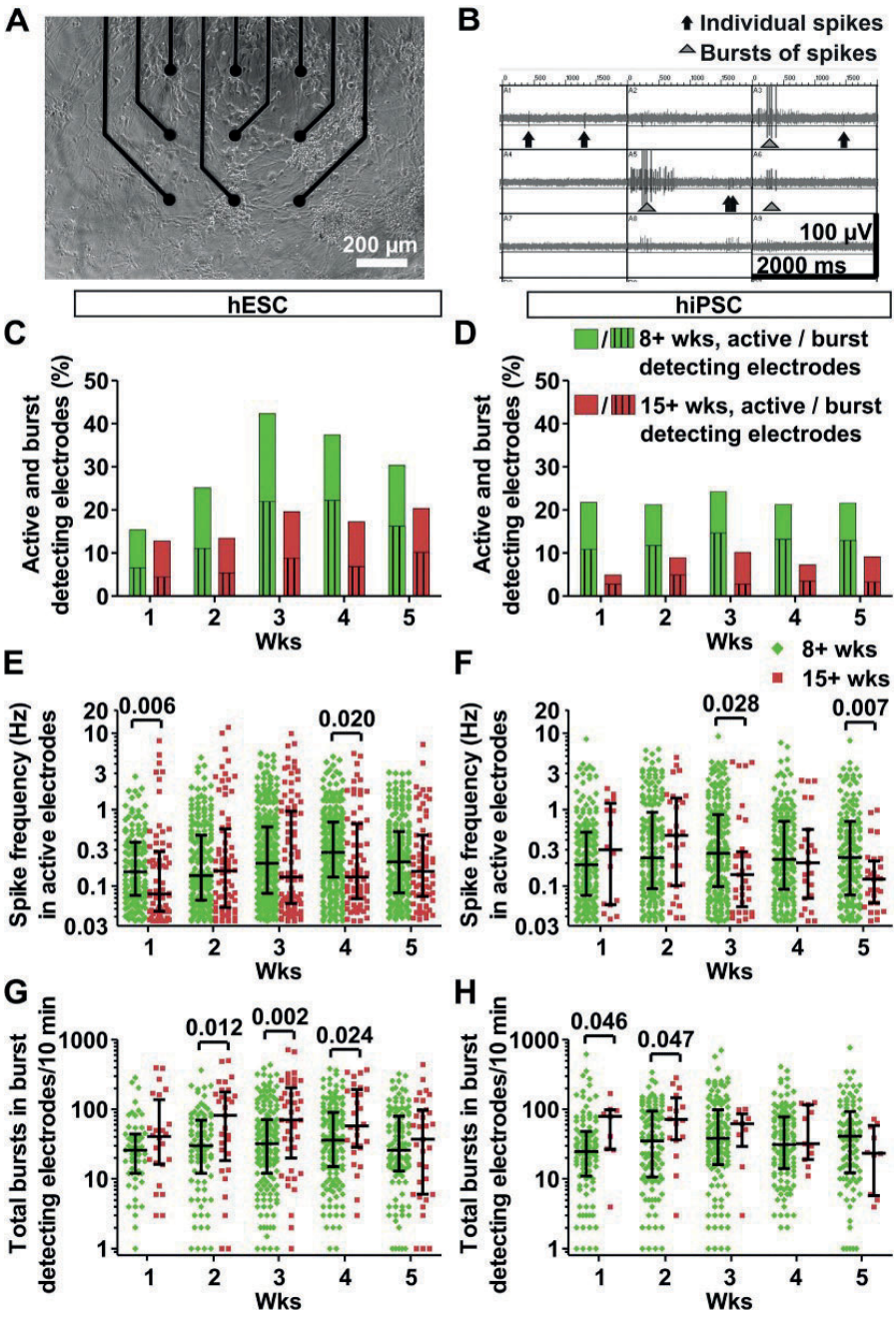

Fig. 4. Spike and burst activity development after standard and prolonged differentiation. (A) Activity was measured with 9 electrodes per well. (B) Spikes were detected when their amplitude exceeded a threshold of 5 × standard deviation of background noise. Vertical scale bar is 100 µV and horizontal 2 s. (C, D) The percentage of active (colored bars, no texture) and burst detecting electrodes (colored bars, striped) was calculated from spike and burst counts determined using a custom-made MATLAB algorithm. (E, F) The spike frequency in active electrodes was calculated from the same data. (G, H) The number of bursts in burst-detecting electrodes was also calculated. The numbers of spikes and bursts (E-H) are presented as scatter plots on a logarithmic scale; each dot represents a single electrode, the horizontal line indicates the median, and whiskers indicate the interquartile range. See also Supplementary Table 3. The numbers of analyzed cultures and electrodes are presented in Supplementary Table 2. Statistical significance was calculated using the Mann-Whitney U test, and a p-value <0.05 was considered significant. Significant p-values are presented in the images.

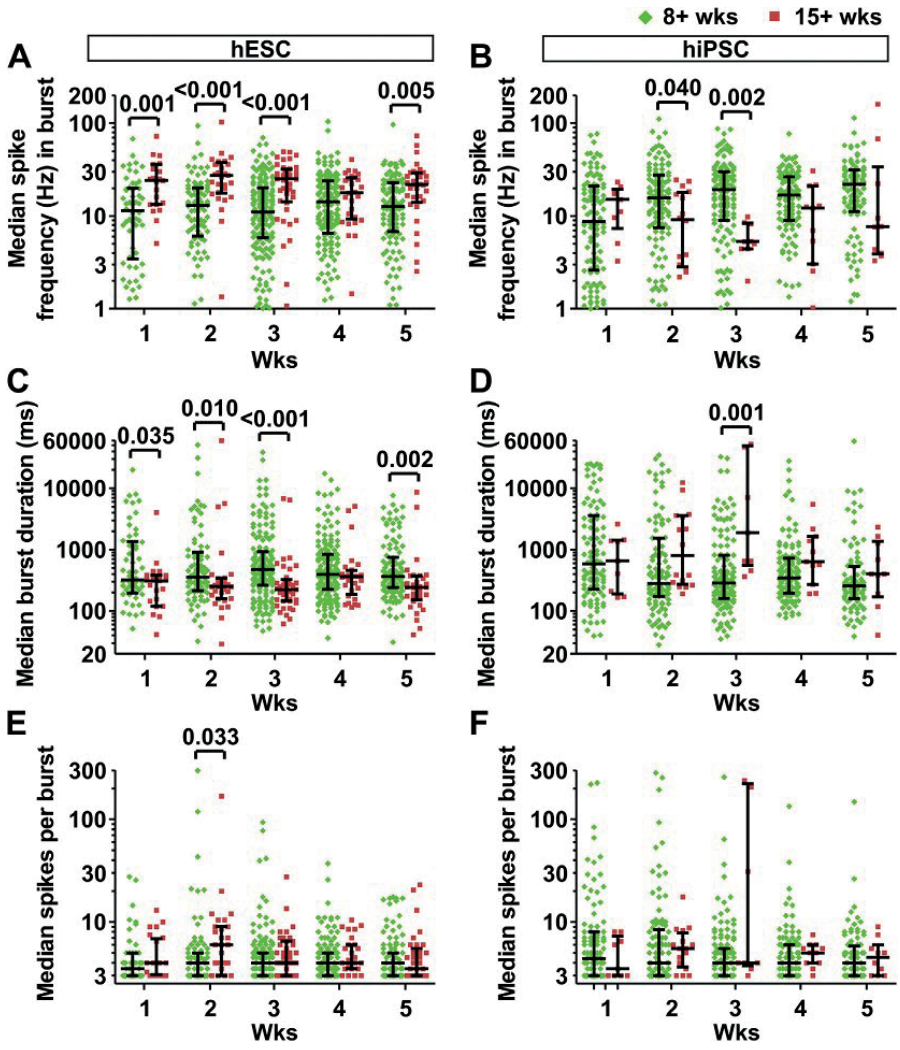

Fig. 5. Burst parameters after standard and prolonged differentiation. (A, B) MEA data were analyzed with a custom-made MATLAB script to determine the spike frequency in bursts. (C, D) Burst duration was also calculated. (E, F) The number of spikes per burst was determined. Each dot in the scatter plot represents the median result from a single electrode on a logarithmic scale. The median and interquartile range are indicated by the line and whiskers, respectively. See also Supplementary Table 4. The numbers of analyzed cultures and electrodes are presented in Supplementary Table 2. Due to high variation in the data, a small number of data points are outside the axis limits (A: 13; B: 4; C: 7; D: 8; E: 3; F: 4; see Supplementary Table 4 for the full range of results). Statistical significances between groups were calculated using the Mann-Whitney U test and significant p-values (<0.05) are indicated in the figure.

Acknowledgements

The authors thank the iPS Cells Facility, University of Tampere, for providing the undifferentiated hiPSCs and Hanna Mäkelä and Eija Hannuksela for technical assistance with cell maintenance and molecular biology analyses. We thank the Imaging Facility and Facility of Electrophysiological Measurements, University of Tampere, and especially Juha Heikkilä and Marco Fabiani for technical assistance with the MEA measurements. We also thank Dr. Laura Ylä-Outinen, PhD, for her advice and constructive criticism throughout the project. This work was supported by the 3DNeuroN project in the European Union's Seventh Framework Programme, Future and Emerging Technologies, grant agreement n°296590. It was also supported by the Human Spare Parts 2 program, The Finnish Funding Agency for Innovation, TEKES. T.P. received support from the Tampere City Science Foundation and Alfred Kordelin Foundation, and A.P. from the Juliana von Wendt Fund.

References

Ben-Ari, Y., Khalilov, I., Kahle, K.T., Cherubini, E., 2012. The GABA excitatory/inhibitory shift in brain maturation and neurological disorders. Neuroscientist 18, 467–486.

Benders, M.J., Palmu, K., Menache, C., Borradori-Tolsa, C., Lazeyras, F., Dubois, J., Vanhatalo, S., Huppi, P.S., 2015. Early Brain Activity Relates to Subsequent Brain Growth in Premature Infants. Cereb. Cortex 25, 3014–3024.

Carpenter, A.E., Jones, T.R., Lamprecht, M.R., Clarke, C., Kang, I.H., Friman, O., Guertin, D.A., Chang, J.H., Lindquist, R.A., Moffat, J., Golland, P., Sabatini, D.M., 2006. CellProfiler: image analysis software for identifying and quantifying cell phenotypes. Genome Biol. 7.

Clarke, L.E., Barres, B.A., 2013. Emerging roles of astrocytes in neural circuit development. Nat. Rev. Neurosci. 14, 311–321.

Du, X., Parent, J.M., 2015. Using patient-derived induced pluripotent stem cells to model and treat epilepsies. Curr. Neurol. Neurosci. Rep. 15.

Emdad, L., D'Souza, S.L., Kothari, H.P., Qadeer, Z.A., Germano, I.M., 2012. Efficient differentiation of human embryonic and induced pluripotent stem cells into functional astrocytes. Stem Cells Dev. 21, 404–410.

Floruta, C.M., Du, R., Kang, H., Stein, J.L., Weick, J.P., 2017. Default patterning produces pan-cortical glutamatergic and CGE/LGE-like GABAergic neurons from human pluripotent stem cells. Stem Cell Rep. 9, 1463–1476.

Forostyak, O., Romanyuk, N., Verkhratsky, A., Sykova, E., Dayanithi, G., 2013. Plasticity of calcium signaling cascades in human embryonic stem cell-derived neural precursors. Stem Cells Dev. 22, 1506–1521.

Frega, M., van Gestel, S.H., Linda, K., van der Raadt, J., Keller, J., Van Rhijn, J.R., Schubert, D., Albers, C.A., Nadif Kasri, N., 2017. Rapid neuronal differentiation of induced pluripotent stem cells for measuring network activity on micro-electrode arrays. J. Vis. Exp. 119.

Fukushima, K., Miura, Y., Sawada, K., Yamazaki, K., Ito, M., 2016. Establishment of a human neuronal network assessment system by using a human neuron/astrocyte co-culture derived from fetal neural stem/progenitor cells. J. Biomol. Screen. 21, 54–64.

Hatada, I., Namihira, M., Morita, S., Kimura, M., Horii, T., Nakashima, K., 2008. Astrocyte-specific genes are generally demethylated in neural precursor cells prior to astrocytic differentiation. PLoS One 3, e3189.

Heikkilä, T.J., Ylä-Outinen, L., Tanskanen, J.M.A., Lappalainen, R.S., Skottman, H., Suuronen, R., Mikkonen, J.E., Hyttinen, J.A.K., Narkilahti, S., 2009. Human embryonic stem cell-derived neuronal cells form spontaneously active neuronal networks in vitro. Exp. Neurol. 218, 109–116.

Hu, B., Weick, J.P., Yu, J., Ma, L., Zhang, X., Thomson, J.A., Zhang, S., 2010. Neural differentiation of human induced pluripotent stem cells follows developmental principles but with variable potency. Proc. Natl. Acad. Sci. U. S. A. 107, 4335–4340.

Itsykson, P., Ilouz, N., Turetsky, T., Goldstein, R.S., Pera, M.F., Fishbein, I., Segal, M., Reubinoff, B.E., 2005. Derivation of neural precursors from human embryonic stem cells in the presence of noggin. Mol. Cell. Neurosci. 30, 24–36.

Johnson, M.A., Weick, J.P., Pearce, R.A., Zhang, S.-., 2007. Functional neural development from human embryonic stem cells: accelerated synaptic activity via astrocyte coculture. J. Neurosci. 27, 3069–3077.

Johnstone, A.F.M., Gross, G.W., Weiss, D.G., Schroeder, O.H., Gramowski, A., Shafer, T.J., 2010. Microelectrode arrays: a physiologically based neurotoxicity testing platform for the 21st century. Neurotoxicology 31, 331–350.

Jones, T.R., Kang, I.H., Wheeler, D.B., Lindquist, R.A., Papallo, A., Sabatini, D.M., Golland, P., Carpenter, A.E., 2008. CellProfiler Analyst: data exploration and analysis software for complex image-based screens. BMC Bioinform. 9.

Kapucu, F.E., Tanskanen, J.M.A., Mikkonen, J., Ylä-Outinen, L., Narkilahti, S., Hyttinen, J.A.K., 2012. Burst analysis tool for developing neuronal networks exhibiting highly varying action potential dynamics. Front. Comput. Neurosci. 6.

Kim, K., Doi, A., Wen, B., Ng, K., Zhao, R., Cahan, P., Kim, J., Aryee, M.J., Ji, H., Ehrlich, L.I.R., Yabuuchi, A., Takeuchi, A., Cunniff, K.C., Hongguang, H., McKinney-Freeman, S., Naveiras, O., Yoon, T.J., Irizarry, R.A., Jung, N., Seita, J., Hanna, J., Murakami, P., Jaenisch, R., Weissleder, R., Orkin, S.H., Weissman, I.L., Feinberg, A.P., Daley, G.Q., 2010. Epigenetic memory in induced pluripotent stem cells. Nature 467, 285–290.

Kreutzer, J., Ylä-Outinen, L., Kärnä, P., Kaarela, T., Mikkonen, J., Skottman, H., Narkilahti, S., Kallio, P., 2012. Structured PDMS chambers for enhanced human neuronal cell activity on MEA platforms. J. Bionic Eng. 9.

Lappalainen, R.S., Salomäki, M., Ylä-Outinen, L., Heikkilä, T.J., Hyttinen, J.A., Pihlajamäki, H., Suuronen, R., Skottman, H., Narkilahti, S., 2010. Similarly derived and cultured hESC lines show variation in their developmental potential towards neuronal cells in long-term culture. Regen. Med. 5, 749–762.

Li, K., Javed, E., Scura, D., Hala, T.J., Seetharam, S., Falnikar, A., Richard, J., Chorath, A., Maragakis, N.J., Wright, M.C., Lepore, A.C., 2015. Human iPS cell-derived astrocyte transplants preserve respiratory function after spinal cord injury. Exp. Neurol. 271, 479–492.

Lindvall, O., 2015. Treatment of Parkinson's disease using cell transplantation. Philos. Trans. R. Soc. B Biol. Sci. 370, 20140370.

Majumder, A., Dhara, S.K., Swetenburg, R., Mithani, M., Cao, K., Medrzycki, M., Fan, Y., Stice, S.L., 2013. Inhibition of DNA methyltransferases and histone deacetylases induces astrocytic differentiation of neural progenitors. Stem Cell Res. 11, 574–586.

Miller, F.D., Gauthier, A.S., 2007. Timing is everything: making neurons versus glia in the developing cortex. Neuron 54, 357–369.

Napoli, A., Obeid, I., 2016. Comparative analysis of human and rodent brain primary neuronal culture spontaneous activity using micro-electrode array technology. J. Cell. Biochem. 117, 559–565.

Nat, R., Nilbratt, M., Narkilahti, S., Winblad, B., Hovatta, O., Nordberg, A., 2007. Neurogenic neuroepithelial and radial glial cells generated from six human embryonic stem cell lines in serum-free suspension and adherent cultures. Glia 55, 385–399.

Odawara, A., Saitoh, Y., Alhebshi, A.H., Gotoh, M., Suzuki, I., 2014. Long-term electrophysiological activity and pharmacological response of a human induced pluripotent stem cell-derived neuron and astrocyte co-culture. Biochem. Biophys. Res. Commun. 443, 1176–1181.

Ojala, M., Prajapati, C., Pölönen, R., Rajala, K., Pekkanen-Mattila, M., Rasku, J., Larsson, K., Aalto-Setälä, K., 2016. Mutation-specific phenotypes in hiPSC-derived cardiomyocytes carrying either myosin-binding protein C or α-tropomyosin mutation for hypertrophic cardiomyopathy. Stem Cells Int. 2016, 1684792.

Pasca, A.M., Sloan, S.A., Clarke, L.E., Tian, Y., Makinson, C.D., Huber, N., Kim, C.H., Park, J., O'Rourke, N.A., Nguyen, K.D., Smith, S.J., Huguenard, J.R., Geschwind, D.H., Barres, B. A., Pasca, S.P., 2015. Functional cortical neurons and astrocytes from human pluripotent stem cells in 3D culture. Nat. Methods 12, 671–678.

Rajala, K., Hakala, H., Panula, S., Aivio, S., Pihlajamäki, H., Suuronen, R., Hovatta, O., Skottman, H., 2007. Testing of nine different xeno-free culture media for human embryonic stem cell cultures. Hum. Reprod. 22, 1231–1238.

Rajala, K., Lindroos, B., Hussein, S.M., Lappalainen, R.S., Pekkanen-Mattila, M., Inzunza, J., Rozell, B., Miettinen, S., Narkilahti, S., Kerkelä, E., Aalto-Setälä, K., Otonkoski, T., Suuronen, R., Hovatta, O., Skottman, H., 2010. A defined and xeno-free culture method enabling the establishment of clinical-grade human embryonic, induced pluripotent and adipose stem cells. PLoS One 5, e10246.

Shi, Y., Kirwan, P., Smith, J., Robinson, H.P.C., Livesey, F.J., 2012. Human cerebral cortex development from pluripotent stem cells to functional excitatory synapses. Nat. Neurosci. 15 (477-U180).

Skottman, H., 2010. Derivation and characterization of three new human embryonic stem cell lines in Finland. In Vitro Cell. Dev. Biol. Anim. 46, 206–209.

Suzuki, I.K., Vanderhaeghen, P., 2015. Is this a brain which I see before me? Modeling human neural development with pluripotent stem cells. Development 142, 3138–3150.

Takahashi, K., Tanabe, K., Ohnuki, M., Narita, M., Ichisaka, T., Tomoda, K., Yamanaka, S., 2007. Induction of pluripotent stem cells from adult human fibroblasts by defined factors. Cell 131, 861–872.

Thomson, J.A., 1998. Embryonic stem cell lines derived from human blastocysts. Science 282, 1145–1147.

Toivonen, S., Ojala, M., Hyysalo, A., Ilmarinen, T., Rajala, K., Pekkanen-Mattila, M., Äänismaa, R., Lundin, K., Palgi, J., Weltner, J., Trokovic, R., Silvennoinen, O., Skottman, H., Narkilahti, S., Aalto-Setälä, K., Otonkoski, T., 2013. Comparative analysis of targeted differentiation of human induced pluripotent stem cells (hiPSCs) and human embryonic stem cells reveals variability associated with incomplete transgene silencing in retrovirally derived hiPSCs lines. Stem Cells Transl. Med. 2, 83–93.

Wagenaar, D.A., Pine, J., Potter, S.M, 2006. An extremely rich repertoire of burstingpatterns during the development of cortical cultures. BMC Neurosci. 7.

Yamamoto, N., López-Bendito, G., 2012. Shaping brainconnections through spontaneous neural activity. Eur. J. Neurosci. 35, 1595–1604.

Ylä-Outinen, L., Heikkilä, J., Skottman, H., Suuronen, R., Äänismaa, R., Narkilahti, S., 2010. Human cell-based micro electrode array platform for studying neurotoxicity. Front. Neuroeng. 3.

Zhang, S., Wernig, M., Duncan, I.D., Brüstle, O., Thomson, J.A., 2001. In vitro differentiation of transplantable neural precursors from human embryonic stem cells. Nat. Biotechnol. 19, 1129–1133.

PUBLICATION II

Functional characterization of human pluripotent stem cell-derived cortical networks differentiated on laminin-521 substrate: comparison to rat cortical cultures

Hyvärinen T, Hyysalo A, Kapucu FE, Aarnos L, Vinogradov A, Eglen SJ, Ylä-Outinen L, Narkilahti S

Scientific Reports. 2019. 9(1):17125.
doi:10.1038/s41598-019-53647-8

SCIENTIFIC REPORTS
nature research

OPEN

Functional characterization of human pluripotent stem cell-derived cortical networks differentiated on laminin-521 substrate: comparison to rat cortical cultures

Tanja Hyvärinen[1], Anu Hyysalo[1,2], Fikret Emre Kapucu[3,4], Laura Aarnos[1], Andrey Vinogradov[1], Stephen J. Eglen[5], Laura Ylä-Outinen[1] & Susanna Narkilahti[1*]

Human pluripotent stem cell (hPSC)-derived neurons provide exciting opportunities for *in vitro* modeling of neurological diseases and for advancing drug development and neurotoxicological studies. However, generating electrophysiologically mature neuronal networks from hPSCs has been challenging. Here, we report the differentiation of functionally active hPSC-derived cortical networks on defined laminin-521 substrate. We apply microelectrode array (MEA) measurements to assess network events and compare the activity development of hPSC-derived networks to that of widely used rat embryonic cortical cultures. In both of these networks, activity developed through a similar sequence of stages and time frames; however, the hPSC-derived networks showed unique patterns of bursting activity. The hPSC-derived networks developed synchronous activity, which involved glutamatergic and GABAergic inputs, recapitulating the classical cortical activity also observed in rodent counterparts. Principal component analysis (PCA) based on spike rates, network synchronization and burst features revealed the segregation of hPSC-derived and rat network recordings into different clusters, reflecting the species-specific and maturation state differences between the two networks. Overall, hPSC-derived neural cultures produced with a defined protocol generate cortical type network activity, which validates their applicability as a human-specific model for pharmacological studies and modeling network dysfunctions.

Human pluripotent stem cell (hPSC)-derived neurons possess great promise for unraveling the mechanisms of diseases with genetic susceptibility[1]. They also provide a human-specific model for *in vitro* research in neurotoxicology and drug discovery with the potential of reducing the use of animal studies[2]. Multiple differentiation protocols have been developed for hPSC-derived cortical neurons, all of which aim at the fast and consistent production of neurons[3–6]. Several methodological advances have improved the controllability of culture conditions, for example, feeder-free cultures of hPSCs and defined mediums devoid of serum[7,8]. Additionally, an efficient neural induction of the default anterior central nervous system (CNS) phenotype has been achieved with a simple dual SMAD inhibition method by blocking the TGF-β and BMP signaling pathways with small molecules[9]. More recently, defined culture matrices such as human recombinant extracellular matrix (ECM) proteins have emerged as potent alternatives for mouse laminin or Matrigel, which are animal-derived products known to suffer from batch-to-batch variation[10–12]. Defined ECM molecules are used both in culture of hPSCs

[1]Faculty of Medicine and Health Technology and BioMediTech, Tampere University, Tampere, Finland. [2]Institute of Biotechnology, HiLIFE, University of Helsinki, Helsinki, Finland. [3]Department of Biomedicine, Aarhus University, Aarhus, Denmark. [4]Danish Research Institute of Translational Neuroscience - DANDRITE, Aarhus University, Aarhus, Denmark. [5]Department of Applied Mathematics and Theoretical Physics, University of Cambridge, Cambridge, United Kingdom. *email: susanna.narkilahti@tuni.fi

and in neural differentiation and have even been shown to improve the functional maturation of neurons[10–13]. These improvements, among others, are essential for making neural differentiation methods more controllable and comparable between different laboratories and pave the way for more reliable findings in the application of hPSC-derived neurons.

The emergence of neuronal network activity during development is important in regulating neuronal migration, differentiation and apoptosis[14–16]. During CNS development, including that of the cerebral cortex, network formation starts as the newly born neurons elongate their axonal projections, find paths and form synaptic connections[16]. After the initial formation of excessive functional connections, the developing networks undergo refinement of some connections and strengthening of others[16]. Large populations of neurons generate synchronous activity that has a central role in fine-tuning connectivity during CNS development[16,17]. These synchronous oscillations have been described in the cerebral cortex of premature human fetuses at approximately 20 weeks of gestation[18,19] and in the mouse and rat cortexes at birth (P0)[20,21]. Wide-ranging oscillatory activities in the cortex dominate throughout development, ensuring neuronal survival and maturation[22,23], and in adults, they are believed to be involved in cognitive and perceptual functions and motor actions[24]. The cerebral cortex and its functional dynamics are also affected in many neurological disorders[25–27]. hPSC-derived neurons have been shown to develop membrane properties similar to native neurons *in vivo* and have been reported to respond to pharmacological manipulation and electrical stimulation, as expected from their *in vivo* counterparts[28–30]. Although network-level events are central in both healthy and pathological states, modeling of network-level activity with hPSC-derived neurons is still less described in the literature[31–34].

Microelectrode arrays (MEA) have been used to measure the connectivity and network activity in neuronal cultures, brain slices and even in awake animals[28,35–37]. A clear advantage of MEAs is that they measure the activity from a population of neurons simultaneously, providing information about network events. They also enable repeated measurements of the same networks over time, allowing follow-up of developmental events or, for example, long-term drug responses[38]. For *in vitro* research, multiwell-format MEAs also facilitate higher throughput analyses[13,39]. These features make MEAs a potential tool for disease modeling, drug screening and toxicology using hPSC-derived neurons. So far, most MEA culture and signal analysis protocols have been established with rodent networks, which are often considered "gold standards" in the field[40,41]. However, direct transfer and validation of these methods to hPSC-derived networks has not been straightforward[28,42–44].

Here, we report that the differentiation of hPSC-derived cortical cultures on defined human recombinant laminin-521 (LN521) substrates is repeatable and results in the generation of cortical neurons, which form functionally active networks. We utilize MEA technology to characterize the development of hPSC-derived neuronal network activity and compare it with the activity of rat embryonic cortical networks *in vitro*. The results confirm that spontaneous activity arises through similar developmental stages and on comparable time scales in both hPSC-derived and rat cortical networks. Both network types show typical synchronous activity; however, hPSC-derived networks present unique characteristics in burst patterns that distinguish them from their rat counterparts. The present data validate hPSC-derived neuronal networks as a reliable model for cortical activity development and consolidate their utilization in applications such as disease modeling, where network malfunctions are considered key characteristics.

Results

Generation of neural progenitor cells on human recombinant LN521 substrate. To achieve controlled, repeatable protocol producing cortical neurons, we utilized and modified previously described methods for culturing hPSCs and differentiation of neurons that can form spontaneously active networks[6,11] (Fig. 1a). The hPSCs were cultured in feeder-free conditions using LN521 substrate and Essential 8 (E8) medium according to the protocol from Hongisto *et al.* (2017). The neural differentiation protocol was modified from Shi *et al.* (2012) and further optimized for the LN521 substrate to achieve more defined culture conditions and to support the functional development of neuronal networks, as we have previously described[13].

To assess the repeatability of the optimized culture protocol, experiments were performed with one human embryonic stem cell (hESC) line (08/023) and two human induced pluripotent stem cell (hiPSC) lines (10212.EURCCs and IMR90-4). All hPSC lines expressed the pluripotency marker Oct4 when grown as a monolayer culture on LN521 substrate in E8 medium (Fig. 1b). After a 12-day neural induction stage with dual SMAD inhibition, the pluripotency marker Oct4 was downregulated, and homogenous expression of neuroectodermal markers Sox2 and Pax6 was apparent, indicating efficient neural conversion (Fig. 1b). In addition, the anterior cortical fate of the cells was identified by FoxG1 staining (Fig. 1b).

After the neural induction stage, vimentin- and Pax6-positive neural stem and progenitor cells (now referred to as NPCs) could be efficiently expanded and differentiated in FGF2-containing media (Fig. 1a,c, Supplementary Fig. S1). Differentiation induced the emergence of first Tbr2- and MAP2-positive cortical neurons (Fig. 1c). Furthermore, NPCs could be cryopreserved at day 21 to create master cell banks. As a comparison to LN521 substrate, we also tested neural induction on the commonly used Matrigel matrix. Cells cultured on Matrigel matrix showed similar homogenous Pax6 staining, and the subsequent differentiation on mouse laminin generated FoxG1- and vimentin-positive NPCs (Supplementary Fig. S2).

After thawing, the NPCs were expanded until day 32 and then used for experiments (Fig. 1a). Neuronal maturation was promoted in the presence of neurotrophic factors BDNF, GDNF, cAMP and ascorbic acid. The number of Pax6-positive NPCs gradually decreased from 93–98% at day 12 to 35–41% at day 46 in all studied hPSC lines, suggesting neuronal maturation (08/023, $p < 0.001$; 10212.EURCCs, $p = 0.009$; and IMR90-4, $p = 0.009$; Fig. 1d). Taken together, neural induction and expansion of NPCs on LN521 substrate was efficient, and the produced cells represented an anterior cortical phenotype.

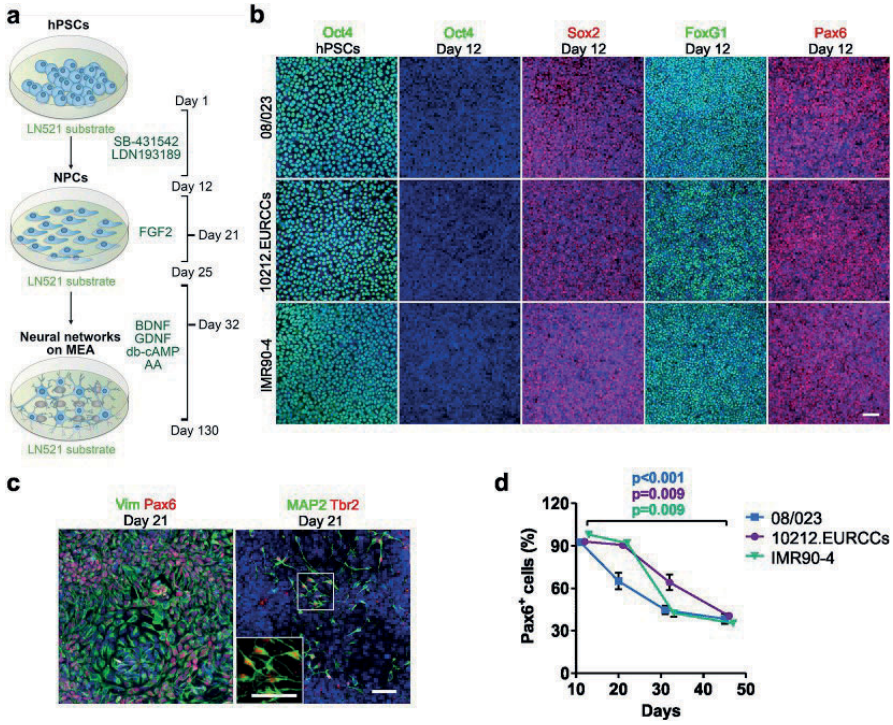

Figure 1. Neural induction of hPSCs. (**a**) Both hPSC culture and neural differentiation were performed on LN521 substrate. Cortical neurons were induced with dual SMAD inhibition, expanded in the presence of FGF2, and matured with support by a selection of neurotrophic factors. Neural progenitor cells (NPCs) could be cryopreserved at day 21 and plated at day 32 for final experiments, including microelectrode array (MEA) measurements. **(b)** Three different hPSC lines (one hESC line, 08/023 and two hiPSC lines, 10212.EURCCs and IMR90-4) were characterized for their efficiency in producing neuroectodermal cells in response to 12-day neural induction by dual SMAD inhibition. Cells were stained for pluripotency marker Oct4 at the pluripotent stage and after 12 days of neural induction. The presence of early neuroectodermal markers was evaluated with Sox2, FoxG1 and Pax6 staining. **(c)** After 21 days of differentiation, the culture contained vimentin- and Pax6-positive NPCs that could be cryopreserved. Additionally, the first Tbr2- and MAP2-positive neurons were detected at this time point. **(d)** The percentages of Pax6-positive cells were quantified at four time points of differentiation (mean ± s.e.m., n = 5–14, data derived from 1–3 independent differentiations). Statistical analysis was performed with the Mann-Whitney U test to compare differences between day 12 and day 46 within each hPSC line, and significant p-values are presented in the image. The scale bar is 50 µm in all images.

Development of cortical layer-specific neurons. Neurogenesis produced neurons specific for both deep and upper cortical layers. The early-born deep layer neurons were identified by immunocytochemical staining of transcription factors COUP-TF-interacting protein 2 (CTIP2) and T-box homeobox protein 1 (Tbr1) (Fig. 2a, Supplementary Fig. S3a), both having similar temporal expression patterns in the studied hPSC lines. Higher CTIP2 expression, 19–35%, was detected at day 46 and decreased thereafter to 16–18% by day 74 (08/023, $p = 0.802$; 10212.EURCCs, $p = 0.001$; and IMR90-4, $p < 0.001$; Fig. 2b). Similarly, Tbr1 expression showed a minor decrease from 6–13% to 3–8% from day 46 to day 74 (08/023, $p < 0.001$; 10212.EURCCs $p = 0.117$, and IMR90–4, $p = 0.066$; Fig. 2b). Additionally, later-born upper layer neurons positive for POU domain transcription factor Brn2 (also known as POU3F2) and special AT-rich sequence-binding protein 2 (Satb2) were detected in the cultures (Fig. 2a, Supplementary Fig. S3a). The Brn2-positive neurons appeared first in all hPSC lines with higher expression at day 46, 30–47%, followed by a decrease to 24–27% at day 74 (08/023, $p = 0.002$; 10212.EURCCs, $p < 0.001$; and IMR90-4, $p = 0.050$; Fig. 2b). The number of Satb2-positive late-born neurons was low at the studied time points (Fig. 2b). A very modest increase was detected, ranging from 0–2% to 0–7% between days 46 and 74 (08/023, $p = 0.052$; 10212.EURCCs, $p < 0.001$; and IMR90-4, $p = 0.371$; Fig. 2b). In conclusion, the differentiation protocol produced both deep and upper layer cortical neurons in a similar manner for all studied hPSC lines.

Maturation of hPSC-derived and rat embryonic cortical cultures. Next, the cell type composition of the hPSC-derived neural cultures differentiated on LN521 substrate was characterized by MAP2 and βIII-tubulin

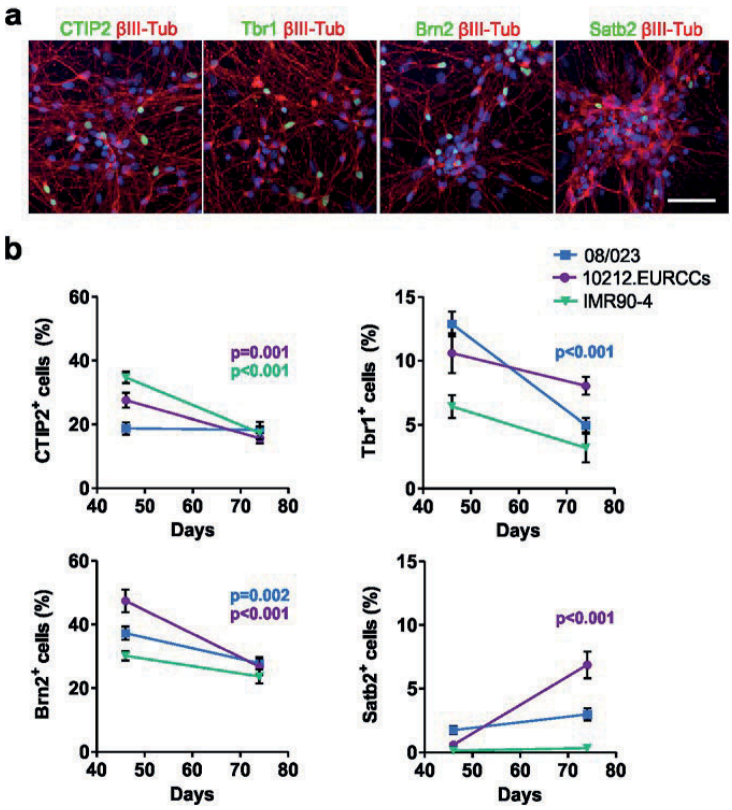

Figure 2. Development of cortical layer-specific neurons. (**a**) Immunocytochemical staining verified the presence of cortical layer-specific neurons expressing the early-born deep layer markers CTIP2 and Tbr1 and the later-born upper layer markers Brn2 and Satb2. Images are representative of the 08/023 hPSC line. Scale bar is 50 µm. **(b)** The number of positive cells for cortical layer-specific markers was quantified from neuronal cultures differentiated from all three hPSC lines at days 46 and 74 of differentiation, and the data are presented as the mean ± s.e.m. (for each hPSC line n = 5–51, data from 1–3 independent differentiations). Mann-Whitney U test was performed to determine statistically significant differences in time within each hPSC line. Significant p-values are presented in the images.

staining for neurons and S100β and GFAP staining for astrocytes (Fig. 3a). For comparison studies on the MEAs, the rat embryonic cortical cells were also cultured and characterized with the same markers (Fig. 3a).

The number of neurons and astrocytes was quantified from hPSC-derived cortical cultures. The percentage of MAP2-positive neurons was 61–79% at day 46 and decreased significantly to 45–51% at day 74 in the studied hPSC lines (08/023, $p = 0.004$; 10212.EURCCs, $p = 0.017$, and IMR90-4; $p < 0.001$; Fig. 3b). In contrast, the number of S100β- and GFAP-positive astrocytes increased in a temporal manner, suggesting subsequent astrogenesis from the common neural progenitor pool. The percentage of S100β-positive astrocytes increased significantly from 2–15% to 30–38% between day 46 and day 74 in the studied hPSC lines (08/023, $p < 0.001$; 10212.EURCCs, $p < 0.001$; and IMR90-4, $p < 0.001$; Fig. 3b). GFAP expression appeared later, as only 0–4% GFAP-positive astrocytes were detected at day 46, while later, at day 74, their number was significantly increased to 15–26% (08/023, $p < 0.001$; 10212.EURCCs, $p < 0.001$; and IMR90-4, $p < 0.001$; Fig. 3b). Interestingly, almost all GFAP-expressing astrocytes were also S100β-positive (Supplementary Fig. S3b). The neuronal population was further characterized as consisting of both vGlut1-expressing glutamatergic neurons and GABA- and GAD67-positive GABAergic neurons (Fig. 3c). Importantly, both hPSC-derived and rat embryonic cortical neurons formed structural synapses identified with juxtaposed synaptophysin and PSD-95 puncta (Fig. 3d). In summary, both rat and hPSC-derived cortical neurons established synaptically connected networks that were intermingled with astroglia.

Development of spontaneous activity in hPSC-derived and rat cortical networks. To study the spontaneous activity of hPSC-derived cortical networks differentiated on LN521 substrate and compare their functional properties to the widely used rat embryonic cortical networks, we followed network development with regular MEA measurements over 100 days. The hPSC-derived cortical cells were plated on MEAs at day 32 of

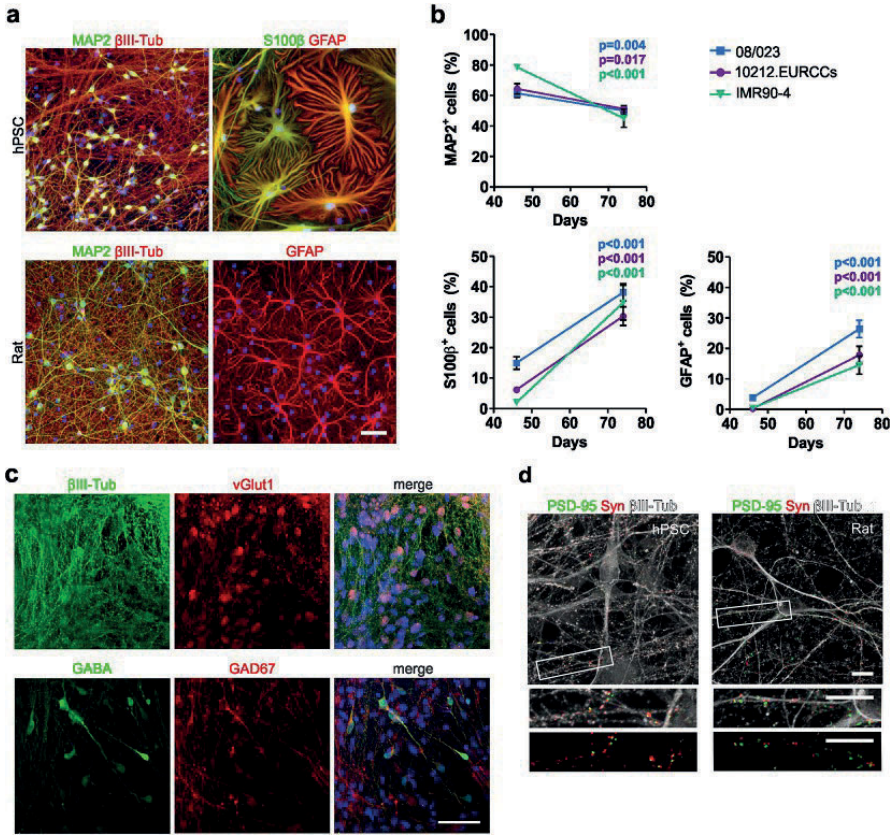

Figure 3. Maturation of hPSC-derived and rat embryonic cortical cultures. (**a**) Immunocytochemical staining of neurons (MAP2 and βIII-tubulin) and astrocytes (GFAP and S100β) in hPSC-derived (hPSC line 08/023) and rat primary cultures. Dapi nuclear staining is shown in blue. Scale bar represents 50 µm. **(b)** The number of neurons and astrocytes was quantified from cultures differentiated from all three hPSC lines at days 46 and 74. Quantitative data are presented as the mean ± s.e.m. (MAP2 n = 7–42, S100β and GFAP n = 9–44, data derived from 1–3 independent differentiations). The Mann-Whitney U test was performed between time points within each hPSC line, and significant p-values are presented in the images. **(c)** The hPSC-derived neuronal cultures consisted of vGlut1-positive glutamatergic and GABA- and GAD67-positive GABAergic neurons. Dapi nuclear staining is shown in blue, and the scale bar represents 50 µm. **(d)** Both hPSC-derived (day 61) and rat embryonic (day 22) cortical cultures formed networks with excitatory synapses positive for synaptophysin (Syn) and PSD-95. Insets show higher magnification, and the scale bars are 10 µm in all images.

differentiation (now called day 1 on MEA), and primary rat cortical neurons (from E17-E18 embryos) were plated directly on MEAs (Fig. 4a). Cell density has been shown to be critical for the timeframe of activity development on MEAs[34,45], and therefore, cells were plated at high densities (Fig. 4b). Measurements performed on 64-electrode MEAs (8 × 8 grid) revealed that this facilitated the detection of activity from hPSC-derived networks soon after plating (Fig. 4c). The hPSC-derived networks expressed widespread activity from day 3 on MEA onwards, and the percentage of active electrodes (>10 spikes/min) ranged from 53% to 84% over 35 days on MEA. The rat networks showed latency in the onset of activity development (Fig. 4c). In the rat networks, the number of active electrodes was 2% at day 3 on MEA, reaching almost 100% on day 21 and then declining towards day 35.

The median spike rate per well increased early in the hPSC-derived networks, starting from day 3 and through day 14 on MEA (Fig. 4d). However, the rat networks showed higher spike rates during the most active state at days 24 to 28 on MEA (Fig. 4d). Here, the peak activity for both groups was detected after 24 days on MEA (hPSC median 4.4 Hz and rat median 6.1 Hz, Fig. 4d). After 35 days, the rat networks experienced a typical terminal decline in activity, while hPSC-derived networks settled on a plateau (Fig. 4d,e). We also looked at activity development in hPSC-derived neurons differentiated on the commonly used mouse laminin substrate (Supplementary Fig. S4). Similar to our earlier reports[13], the activity development of hPSC-derived neurons was more efficient on LN521 substrate compared to mouse laminin, as indicated by both the number of active electrodes and spike rate in the networks.

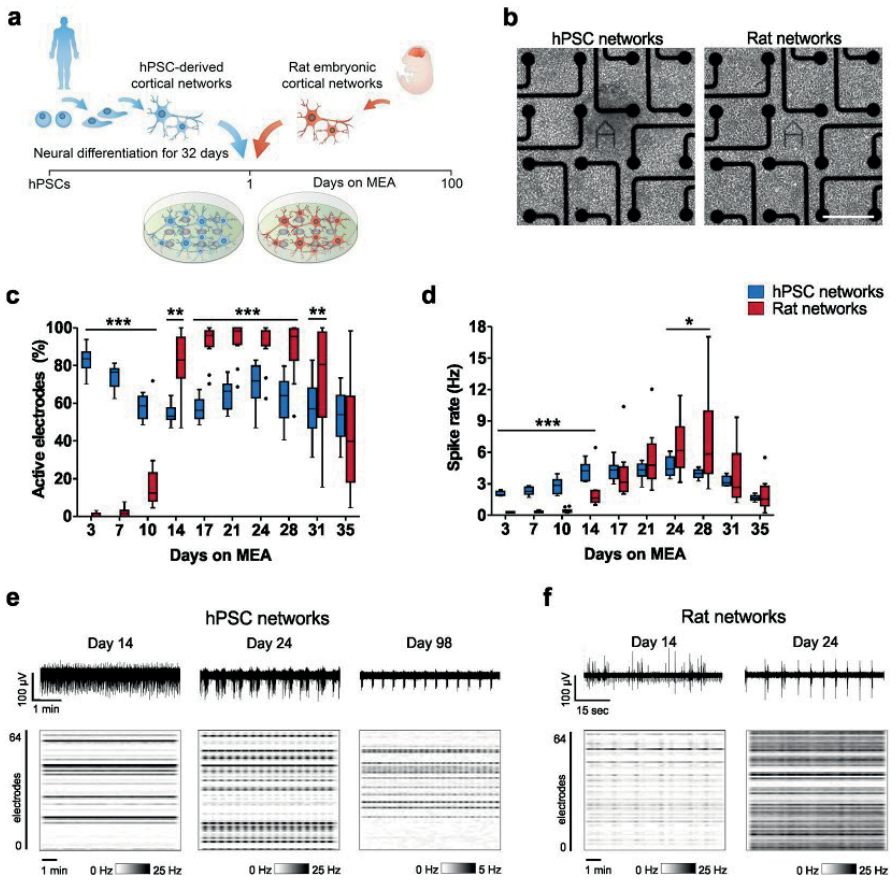

Figure 4. Developmental changes in the spontaneous activity of hPSC-derived and rat cortical networks on MEA. **(a)** hPSC-derived cortical neurons were differentiated for 32 days before plating on MEAs. Rat cortical neurons were dissected from E17-E18 embryos and directly plated on MEAs. **(b)** Phase contrast images showing hPSC-derived and rat networks on a MEA. The scale bar is 200 µm. **(c)** Percentage of active electrodes per MEA well in hPSC-derived and rat networks over time. Electrodes detecting >10 spikes/min were considered active. **(d)** Development of spike rate (Hz) per MEA well in hPSC-derived and rat networks over time. hPSC network data are from line 08/023. Both hPSC and rat network data consist of n = 12 networks per group. Data are presented as Tukey box plots. Mann-Whitney U test was performed to compare differences between hPSC-derived and rat networks, and significance within each time point is denoted in the images as $*p < 0.05$, $**p < 0.01$ and $***p < 0.001$. **(e)** Representative images of the spontaneous activity recorded from single electrodes of hPSC-derived networks over 5 minutes and **(f)** from rat networks over 1 minute at different time points. Raster plots below show the intensity of spike activity on a MEA during a 10 min recording.

Representative images of firing patterns detected with single electrodes and entire MEA arrays revealed the developmental organization of uncorrelated spike trains into highly synchronous bursts in both hPSC-derived and rat networks from day 14 to 24 on MEA (Fig. 4e,f). In hPSC-derived networks, this synchronous bursting was still apparent after 98 days on MEA (Fig. 4e). Taken together, hPSC-derived networks differentiated on LN521 substrate develop activity across the MEA array in a comparable time period to the rat networks. They can reach spike rates close to that of the rat counterparts and maintain activity for almost 100 days on MEA.

Both hPSC-derived and rat neurons form highly connective networks. Functional connectivity is typically measured as simultaneously occurring events of activity originating from spatially distant areas[46]. To determine how array-wide activity develops in hPSC- and rat-derived networks, we performed connectivity analysis based on the entropy between electrode pairs[47]. Representative connectivity maps showing results from one network of hPSC and rat groups over 10 minutes of recording revealed a gradual increase in functional connections over time (Fig. 5a,b). The first functional connections were observed in hPSC-derived networks after 21 days on MEA and in rat networks after 14 days on MEA (Fig. 5a,b). Connections expanded and strengthened

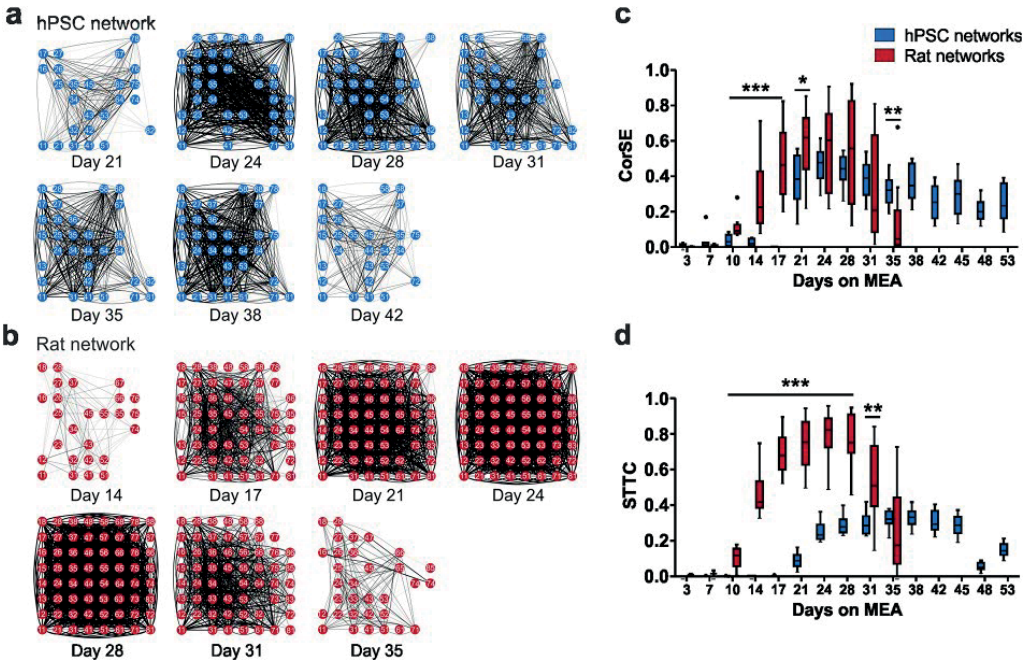

Figure 5. Analysis of functional connectivity development. (**a**) Functional connectivity maps from the hPSC-derived network over 10 minutes of recording between days 21 and 42 on MEA and **(b)** from the rat network between days 14 and 35 on MEA. Electrodes in an 8 × 8 array with functional connections (lines) are presented during the measurement time. An arbitrary connectivity strength (CorSE) value of 0.7 was used as the threshold for plotting. **(c)** Average connectivity strength (CorSE) is calculated from all channel pairs for hPSC-derived and rat networks. **(d)** Network synchronization of hPSC-derived and rat networks described by the spike time tiling coefficient (STTC). Data hPSC data are from line 08/023. Both hPSC and rat network data consist of n = 12 networks per group; data are shown as Tukey box plots. Mann-Whitney U test was performed to compare the two groups at each time point. Statistical significances are marked as *$p < 0.05$, **$p < 0.01$ and ***$p < 0.001$.

progressively in both hPSC-derived and rat networks (Fig. 5a,b). When connectivity strength (CorSE) values were quantified, a considerably higher level of connectivity was observed in rat networks compared to hPSC-derived networks between 10 and 21 days on MEA (Fig. 5c). The strongest network connectivity was detected after 24 days on MEA (hPSC median CorSE 0.48 and rat median CorSE 0.60). While rat networks were silenced after 35 days on MEA, in hPSC-derived networks, the connectivity persisted between certain areas of the networks over several days (Fig. 5a–c). We further complemented the analysis by calculating the spike time tiling coefficient (STTC), which measures network synchronization in pairs of electrodes[48]. The results from STTC analysis confirmed the earlier observations with CorSE analysis, showing that although both hPSC-derived and rat networks form connections across the culture, in the rodent data, the synchronous activity was initiated earlier and involved a larger fraction of the network (Fig. 5d).

Bursting behavior differs between hPSC-derived and rat networks. Spontaneous bursts arise during early activity development in the cerebral cortex and are important for neuronal circuit formation[16]. The tonic firing detected soon after cell plating gradually transformed into bursts with a rich repertoire of patterns, which could be reliably detected from both hPSC-derived and rat neuronal signals (Fig. 6a). The number of bursts and the percentage of spikes participating in the bursts progressively increased in both network types (Fig. 6b,c). During the peak of activity, the percentage of spikes recruited into bursts was generally higher in rat networks than in hPSC-derived networks, which also presented substantial spiking between condensed bursts (Fig. 6a,c). The hPSC-derived networks initially fired short bursts at a high frequency (Fig. 6b,d). When the well median values were examined at day 14, the burst frequency was 33 bursts per min, the burst duration was 0.4 sec, and bursts contained fewer than 13 spikes (Fig. 6b,d,e). Once networks matured, less frequently occurring and longer-duration bursts became the more dominant form of activity (Fig. 6a,b,d). During the peak of activity at day 24, the burst frequency was 11 bursts per min, the burst duration was 0.7 sec, and bursts contained 34 spikes (Fig. 6b,d,e). In the rat networks, the generation of bursting activity was steady, and the highest number of bursts, 15 per min, was detected during the peak of activity on day 24 (Fig. 6b). At that point, the median burst duration was 0.3 sec (Fig. 6d). Thus, hPSC-derived networks expressed longer bursts than the rat networks. Although rat bursts consisted of a similar number of spikes as observed in hPSC-derived networks (Fig. 6e), the spike

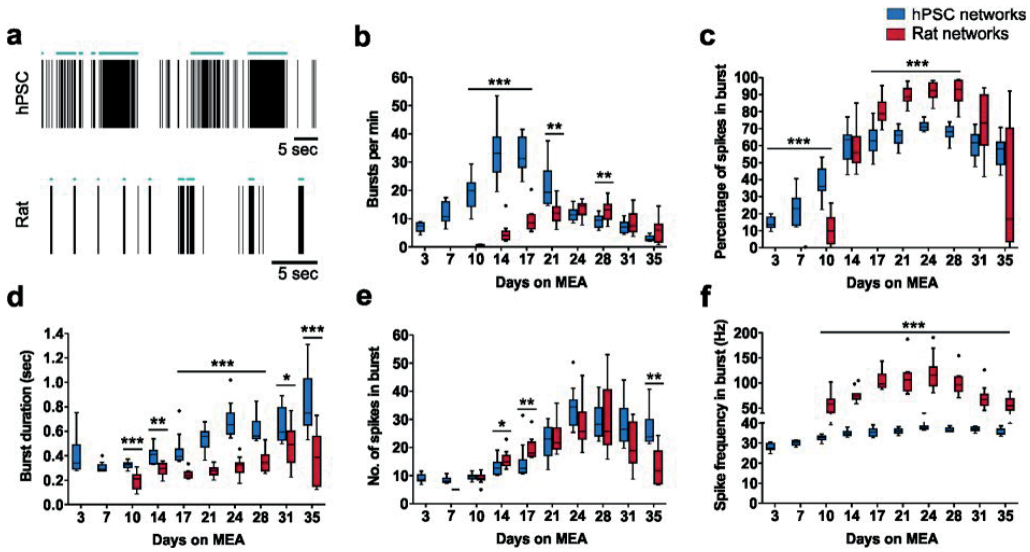

Figure 6. Burst features in hPSC-derived and rat cortical networks. (**a**) Raster plots showing typical spike and burst activity of one electrode from both hPSC-derived and rat data at day 24 on MEA. The green horizontal lines denote detected bursts. Temporal changes in burst features including **(b)** number of bursts per minute, **(c)** percentage of spikes in burst, **(d)** burst duration, **(e)** number of spikes in bursts, and **(f)** spike frequency in bursts. Data consist of n = 12 networks for both hPSC-derived (hPSC line 08/023) and rat networks and are presented as Tukey box plots. Mann-Whitney U test was performed to compare differences between the two groups at each time point, and significance is denoted as *$p < 0.05$, **$p < 0.01$ and ***$p < 0.001$.

frequencies in bursts were different across all time points (Fig. 6f). The median spike frequency in bursts was below 40 Hz in the hPSC-derived networks, whereas in rat networks, up to 100 Hz was observed during the peak of activity (Fig. 6f). Taken together, the hPSC-derived and rat networks express bursts that differ mostly in four properties: temporal development of bursts, burst duration, percentage of spikes recruited in bursts and spike frequency inside bursts.

hPSC-derived and rat networks show similar pharmacological responses. Next, we evaluated whether the observed network activity was synaptically driven and whether we could pharmacologically manipulate activity in both network types. Experiments were carried out once synchronous activity was well established after 29 days on MEA for hPSC-derived networks and after 22 days on MEA for rat networks. Typical firing patterns showed that common glutamatergic and GABAergic agonists and antagonists evoked similar responses in both hPSC-derived and rat networks (Fig. 7a,b). The glutamatergic agonist kainic acid reduced the spiking activity and disorganized the synchronous network bursts down to tonic spike trains in both groups similarly (Fig. 7a–c), as observed earlier[49]. A concentration-dependent response to kainic acid was also observed with the rat networks (Supplementary Fig. S5). In both network types, the glutamatergic AMPA/kainate antagonist CNQX and the NMDA antagonist D-AP5 both efficiently reduced activity, verifying that the synchronous network events involve synaptic inputs (Fig. 7a–c).

The presence of the inhibitory system is not often observed in hPSC-derived forebrain cortical cultures[50], and therefore, we tested the effect of the GABA and $GABA_A$ receptor antagonist gabazine on network activity (Fig. 7a,b). GABA suppressed the excitatory activity in both groups but more efficiently in the rat networks (Fig. 7c). Gabazine blocked GABAergic signaling in both rat and hPSC-derived networks, leading to increased spike rates (Fig. 7c). Finally, we confirmed that the activity recorded with MEAs originated from neuronal excitation, since all activity was silenced with the voltage-dependent sodium channel blocker tetrodotoxin (TTX, Fig. 7a–c). In summary, both hPSC-derived and rat networks presented network activity that was sensitive to synaptic modulators, and most importantly, the networks contained a functional inhibitory system.

Principal component analysis of the features of MEA activity distinguishes hPSC- and rat-derived networks. Principal component analysis (PCA) can efficiently cluster MEA data based on activity feature profiles and has been used for studying the properties of various brain region-specific cells and the effects of chemical exposure[40,51]. Therefore, we applied PCA to obtain conclusive results from the functional comparison between the hPSC-derived and rat networks. Both network types may have variability in the onset of activity and synchrony; therefore, analysis was performed on three separate experiments at the time point showing the highest spike rate and two of its neighboring measurement days (Supplementary Figs. S6 and S7). To measure the differences, we used several spike, burst and synchrony features. A clear segregation of the

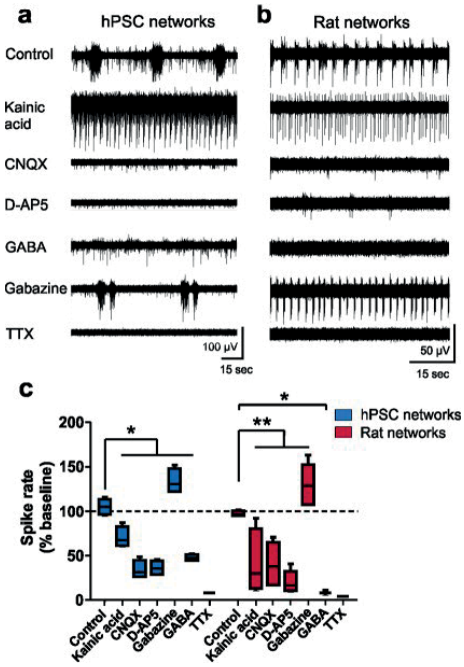

Figure 7. Pharmacological responses of hPSC-derived and rat cortical networks. (**a**) Typical activity patterns in response to different pharmacological treatments recorded from single electrodes of hPSC-derived networks at 29 days on MEA over 2 minutes and **(b)** from rat networks at 22 days on MEA over 1 minute. **(c)** Percentage change in spike rate compared to baseline measurement from the same well. Data consist of n = 4 networks for hPSC networks (hPSC line 08/023) and n = 7 for rat networks and are presented as a Tukey box plots. Mann-Whitney U test was performed to compare differences between the treatment groups, and significance is marked as *$p < 0.05$, **$p < 0.01$ and ***$p < 0.001$.

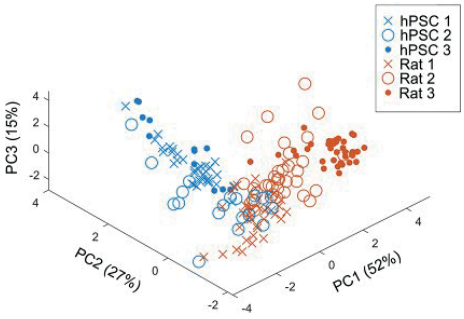

Figure 8. Principal component analysis of features of MEA activity of hPSC-derived and rat datasets. Principal component analysis (PCA) was performed to cluster hPSC-derived and rat MEA data based on seven activity features. Analysis was performed on three separate hPSC-derived (hPSC 1–3) and rat data sets (Rat 1–3) that all included 4–12 networks. Data were analyzed from time points showing the highest spike rates during development and two of their neighboring measurement time points. Data are plotted in 3-dimensional space, where each of the principal components accounts for the amount of variation of the data shown in parenthesis. Each data point in the scatter plot represents one network at a particular time point.

hPSC-derived and rat recordings was observed when the 7-dimensional feature vectors were plotted onto the first three principal components (Fig. 8). The first principal component (PC1) accounted for more than half of the variation (52%) between the two networks, and PC2 and PC3 explained 27% and 14% of the variation, respectively. However, there was a slight overlap between the second hPSC batch (hPSC 2) and the first rat batch (Rat 1), suggesting that single datasets cannot be reliably used to discriminate between two types of recordings. In fact, in

the rat networks group, internal variation among the three individual experiments was well explained by the first PC. The hPSC-derived networks were better explained by the second PC, and although variability within experiments was observed, a clear segregation between the three independent hPSC experiments (hPSC 1-hPSC 3) was not evident. In conclusion, PCA was used as a promising tool for summarizing multiple activity features from different MEA experiments. It successfully displayed differences in the individual MEA recordings and identified two separate clusters for hPSC-derived and rat networks suggestive of their distinct functional characteristics.

Discussion

We established here hPSC-derived cortical networks using highly defined culture methods resulting in consistency of differentiation and distinct functional properties. We have previously shown improved functionality of neurosphere-differentiated networks on MEA with laminin alpha5 substrates[13]. We now apply LN521 substrate for hPSC culture[11] and the subsequent adherent neuronal differentiation, and for the first time, we show a detailed network-level functional comparison between hPSC-derived and rat embryonic cortical cultures. The results demonstrate that hPSC-derived cortical networks present unique activity patterns, but the stages of development over time reflect those observed in rat cortical networks. Thus, these results validate the hPSC-derived networks as a representative model for cortical activity development *in vitro*.

Over the years, increasing knowledge of the key signaling molecules involved in neurodevelopment has been utilized for the improvement of neuronal differentiation methods[9,52]. Less attention has been drawn to the ECM components, although they are known to mediate cellular effects through signaling via membrane receptors[53,54]. Laminins are a major class of ECM molecules and are essential during embryogenesis and neural development, regulating neuronal proliferation, differentiation and migration[53,55]. The human recombinant laminin isoform LN521 has been shown to support the pluripotency of hPSCs in feeder-free culture[7,11,12] and has been applied to dopaminergic differentiation of multiple hESC and hiPSC lines[10,56]. We have also demonstrated that laminin α5 substrates, including LN521, improve the functional activity of hPSC-derived neuronal networks on MEA[13]. Therefore, here LN521 was chosen as the sole substrate for maintaining the undifferentiated hPSCs[11] and for supporting efficient neural induction, cortical differentiation and functional development. Using optimized methods, all three of the studied hPSC lines presented over 90% neural conversion as shown by Pax6 staining after dual SMAD inhibition, and the generated NPCs expressed typical markers of the forebrain cortical phenotype. Importantly, the NPCs were cryopreservable, and with further maturation, they readily differentiated into mature neural cell types, neurons and astrocytes. The neuron population showed typical temporal profiles of cortical layer marker expression, in which the deep layer neurons were produced first followed by generation of upper layer neurons, similar to previous reports[6]. The majority of the neurons consisted of glutamatergic projection neurons and GABAergic interneurons, and the formation of structurally mature synapses was observed.

Both neurons and astrocytes are derived from the same neuroepithelial pool in a distinct temporal order with neurogenesis preceding astrogenesis[57]. Here, the glial switch was apparent during differentiation, as all hPSC lines produced first MAP2-positive neurons followed by an increased expression of S100β and GFAP, phenotypical markers for astrocyte progenitors and mature astrocytes, respectively. After 74 days of differentiation, over 30% of the cell population consisted of S100β-expressing astrocytes, of which at least half were double-positive for GFAP, while neurons accounted for approximately 50% of the cells in the culture. Many of the previous cortical differentiation protocols have described lower amounts of astrocytes (<10%), even after 80–100 days of differentiation[4,6,58]. Astrocytes are known to promote synaptogenesis and functional maturation of neurons and are also important for the synchronization of networks[59,60]. Consequently, hPSC-derived neurons are often cocultured with rodent astrocytes to improve functional activity[29,38]. However, major drawbacks of these cocultures include species differences and the risk of masking the phenotypes of hiPSC-derived neurons, which is particularly critical for studies focused on disease modeling[61]. Attempts have been made to overcome the species differences by replacing rodent cells with hPSC-derived astrocytes[31,62]. We and others have previously shown functionally active networks with neurons and astrocytes differentiated through EB or neurosphere aggregate stage[34,63,64]. Here, we also present a humanized, fully adherent culture where astrocytes originate endogenously from the same NPCs as neuronal cells and are able to support the functional development of the networks.

Functional activity arises during early embryonic development and is essential for neuronal survival, migration and differentiation[14,17]. The hPSC-derived neuronal cells are generally considered functionally immature, resembling those of the late embryonic stages in rodents, and indeed, transcriptional profiling has shown similarity between hPSC-derived neural cultures and the cells of mid-gestational human embryos[4,65,66]. Here, we show that the time scale for *in vitro* functional activity development between late-embryonic stage rat cortical networks and hPSC-derived cortical networks predifferentiated for one month are highly similar. Measurements in high-throughput multiwell MEAs demonstrate that activity can be detected from the hPSC-derived networks starting already from the early recording days, and the most active stage can be reached within a comparable time to that of rat cortical networks. Rat cortical cells developed functionally connected networks in 14–21 days on MEA, as similarly described by others[41,42]. Additionally, hPSC-derived neuronal networks formed robust synchrony across the culture as early as 21 days (3 weeks) on MEA. Previous studies have typically reported longer times, up to 20 weeks on MEA, for hPSC-derived networks to reach full maturation[32,38,62]. Furthermore, our data reveal that the hPSC-derived and rat cortical networks undergo similar phases of development in activity patterns. Both networks initially fire uncorrelated single spikes and tonic spike trains, and upon maturation, an increasing connectivity is observed when the activity is orchestrated into highly synchronous network bursts.

Spontaneous bursting is observed in the developing cerebral cortex and is considered important for the formation of neuronal circuits[16]. The hPSC-derived networks initially fired comparatively short bursts at high frequency, but as the networks matured, the bursts became less frequent and longer in duration. Over the recoding period, hPSC-derived cortical networks were characterized by bursts with longer durations and lower spike frequencies compared to rat counterparts. Additionally, they presented a higher number of spikes outside the bursts,

all of which may reflect species-specific differences or different states of maturity between the two cell types. In both hPSC-derived and rat cortical networks, activity was synaptically driven, as shown by the inhibition with glutamatergic antagonists and application of GABA. We also confirmed the presence of a functional inhibitory system in both networks, as demonstrated by the increased activity upon pharmacological modulation with a $GABA_A$ receptor antagonist. To date, only a few studies have reported robust burst firing of hPSC-derived neuronal cultures[31,34,38,67], and the activity often arises from purely excitatory glutamatergic networks lacking inhibitory GABAergic inputs[50].

We demonstrated an extensive, direct *in vitro* comparison between rat cortical networks held as the "gold standard" in the MEA field and human-derived networks, which have been less covered by previous reports[68–71]. PCA analysis based on spike rates, network synchronization and burst features effectively identified differences between the two network types; thus, this approach seems potential for future studies. There is an increasing interest in disease modeling to better understand pathology at the network level and to exploit hPSC-derived neurons in drug screening and neurotoxicological studies[31,72–74]. Validation of methods is of importance[70,74], as variability in hPSC-derived neuronal culture protocols, functional measurements and analysis procedures may at worst lead to falsely assumed conclusions on disease-specific phenotypes. Standardization also supports evaluations of human and rodent networks for drug screening and toxicological analysis and helps to avoid false negative or positive hits that may compromise further studies.

Based on our results, we report reproducible differentiation of hPSC-derived cortical networks and their stable functional development on MEA. The hPSC-derived networks differ from rat *in vitro* counterparts mostly by their unique bursting properties, whereas the stages of activity development reflect the rodent cortical networks in many ways. Detailed quantification of the functional similarities and differences between the rodent and human *in vitro* networks utilizing the current state-of-the-art methods offers a foundation for future studies involving healthy and pathological networks.

Methods

Maintenance of human pluripotent stem cells. The hPSC lines used in this study consist of the in-house derived hESC line Regea 08/023[75] (total passages 29–31, feeder-free passages 6–8), the in-house derived hiPSC line 10212.EURCCs[76] (total passages 38, feeder-free passages 6) and the commercial hiPSC line IMR90-4[77] (WiCell, total passages 46, feeder-free passages 5–9). Lines Regea 08/023 and 10212.EURCCs were derived at the Faculty of Medicine and Health Technology (MET), Tampere University, Finland, which has approval from the Finnish Medicines Agency (FIMEA) for research utilizing human embryos (Dnro 1426/32/300/05) and supportive statements from the regional ethics committee of Pirkanmaa Hospital District for the derivation, culture, and differentiation of hESCs (R05116) and hiPSCs (R08070). Informed consent was obtained from all subjects who provided cell samples. All methods were carried out in accordance with relevant guidelines and regulations. The hPSC lines were maintained on top of a human foreskin fibroblast feeder cell layer in Dulbecco's modified Eagle's medium (DMEM) containing 20% KnockOut Serum Replacement (both from Thermo Fisher Scientific) as described previously[78]. Before neural differentiation, hPSCs were transferred and expanded in feeder-free culture on recombinant human laminin-521 (LN521, Biolamina, Sweden) and E8 medium (Thermo Fisher Scientific) according to a previous publication[11]. The pluripotency of hPSC lines was regularly monitored with immunocytochemical staining of Nanog, Oct-3/4, SSEA-3, SSEA-4, TRA-1-81 and TRA-1-60, and the capacity to produce different germ layers in the EB formation assay was verified by staining for α-smooth muscle actin, α-fetoprotein, and Nestin. All cultures maintained normal karyotypes and were mycoplasma free.

Neural differentiation. The neural differentiation protocol was modified from a previously published method[6]. hPSCs were detached using TrypLE Select (Thermo Fisher Scientific) and plated at a density of 5×10^5 cells/cm^2 on 100 µg/ml poly-L-ornithine (PO, Sigma) and 15 µg/ml LN521 or Matrigel matrix (Corning)-coated plates in E8 medium containing 10 µM ROCK inhibitor (Y-27632, Sigma). Neural maintenance medium was used as a basal medium and consisted of 1:1 DMEM/F12 with Glutamax and Neurobasal, 0.5% N2, 1% B27 with Retinoic Acid, 0.5 mM GlutaMAX, 0.5% NEEA, 50 µM 2-mercaptoethanol (all from Thermo Fisher Scientific), 2.5 µg/ml Insulin (Sigma) and 0.1% penicillin/streptomycin (Thermo Fisher Scientific). During the neural induction stage (days 1–12, Fig. 1a), the maintenance medium was supplemented with 100 nM LDN193189 and 10 µM SB431542 (both from Sigma), and the medium was changed daily. At day 12, the cells were detached with StemPro Accutase (Thermo Fisher Scientific) and plated at a density of 2.5×10^5 cells/cm^2 on PO and either LN521 or mouse laminin (Sigma)-coated well plates in neural induction medium containing 10 µM ROCK inhibitor. For neural proliferation (days 13–25), the maintenance medium was supplemented with 20 ng/ml fibroblast growth factor-2 (FGF2, Thermo Fisher Scientific). At days 17, 21 and 25, the neural progenitor cells were passaged with StemPro Accutase and replated in medium containing 10 µM ROCK inhibitor. At day 21, the NPCs were cryopreserved in the same medium containing 10% DMSO (Sigma). For final maturation (days 26–130), the medium was changed to maintenance medium supplemented with 20 ng/ml brain-derived neurotrophic factor (BDNF, R&D Systems), 10 ng/ml glial-derived neurotrophic factor (GDNF, R&D Systems), 500 µM dibutyryl-cyclicAMP (db-cAMP, Sigma) and 200 µM ascorbic acid (AA, Sigma). At day 32, the cells were plated for experiments at a density of 50,000 cells/cm^2 on plastic well plates or 1×10^6 cells/cm^2 on microelectrode arrays (MEAs). Plastic well plates were coated with PO and either LN521 or mouse laminin as before and MEAs with 0.1% poly-ethylene-imide (PEI, Sigma) and either 50 µg/ml LN521 or mouse laminin. Medium changes were performed every two to three days.

Primary rat cultures. Cortex tissue was harvested from embryonic days 17–18 Wistar rat embryos as described previously[79]. Local authority approved the animal license (County Administrative Board of Southern

Finland, ESAVI/10300/04.10.07/2016) to conduct the described procedures. All experiments were performed according to institutional guidelines and regulations (University of Helsinki internal license number: KEK17-016). The medium consisted of Neurobasal, 2% B27, 2 mM GlutaMAX and 1% penicillin/streptomycin (Thermo Fisher Scientific). The plating density for the experiments was 100,000 cells/cm^2 on plastic cell culture wells or 2.5×10^5 cells/cm^2 on MEAs. Plastic well plates and MEAs were coated with 25 µg/ml poly-D-lysine (PDL, Sigma). The media was changed every two or three days.

Immunocytochemical staining. Immunocytochemistry was performed as previously described[80]. Primary antibodies consisted of βIII-tubulin (rabbit, 1:2000, GenScript: A01627), βIII-tubulin (chicken, 1:200, Abcam: ab41489), Brn2 (goat, 1:400 Santa Cruz: sc-6029), Ctip2 (rat, 1:500, Abcam: ab18465), FoxG1 (rabbit, 1:500, Abcam: ab18259), GABA (rabbit, 1:1000, Sigma-Aldrich: A2052), GAD67 (mouse, 1:100, Millipore: MAB5406), GFAP (chicken, 1:4000, Abcam: ab4674), MAP2 (rabbit, 1:400, Millipore: AB5622), MAP2 (chicken, 1:4000, Novus Biologicals: NB300-213), Oct4 (goat, 1:200, R&D Systems, AF1759), Pax6 (rabbit, 1:1000, BioLegend: 901301), PSD-95 (mouse, 1:50, Abcam: ab2723), Satb2 (mouse, 1:200, Abcam; ab51502), S100β (mouse, 1:500, Abcam: ab11178), Sox2 (mouse, 1:200, R&D Systems: MAB2018), synaptophysin (rabbit, 1:2000, Abcam: ab32127), Tbr1 (rabbit, 1:1500, Abcam: ab31940), Tbr2 (rabbit, 1:1000, Abcam: ab23345), vGlut1 (rabbit, 1:2000, Synaptic Systems: 135303) and vimentin (mouse, 1:500, Dako: M0725). Secondary antibodies consisted of Alexa Fluor 488 (1:400), Alexa Fluor 568 (1:400) or Alexa Fluor 647 (1:200) dyes (all Thermo Fisher Scientific). The cells were imaged using an Olympus IX51 microscope with an Olympus DP30BW camera (Olympus Corporation, Hamburg, Germany), an LSM780 laser scanning confocal microscope with a Quasar spectral GaAsP detector (all from Carl Zeiss, Jena, Germany) and a Nikon A1R + laser scanning confocal microscope with an A1-DUG GaAsP Multi Detector Unit. CellProfiler[81] and CellProfiler Analyst[82] software were used for quantification.

Microelectrode array measurements. Extracellular recordings were obtained with an Axion Maestro system controlled by AxIS software (Axion Biosystems, Atlanta, GA, USA) with a 12.5 kHz sampling rate. Cells were plated on CytoView MEA 12 for recording spontaneous activity development and on CytoView MEA 48 for pharmacological experiments (both from Axion Biosystems). CytoView MEA 12 and 48 plates contained 64 or 16 electrodes per well, respectively. Recordings were performed under 37 °C temperature control, and a 5% CO_2 atmosphere was provided during measurements exceeding 10 min. Spontaneous activity was measured twice a week for 10 min for a total of 14 weeks.

For pharmacological tests, 30 min of baseline activity was measured followed by a 30 min treatment follow-up. Pharmacological experiments were performed on rat cortical networks after 22 days on MEA and for hPSC-derived networks after 29 days on MEA. The pharmacological reagents used included kainic acid (1–5 µM, Sigma), α-amino-3-hydroxy-5-methyl-4-isoxazolepropionic acid (AMPA)/kainate receptor antagonist 6-cyano-7-nitroquinoxaline-2,3-dione (CNQX, 50 µM, Abcam), N-methyl-D-aspartate (NMDA) receptor antagonist D-(-)-2 amino-5-phosphonopentanoic acid (D-AP5, 50 µM, Sigma), γ-aminobutyric acid (GABA, 10 µM, Sigma), $GABA_A$ receptor antagonist gabazine (30 µM, Sigma) and voltage-gated sodium channel blocker tetrodotoxin (TTX, 1 µM, Tocris). All pharmacological agents were added into separate MEA wells in 30 µl volumes with higher concentrations, thus resulting in the final concentrations as stated above.

Microelectrode array data analysis. Spike detection was performed according to the stationary wavelet transform-based Teager energy operator (SWTTEO) algorithm that was presented previously[83] and revised for biological data[43]. The algorithm was implemented in a custom-made MATLAB (MathWorks) script. During initial method testing, it was confirmed that the method reliably detects low-amplitude signals typical for hPSC-derived networks and the pharmacologically evoked fast tonic spiking that can be challenging to separate from the baseline noise, as shown in the examples in Supplementary Fig. S8. In short, data were prefiltered with an elliptic bandpass filter with a 200 Hz lower passband and a 3000 Hz upper passband frequencies. The spike detection method uses a low threshold value for the initial threshold-based spike detection to detect low amplitude spikes. Here, a threshold value of 4.5 × the estimate of the noise standard deviation was applied according to previous publication[84]. Next, extra steps were performed to remove possible false positive spikes using the SWTTEO algorithm. The number of spikes extracted by threshold detection was fed to the SWTTEO analysis, and the corresponding spike list was produced. Finally, only the spikes detected by both methods were considered true positive events. Electrodes detecting >10 spikes per minute were considered active electrodes and included in the analysis.

Burst analysis was performed utilizing the R-package meaRtools[85]. For burst detection, the logISI algorithm was integrated into the analysis code[86] with minor modifications. When calculating burst features, only bursting electrodes were concerned. Parameters were set according to the original publication except for the minimum number of spikes in the burst, which was set to 5. A single modification to the original algorithm was added to merge short bursts in cases when the computed inter-spike interval threshold was less than 100 ms. Here, a cutoff of 100 ms was applied as the minimum time required between bursts.

Connectivity analysis was performed using the correlated spectral entropy (CorSE) method described previously[47]. Functional connectivity was calculated between all electrode pairs of the MEA during the measurement period. Briefly, CorSE quantifies the synchronization of signals by correlation of the temporal changes in their spectral contents. Magnitude of correlation gives the connectivity strength. Average CorSE values are calculated from all the MEA channels to assess the overall connectivity strength of the whole network. To observe the changes in the network formation of the most robust network participants, connectivity maps were plotted for the channel pairs, which have CorSE > 0.7.

Principal component analysis (PCA) was used as previously described[87] to segregate MEA results from different experiments. The data were derived from two differentiations of hESC line 08/023 (named hPSC 1 and 2) and

one differentiation of hiPSC line 10212.EURCCs (named hPSC 3). Additionally, MEA data were derived from three independent batches of rat embryonic neurons (named Rat 1–3). From each cell batch, the developmental time point showing the most significant activity (maximum spike rate) and two of its surrounding time points were selected for PCA analysis. The selected time points (days on MEA) were 21, 24 and 28 for hPSC 1 and 2; 70, 73 and 77 for hPSC 3; 21, 24 and 28 for Rat 1 and 2; and 24, 28 and 31 for Rat 3. A total of 7 features from spike, burst and network synchronization analysis were selected. These included the mean firing rate (MFR), burst rate, burst duration, spike frequency in burst, spikes in burst, percentage of spikes in bursts and spike time tiling coefficient (STTC, using default time bin 50 msec). All values were normalized using the standard score method. PCA was performed in MATLAB and plotted against the three major principal components.

Statistical analysis. Due to the non-Gaussian distribution of the data, the nonparametric Mann-Whitney U test was used. A p-value < 0.05 was considered significant. All statistical tests were performed with SPSS Statistics software (version 25.0). Tampere University statistician Heini Huhtala was consulted for the statistical tests.

Data availability

The datasets generated and/or analyzed during the current study are available from the corresponding author on reasonable request. We are planning to publish the MEA data in a subsequent publication, currently in preparation.

Received: 29 August 2019; Accepted: 1 November 2019;
Published online: 20 November 2019

References

1. Sandoe, J. & Eggan, K. Opportunities and challenges of pluripotent stem cell neurodegenerative disease models. *Nat. Neurosci.* **16**, 780 (2013).
2. Avior, Y., Sagi, I. & Benvenisty, N. Pluripotent stem cells in disease modelling and drug discovery. *Nat. Rev. Mol. Cell Biol.* **17**, 170–182 (2016).
3. Zhang, Y. *et al*. Rapid single-step induction of functional neurons from human pluripotent stem cells. *Neuron* **78**, 785–798 (2013).
4. Pasca, A. M. *et al*. Functional cortical neurons and astrocytes from human pluripotent stem cells in 3D culture. *Nat. Methods* **12**, 671–678 (2015).
5. Mariani, J. *et al*. Modeling human cortical development *in vitro* using induced pluripotent stem cells. *Proc. Natl. Acad. Sci. USA* **109**, 12770 (2012).
6. Shi, Y., Kirwan, P., Smith, J., Robinson, H. P. & Livesey, F. J. Human cerebral cortex development from pluripotent stem cells to functional excitatory synapses. *Nat. Neurosci.* **15**(47-86), S1 (2012).
7. Chen, G. *et al*. Chemically defined conditions for human iPSC derivation and culture. *Nat Methods* **8**, 424 (2011).
8. Ludwig, T. E. *et al*. Derivation of human embryonic stem cells in defined conditions. *Nat. Biotechnol.* **24**, 185 (2006).
9. Chambers, S. M. *et al*. Highly efficient neural conversion of human ES and iPS cells by dual inhibition of SMAD signaling. *Nat. Biotechnol.* **27**, 275 (2009).
10. Niclis, J. C. *et al*. Efficiently Specified Ventral Midbrain Dopamine Neurons from Human Pluripotent Stem Cells Under Xeno-Free Conditions Restore Motor Deficits in Parkinsonian Rodents. *Stem Cells Transl Med* **6**, 937–948 (2017).
11. Hongisto, H., Ilmarinen, T., Vattulainen, M., Mikhailova, A. & Skottman, H. Xeno- and feeder-free differentiation of human pluripotent stem cells to two distinct ocular epithelial cell types using simple modifications of one method. *Stem Cell Res Ther* **8**, 291 (2017).
12. Nakagawa, M. *et al*. A novel efficient feeder-free culture system for the derivation of human induced pluripotent stem cells. *Sci Rep* **4**, 3594 (2014).
13. Hyysalo, A. *et al*. Laminin alpha5 substrates promote survival, network formation and functional development of human pluripotent stem cell-derived neurons *in vitro*. *Stem Cell. Res.* **24**, 118–127 (2017).
14. Kilb, W., Kirischuk, S. & Luhmann, H. J. Electrical activity patterns and the functional maturation of the neocortex. *Eur. J. Neurosci.* **34**, 1677–1686 (2011).
15. Spitzer, N. C. Electrical activity in early neuronal development. *Nature* **444**, 707 (2006).
16. Zhang, L. I. & Poo, M. Electrical activity and development of neural circuits. *Nat. Neurosci.* **4**, 1207 (2001).
17. Blankenship, A. G. & Feller, M. B. Mechanisms underlying spontaneous patterned activity in developing neural circuits. *Nat. Rev. Neurosci.* **11**, 18–29 (2010).
18. Khazipov, R. & Luhmann, H. J. Early patterns of electrical activity in the developing cerebral cortex of humans and rodents. *Trends Neurosci.* **29**, 414–418 (2006).
19. Moore, A. R., Zhou, W. L., Jakovcevski, I., Zecevic, N. & Antic, S. D. Spontaneous electrical activity in the human fetal cortex *in vitro*. *J. Neurosci.* **31**, 2391–2398 (2011).
20. Allène, C. *et al*. Sequential Generation of Two Distinct Synapse-Driven Network Patterns in Developing Neocortex. *J. Neurosci.* **28**, 12851 (2008).
21. Corlew, R., Bosma, M. M. & Moody, W. J. Spontaneous, synchronous electrical activity in neonatal mouse cortical neurones. *J. Physiol.* **560**, 377–390 (2004).
22. Golbs, A., Nimmervoll, B., Sun, J., Sava, I. E. & Luhmann, H. J. Control of programmed cell death by distinct electrical activity patterns. *Cereb. Cortex* **21**, 1192–1202 (2011).
23. Egorov, A. V. & Draguhn, A. Development of coherent neuronal activity patterns in mammalian cortical networks: common principles and local hetereogeneity. *Mech. Dev.* **130**, 412–423 (2013).
24. Schnitzler, A. & Gross, J. Normal and pathological oscillatory communication in the brain. *Nat. Rev. Neurosci.* **6**, 285 (2005).
25. Ebert, D. H. & Greenberg, M. E. Activity-dependent neuronal signalling and autism spectrum disorder. *Nature* **493**, 327 (2013).
26. Kramer, M. A. & Cash, S. S. Epilepsy as a Disorder of Cortical Network Organization. *Neuroscientist* **18**, 360–372 (2012).
27. Pievani, M., Filippini, N., van, d. H., Cappa, S. F. & Frisoni, G. B. Brain connectivity in neurodegenerative diseases—from phenotype to proteinopathy. *Nat. Rev. Neurol.* **10**, 620 (2014).
28. Heikkilä, T. J. *et al*. Human embryonic stem cell-derived neuronal cells form spontaneously active neuronal networks *in vitro*. *Exp. Neurol.* **218**, 109–116 (2009).
29. Johnson, M. A., Weick, J. P., Pearce, R. A. & Zhang, S. C. Functional neural development from human embryonic stem cells: Accelerated synaptic activity via astrocyte coculture. *J. Neurosci.* **27**, 3069–3077 (2007).
30. Odawara, A., Katoh, H., Matsuda, N. & Suzuki, I. Induction of long-term potentiation and depression phenomena in human induced pluripotent stem cell-derived cortical neurons. *Biochem. Biophys. Res. Commun.* **469**, 856–862 (2016).

31. Tukker, A. M., Wijnolts, F. M. J., de Groot, A. & Westerink, R. H. S. Human iPSC-derived neuronal models for *in vitro* neurotoxicity assessment. *Neurotoxicology* **67**, 215–225 (2018).
32. Deneault, E. *et al*. Complete Disruption of Autism-Susceptibility Genes by Gene Editing Predominantly Reduces Functional Connectivity of Isogenic Human Neurons. *Stem Cell. Reports* **11**, 1211–1225 (2018).
33. Mäkinen, M. E., Ylä-Outinen, L. & Narkilahti, S. GABA and Gap Junctions in the Development of Synchronized Activity in Human Pluripotent Stem Cell-Derived Neural Networks. *Front Cell Neurosci* **12**, 56 (2018).
34. Izsak, J. *et al*. Robust Generation of Person-Specific, Synchronously Active Neuronal Networks Using Purely Isogenic Human iPSC-3D Neural Aggregate Cultures. *Front Neurosci* **13**, 351 (2019).
35. An, S., Yang, J., Sun, H., Kilb, W. & Luhmann, H. J. Long-Term Potentiation in the Neonatal Rat Barrel Cortex *In Vivo*. *J. Neurosci.* **32**, 9511 (2012).
36. Jimbo, Y., Tateno, T. & Robinson, H. P. C. Simultaneous Induction of Pathway-Specific Potentiation and Depression in Networks of Cortical Neurons. *Biophys. J.* **76**, 670–678 (1999).
37. Sun, J. & Luhmann, H. J. Spatio-temporal dynamics of oscillatory network activity in the neonatal mouse cerebral cortex. *Eur. J. Neurosci.* **26**, 1995–2004 (2007).
38. Odawara, A., Katoh, H., Matsuda, N. & Suzuki, I. Physiological maturation and drug responses of human induced pluripotent stem cell-derived cortical neuronal networks in long-term culture. *Sci Rep* **6**, 26181 (2016).
39. Cotterill, E. *et al*. Characterization of Early Cortical Neural Network Development in Multiwell Microelectrode Array Plates. *J Biomol Screen* **21**, 510–519 (2016).
40. Charlesworth, P., Cotterill, E., Morton, A., Grant, S. G. N. & Eglen, S. J. Quantitative differences in developmental profiles of spontaneous activity in cortical and hippocampal cultures. *Neural Dev* **10** (2015).
41. Wagenaar, D. A., Pine, J. & Potter, S. M. An extremely rich repertoire of bursting patterns during the development of cortical cultures. *BMC Neurosci*. **7** (2006).
42. Cotterill, E., Charlesworth, P., Thomas, C. W., Paulsen, O. & Eglen, S. J. A comparison of computational methods for detecting bursts in neuronal spike trains and their application to human stem cell-derived neuronal networks. *J. Neurophysiol*. **116**, 306–321 (2016).
43. Mayer, M. *et al*. Electrophysiological investigation of human embryonic stem cell derived neurospheres using a novel spike detection algorithm. *Biosens. Bioelectron*. **100**, 462–468 (2018).
44. Ylä-Outinen, L. *et al*. In *In Vitro Neuronal Networks - From Culturing Methods to* Neuro-Technological *Applications* (eds Chiappalone, M., Pasquale, V. & Frega, M.) 299–329 (Springer book series, 2019).
45. Okujeni, S., Kandler, S. & Egert, U. Mesoscale Architecture Shapes Initiation and Richness of Spontaneous Network Activity. *J. Neurosci.* **37**, 3972–3987 (2017).
46. Luhmann, H. J. *et al*. Spontaneous Neuronal Activity in Developing Neocortical Networks: From Single Cells to Large-Scale Interactions. *Front Neural Circuits* **10**, 40 (2016).
47. Kapucu, F. E. *et al*. Spectral Entropy Based Neuronal Network Synchronization Analysis Based on Microelectrode Array Measurements. *Front Comput Neurosci* **10**, 112 (2016).
48. Cutts, C. S. & Eglen, S. J. Detecting pairwise correlations in spike trains: an objective comparison of methods and application to the study of retinal waves. *J. Neurosci.* **34**, 14288–14303 (2014).
49. Scelfo, B. *et al*. Application of multielectrode array (MEA) chips for the evaluation of mixtures neurotoxicity. *Toxicology* **299**, 172–183 (2012).
50. Kirwan, P. *et al*. Development and function of human cerebral cortex neural networks from pluripotent stem cells *in vitro*. *Development (Cambridge)* **142**, 3178–3187 (2015).
51. Mack, C. M. *et al*. Burst and principal components analyses of MEA data for 16 chemicals describe at least three effects classes. *Neurotoxicology* **40**, 75–85 (2014).
52. Stern, C. D. Neural induction: old problem, new findings, yet more questions. *Development* **132**, 2007–2021 (2005).
53. Domogatskaya, A., Rodin, S. & Tryggvason, K. Functional diversity of laminins. *Annu. Rev. Cell Dev. Biol.* **28**, 523–553 (2012).
54. Long, K. R. & Huttner, W. B. How the extracellular matrix shapes neural development. *Open Biol* **9**, 180216 (2019).
55. Miner, J. H., Cunningham, J. & Sanes, J. R. Roles for laminin in embryogenesis: exencephaly, syndactyly, and placentopathy in mice lacking the laminin alpha5 chain. *J. Cell Biol.* **143**, 1713–1723 (1998).
56. Lu, H. F. *et al*. A defined xeno-free and feeder-free culture system for the derivation, expansion and direct differentiation of transgene-free patient-specific induced pluripotent stem cells. *Biomaterials* **35**, 2816–2826 (2014).
57. Qian, X. *et al*. Timing of CNS cell generation: a programmed sequence of neuron and glial cell production from isolated murine cortical stem cells. *Neuron* **28**, 69–80 (2000).
58. Rigamonti, A. *et al*. Large-Scale Production of Mature Neurons from Human Pluripotent Stem Cells in a Three-Dimensional Suspension Culture System. *Stem Cell Reports* **6**, 993–1008 (2016).
59. Bellot-Saez, A. *et al*. Astrocytic modulation of cortical oscillations. *Sci Rep* **8**, 11565 (2018).
60. Fellin, T. *et al*. Neuronal synchrony mediated by astrocytic glutamate through activation of extrasynaptic NMDA receptors. *Neuron* **43**, 729–743 (2004).
61. Engle, S. J., Blaha, L. & Kleiman, R. J. Best Practices for Translational Disease Modeling Using Human iPSC-Derived Neurons. *Neuron* **100**, 783–797 (2018).
62. Odawara, A., Matsuda, N., Ishibashi, Y., Yokoi, R. & Suzuki, I. Toxicological evaluation of convulsant and anticonvulsant drugs in human induced pluripotent stem cell-derived cortical neuronal networks using an MEA system. *Sci Rep* **8**, 10416 (2018).
63. Paavilainen, T. *et al*. Effect of prolonged differentiation on functional maturation of human pluripotent stem cell-derived neuronal cultures. *Stem Cell Res* **27**, 151–161 (2018).
64. Gunhanlar, N. *et al*. A simplified protocol for differentiation of electrophysiologically mature neuronal networks from human induced pluripotent stem cells. *Mol. Psychiatry* **23**, 1336–1344 (2018).
65. Weick, J. P. Functional Properties of Human Stem Cell-Derived Neurons in Health and Disease. *Stem Cells Int* **2016**, 4190438 (2016).
66. Stein, J. L. *et al*. A quantitative framework to evaluate modeling of cortical development by neural stem cells. *Neuron* **83**, 69–86 (2014).
67. Trujillo, C. A. *et al*. Complex Oscillatory Waves Emerging from Cortical Organoids Model Early Human Brain Network Development. *Cell Stem Cell* **25**, 55–569.e7 (2019).
68. Napoli, A. & Obeid, I. Comparative Analysis of Human and Rodent Brain Primary Neuronal Culture Spontaneous Activity Using Micro-Electrode Array Technology. *J. Cell. Biochem.* **117**, 559–565 (2016).
69. Kasteel, E. E. J. & Westerink, R. H. S. Comparison of the acute inhibitory effects of Tetrodotoxin (TTX) in rat and human neuronal networks for risk assessment purposes. *Toxicol. Lett.* **270**, 12–16 (2017).
70. Tukker, A. M. *et al*. Is the time right for *in vitro* neurotoxicity testing using human iPSC-derived neurons? *ALTEX* **33**, 261–271 (2016).
71. Moakley, D. *et al*. Pharmacological Profiling of Purified Human Stem Cell-Derived and Primary Mouse Motor Neurons. *Sci Rep* **9**, 10835 (2019).
72. Mehta, S. R. *et al*. Human Huntington's Disease iPSC-Derived Cortical Neurons Display Altered Transcriptomics, Morphology, and Maturation. *Cell Rep* **25**, 108–1096.e6 (2018).
73. Russo, F. B. *et al*. Modeling the Interplay Between Neurons and Astrocytes in Autism Using Human Induced Pluripotent Stem Cells. *Biol. Psychiatry* **83**, 569–578 (2018).

74. Grainger, A. I. *et al*. *In vitro* Models for Seizure-Liability Testing Using Induced Pluripotent Stem Cells. *Front Neurosci* **12**, 590 (2018).
75. Skottman, H. Derivation and characterization of three new human embryonic stem cell lines in Finland. *In Vitro Cell Dev Biol Anim* **46**, 206–209 (2010).
76. Kiamehr, M. *et al*. Compromised Barrier Function in Human Induced Pluripotent Stem-Cell-Derived Retinal Pigment Epithelial Cells from Type 2 Diabetic Patients. *Int J Mol Sci* **20** (2019).
77. Yu, J. *et al*. Induced Pluripotent Stem Cell Lines Derived from Human Somatic Cells. *Science* **318**, 1917 (2007).
78. Rajala, K. *et al*. Testing of nine different xeno-free culture media for human embryonic stem cell cultures. *Hum. Reprod.* **22**, 1231–1238 (2007).
79. Sahu, M., Nikkilä, O., Lågas, S., Kolehmainen, S. & Castrén, E. Culturing primary neurons from rat hippocampus and cortex. *Neuronal Signal.* **3**, NS20180207 (2019).
80. Lappalainen, R. S. *et al*. Similarly derived and cultured hESC lines show variation in their developmental potential towards neuronal cells in long-term culture. *Regenerative Med.* **5**, 749–762 (2010).
81. Carpenter, A. E. *et al*. CellProfiler: Image analysis software for identifying and quantifying cell phenotypes. *Genome Biol.* **7** (2006).
82. Jones, T. R. *et al*. CellProfiler Analyst: Data exploration and analysis software for complex image-based screens. *BMC Bioinform.* **9** (2008).
83. Lieb, F., Stark, H. & Thielemann, C. A stationary wavelet transform and a time-frequency based spike detection algorithm for extracellular recorded data. *J Neural Eng* **14**, 036013 (2017).
84. Quiroga, R. Q., Nadasdy, Z. & Ben-Shaul, Y. Unsupervised spike detection and sorting with wavelets and superparamagnetic clustering. *Neural Comput* **16**, 1661–1687 (2004).
85. Gelfman, S. *et al*. meaRtools: An R package for the analysis of neuronal networks recorded on microelectrode arrays. *PLoS Comput. Biol.* **14**, e1006506 (2018).
86. Pasquale, V., Martinoia, S. & Chiappalone, M. A self-adapting approach for the detection of bursts and network bursts in neuronal cultures. *J. Comput. Neurosci.* **29**, 213–229 (2010).
87. Ylä-Outinen, L. *et al*. Screening of Hydrogels for Human Pluripotent Stem Cell-Derived Neural Cells: Hyaluronan-Polyvinyl Alcohol-Collagen-Based Interpenetrating Polymer Network Provides an Improved Hydrogel Scaffold. *Macromol Biosci* **19**, e1900096 (2019).

Acknowledgements

The authors thank Senior Scientist Tina C. Stummann, PhD (H. Lundbeck A/S, Denmark) for her contribution in establishing the neural differentiation methods. We thank Prof. Ellen Fritsche (Heinrich Heine University Düsseldorf, Germany) for help establishing the IMR90-4 culture. The authors thank Prof. Eero Castrén and the Neuronal Cell Culture Unit at the University of Helsinki for the primary rat cortical cells. Additionally, we thank the iPS Cells core facility, Tampere University, for providing the undifferentiated hiPSCs and Hanna Mäkelä and Eija Hannuksela for technical assistance with cell maintenance and molecular biology analyses. The authors thank the Tampere Imaging Facility and Outi Paloheimo for technical assistance and illustrations. We thank the Tampere Facility of Electrophysiological Measurements, Tampere University, and Juha Heikkilä for technical assistance with the MEA measurements. This work was supported by Business Finland and the Academy of Finland (grant number 312414 to S.N. and 286990 to L.Y.-O.). T.H. received support from the Finnish Cultural Foundation (grant number 00170805) and the doctoral program at the Faculty of Medicine and Health Technology, Tampere University.

Author contributions

T.H., A.H., L.Y.-O. and S.N. designed the study; T.H., A.H., and L.A. performed experiments; S.J.E., L.A. and A.V. contributed new analysis tools; T.H., L.Y.-O. and F.E.K. analyzed the data; T.H. and S.N. wrote the paper. All authors edited the article.

Competing interests

The authors declare no competing interests.

Additional information

Supplementary information is available for this paper at https://doi.org/10.1038/s41598-019-53647-8.

Correspondence and requests for materials should be addressed to S.N.

Reprints and permissions information is available at www.nature.com/reprints.

Publisher's note Springer Nature remains neutral with regard to jurisdictional claims in published maps and institutional affiliations.

PUBLICATION III

Co-stimulation with IL-1β and TNF-α induces an inflammatory reactive astrocyte phenotype with neurosupportive characteristics in a human pluripotent stem cell model system

Hyvärinen T, Hagman S, Ristola M, Sukki L, Veijula K, Kreutzer J, Kallio P, Narkilahti S

Scientific Reports. 2019. 9(1):16944.
doi:10.1038/s41598-019-53414-9

SCIENTIFIC REPORTS
nature research

OPEN

Co-stimulation with IL-1β and TNF-α induces an inflammatory reactive astrocyte phenotype with neurosupportive characteristics in a human pluripotent stem cell model system

Tanja Hyvärinen[1,3], Sanna Hagman[1,3], Mervi Ristola[1], Lassi Sukki[2], Katariina Veijula[1], Joose Kreutzer[2], Pasi Kallio[2] & Susanna Narkilahti[1*]

Astrocyte reactivation has been discovered to be an important contributor to several neurological diseases. *In vitro* models involving human astrocytes have the potential to reveal disease-specific mechanisms of these cells and to advance research on neuropathological conditions. Here, we induced a reactive phenotype in human induced pluripotent stem cell (hiPSC)-derived astrocytes and studied the inflammatory natures and effects of these cells on human neurons. Astrocytes responded to interleukin-1β (IL-1β) and tumor necrosis factor-α (TNF-α) treatment with a typical transition to polygonal morphology and a shift to an inflammatory phenotype characterized by altered gene and protein expression profiles. Astrocyte-secreted factors did not exert neurotoxic effects, whereas they transiently promoted the functional activity of neurons. Importantly, we engineered a novel microfluidic platform designed for investigating interactions between neuronal axons and reactive astrocytes that also enables the implementation of a controlled inflammatory environment. In this platform, selective stimulation of astrocytes resulted in an inflammatory niche that sustained axonal growth, further suggesting that treatment induces a reactive astrocyte phenotype with neurosupportive characteristics. Our findings show that hiPSC-derived astrocytes are suitable for modeling astrogliosis, and the developed *in vitro* platform provides promising novel tools for studying neuron-astrocyte crosstalk and human brain disease in a dish.

Astrocytes are the most abundant cell type in the central nervous system (CNS) and play important roles in supporting neuronal cell functions by releasing energy substrates and trophic factors, maintaining homeostatic functions and regulating neuronal synaptogenesis and synaptic transmission[1–4]. During CNS injury and disease, astrocytes transform into a reactive phenotype with changed morphology and altered gene expression and secretion profiles[4,5]. These astrocytes are regarded as immunocompetent cells that can respond to complex inflammatory events by secreting cytokines and chemokines, thereby controlling immune cell activation and migration to sites of damage[5,6]. Astrocytes are considered to play a dual role in CNS pathophysiology, as they can both support regeneration and exert detrimental effects on surrounding cells and brain parenchyma[6,7]. Interestingly, two distinct astrocyte phenotypes were recently described in rodent studies: a detrimental A1 type and a beneficial A2 type[8,9]. Of these, A2 astrocytes were associated with ischemia-induced CNS lesions, while A1 astrocytes dominated in inflammation-induced lesions reflecting those in diseases such as multiple sclerosis (MS). However, reactivation of astrocytes is a complex phenomenon that possibly results in a mixture of the two phenotypes or even several distinct yet unidentified activation states[10].

[1]NeuroGroup, Faculty of Medicine and Health Technology, Tampere University, Tampere, Finland. [2]Micro and Nanosystems Research Group, Faculty of Medicine and Health Technology, Tampere University, Tampere, Finland. [3]These authors contributed equally: Tanja Hyvärinen and Sanna Hagman. *email: susanna.narkilahti@tuni.fi

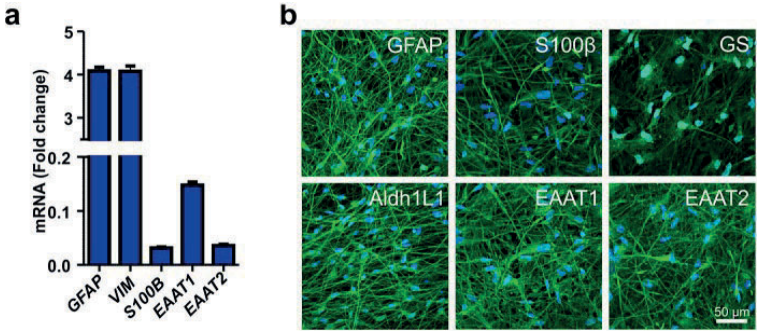

Figure 1. Characterization of hiPSC-derived astrocytes. (**a**) The hiPSC-derived astrocytes expressed several astrocyte-specific genes, including *GFAP, VIM, S100B, EAAT1* and *EAAT2*. The data are presented as the mean ± s.e.m. (n = 2 with three technical replicates; the data are representative of two experiments). (**b**) Immunocytochemical staining was used to confirm the expression of the major astrocyte markers GFAP, S100β, GS, Aldh1L1, EAAT1 and EAAT2.

The majority of the knowledge on reactive astrocytes has been gathered from rodent studies, whereas the inflammatory nature of human astrocytes has received less attention[9–11]. Nevertheless, growing evidence shows significant structural and functional differences between human and rodent astrocytes, underlining the relevance of further studies focusing on human astrocytes and their behaviors[12–14]. *In vitro* studies with human cells have typically utilized astrocytes from primary fetal or adult tissues or immortalized astrocytoma cell lines[14–17]; however, the availability of human primary astrocytes is limited, and immortalized cells are often criticized as model systems. Advancements in the field of stem cell biology have enabled the differentiation of astrocytes from human pluripotent stem cells (hPSCs)[18–22], providing an unlimited cell source and an option to create disease-specific cell lines. Despite these advancements, only a few studies have described the reactivation of hPSC-derived astrocytes[18,22–25], and even fewer studies have reported the interplay of inflammation or reactive astrocytes with human neuronal cells[24,26,27].

The development of newly engineered *in vitro* platforms based on hPSC-derived cells is a promising approach for studying the mechanisms of CNS functions and disorders[28–30]. Microfluidic devices are potent research tools for studying the interactions of several cell types in controlled, compartmentalized culture environments[31,32]. For example, multiple cell compartments can be connected via microtunnels, allowing the growth of axons while restricting neuronal somas thus facilitating experimentation on cellular processes and cell-to-cell interactions[31]. Advantages in microfluidic technology have already been validated, for instance, in axonal transport and myelination studies[33–39]. However, less data are available on neuron-astrocyte interactions and neuroinflammatory activity[26,31]. Understanding the complex cellular interplay among several neural cell types can help to reveal underlying mechanisms in neurodegenerative diseases and create opportunities for drug discovery.

Here, we studied reactivation using human induced pluripotent stem cell (hiPSC) -derived astrocytes and observed their transformation into cells with reactive proinflammatory phenotypes with neurosupportive characteristics. Furthermore, we designed a novel microfluidic co-culture platform including neurons, astrocytes and an inflammatory environment that was validated for studying reactive astrocyte-neuron interactions. We are convinced that hiPSC-astrocyte model systems can facilitate investigation of specific human cell properties and ultimately model human CNS diseases in a dish.

Results

Characterization of hiPSC-derived astrocytes. HiPSC-derived astrocytes were first characterized in their quiescent resting state for the expression of astrocyte-specific markers at the gene and protein levels. Gene expression analysis revealed expression of transcripts typical for developing astrocytes, including S100 calcium-binding protein beta (*S100β*) and vimentin (*VIM*) (Fig. 1a). Additionally, mature astrocyte genes, such as glial fibrillary acidic protein (*GFAP*) and excitatory amino acid transporters 1 and 2 (*EAAT1* and *EAAT2*, respectively), were expressed (Fig. 1a). Major astrocyte-specific markers were also confirmed by immunocytochemical staining of GFAP, S100β, glutamine synthetase (GS), aldehyde dehydrogenase 1 family member (Aldh1L1), EAAT1 and EAAT2 (Fig. 1b). To confirm that the astrocytes were mostly negative for neuronal markers, the cells were stained for microtubule-associated protein 2 (MAP2) (Supplementary Fig. S1). Thus, the culture consisted of a heterogeneous astrocyte population with a cell type-specific expression signature.

Treatment of hiPSC-derived astrocytes with IL-1β and TNF-α induces a reactive phenotype. To induce a reactive astrocyte phenotype with inflammatory cytokines and to characterize astrocyte properties, an extended seven-day co-stimulation with IL-1β and TNF-α was performed (Fig. 2a). First, the presence of cytokine receptors for IL-1β and TNF-α in hiPSC-derived astrocytes was analyzed in the quiescent resting state. The expression of IL-1 receptor 1 (*IL1R*) and IL-1 receptor accessory protein (*IL1RAP*), as well as that of tumor necrosis factor receptor superfamily 1 A (*TNFRSF1A*), which is important for mediating the signals of these

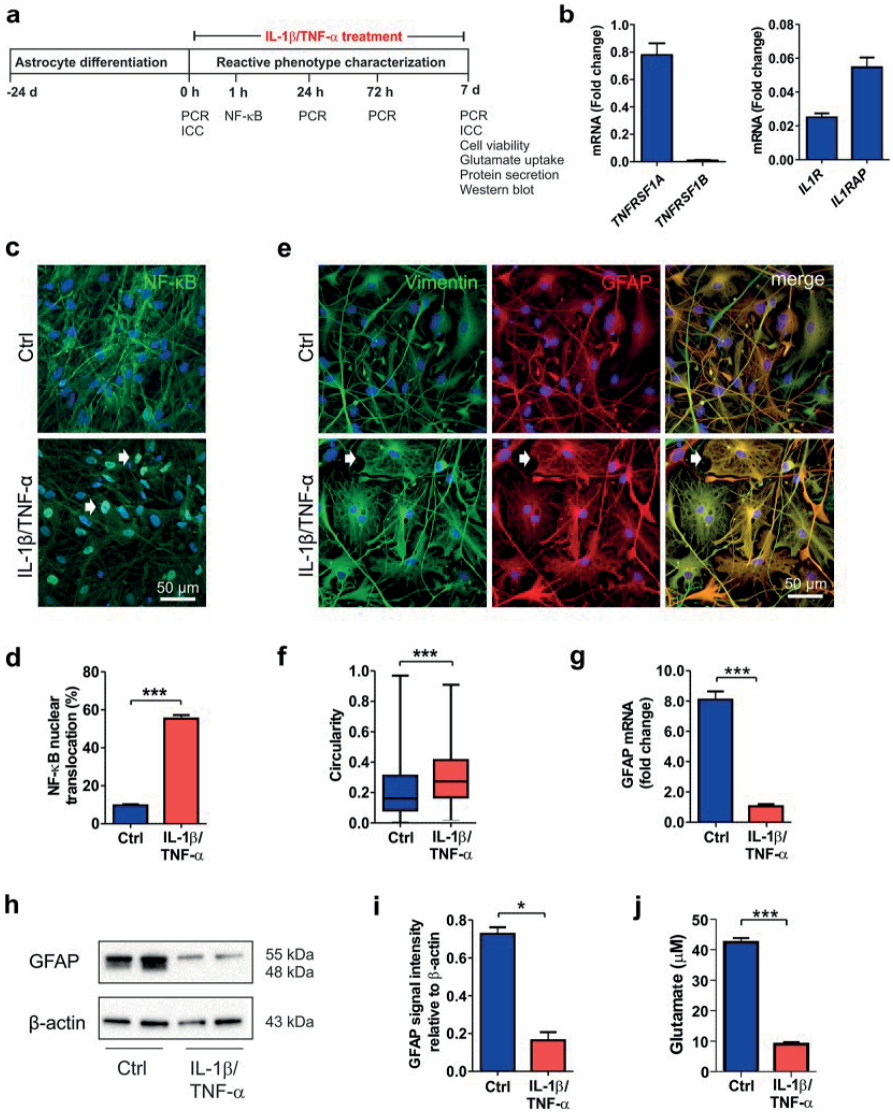

Figure 2. IL-1β and TNF-α treatment induces a reactive astrocyte phenotype. (**a**) Experimental setup for astrocyte stimulation with IL-1β and TNF-α and astrocyte characterization. (**b**) Gene expression analysis revealed the presence of TNFRSF1A, IL1R, and IL1RAP transcripts in the astrocytes (n = 2 with three technical replicates; the data are representative of two experiments). (**c**) In control astrocytes, NF-κB was ubiquitously expressed in the cytoplasm, whereas after 60 minutes cytokine stimulation, it was activated and translocated to the nucleus (white arrows). (**d**) NF-κB activation was quantified as the percentage of nuclei with translocation among the total nuclei (n = 6 cultures; the data were analyzed from two experiments). (**e**) Immunocytochemical staining of the intermediate filament proteins vimentin and GFAP showed morphological changes from filamentous to flattened shapes (white arrows) in response to cytokine stimulation. (**f**) Morphological change was quantified based on the vimentin staining of samples on day 7. The circularity of the cells in each group is presented as the median and interquartile range, with the whiskers showing the minimum and maximum values. Images were analyzed from six cultures derived from three experiments. (**g**) *GFAP* expression levels decreased following cytokine stimulation (n = 2 with three technical replicates; the data are representative of two experiments). (**h**) GFAP was analyzed at the protein level by western blot analysis, representative cropped images of the membranes for the GFAP and β-Actin are shown here and full length of membranes are presented in the Supplementary Fig. S4. (**i**) Quantification of GFAP and β-Actin showed a reduction after cytokine treatment. β-Actin was used as a loading control (n = 2; the data are representative of three experiments). (**j**) Cytokine treatment impaired the glutamate uptake capacity of astrocytes (n = 3; the data are representative

of two experiments). The data are presented as the mean ± s.e.m. Statistical analysis was performed with independent-sample t-tests except in (**f**), in which statistical analysis was performed with the Mann-Whitney U test. Statistical significance: * $p < 0.05$, ** $p < 0.01$, and *** $p < 0.001$.

cytokines, was confirmed (Fig. 2b). However, *TNFRSF1B* was not detectable in the hiPSC-derived astrocytes (Fig. 2b).

Nuclear factor kappa B (NF-κB) is a key transcription factor that has been shown to be activated in reactive astrocytes during neuroinflammation[6]. Here, NF-κB was ubiquitously present in the cytoplasm of quiescent astrocytes but was only present in low amounts in the nuclei (Fig. 2c). However, soon after the initiation of cytokine treatment, NF-κB was activated and translocated to the nucleus (Fig. 2c, Supplementary Fig. S2). After 60 min of cytokine stimulation, a significant portion (over 50%) of the astrocytes showed activation of the NF-κB pathway (control [Ctrl] 9.7 ± 0.6 vs. IL-1β/TNF-α treated [Trt] 55.3 ± 1.9, $p < 0.001$, Fig. 2d).

Reactive astrocytes undergo changes in morphology typically characterized by hypertrophy of main cellular processes[40]. Over the 7-day cytokine treatment period, the astrocytes gradually exhibited a morphological change from a highly filamentous shape to a flattened polygonal appearance (Supplementary Fig. S3). This typical response was most notable upon the staining of the intermediate filament proteins vimentin and GFAP, both of which contribute to astrocyte morphology (Fig. 2e). The morphology of the control and treated astrocytes was quantified based on vimentin staining at the 7-day time point (Fig. 2f). The circularity index was calculated according to the area and perimeter metrics of each cell, with a value of 1 describing a perfectly circular object. Quantification confirmed that the astrocytes lost their filamentous shape and adopted a more circular morphology in response to cytokine activation (medians Ctrl 0.16 vs. Trt 0.27, $p < 0.001$, Fig. 2f).

Changes in intermediate filament protein expression have often been considered to be hallmarks of reactive astrocytes[10]. Although the cytokine-stimulated reactive astrocytes showed positive staining for GFAP (Fig. 2e), we observed an 8-fold decrease in mRNA levels after the 7-day treatment in the treated cells compared to the controls (Ctrl 8.81 ± 0.54 vs. Trt 1.05 ± 0.15, $p < 0.001$, Fig. 2g). The GFAP protein levels were also confirmed by western blot analysis, showing similar decreases as a result of IL-1β and TNF-α treatment (Ctrl 0.73 ± 0.04 vs. Trt 0.16 ± 0.06, $p = 0.010$, Fig. 2h–i, Supplementary Fig. S4). Additionally, the vimentin protein levels were studied and were found to remain more stable than GFAP protein levels after cytokine treatment (Supplementary Fig. S4).

Uptake of glutamate from the extracellular space is an important function of astrocytes that sustains healthy synaptic transmission of neurons[4]. Impairment in the uptake of glutamate from the culture medium was revealed in cytokine-stimulated astrocytes compared to control astrocytes (Ctrl 42.4 ± 1.4 vs. Trt 9.0 ± 0.66, $p < 0.001$, Fig. 2j). In summary, treatment with the cytokines IL-1β and TNF-α activated astrocytes, modified their intermediate filament cytoskeleton and transformed them morphologically and functionally into cells with a reactive phenotype.

Cytokine treatment induces astrocyte proliferation and reduces viability. Next, we studied the effects of cytokines on the viability and proliferation of astrocytes after a 7-day treatment regimen. Immunocytochemical staining with the proliferation marker Ki67 showed a slight (5%) but significant increase in proliferation in cytokine-treated cells compared to control cells (Ctrl 6.8 ± 0.9 vs. Trt 11.8 ± 0.7, $p < 0.001$, Fig. 3a–b). However, this increase did not significantly affect the total nuclei count (Ctrl 1094 ± 28 vs. Trt 1040 ± 55, Fig. 3c) or the total DNA amount (Ctrl 95476.7 ± 8299.5 vs. Trt 89263.8 ± 8779.2, Fig. 3d). Upon assessing the viability of astrocytes after cytokine treatment, a significant increase in cytotoxicity (Ctrl 1053.0 ± 55.8 vs. Trt 2677.3 ± 461.2, $p = 0.017$) and a decrease in viability (Ctrl 38938.2 ± 2347.3 vs. Trt 17999.2 ± 3352.4, $p < 0.001$) in the treated cells compared to the control cells were found (Fig. 3e). In the apoptosis metrics, no statistically significant differences were detected between the groups (Ctrl 26026.8 ± 4362.3 vs. Trt 20265.8 ± 3629.6, Fig. 3e). In conclusion, cytokine treatment of hiPSC-derived astrocytes caused minor proliferation, but the total cell number remained stable due to cytotoxicity.

Reactivation induces a proinflammatory response in astrocytes. To reveal whether the astrocytes were able to produce an immune response, the gene expression and secretion profiles of inflammatory markers were characterized. First, the effects of IL-1β and TNF-α treatment on the expression of the inflammation-related genes *CCL5*, *CXCL8*, complement component 3 (*C3*) and lipocalin-2 (*LCN2*) were studied (Fig. 4a–d). At the basal level, none of the transcripts were expressed, whereas treatment for 24 h led to over 300-fold increases in the expression of the chemokines *CCL5* and *CXCL8* (Fig. 4a–b). Recently, C3 has been linked to astrocyte reactivity[8,41]. Here, *C3* expression increased in a time-dependent manner after cytokine treatment, reaching over a 200-fold change compared to the control level at the 7-day time point (Fig. 4c). The gene expression of *LCN2* also considerably increased over 7 days, although the change was not as prominent as that for the other transcripts (Fig. 4d).

Next, the secretion of 105 inflammatory proteins (see full list in Supplementary Table 1) from cytokine-stimulated astrocytes was studied (Fig. 4e; Supplementary Fig. S5a). Treatment induced widespread protein secretion at the 24 h and 7-day time points (Fig. 4e and Supplementary Fig. S4a). The most highly secreted proteins were chemokines (CXCL10, CXCL5, CXCL8, CCL2, CXCL1, and CCL5), but other inflammatory factors, such as pentraxin 3 (PTX3), osteopontin (OPN), chitinase-3 like 1 (CHI3L1), Serpin E1 and adhesion molecule vascular cell adhesion protein-1 (VCAM1), were also secreted. Among the cytokines, IL-6, IL-1β, TNF-α and macrophage migration inhibitory factor (MIF) were detected on medium obtained from the cytokine-treated astrocytes.

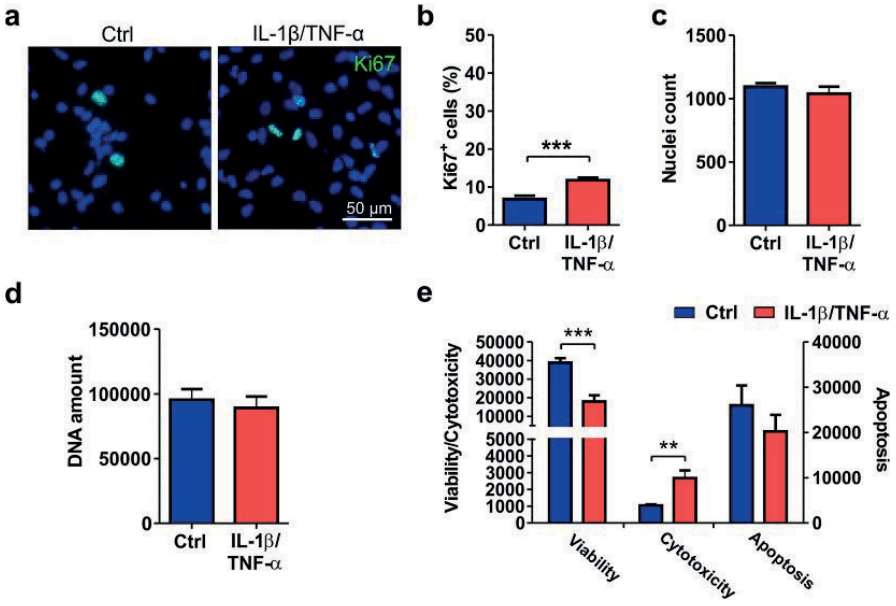

Figure 3. Viability and proliferation of cytokine-treated astrocytes. (**a**) Immunocytochemical staining of proliferating Ki67-positive cells in control and IL-1β/TNF-α-treated cultures. (**b**) The number of proliferating cells was increased after cytokine treatment. (**c**) The nuclei count quantified from DAPI staining remained similar between the control and treated groups. For Ki67 staining and nuclei counts, images were analyzed from 11 cultures derived from four experiments. (**d**) Additionally, the amount of DNA was similar between the groups (n = 6 with two technical replicates; the data are from two experiments). (**e**) The viability assay showed decreased viability and increased cytotoxicity but no significant difference in apoptosis following cytokine treatment (n = 3; the data are representative from two experiments). The quantification data are presented as the mean ± s.e.m. All statistical analysis was performed using independent-sample t-tests. The significant p-values are presented in the graphs. Statistical significance: * $p < 0.05$, ** $p < 0.01$, and *** $p < 0.001$.

IL-6 is a classic inflammatory mediator known to be secreted from astrocytes after reactivation[42]; therefore, the secretion of IL-6 was further investigated. Control astrocytes did not secrete IL-6, but cytokine-stimulated astrocytes gradually secreted IL-6, the levels of which reached 2000 pg/ml at the 7-day time point (Fig. 4f). In summary, astrocytes responded to cytokine treatment with changes in gene expression and broad secretion of proinflammatory factors.

Astrocyte conditioned medium sustains neuronal viability and supports functional activity. Astrocyte activation resulted in widespread secretion of inflammatory molecules; therefore, we next studied whether astrocyte conditioned medium (ACM) has an effect on neurons. Astrocytes were treated with IL-1β and TNF-α for seven days; the treatment was then washed out, and the ACM was collected 48 h later. At this stage, the astrocytes still secreted a broad profile of inflammatory factors (Supplementary Fig. S5b). In-house-differentiated hPSC-derived neurons were exposed to ACM for 48 h, after which they still retained a normal branched neuronal morphology (Fig. 5a). Additionally, ACM treatment did not cause any changes in viability or apoptosis or cause cytotoxicity, confirming that the produced reactive astrocytes did not secrete neurotoxic factors at detrimental levels (Fig. 5b). Similar results were obtained with commercial hiPSC-derived neurons (Supplementary Fig. S6a–b).

The effect of ACM on neuronal functionality was studied with a microelectrode array (MEA) setup, which allowed repeated measurements from the same network. In-house-differentiated hPSC-derived neuronal cells were first cultured on MEAs for five weeks until mature bursting and synchronic activity was achieved throughout the network (Fig. 5c–d). Once array-wide activity had developed, the cultures were treated with control ACM or reactive ACM, and measurements were performed immediately (acute) and at 1 h, 4 h and 24 h after ACM application (Fig. 5e). A naïve control group received the same volume of intact medium (held for 48 h in an incubator similar to that in which the collected ACM was held). Overall, addition of the media induced increases in spike rates in all studied groups and, to a lesser extent, increases in burst counts during the 24 h follow-up period (Fig. 5e–f, Supplementary Table 2). The magnitudes of these changes were not as great in the commercial neurons as in the in-house-differentiated neurons (Supplementary Fig. S6d–e).

Next, activity changes in relation to baseline measurements were studied between the different treatment groups (Fig. 5g–h). The control ACM- and reactive ACM-treated networks responded similarly, as no significant

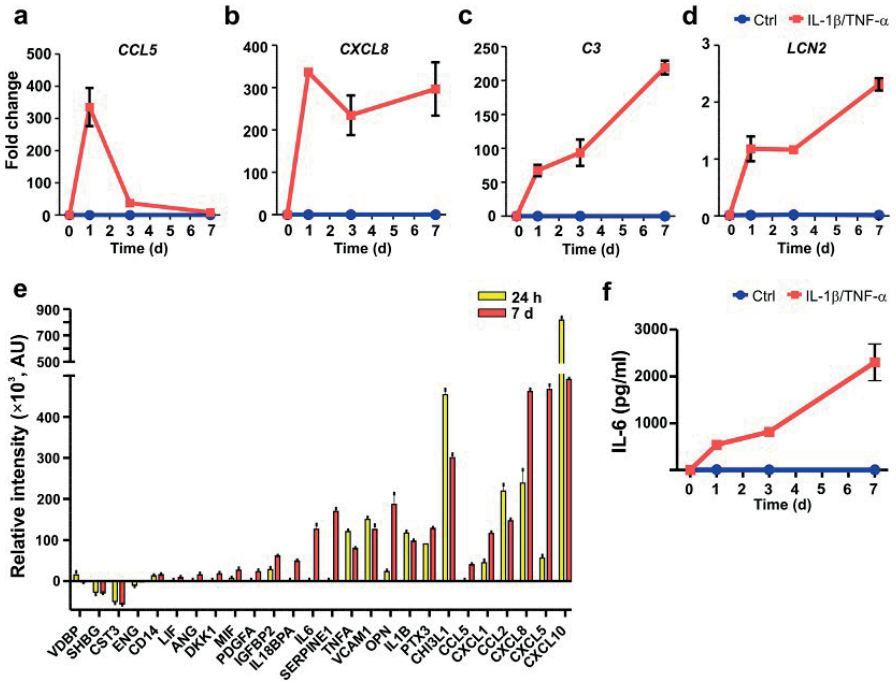

Figure 4. Cytokine treatment results in the inflammatory activation of astrocytes. (**a–d**) The gene expression levels of (**a**) *CCL5*, (**b**) *CXCL8*, (**c**) *C3*, and (**d**) *LCN2* were analyzed in cytokine-treated and control astrocytes at the 0-, 1-, 3- and 7-day time points. Robust increases in the expression of all studied genes were detected after cytokine treatment (n = 2 with three technical replicates; the data are representative of two experiments). (**e**) Secretion of inflammatory factors into the medium was analyzed at the 24 h and 7-day time points. The relative intensity values for the different analytes were calculated by subtracting the intensity values of the control samples from those of the cytokine-treated samples at each time point (n = 1 with two technical replicates; the data are representative of two experiments). (**f**) The levels of IL-6 were analyzed at 0, 1, 3 and 7 day in cytokine-treated and control astrocytes. IL-6 levels increased in a time-dependent manner over 7 days in the cytokine-treated samples, while under control conditions, the levels were undetectable (n = 2 with two technical replicates; the data are representative of two experiments). The quantification data are presented as the mean ± s.e.m.

differences between them were detected in spike or burst rates (Fig. 5g–h). This result was confirmed with both in-house-produced (Fig. 5g–h) and commercial neurons (Supplementary Fig. S6f–g).

In comparison to the control group, the reactive ACM group demonstrated an immediate increase in spike activity (Ctrl -0.168 ± 0.039 vs. reactive ACM 0.025 ± 0.036, p = 0.033) and a decrease in activity at the 24 h time point (Ctrl 0.470 ± 0.066 vs. reactive ACM 0.250 ± 0.087, p = 0.045, Fig. 5g–h). However, the control ACM group exhibited both increased spike activity (Ctrl 0.349 ± 0.067 vs. Ctrl ACM 0.576 ± 0.095, p = 0.039) and increased burst rate (Ctrl 0.579 ± 0.377 vs. Ctrl ACM 2.048 ± 0.535, p = 0.02) at the 1 h time point compared to the control group. Similar changes in spike and burst rates were also confirmed with commercial neurons (Supplementary Fig. S6f–g). Thus, conditioned medium from reactive astrocytes did not cause any detectable cytotoxicity or functional silencing of neuronal networks. In fact, both control and reactive ACM supported functional activity, suggesting that astrocytes were neurosupportive rather than neurotoxic under these conditions.

Generation of a controlled astrocyte-neuron co-culture system utilizing a microfluidic device. Next, we established a novel platform enabling controlled co-culture of neurons and astrocytes, targeted stimulation of astrocytes, and study of neuron-astrocyte interactions (Fig. 6a). The microfluidic device is composed of separate compartments for neurons and astrocytes, which are connected via microtunnels and axonal compartment (Fig. 6a,b, Supplementary Fig. S7). Immunofluorescence staining demonstrated that β-tubulin-positive neuronal somas were restricted to their designated compartments (Fig. 6c–e), while NF-H-positive axons grew readily through the microtunnels into the axonal compartment (Fig. 6d). GFAP-positive astrocytes were restricted to the astrocyte compartment (Fig. 6c), and direct cell-to-cell interactions could be verified, as astrocyte processes extended through the microtunnels and connected to neuronal axons in the neighboring compartment (Fig. 6e,f).

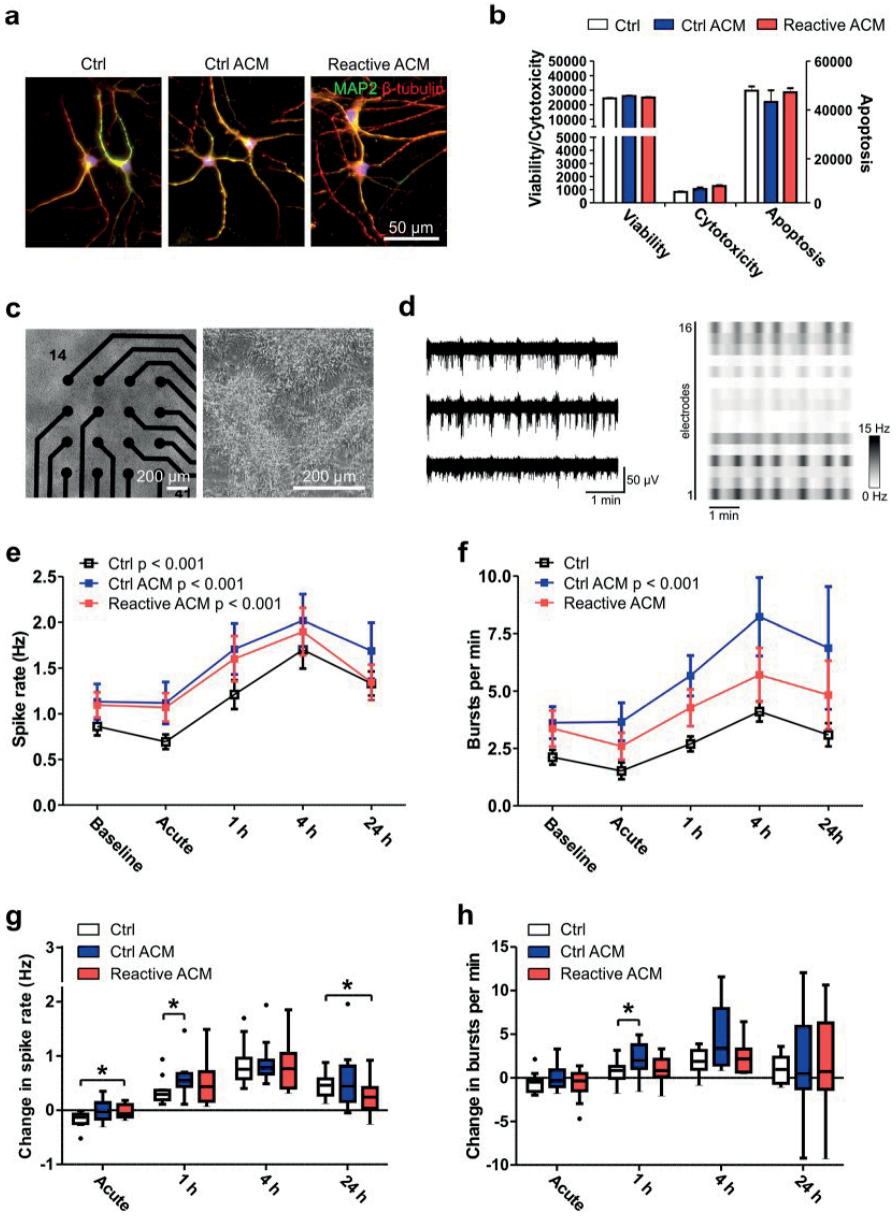

Figure 5. Viability and functionality of neuronal cells after exposure to reactive astrocyte conditioned medium. (**a**) Immunocytochemical staining of hPSC-derived neuronal cells exposed to control medium (Ctrl), control ACM (Ctrl ACM) and reactive ACM. Neuronal cells stained positive for MAP2 (green) and β-tubulin (red). DAPI nuclear staining is shown in blue. (**b**) The reactive astrocyte conditioned medium did not show an effect on the viability, cytotoxicity or apoptosis of neuronal cells after 48 h of exposure (the data are representative of two experiments; in each experiment n = 3–6 per group). Statistical analysis was performed using independent-sample t-tests. (**c**) The effect of ACM on neuronal functionality was studied with microelectrode array (MEA) measurements. The phase-contrast images show neuronal cells cultured on MEAs. (**d**) Typical spontaneous activity in neuronal networks recorded from three electrodes over 5 minutes. The raster blot shows the typical network-wide activity from all 16 electrodes of one well over 5 minutes. (**e**) Spike rate (Hz) development for active electrodes before (baseline) and after different medium exposures (acute, 1 h, 4 h and 24 h). (**f**) Number of bursts per minute before and after different medium exposures. For the MEA data, n = 12 networks derived from one differentiation. The data are presented as the mean ± s.e.m., and statistical analysis was performed using the Friedman test. (**g**-**h**) To highlight significant differences between treatment groups, the data from

panels e-f were reused and are presented as the changes in spike and burst rates compared to the baseline measurements. The data are shown as Tukey boxplots. Statistical significances was determined with the Mann-Whitney U test; * $p < 0.05$, ** $p < 0.01$, and *** $p < 0.001$.

Fluidic isolation of the astrocyte compartment from the neuron compartment was demonstrated with FITC-conjugated dextran particles, which did not diffuse to the neuron compartment, as detected by fluorescence imaging (Fig. 6g) and measurements of particle concentrations after 24 h (Fig. 6h). However, over 24 h, particles did diffuse from the astrocyte compartment into the axonal compartment, verifying the possibility of studying humoral effects on axons with this system (Fig. 6g). In summary, the generated platform enabled the isolation of different cell types and cell parts, and the control of cell-to-cell interactions and fluid flow.

Reactive astrocytes and an inflammatory environment affect axonal growth in the microfluidic platform. The last aim was to induce the reactive astrocyte phenotype in the microfluidic platform and study the effect of reactive astrocytes on axon growth in the axonal compartment (Fig. 7a). To treat astrocytes, IL-1β and TNF-α were applied to the astrocyte compartment after the neurons and astrocytes were both plated into the microfluidic platform (Fig. 7a). The 72 h cytokine treatment did not cause any major cytotoxic effects on either cell type, as only a few dead cells were detected among viable cells (Fig. 7b). Similar to the findings under open-well conditions described above, the reactive astrocytes secreted a wide range of inflammatory factors (e.g., VCAM1, CCL2, CXCL8, CXCL5, and CHI3L1) (Fig. 7c, Supplementary Fig. S8).

After confirming the proinflammatory phenotype of the astrocytes, the effect of these astrocytes on axonal growth was studied by quantifying the number and density of axons extending to the axonal compartment (Fig. 7d–g). In addition to devices with co-cultures of control or reactive astrocytes with neurons (treatment groups: Neu + Ctrl astro and Neu + Reactive astro), devices with only neurons were included in the study to elucidate whether treatment with IL-1β and TNF-α alone had an effect on axons (treatment groups: Neu and Neu + IL-1β/TNF-α). Over the 72 h follow-up period, no statistically significant differences were detected in axon counts between the groups (Fig. 7e). Furthermore, axonal density was assessed with live-cell calcein-AM color staining by quantifying the area coverage in the axonal compartment 72 h after cytokine treatment (Fig. 7f,g). The results showed that reactive astrocytes increased axonal density compared to control astrocytes (Neu + Ctrl astro 4.7 ± 0.6 vs. Neu + Reactive astro 8.2 ± 1.3, $p = 0.028$, Fig. 7g). Taken together, the results indicate that selective cytokine stimulation of astrocytes resulted in an inflammatory environment that had a positive effect on axonal growth, demonstrating the suitability of the developed cell model for studying axonal biology.

Discussion

Astrocytes are an acknowledged partner in the inflammatory processes in many neurodegenerative diseases and injuries of the CNS[5,11]. Astrocytes regulate the homeostasis of their surroundings and can have direct effects on neurons, both beneficial and detrimental. Human astrocytes are known for their complexity and heterogeneity, and some of their structural and functional traits differ from those of rodent astrocytes[12–14]. Therefore, in this study, we used hiPSC-derived astrocytes to create a human cell model system to study the inflammatory activation of astrocytes and the effects of activated astrocytes on neuronal functionality and axonal growth.

A variety of inflammatory molecules have been studied for their ability to induce a reactive astrocyte phenotype *in vitro*[8,23,43]. Here, astrocytes were treated with a combination of the cytokines IL-1β and TNF-α, which are typically released by activated microglia during neuroinflammation and are capable of stimulating astrogliosis *in vivo*[5,44,45] and *in vitro*[18,46–48]. Furthermore, co-stimulation with IL-1β and TNF-α has been demonstrated to be a more potent trigger of reactivity that stimulation with either of the cytokines independently[8,23]. To date, few reports have described the responses of hiPSC-derived astrocytes to cytokine treatments[18,22–25,41]. However, many astrocyte differentiation protocols use serum to enhance astrocytes production that can promote astrocyte reactivation[14,23]. Here, astrocytes were cultured in serum-free medium, and under control conditions, the astrocytes remained in a quiescent state according to the results of gene expression and secretion profile analysis. We also treated astrocytes with the inflammatory cytokines for 7 days as described previously[18] to mimic chronic effects. During the 7-day activation, we observed a gradual change in the morphology of the astrocytes from fibrous to polygonal and a reorganization of intermediate filament proteins, which are typical hallmarks of astrogliosis *in vivo*[6]. This clear morphological change has previously been demonstrated *in vitro* with human fetal astrocytes[14,46] but not reported with hiPSC-derived astrocytes[18,22,25]. Additionally, upregulation of GFAP has been commonly described in relation to astrogliosis *in vivo*[10]. Interestingly, even though both control and reactive astrocytes stained positive for GFAP, more detailed analysis revealed downregulation of GFAP at both the gene and total protein levels upon cytokine treatment. Consistent with our data, reductions in GFAP have been reported in IL-1-treated human fetal astrocytes[49] and in IL-1β- and TNF-α-treated rodent astrocytes at both the gene and protein levels[8,43]. Overall, we showed morphological transformation and alterations in the structural proteins of reactive astrocytes following 7-day IL-1β and TNF-α treatment.

Astrocytes are immunocompetent cells, and inflammatory activity upon stimulation is therefore their important feature[6]. The key signaling pathways involved in astrocyte reactivation include NF-κB pathway, which was acutely activated after cytokine treatment in the present study. NF-κB activation is known to induce the production of proinflammatory cytokines, chemokines and adhesion molecules, which mediate leukocyte recruitment to the CNS, leading to neuroinflammation[7,10,50]. Here, we demonstrated the secretion of a wide variety of chemokines, cytokines and other inflammatory factors by reactive astrocytes. For example, secretion of the typical inflammatory markers CCL5, CXCL8 and IL-6 was temporally induced after cytokine treatment, which has also been previously reported in studies on IL-1β- and TNF-α-treated hiPSC-derived astrocytes[18,22]. Interestingly,

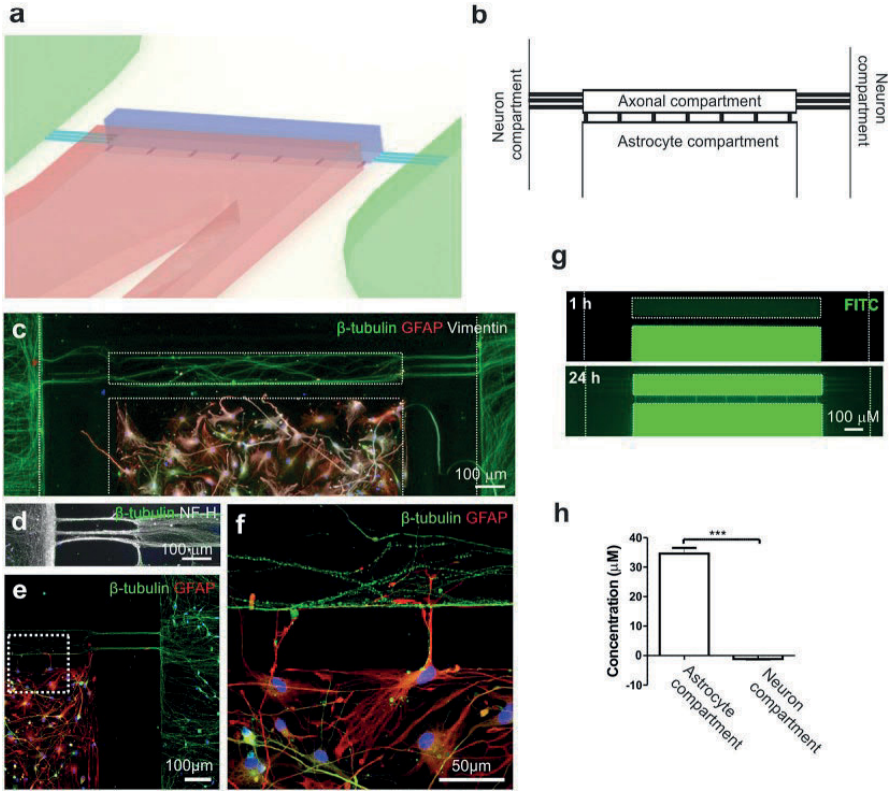

Figure 6. Description of the microfluidic device for co-culture of neurons and astrocytes and the fluidic isolation of the cell compartments. (**a**) Schematic showing a 3D illustration of the microfluidic device. (**b**) The microfluidic device consisted of two opposing compartments for neurons and a separate compartment for astrocytes, all of which were connected to an axonal compartment via microtunnels. (**c**) Immunocytochemical staining showing successful co-culture of β-tubulin-positive neurons and GFAP- and vimentin-positive astrocytes in the device and (**d**) the presence of NF-H-positive axons growing into the axonal compartment. (**e**) GFAP-positive astrocytes were placed close to the microtunnels leading to the axonal compartment, and (**f**) enlargement of the image illustrates cell-to-cell interactions between astrocytic processes and axons. (**g**) To evaluate the fluidic isolation of the astrocyte compartment, dextran-conjugated FITC was added to the astrocyte compartment, and its diffusion was evaluated by imaging with fluorescence microscopy at 1 h and 24 h. Fluorescence was detected in the axonal compartment after 24 h but was absent in the neuronal compartment (the compartments are shown with white dotted lines). (**h**) The concentration of dextran-FITC was measured after 24 h from medium collected from the astrocyte and neuron compartments. The data are shown as the mean ± s.e.m. (n = 6; the data are from one experiment). Statistical analysis was performed with independent-sample t-tests, and statistical significance is denoted as * $p < 0.05$, ** $p < 0.01$, and *** $p < 0.001$.

we observed upregulation of complement component 3 (C3), which has been linked to the neuroinflammatory phenotype of reactive astrocytes and has also been detected in demyelinating lesions of MS patients[8,9]. For the first time, we detected CHI3L1, OPN, and PTX3, known astrogliosis-associated markers *in vivo*[9], in hiPSC-derived reactive astrocytes; these proteins are also considered candidate diagnostic and prognostic biomarkers for CNS diseases[51,52]. Thus, a broad range of inflammatory factors were discovered in a human model system of astrogliosis; however, the specific roles of these factors in neuroinflammatory processes remain to be explained.

Only a handful of studies have addressed interactions between reactive astrocytes and neurons *in vitro* using human cells[8,24,26,53]. Here, humoral signaling by reactive astrocytes sustained neuronal viability, suggesting that the astrocyte secretion profile was not primarily neurotoxic. In contrast, previous studies have described decreased numbers of neurons in direct co-cultures of human neurons and IL-1β-stimulated astrocytes[24], and the humoral effects of TNF-α, IL-1α and complement component 1q (C1q) -stimulated rodent astrocytes have been reported to be toxic to human neurons[8]. Here, responses were also studied on a more sensitive neuronal network functionality level[54]. ACM exposure did not silence neuronal network activity but rather supported functionality, suggesting the polarization of astrocytes into a neurosupportive state. Previous studies have shown that secreted factors as well as direct cell-to-cell contact with rodent astrocytes can increase the activity of networks

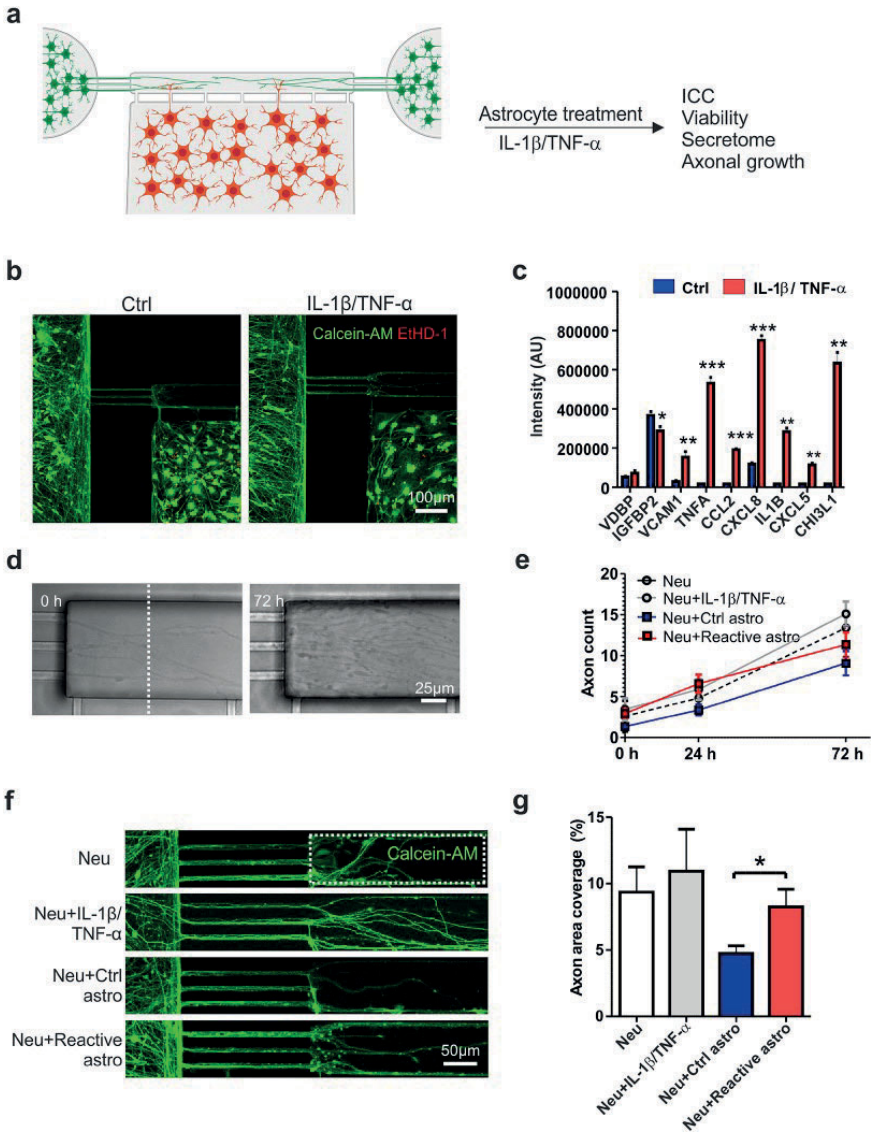

Figure 7. *In vitro* model for astrogliosis and axonal growth. (**a**) Experimental design for co-culture of astrocytes and neurons in the microfluidic device and astrocyte activation with IL-1β and TNF-α. (**b**) Both cell types remained viable (based on calcein-AM staining) on the platform after cytokine treatment, and very few dead cells (revealed by EtHD-1 staining) were observed. (**c**) Cytokine-treated astrocytes secreted significantly higher levels of several inflammatory factors than controls (n = 2; the data are from one experiment). (**d**) Phase-contrast images showing axons extending into the axonal compartment at 0 h and 72 h after cytokine treatment. (**e**) The number of axons extending into the axonal compartment (crossing the distance marked with the white dotted line) was quantified over 72 h. In addition to devices with co-cultures of control or reactive astrocytes and neurons (the Neu + Ctrl astro and Neu + Reactive astro groups), devices with cultures of only neurons were established to determine the effects of IL-1β and TNF-α treatment on axons (the Neu and Neu + IL-1β/TNF-α group) (n = 4–8 for each group; the data are from two experiments). (**f**) Axonal growth was also visualized with live-cell calcein-AM color staining to estimate coverage in the axonal compartment (the white dotted line). (**g**) Quantification of the area coverage in the axonal compartment revealed that reactive astrocytes supported axonal growth compared to control astrocytes (n = 6–13 for each group; the data are from one independent experiment). All data are presented as the mean ± s.e.m. Statistical analysis between groups was performed with independent-sample t-tests. P-values less than 0.05 were considered to indicate significance, and significant differences compared to the control group are presented in the graphs as * $p < 0.05$, ** $p < 0.01$, and *** $p < 0.001$.

on MEAs[55,56]. On the other hand, neurotoxic astrocytes have failed to promote synapse function[8]. Altogether, our results suggest that 7-day stimulation of hiPSC-derived astrocytes with cytokines results in an inflammatory phenotype that has a supportive rather than a harmful effect on neuronal cells.

To reveal the underlying mechanisms of CNS disorders, the complex cellular interactions between glial and neuronal cells should be investigated in more detail. Microfluidic technology can provide *in vitro* research tools that go beyond conventional cell culture methods with the aim of better modeling *in vivo* environments[31,32]. Here, our microfluidic platform was developed to co-culture the two cell types in a compartmentalized, controlled manner to specifically study axonal interactions with glial cells. Co-culture of human neurons and astrocytes was successful in the platform, which allowed direct contact between astrocyte processes and axons. Moreover, fluidic isolation enabled targeted stimulation of astrocytes in their compartment while also permitting humoral effects on neuronal axons extending into the axonal compartment. Activation of astrocytes with IL-1β and TNF-α was reproduced selectively in the microfluidic platform, and the inflammatory niche promoted axonal growth, further suggesting neurosupportive characteristics. This interpretation is supported by a recent report in which IL-1β mediated a potentially neuroprotective astrocyte phenotype expressing axonal permissive transcripts[57]. A microfluidic platform has been previously used for analysis of the neuroinflammatory mechanisms of astrocytes and microglia in the neurotoxic environment of Alzheimer's disease[26]. Our results present a unique microfluidic device designed for studying the interactions of axons and glial cells and further validate the suitability of microfluidic platforms as tools for studying the complex interplay among multiple cell types in the contexts of neuroinflammation and neurodegeneration.

In conclusion, our results suggest that extended co-stimulation with IL-1β and TNF-α produces a reactive astrocyte phenotype with a broad inflammatory secretion profile that displays neurosupportive characteristics with regard to neuronal viability, functionality and axonal growth. The mechanism behind the neurosupportive effects need to be clarified in the future studies. Furthermore, an *in vitro* model combining human cells and microfluidic technology was developed, and the usefulness of the proposed novel microfluidic platform for investigation of neuron-astrocyte interactions in an inflammatory environment was demonstrated. Advancing the field of *in vitro* modeling and creating tools for studying intricate cellular interactions in neurological disorders will promote the discovery of novel neuroprotective therapeutic targets in the future.

Methods

Human pluripotent stem cells and differentiation of neurons and astrocytes. The hPSC lines Regea 08/023[58] and 10212.EURCCs[59] used in this study were derived at the Faculty of Medicine and Health Technology (MET), Tampere University, Finland. MET has approval from the Finnish Medicines Agency (FIMEA) for research utilizing human embryos (Dnro 1426/32/300/05) and has received supportive statements from the regional ethics committee of Pirkanmaa Hospital District for the derivation, culture, and differentiation of hESCs (R05116) and hiPSCs (R08070). An informed consent was obtained from all subjects who provided cell samples. All methods were carried out in accordance with relevant guidelines and regulations. The hiPSC line 10212.EURCCs was derived from human skin fibroblasts using Sendai virus technology[60]. The hPSC lines were expanded in feeder-free culture as described earlier[61]. The in-house-produced neurons were differentiated according to the methods in a previous publication[62], with some modifications (details in the Supplementary methods).

Commercial hiPSC-derived neurons (ax0018) and astrocyte progenitors (ax0083) from healthy donors were cultured according to the manufacturer's protocol (both from Axol Bioscience Inc., UK). The astrocyte progenitors were differentiated for 24 days in culture and then treated for 7 days with 10 ng/ml human recombinant TNF-α and 10 ng/ml human recombinant IL-1β (PeproTech Inc.). Samples for astrocyte characterization were collected during the treatment at the 0 h, 24 h, 72 h and 7 day time points (Fig. 2a).

RNA isolation and quantitative PCR. RNA was isolated from astrocytes with a NucleoSpin RNA kit (Macherey-Nagel). The concentration and purity of RNA were quantified with a NanoDrop 1000 (Thermo Fisher Scientific). RNA was converted to cDNA using a High Capacity cDNA Reverse Transcription Kit (Thermo Fisher Scientific). The expression levels of *CCL5, CXCL8, GFAP, LCN2, C3, GFAP, VIM, S100B, IL1R, IL1RAP, TNFRSF1A* and *TNFRSF1B* (Supplementary Table 3) were analyzed with TaqMan assays using an ABI Prism 7300 real-time PCR system (Thermo Fisher Scientific). The data were analyzed using the delta Ct method using GUSB and GAPDH as endogenous controls.

Immunocytochemical staining. Immunocytochemical staining was performed according to the methods in a previous publication[63]. The used primary and secondary antibodies are listed in the Supplementary Table 4. Images were acquired with an Olympus IX51 microscope equipped with an Olympus DP30BW camera (Olympus Corporation, Germany) or an LSM780 laser-scanning confocal microscope equipped with a Quasar spectral GaAsP detector (all from Carl Zeiss, Germany). CellProfiler[64] and CellProfiler Analyst[65] software was used to perform image analysis. For evaluation of astrocyte morphology, the FormFactor module of CellProfiler software was used to calculate circularity index according to the area and perimeter metrics of each cell. Circularity index was calculated as $4*\pi*\text{Area}/\text{Perimeter}^2$, with a value of 1 describing a perfectly circular object.

Glutamate uptake. Glutamate uptake by cultured cells was analyzed with a glutamate assay kit (Abcam). The cells were washed with PBS and with 0.1% BSA in PBS for 30 min + 37 °C. The cells were then incubated with 100 μM glutamate in PBS for 1 h + 37 °C. Finally, the cells were washed with PBS and lysed with assay buffer. The concentration of glutamate in the cell lysate was analyzed according to the manufacturer's protocol.

Cell proliferation assay. A CyQUANT Cell Proliferation Assay (Thermo Fisher Scientific) was used to analyze the DNA amounts in cultured cells according to the manufacturer's protocol. Fluorescence was measured at 520 nm (Wallac Victor 1420, PerkinElmer).

Cell viability and apoptosis assay. Cell viability and caspase-3/7 activation were detected in cultured cells with an ApoTox-Glo Triplex Assay (Promega). For positive controls, cells were treated with 1.25 µM staurosporine and 25 µM ionomycin (both from Sigma) for 6 h. Fluorescence was measured at 505 nm and 520 nm for viability and cytotoxicity, respectively. Luminescence was measured to detect apoptosis (Wallac Victor 1420).

Collection of astrocyte conditioned medium. Astrocyte conditioned medium (ACM) from cytokine-treated and control astrocytes was collected at the 9-day time point. First, astrocytes were treated for 7 days with the cytokines IL-1β and TNF-α; thereafter, the cells were washed with PBS, and fresh medium was added to the cells. At day 9, the medium was harvested and centrifuged at 400 × *g* for 5 min at RT, and the supernatant was collected and stored at -80 °C until use. Neuronal cells (in-house-derived hESC line Regea 08/023) were exposed to ACM or control medium for 24 h (MEA analysis) or 48 h (viability assay) before analysis. The experiments with ACM also included a control group; the control medium was prepared similarly to the ACM but without astrocytes.

Cytokine array and ELISA. Protein secretion (see the list of analytes in Supplementary Table 1) into the astrocyte culture medium was measured using a Proteome Profiler Antibody Array (Human XL Cytokine Array Kit, ARY022B, R&D Systems) according to the manufacturer's protocol. The membranes were imaged with a ChemiDoc imaging system (Bio-Rad), and the intensity of the spots was quantified with Image Lab software (Bio-Rad).

The levels of IL-6 in the medium were measured with a human IL-6 uncoated ELISA kit (#88-7066-22, Thermo Fisher Scientific) according to the manufacturer's protocol. The absorbance was measured at 450 nm (Wallac Victor 1420).

Viability staining. A viability/cytotoxicity kit for mammalian cells (Thermo Fisher Scientific) was used to evaluate the viability of cells after ACM treatment and culture in the microfluidic platform. The cultures were incubated for 30 min to 1 h at 37 °C with green-fluorescent calcein-AM (0.5 µM) for detection of live cells and with red-fluorescent ethidium homodimer-1 (0.5 µM) for detection of dead cells. The samples were imaged immediately with an Olympus IX51 microscope equipped with an Olympus DP30BW camera (Olympus Corporation) and an LSM780 laser-scanning confocal microscope equipped with a Quasar spectral GaAsP detector (Carl Zeiss).

Microelectrode array measurements. Neuronal network activity was recorded with an Axion Maestro system controlled by AxIS Software (Axion Biosystems, Atlanta, GA, USA) with 12.5 kHz sampling rate as described previously[66]. The hPSC-derived cortical neurons (in-house-derived hESC line Regea 08/023 or commercial hiPSC-derived neurons, ax0018) were plated on CytoView MEA 48 plates with 16 electrodes per array. Recordings were obtained under a controlled temperature of 37 °C. Spontaneous activity development was examined once a week with 10-minute recordings. After five weeks, when synchronous network activity had developed, the experiments with astrocyte conditioned medium (ACM) were initiated. The responses to control medium, control ACM or reactive ACM were measured for 10 min immediately and at 1 h, 4 h and 24 h after application. Analysis methods for spike and burst detection are described in the Supplementary methods section.

Design of the microfluidics device. An in-house-developed microfluidics polydimethylsiloxane (PDMS) device (Patent: WO2015092141A1) was used (Fig. 6a, Supplementary Fig. S7). The device contains three separate cell compartments and an axonal compartment that are interconnected by microtunnels (Fig. 6b, Supplementary Fig. S7). There are two neuronal compartments (length = 4250 µm, width = 3000 µm) that are connected to the axonal compartment (length = 1000 µm, height = 100 µm, width = 100 µm) with three microtunnels (length = 250 µm, height = 3 µm, width = 10 µm). The microtunnels allow the extension of axons but prevent the migration of neuronal somas from the neuronal compartment into the axonal compartment (Fig. 6b,c). The flow-based astrocyte compartment is connected to the axonal compartment with seven microtunnels (length = 50 µm, height = 3.5 µm, width = 10 µm) (Supplementary Fig. S7). The fabrication of PDMS devices are described in the Supplementary methods.

Co-culture of neurons and astrocytes in the microfluidic platform. HiPSC-derived cortical neurons (10212.EURCCs) and commercial hiPSC-derived astrocytes (ax0083) were seeded into the neuronal compartments and astrocyte compartment, respectively (see details on Supplementary methods). Three days after cell plating, 10 ng/ml IL-1β- and TNF-α-containing medium was added into the astrocyte compartment, and treatment continued for 3 days. After cytokine treatment, the viability of cells was assessed with viability staining, and astrocyte-secreted inflammatory factors were analyzed in medium collected from the astrocyte compartment. To characterize the astrocytes and neurons in the co-cultures, immunofluorescence staining was performed. First, the microfluidics devices were separated manually from the coverslips, and then the cells were fixed with 4% PFA and stained according to an immunocytochemical protocol. To evaluate the influences of the astrocytes and cytokines on axonal growth, the following experimental groups were established: 1) a group in which neurons were seeded in the neuronal compartments (the Neu group), 2) a group in which neurons were seeded in the neuronal compartments and cytokine treatment was conducted via the astrocyte compartment (the Neu + IL-1β/TNF-α group), 3) a group in which neurons and astrocytes were seeded in their compartments (the Neu + Ctrl

astro group), and 4) a group in which neurons and astrocytes were seeded in their compartments and cytokine treatment was conducted via the astrocyte compartment (the Neu + Reactive astro group). The cells in the devices were imaged with phase-contrast microscopy at baseline and at 24 h and 72 h after cytokine treatment. The individual axons entering the axonal compartment were counted manually from the images at a distance of 80 µm from the axonal microtunnels (the white dotted line in Fig. 7d). The density of the axons in the axonal compartment was evaluated by analyzing the area covered with calcein-AM-stained axons at 72 h after cytokine treatment. The analyzed area was a 0.033 mm^2 (325 µm × 100 µm) region next to the axonal microtunnels (the white dotted line in Fig. 7f), and analysis was performed using CellProfiler software.

Statistical analysis. Statistical analysis of Gaussian-distributed data was performed with independent-sample T-tests. If the data followed a non-Gaussian distribution, the nonparametric Mann-Whitney U-test was used. Bonferroni correction was used for multiple comparisons.

The MEA data followed a non-Gaussian distribution; therefore, nonparametric tests were selected. To study changes in activity within treatment groups over time, the Friedman test for related samples was performed followed by the Wilcoxon signed-rank test to compare two related samples. To study differences between groups, delta values were calculated (by subtracting the baseline values from the values obtained immediately (acute), 1 h, 4 h, or 24 h after treatment), and Mann-Whitney U-tests were performed.

A p-value < 0.05 was considered to indicate significance. Statistical significance is denoted as * $p < 0.05$, ** $p < 0.01$, and *** $p < 0.001$. All statistical tests were performed with SPSS Statistics software (version 25.0).

Data availability

The datasets generated during and/or analyzed during the current study are available from the corresponding author on reasonable request.

Received: 14 June 2019; Accepted: 31 October 2019;
Published online: 15 November 2019

References

1. Araque, A., Parpura, V., Sanzgiri, R. P. & Haydon, P. G. Tripartite synapses: glia, the unacknowledged partner. *Trends in Neurosciences* **22**, 208–215 (1999).
2. Papouin, T., Dunphy, J., Tolman, M., Foley, J. C. & Haydon, P. G. Astrocytic control of synaptic function. *Philosophical transactions of the Royal Society of London.Series B, Biological sciences* **372**, 20160154 (2017).
3. Allen, N. J. Astrocyte Regulation of Synaptic Behavior. *Annu. Rev. Cell Dev. Biol.* **30**, 439–463 (2014).
4. Allaman, I., Belanger, M. & Magistretti, P. J. Astrocyte-neuron metabolic relationships: for better and for worse. *Trends Neurosci.* **34**, 76–87 (2011).
5. Ben Haim, L., Carrillo-de Sauvage, M., Ceyzériat, K. & Escartin, C. Elusive roles for reactive astrocytes in neurodegenerative diseases. *Frontiers in Cellular Neuroscience* **9**, 278 (2015).
6. Colombo, E. & Farina, C. Astrocytes: Key Regulators of Neuroinflammation. *Trends Immunol.* **37**, 608–620 (2016).
7. Correale, J. & Farez, M. F. The Role of Astrocytes in Multiple Sclerosis Progression. *Front Neurol* **6**, 180 (2015).
8. Liddelow, S. A. *et al*. Neurotoxic reactive astrocytes are induced by activated microglia. *Nature* **541**, 481–487 (2017).
9. Zamanian, J. L. *et al*. Genomic analysis of reactive astrogliosis. *J. Neurosci.* **32**, 6391–6410 (2012).
10. Liddelow, S. A. & Barres, B. A. Reactive Astrocytes: Production, Function, and Therapeutic Potential. *Immunity* **46**, 957–967 (2017).
11. Sofroniew, M. V. Molecular dissection of reactive astrogliosis and glial scar formation. *Trends Neurosci.* **32**, 638–647 (2009).
12. Oberheim, N. A. *et al*. Uniquely hominid features of adult human astrocytes. *The Journal of neuroscience: the official journal of the Society for Neuroscience* **29**, 3276–3287 (2009).
13. Tarassishin, L., Suh, H. & Lee, S. C. LPS and IL-1 differentially activate mouse and human astrocytes: role of CD14. *Glia* **62**, 999–1013 (2014).
14. Zhang, Y. *et al*. Purification and Characterization of Progenitor and Mature Human Astrocytes Reveals Transcriptional and Functional Differences with Mouse. *Neuron* **89**, 37–53 (2016).
15. Hoffmann, F. S. *et al*. Fingolimod induces neuroprotective factors in human astrocytes. *J Neuroinflammation* **12**, 184 (2015).
16. van Scheppingen, J. *et al*. miR147b: A novel key regulator of interleukin 1 beta-mediated inflammation in human astrocytes. *Glia* **66**, 1082–1097 (2018).
17. van Kralingen, C., Kho, D. T., Costa, J., Angel, C. E. & Graham, E. S. Exposure to inflammatory cytokines IL-1β and TNFα induces compromise and death of astrocytes; implications for chronic neuroinflammation. *PLoS ONE* **8**, e84269 (2013).
18. Roybon, L. *et al*. Human stem cell-derived spinal cord astrocytes with defined mature or reactive phenotypes. *Cell. Rep.* **4**, 1035–1048 (2013).
19. Serio, A. *et al*. Astrocyte pathology and the absence of non-cell autonomy in an induced pluripotent stem cell model of TDP-43 proteinopathy. *Proc. Natl. Acad. Sci. USA* **110**, 4697–4702 (2013).
20. Shaltouki, A., Peng, J., Liu, Q., Rao, M. S. & Zeng, X. Efficient generation of astrocytes from human pluripotent stem cells in defined conditions. *Stem Cells* **31**, 941–952 (2013).
21. Krencik, R., Weick, J. P., Liu, Y., Zhang, Z. J. & Zhang, S. C. Specification of transplantable astroglial subtypes from human pluripotent stem cells. *Nat. Biotechnol.* **29**, 528–534 (2011).
22. Lundin, A. *et al*. Human iPS-Derived Astroglia from a Stable Neural Precursor State Show Improved Functionality Compared with Conventional Astrocytic Models. *Stem Cell. Reports* **10**, 1030–1045 (2018).
23. Perriot, S. *et al*. Human Induced Pluripotent Stem Cell-Derived Astrocytes Are Differentially Activated by Multiple Sclerosis-Associated Cytokines. *Stem Cell Reports* **11**, 1199–1210 (2018).
24. Santos, R. *et al*. Differentiation of Inflammation-Responsive Astrocytes from Glial Progenitors Generated from Human Induced Pluripotent Stem Cells. *Stem Cell. Reports* **8**, 1757–1769 (2017).
25. Tcw, J. *et al*. An Efficient Platform for Astrocyte Differentiation from Human Induced Pluripotent Stem Cells. *Stem cell reports* **9**, 600–614 (2017).
26. Park, J. *et al*. A 3D human triculture system modeling neurodegeneration and neuroinflammation in Alzheimer's disease. *Nat. Neurosci.* **21**, 941–951 (2018).
27. Hagman, S. *et al*. Effects of inflammatory cytokines IFN-γ, TNF-α and IL-6 on the viability and functionality of human pluripotent stem cell-derived neural cells. *J. Neuroimmunol.* **331**, 36–45 (2019).

28. Bigler, R. L., Kamande, J. W., Dumitru, R., Niedringhaus, M. & Taylor, A. M. Messenger RNAs localized to distal projections of human stem cell derived neurons. *Sci Rep* **7**, 611 (2017).
29. Fantuzzo, J. A. *et al*. Neurocircuitry: Establishing *in vitro* models of neurocircuits with human neurons. *Technology (Singap World Sci)* **5**, 87–97 (2017).
30. Sarkar, A. *et al*. Efficient Generation of CA3 Neurons from Human Pluripotent Stem Cells Enables Modeling of Hippocampal Connectivity *In Vitro*. *Cell Stem Cell*, **22**, 697.e9 (2018).
31. Neto, E. *et al*. Compartmentalized Microfluidic Platforms: The Unrivaled Breakthrough of *In Vitro* Tools for Neurobiological Research. *J. Neurosci.* **36**, 11573–11584 (2016).
32. Taylor, A. M. *et al*. A microfluidic culture platform for CNS axonal injury, regeneration and transport. *Nat. Methods* **2**, 599–605 (2005).
33. Brahic, M., Bousset, L., Bieri, G., Melki, R. & Gitler, A. D. Axonal transport and secretion of fibrillar forms of α-synuclein, Aβ42 peptide and HTTExon 1. *Acta Neuropathol.* **131**, 539–548 (2016).
34. Chen, M. *et al*. A new method for quantifying mitochondrial axonal transport. *Protein Cell* **7**, 804–819 (2016).
35. Lu, X., Kim-Han, J. S., O'Malley, K. L. & Sakiyama-Elbert, S. E. A microdevice platform for visualizing mitochondrial transport in aligned dopaminergic axons. *J. Neurosci. Methods* **209**, 35–39 (2012).
36. Malone, M. *et al*. Neuronal activity promotes myelination via a cAMP pathway. *Glia* **61**, 843–854 (2013).
37. Ristola, M. *et al*. A compartmentalized neuron-oligodendrocyte co-culture device for myelin research: design, fabrication and functionality testing. *J Micromech Microengineering* **29**, 065009 (2019).
38. Yang, I. H. *et al*. Axon myelination and electrical stimulation in a microfluidic, compartmentalized cell culture platform. *Neuromolecular Med.* **14**, 112–118 (2012).
39. Virlogeux, A. *et al*. Reconstituting Corticostriatal Network on-a-Chip Reveals the Contribution of the Presynaptic Compartment to Huntington's Disease. *Cell Rep* **22**, 110–122 (2018).
40. Pekny, M., Wilhelmsson, U., Tatlisumak, T. & Pekna, M. Astrocyte activation and reactive gliosis-A new target in stroke? *Neurosci. Lett.* **689**, 45–55 (2019).
41. Ponath, G. *et al*. Enhanced astrocyte responses are driven by a genetic risk allele associated with multiple sclerosis. *Nat Commun* **9**, 5337 (2018).
42. Schönrock, L. M., Gawlowski, G. & Brück, W. Interleukin-6 expression in human multiple sclerosis lesions. *Neuroscience Letters* **294**, 45–48 (2000).
43. Ronco, V. *et al*. Differential deregulation of astrocytic calcium signalling by amyloid-β, TNFα, IL-1β and LPS. *Cell Calcium* **55**, 219–229 (2014).
44. Clausen, B. H. *et al*. Interleukin-1beta and tumor necrosis factor-alpha are expressed by different subsets of microglia and macrophages after ischemic stroke in mice. *J Neuroinflammation* **5**, 46 (2008).
45. Shinozaki, Y. *et al*. Transformation of Astrocytes to a Neuroprotective Phenotype by Microglia via P2Y1 Receptor Downregulation. *Cell Rep* **19**, 1151–1164 (2017).
46. Choi, S. S., Lee, H. J., Lim, I., Satoh, J. & Kim, S. U. Human astrocytes: secretome profiles of cytokines and chemokines. *PLoS ONE* **9**, e92325 (2014).
47. Rivieccio, M. A. *et al*. The cytokine IL-1beta activates IFN response factor 3 in human fetal astrocytes in culture. *J. Immunol.* **174**, 3719–3726 (2005).
48. Croitoru-Lamoury, J. *et al*. Expression of chemokines and their receptors in human and simian astrocytes: evidence for a central role of TNF alpha and IFN gamma in CXCR4 and CCR5 modulation. *Glia* **41**, 354–370 (2003).
49. John, G. R., Lee, S. C., Song, X., Rivieccio, M. & Brosnan, C. F. IL-1-regulated responses in astrocytes: relevance to injury and recovery. *Glia* **49**, 161–176 (2005).
50. Ponath, G., Park, C. & Pitt, D. The Role of Astrocytes in Multiple Sclerosis. *Front Immunol* **9**, 217 (2018).
51. Comabella, M., Sastre-Garriga, J. & Montalban, X. Precision medicine in multiple sclerosis: biomarkers for diagnosis, prognosis, and treatment response. *Curr. Opin. Neurol.* **29**, 254–262 (2016).
52. Agah, E. *et al*. Osteopontin (OPN) as a CSF and blood biomarker for multiple sclerosis: A systematic review and meta-analysis. *PLoS ONE* **13**, e0190252 (2018).
53. Russo, F. B. *et al*. Modeling the Interplay Between Neurons and Astrocytes in Autism Using Human Induced Pluripotent Stem Cells. *Biol. Psychiatry* **83**, 569–578 (2018).
54. Ylä-Outinen, L. *et al*. Human cell-based micro electrode array platform for studying neurotoxicity. *Front Neuroeng* **3**, 111 (2010).
55. Fukushima, K., Miura, Y., Sawada, K., Yamazaki, K. & Ito, M. Establishment of a Human Neuronal Network Assessment System by Using a Human Neuron/Astrocyte Co-Culture Derived from Fetal Neural Stem/Progenitor Cells. *J Biomol Screen* **21**, 54–64 (2016).
56. Odawara, A., Saitoh, Y., Alhebshi, A. H., Gotoh, M. & Suzuki, I. Long-term electrophysiological activity and pharmacological response of a human induced pluripotent stem cell-derived neuron and astrocyte co-culture. *Biochem. Biophys. Res. Commun.* **443**, 1176–1181 (2014).
57. Teh, D. B. L. *et al*. Transcriptome Analysis Reveals Neuroprotective aspects of Human Reactive Astrocytes induced by Interleukin 1β. *Sci Rep* **7**, 13988 (2017).
58. Skottman, H. Derivation and characterization of three new human embryonic stem cell lines in Finland. *In Vitro Cell. Dev. Biol. Anim.* **46**, 206–209 (2010).
59. Mostafa, K. Compromised Barrier Function in Human Induced Pluripotent Stem-Cell-Derived Retinal Pigment Epithelial Cells from Type 2 Diabetic Patients. *International Journal of Molecular Sciences* **20**(15), 3773 (2019).
60. Ojala, M. *et al*. Mutation-Specific Phenotypes in hiPSC-Derived Cardiomyocytes Carrying Either Myosin-Binding Protein C Or α-Tropomyosin Mutation for Hypertrophic Cardiomyopathy. *Stem Cells International* **2016**, 1684792 (2016).
61. Hongisto, H., Ilmarinen, T., Vattulainen, M., Mikhailova, A. & Skottman, H. Xeno- and feeder-free differentiation of human pluripotent stem cells to two distinct ocular epithelial cell types using simple modifications of one method. *Stem cell research & therapy* **8**, 291 (2017).
62. Shi, Y., Kirwan, P., Smith, J., Robinson, H. P. & Livesey, F. J. Human cerebral cortex development from pluripotent stem cells to functional excitatory synapses. *Nat. Neurosci.* **15**(86), S1 (2012).
63. Lappalainen, R. S. *et al*. Similarly derived and cultured hESC lines show variation in their developmental potential towards neuronal cells in long-term culture. *Regenerative Med.* **5**, 749–762 (2010).
64. Carpenter, A. E. *et al*. CellProfiler: image analysis software for identifying and quantifying cell phenotypes. *Genome Biol.* **7**, R100 (2016).
65. Thouis, R. Jones. CellProfiler Analyst: data exploration and analysis software for complex image-based screens. *BMC Bioinformatics* **9**(1), 482 (2008).
66. Hyysalo, A. *et al*. Laminin alpha5 substrates promote survival, network formation and functional development of human pluripotent stem cell-derived neurons in vitro. *Stem Cell. Res.* **24**, 118–127 (2017).

Acknowledgements

We thank the iPS Cell Core Facility, Tampere University, for providing the undifferentiated hiPSCs, and we thank Hanna Mäkelä and Eija Hannuksela for their technical assistance with cell maintenance and the molecular biology analyses. The authors thank the Tampere Imaging Facility and Outi Paloheimo for technical assistance and illustrations. We also thank the Facility of Electrophysiological Measurements, Tampere University. We appreciate the technical help received from Laura Hyväri and Janne Koivisto (Tampere University). This work was supported by Business Finland and the Academy of Finland (grant number 312414 to SN and 312411 to PK, grant number 296415 to MR), the Finnish Cultural Foundation (grant number 50191927 to SH, grant number 00170805 to TH) and the Tampere University Graduate School for Medicine and Life Sciences (TH).

Author contributions

T.H., S.H., S.N. and P.K. designed the study; T.H., S.H., M.R., L.S., K.V. and J.K. performed the experiments; S.H., T.H. and K.V. analyzed the data; and S.H. and T.H. wrote the paper. All authors edited the article.

Competing interests

The authors declare no competing interests.

Additional information

Supplementary information is available for this paper at https://doi.org/10.1038/s41598-019-53414-9.

Correspondence and requests for materials should be addressed to S.N.

Reprints and permissions information is available at www.nature.com/reprints.

Publisher's note Springer Nature remains neutral with regard to jurisdictional claims in published maps and institutional affiliations.